Stony Brook University

QCD factorization for heavy quarkonium production and fragmentation functions

A Dissertation Presented

by

Hong Zhang

to

The Graduate School

in Partial Fulfillment of the Requirements

for the Degree of

Doctor of Philosophy

in

Physics

Stony Brook University

August 2014

Stony Brook University

The Graduate School

Hong Zhang

We, the dissertation committee for the above candidate for the Doctor of Philosophy degree, hereby recommend acceptance of this dissertation.

Jian-Wei Qiu – Dissertation Advisor
Brookhaven Professor, C.N. Yang Institute for Theoretical Physics,
Senior Physicist, Brookhaven National Laboratory

George Sterman – Chairperson of Defense
Distinguished Professor and Director, C.N. Yang Institute for Theoretical Physics

Abhay L. Deshpande
Professor, Department of Physics and Astronomy

Thomas C. Weinacht
Professor, Department of Physics and Astronomy

David P. Morrison
Physicist
Brookhaven National Laboratory

This dissertation is accepted by the Graduate School.

Charles Taber
Dean of the Graduate School

Abstract of the Dissertation

QCD factorization for heavy quarkonium production and fragmentation functions

by

Hong Zhang

Doctor of Philosophy

in

Physics

Stony Brook University

2014

From the Tevatron and the LHC data, it is clear that current models for the heavy quarkonium production are not able to explain the polarization of produced heavy quarkonia at large transverse momentum p_T. A new approach to evaluate the heavy quarkonium production, by expanding the cross section in powers of $1/p_T$ before the expansion in powers of α_s, was proposed recently. In terms of the QCD factorization, it is proved that both the leading and next-to-leading power terms in $1/p_T$ for the cross sections can be systematically factorized to all orders in powers of α_s. The predictive power of this new QCD factorization formalism depends on several unknown but universal fragmentation functions (FFs) at an input scale of the order of heavy quarkonium mass m_Q. These FFs should be extracted from the data in principle. However, fitting so many unknown multi-variable functions from the data is formidable practically. The lack of knowledge of the input FFs impedes the application of the QCD factorization.

In this dissertation, inspired by the fact that these input FFs de-

pend on $m_Q \gg \Lambda_{QCD}$, we apply the NRQCD factorization formalism to further separate the perturbative and non-perturbative interactions. With our calculations, all the input unpolarized FFs are expressed as complicated functions with a few unknown NRQCD long-distance matrix elements (LDMEs). In addition, by general symmetry arguments, we successfully generalize the polarized NRQCD four-fermion operators to d dimensions and calculate the polarized FFs with conventional dimensional regularization.

In the first application of the QCD factorization to unpolarized J/ψ production, we find those NRQCD channels, which are expected to be important in the J/ψ polarization, are actually dominated by the next-to-leading-power term in the p_T expansion at current collider energies. Therefore the QCD factorization is very promising to solve the long standing heavy quarkonium polarization puzzle.

Contents

List of Figures

List of Tables

Acknowledgements

First and foremost, I would like to express my sincere gratitude to my Ph.D. advisor Dr. Jian-Wei Qiu for the guidance, patience and encouragement in my research and the writing of this dissertation. I thank him for giving me the freedom to explore on my own, and at the same time the insightful guidance when I feel lost confronting different ideas in the literature, or when I have technical problems in the calculation. He taught me how to question thoughts, express my ideas, and test my ideas with calculation. Without his guidance and persistent help, this dissertation would not have been possible.

I am deeply grateful to Dr. George Sterman for showing me the beauty of quantum field theory in his lectures, and for answering my questions in an understandable way. I would also like to thank my collaborator and the best roommate Dr. Yan-Qing Ma for his generous help when I struggled in NRQCD and programming. I appreciate the numerous discussions we ever had, on physics and beyond. I also thank Dr. Zhong-Bo Kang for many beneficial discussions on physics, and for his encouragement and valuable suggestions about the career.

I would like to thank Heng-Tong Ding, Xiao-Feng Guo, Ying-Chuan Li, Jin-Feng Liao, Shu Lin and many other friends in Brookhaven National Laboratory for their friendship and for their encouragement. Thanks must also go to my friends Xu-Gang He, Jun Nian, Mao Zeng, Yi-Ming Zhong and many others in Stony Brook University for many encouraging discussions on the homework problems.

I wish to thank my parents, Feng Lu and Yun-Cheng Zhang, and my grandfather Hua-Ji Lu for the unconditional love, for always believing in me, for celebrating my successes and forgiving my failures in every step of my life. I would also like to thank my girlfriend Ke Fang for her support and patience in the last six years. Perhaps none of this work would be completed without their love.

Chapter 1

Introduction

> The most incomprehensible thing about
> the universe is that it is comprehensible.
>
> Albert Einstein, 1936

As an important part of the Standard Model, Quantum Chromodynamics (QCD) is an $SU(3)_c$ gauge theory for strong interaction. One of the main successes in our understanding of QCD is the running of strong coupling and asymptotic freedom. Asymptotic freedom implies the validity of perturbation method when the transferred energy is larger than a few GeV. With factorization theorems, perturbative QCD (pQCD) has been widely tested in different processes and is successful in describing almost all experimental data on high-energy, large-momentum-transfer cross sections. On the other hand, the quark and gluon degrees of freedom at short distance cannot be observed at long distance due to QCD color confinement. In this low-energy region, QCD on the lattice has achieved many successes in calculating non-perturbative quantities, such as the hadron spectra. The tremendous successes of pQCD and lattice QCD convince us that QCD is the correct theory for strong interaction over all energy ranges.

However, there are still many problems we do not have many clues for, in particular, the transition from asymptotic freedom at short-distance ($< 1/10$ fm) to the color confinement at longer distance ($\gtrsim 1$ fm), or the hadronization process. There are many questions to be answered, such as how the quarks and gluons bind themselves together to form hadrons, is the hadronization process a total chaos or are there some patterns of the ordering, just to list a few. A natural idea for addressing these questions is to start with the production of the simplest strongly-interacting bound state, just as physicists

study the formation of the hydrogen atom to test their understanding of atomic structure.

Heavy quarkonium is one of the simplest systems. Inside heavy quarkonia, the large heavy quark mass $m_Q \gg \Lambda_{QCD}$ implies that they are localized heavy color charges. It is then natural to conjecture that the binding of heavy quarkonium is dominated by two-body interactions. Based on this picture, people introduce potential to describe the interaction between the heavy quark pair. This model, known as the potential model, achieves remarkable successes in explaining both the heavy quarkonium spectrum and transition rate between different states [26].

Nevertheless, as a low energy theory, the potential model itself is not able to explain the hadronization of heavy quarkonium, which involves both low-energy and high-energy dynamics. Indeed, the formation of heavy quarkonium is still a mystery 40 years after the discovery of the first quarkonium J/ψ. Because the heavy quark mass m_Q is much larger than $\Lambda_{\rm QCD}$, the production of the heavy quark pair could be calculated perturbatively [27]. The transformation or hadronization of the pair to a heavy quarkonium is intrinsically non-perturbative. It is thus natural to conjecture the factorization between a short-distance part describing the production of a heavy quark pair in hard scattering and a factor describing the non-perturbative hadronization of the pair. Different treatments of the hadronization process lead to various factorization models for heavy quarkonium production.

The color singlet model (CSM) [28–35] assumes the produced heavy quark pair in the hard scattering hadronizes without emitting gluons. Under this assumption, the heavy quark pair must take the same quantum numbers (spin, color, etc.) as the observed heavy quarkonium. Moreover, the non-perturbative factors in CSM are related to the heavy quarkonium wave function (or its derivatives), which can be extracted from heavy quarkonium decay data or calculated from the potential model. The CSM was quite successful explaining the S-wave heavy quarkonium production in low energy experiments until around 1995, when Tevatron data showed that the production rate is larger than LO CSM prediction by more than an order of magnitude. Even after taking into account the large high-order corrections, the CSM still under-predicts the Tevatron data by a large amount (see Fig. 3.6). On the other hand, the calculation of P-wave heavy quarkonium production based on the CSM suffers from uncanceled logarithmic infrared (IR) divergence. All these flaws show that some important piece of physics is missing from the CSM.

The non-relativistic QCD (NRQCD) model [36], which includes CSM as its special case, is basically an effective field theory approach relying on the sep-

aration of momentum scales in heavy quarkonium production. The NRQCD model assumes that a heavy quark pair produced in the hard scattering has a non-zero probability to evolve into any heavy quarkonium. The net transition rate depends on the heavy quark pair's relative velocity v, its spin and color states, and is given by universal NRQCD long-distance elements (LDMEs), which are non-perturbative and whose magnitude follows the NRQCD power-counting rule. Summing over all possible spin and color states of the pair gives the total inclusive cross section. With the perturbative hard parts calculated to next-to-leading order (NLO) in α_s and carefully fitted LDMEs, NRQCD is very successful in interpreting the data on the production rate of χ_{cJ}, J/ψ and Υ from the Tevatron and the LHC [11, 17, 37–39].

However, with additional large scales other than the heavy quark mass, potentially, the perturbative expansion of the hard parts of NRQCD factorization approach could be unstable. For example, for heavy quarkonium produced at large transverse momentum p_T, large $\ln(p_T^2/m_Q^2)$-type logarithms need to be systematically resummed. Moreover, high-order corrections may receive huge power enhancements in terms of p_T^2/m_Q^2, which could overwhelm the suppression of α_s at large p_T [24, 40].

Several inconsistencies between NLO NRQCD calculations and experimental data have been realized recently. The combination of color-octet LDMEs for J/ψ production, $M_{0,3.9}^{J/\psi} = 7.4 \times 10^{-2}$ GeV^3 [11], obtained by fitting hadron collider data based on NLO NRQCD calculation, contradicts the upper limit, 2.0×10^{-2} GeV^3, derived from e^+e^- data [41]. The first attempt of global fitting on J/ψ production in Ref. [38] effectively confirmed this inconsistency, where the minimum χ^2 per degree of freedom of the fitting is larger than 4. In addition, the full NLO NRQCD calculation has difficulties explaining the polarization of the exited state, ψ', measured at the Tevatron and the LHC (Fig. 3.14) [5], as well as the polarization of heavier quarkonium, such as $\Upsilon(3S)$ measured by CMS at the LHC [17, 42], although it is capable of explaining the data on the J/ψ polarization [12, 18]. Because of the large logarithms and possible huge power enhancement at higher orders, it is difficult to determine whether such inconsistencies are from large high order corrections or from the failure of NRQCD factorization conjecture.

Recently, a new QCD factorization approach to high p_T heavy quarkonium production at collider energies was proposed [23, 24, 40, 43]. A similar factorization approach based on soft-collinear effective theory (SCET) was also proposed [44]. In the QCD factorization approach, the cross section is first expanded by powers of $1/p_T^2$. As argued in Refs. [24, 40], both the leading-power (LP) term and next-to-leading-power (NLP) term of the expansion could be factorized systematically into infrared-safe short-distance partonic hard parts

convoluted with universal fragmentation functions (FFs), plus parton distribution functions (PDFs) in the case of hadronic collisions. Unlike the NRQCD factorization approach, the short-distance hard parts calculated by using the QCD factorization formalism are free of large logarithms and the power enhancements. All powers of $\ln(p_T^2/m_Q^2)$-type logarithms are resummed by solving a closed set of evolution equations of FFs [40]. Because of its better control on high order corrections, the QCD factorization approach is a powerful tool to study the mechanism of heavy quarkonium production.

Similar to the inclusive production of a light hadron at high p_T, the predictive power of QCD factorization approach to heavy quarkonium production requires our knowledge of the FFs, in addition to the systematically calculated short-distance partonic hard parts. With the perturbatively calculated evolution kernels, we only need the FFs at an input scale $\mu_0 \gtrsim 2m_Q$, while the evolution equations could generate the FFs to any other scales. However, because of the inclusion of NLP contribution to the cross section, it requires many more unknown input FFs. For the LP term, we need a minimum of *two* single parton (light quark + gluon) FFs to each heavy quarkonium state, if we assume that all light quark/antiquark flavors share the same FF, plus one or two more input FFs if we include fragmentation contribution from a heavy quark, whose mass $m_Q \ll p_T$. For the NLP term, we need at least *six* multi-variable heavy quark-pair FFs due to the pair's two color and four spin states (vector, axial vector, and tensor states), if we do not distinguish the two tensor states. Combining the LP and NLP contributions, we need a minimum of *eight* to *ten* unknown multi-variable input FFs to describe the production of each heavy quarkonium state. Although contributions from some fragmentation channels, such as the tensor channels, could be less important, it still requires a lot of information/data to extract these FFs, which makes it difficult to test this factorization formalism precisely.

Like all QCD factorization approaches to high p_T hadron production, it is the FFs at the input scale that are most sensitive to the properties of the heavy quarkonium produced, since the perturbatively calculated partonic hard parts and evolution kernels are insensitive to any long-distance characteristics, such as the spin and polarization, of the produced quarkonium. That is, the knowledge of heavy quarkonium FFs at the input scale is extremely important for understanding the production and formation of different heavy quarkonia at collider energies.

Unlike the light hadron FFs, heavy quarkonium FFs have an intrinsic hard scale - the heavy quark mass m_Q, which could be large enough to be considered as a perturbative scale. With the input scale $\mu_0 \gtrsim 2m_Q \gg \Lambda_{QCD}$, NRQCD could be a good effective theory to be used to factorize these unknown input

FFs into LDMEs and perturbatively calculated coefficient functions, which cover the phase space between NRQCD factorization scale $\mu_\Lambda \sim m_Q$ and μ_0, and do not have large logarithmic terms or the huge power enhancement found in the NLO NRQCD calculation at high p_T. Although there is no formal proof that NRQCD factorization works for evaluating these universal input FFs perturbatively to all orders in α_s and all powers in expansion of heavy quark velocity, v, applying NRQCD factorization to evaluate heavy quarkonium FFs should at least give a reasonable model calculation of these FFs, and provide some ideas on the relative strength and functional form of these FFs to various states of quarkonia. In addition, this approach could reduce the large number of unknown FFs into a few universal NRQCD LDMEs with perturbatively calculated coefficients.

Therefore, it is very important to calculate these FFs with the NRQCD factorization to bridge the gap between the QCD factorization formalism and its phenomenological application. The objective of this dissertation is to derive all these universal FFs in terms of the NRQCD factorization, and demonstrate their importance in phenomenological applications of heavy quarkonium production.

With NRQCD factorization, we have derived the FFs from a perturbatively produced single parton or a heavy quark pair for all unpolarized partonic channels at $\mathcal{O}(\alpha_s^0)$ and $\mathcal{O}(\alpha_s)$ [45, 46]. By generalizing the definitions of NRQCD LDMEs to d dimensions, we have also derived the polarized FFs for all partonic channels to the first non-trivial order. All heavy quarkonium FFs from our calculation have an explicit and definite dependence on momentum fractions z and the input factorization scale μ_0, which should be a parameter to be determined by fitting experimental data, along with a few unknown NRQCD LDMEs for each physical heavy quarkonium state. From the existing phenomenological success of NRQCD factorization approach to inclusive production of heavy quarkonia, and the clear separation of momentum scales, we expect that our results should provide a reasonable description of these non-perturbative FFs at the input scale. With our calculated input FFs, the evolution kernels of FFs in Ref. [40], and the short-distance perturbative hard parts from Ref. [24], QCD factorization approach is now ready to be applied to both the unpolarized and polarized heavy quarkonium production process.

The power of QCD factorization starts to show its strength in our first numerical work on unpolarized J/ψ production [47]. By considering both LP and NLP at leading order in α_s, QCD factorization naturally reproduces all results from the formidable NLO NRQCD factorization calculation at $p_T \gtrsim 10$ GeV. The systematic treatment of NLP contribution is very crucial. Some channels ($^1S_0^{[8]}$ and $^3S_1^{[1]}$) are dominated by NLP contribution at current collider energies.

Moreover, recent studies [11, 18, 48] show the sum of LP contributions from ${}^3S_1^{[8]}$ and ${}^3P_J^{[8]}$ is relatively small. If this is indeed the case, the J/ψ production at current collider energies is dominated by ${}^1S_0^{[8]}$ channel, which answers the long standing question why the produced J/ψ is almost unpolarized.

The rest of the dissertation is organized as follows. In chapter 2, we give a brief review of QCD, including the Lagrangian, renormalization, asymptotic freedom, and factorization theorems. In chapter 3, we review some historical models for heavy quarkonium production. Our focus will be on NRQCD, because of its importance in our calculation of FFs. At the end of this chapter, we also explain the large high-order corrections in CSM and NRQCD. In chapter 4, we will introduce the recently proposed QCD factorization approach: factorization formula, FFs and evolution equations. From chapter 5, we show in detail our calculation of input FFs with NRQCD factorization. In chapter 5, we first discuss the matching of FFs to NRQCD, then introduce the projection method we use in the calculation. By inspection of the symmetries of the FFs, we gain a lot of information about their structure, which is also discussed in chapter 5. Then in chapter 6 and 7, we explain the details of our calculation for unpolarized S-wave and P-wave heavy quarkonium FFs, respectively. In chapter 8, we explain our method of generalizing the polarized NRQCD LDMEs to d dimensions, which is compatible with conventional dimensional regularization. We do not show the details of the calculation but give our results, since the calculation is very similar to the unpolarized case. In chapter 9, we show how the LO results of QCD factorization with both LP and NLP reproduce the formidable NLO NRQCD calculation. Finally the summary and outlook is given in chapter 10.

Chapter 2

Quantum chromodynamics: Overview

This chapter is a brief survey of the QCD theory. In Sec. 2.1 is a short review of history toward QCD. Then in Sec. 2.2 we review the QCD Lagrangian and the running coupling. Finally in Sec. 2.3 we review the perturbative QCD and collinear factorization theorems.

2.1 History toward QCD

In 1911, Ernest Rutherford bombarded gold foil with alpha rays and realized the existence of a small positively-charged nucleus in an atom. Later in 1932, James Chadwick discovered the neutron. At that time, it was generally accepted that all matter in the universe is made of atoms. Each atom has a heavy nucleus surrounded by the electron cloud. The nucleus is further composed of protons and neutrons, collectively called nucleons.

From late 1920s to the year 1964, with the development of accelerators and detectors, many strongly-interacting particles previously observed only in cosmic rays, were confirmed in scattering experiments. Many new particles were also detected and their decay rates and decay products were well measured. Varied by their masses and spins, these new particles fall into two categories. The fermions, all with masses close or above 1 GeV, are called baryons. The bosons, usually with smaller masses, are named mesons. It turned out that protons and neutrons are just the lightest particles in the baryon spectrum.

It is very unlikely that these new particles are independent. In 1961, Murray Gell-mann generalized the $SU(2)$-isospin symmetry to $SU(3)$ symmetry and named it "Eightfold way" [49]. The same theory was independently proposed by Yuval Ne'eman in the same year [50]. In this Eightfold way, mesons

are organized into singlet and octet, while spin-1/2 and spin-3/2 baryons are organized into octet and decuplet, respectively. Back then, one of the particles in the decuplet was not observed. Gell-mann called this particle Ω^- and predicted in 1962 that it would have strangeness -3, electric charge -1 and a mass near 1680 MeV. In 1964, a team led by Nicholas Samios discovered the Ω^- in the Alternating Gradient Synchrotron (AGS) at Brookhaven National Laboratory (BNL).

The "Eightfold way" has many problems. For example, it cannot explain why meson $\phi(1020)$ is much more sTable than $\omega(782)$. In 1964, Gell-mann [51] and George Zweig [52] proposed that the "Eightfold way" can be naturally explained by assuming hadrons are made of three-flavor quarks: up (u), down (d) and strange(s) (Zweig called them aces: A_1, A_2 and A_3) and their antiparticles. This is the first version of the quark model. In this model, baryons are made of three quarks, while mesons are made of a quark-antiquark pair. The "Eightfold way" is a result of the approximate symmetry $SU(3)_{flavor}$. In this quark model, the long life of $\phi(1020)$ can be explained by what is now known as OZI rule [52–54]. In 1969, Gell-mann was awarded the Nobel Prize in physics "for his contributions and discoveries concerning the classification of elementary particles and their interactions"[1].

However, it was soon realized that the quark model explicitly violates the Pauli exclusion principle. To fit the data, the quark model requires that the configuration of quarks in the observed baryons must be symmetric under permutations. A commonly-used example is Δ^{++}, which is made of three spin-up u quarks and has a S-wave orbital wave-function. At the end of year 1964, Han and Numbu [55] proposed that this contradiction could be resolved by introducing a hidden three-value charge, which is now known as color: *red, green* or *blue*. To avoid proliferating the number of states, it is further assumed that all hadron states observed in nature must be "colorless". In other words, all hadrons and mesons are color-singlet.

In brief, the quark model says that all hadrons are made of three-flavor quarks and antiquarks. Each quark takes a hidden color degree of freedom. There is an approximate $SU(3)_{flavor}$ symmetry and an exact $SU(3)_{color}$ symmetry. All hadron states must be color-singlet. The quark model successfully describes most of the basic properties and the qualitative features of the observed low-lying hadronic states. However, it doesn't say anything of the interactions between quarks and the formation of bound states.

It is then natural to try to detect the quarks and explore the dynamics of their interaction experimentally. In late 1967, the first attempt to directly observe the substructure of the proton was carried out at Stanford Linear Ac-

[1]From http://www.nobelprize.org/.

celerator Center (SLAC)[2], in a Rutherford-type experiment with an energetic electron beam scattered off a proton target, known as the inclusive lepton-hadron deep inelastic scattering (DIS). By measuring the momentum and angular distribution of outgoing electrons, information of the proton structure can be extracted. It turned out that the DIS data agreed with predictions based on the conjecture that the proton are made of freely-moving spin-1/2 point-like fermions[3]. Among these predictions, the most important ones are the Callan-Gross relation [56] and Bjorken scaling rule [57].

Inspired by the discovery of DIS experiment, Richard Feynman proposed his parton model [58, 59] in 1969. In the parton model, the hadrons are composed of point-like spin-1/2 partons (similar to quarks in the quark model), interacting weakly at high energy by exchanging spin-1 partons (gluons). The probability of finding a parton with flavor i and longitudinal momentum fraction x in the parent proton is described by a function $f_i(x)$, which is known as the Parton Distribution Function (PDF). Compared to the quark model which treats hadrons as a bag of three quarks or a quark-antiquark pair, Feynman's parton model indicates that more quarks with different flavors can be pair-produced by interaction inside a hadron. For example, there is a nonzero probability to find a s quark in a proton (uud in the quark model) because $s\bar{s}$ can be pair-produced from gluon annihilation. Conventionally, for a specific hadron, the quarks giving flavor quantum number to the hadron are called valence quarks, while other quarks are called sea quarks.

Until 1973, the only quarks had been discovered were u, d and s quarks, collectively called light quarks. In 1974, a new flavor of quark, called charm or c, was discovered independently by two teams at BNL [60] and SLAC [61, 62], which started the well-known "November Revolution"[4]. In 1977, the fifth flavor, bottom or b, was discovered at Fermi National Accelerator Laboratory (Fermilab) [63]. In 1979, three-jets events were observed in the Deutsches Elektronen-Synchrotron (DESY) in e^+e^- annihilation [64], which is considered a direct evidence for the existence of the gluon. Finally in 1995, the top quark, or t, was discovered at Fermilab [65, 66]. The c, b and t quarks, because their heavy masses, are called heavy quarks. The six quarks and the gluon are all the participants of strong interaction we have discovered so far.

At the same time, it was gradually realized that the gluon plays a very important role inside hadrons. As early as the 1970s, by adding up the mo-

[2]The first run starting in 1966 at lower energy didn't see any hard core inside the proton

[3]Because the indispensable contribution of this DIS experiment to our understanding of hadron structure and strong interactions, the leaders of the SLAC experiment Jerome Friedman, Henry Kendall and Richard Taylor were awarded the Nobel Prize in 1990.

[4]In 1976, the leaders of the two teams, Samuel Ting and Burton Richter, respectively, were awarded the Nobel Prize for the discovery of charm quark.

mentum fraction of all quark flavors measured in the SLAC DIS experiment, people found that quarks take only 50% of the momentum of the proton, which implies that gluons must take the remaining 50%. Later in 1988, a measurement by European Muon Collaboration showed that the spins of quarks and antiquarks contribute only a small fraction to the proton spin [67], which is now generally accepted as 30%.

Theoretically, Feynman's parton model has an acute problem: if the partons are shown to be loosely bound in DIS experiments, why has no isolated parton ever been observed experimentally? To answer this question, the parton model needed to be developed into a theory with the dynamics of the strong interaction. Following the pioneering work on non-Abelian gauge theory by Chen Ning Yang and Robert Mills [68], Fritzsch et al. introduced Quantum Chronodynamics (QCD) to describe the strong interaction in 1973 [69]. QCD is a non-Abelian gauge theory of quarks, gluons and their interaction, which preserves local $SU(3)_{\text{color}}$ gauge symmetry. It was soon realized that QCD has a "counter-intuitive" feature that the interaction between partons is very weak at short distance ($\lesssim 1/10$ fm), which is called asymptotic freedom [70, 71][5], and gets stronger when distance increases, until very strong at the size of a typical hadron (~ 1 fm), which implies color confinement. This feature explains why the partons behave like free particles in DIS and other high-energy processes, but no isolated parton has ever been observed.

The feature of asymptotic freedom allows us to apply perturbation method to calculate the physical observables at large energy scale in powers of the small coupling α_s. However, any physical observable involving identified hadrons is sensitive to the binding energies of these hadrons, which are too strong for perturbative QCD. This problem is solved by factorization theorems, which factorized physical observables into convolutions of process-dependent short-distance coefficients, which can be calculated perturbatively, and some non-perturbative but universal distribution functions. With these distribution functions fitted from some experiments (or through a global fitting procedure), and the perturbatively-calculated short-distance coefficients for each process, the factorization theorems can be used to make predictions. Factorization theorems have been very successful and have provided us lots of insight of strong interaction and QCD.

[5]Gross, Wilczek and Politzer (authors of Ref. [70, 71]) shared the Nobel Prize in 2004 for the discovery of the asymptotic freedom.

2.2 QCD Lagrangian, running coupling and factorization

2.2.1 QCD Lagrangian density

QCD is a quantum gauge field theory of six quark flavors and the gluon which take $SU(3)$ color charges. The kinetics of classical quarks and gluon as well as their interaction are described by the classical Yang-Mills Lagrangian:

$$\mathcal{L}_{\text{invariant}} = \sum_f \bar{\psi}_{f,i}(i\gamma^\mu D_{\mu,ij} - m_f\delta_{ij})\psi_{f,j} - \frac{1}{4}(G^a_{\mu\nu})^2, \tag{2.1}$$

where $D_\mu \equiv \partial_\mu + ig_s A^a_\mu t^a$, g_s is the gauge coupling, $\psi_{f,i}$ is the quark field with flavor $f = u, d, c, s, t, b$ and color $i = 1, 2, 3$, A^a_μ is the gluon field with color $a = 1, 2, \ldots, 8$, $G^a_{\mu\nu}$ is the gluon field-strength tensor with color a which is defined as

$$G^a_{\mu\nu} = \partial_\mu A^a_\nu - \partial_\nu A^a_\mu - g_s f^{abc} A^b_\mu A^c_\nu, \tag{2.2}$$

with f^{abc} the structure constant of $SU(3)$ group.

The QCD Lagrangian is manifestly Lorentz invariant, as well as time-reversal, parity and charge-conjugation invariant. Most importantly, it also exhibits $SU(3)$ local gauge symmetry, which distinguishes QCD Lagrangian from other gauge theories. The local $SU(3)_{color}$ gauge symmetry is defined as the invariance of Lagrangian under the following transformation:

$$\psi'_{f,i}(x) = U_{ij}(x)\psi_{f,j}(x), \tag{2.3a}$$

$$A'_\mu(x) = U(x)A_\mu(x)U^{-1}(x) + \frac{i}{g_s}[\partial_\mu U(x)]U^{-1}(x), \tag{2.3b}$$

where $A_\mu(x) = A^a_\mu(x)T^a$ with T^a being the Gell-Mann matrices, $U(x)$ is the gauge transformation matrix defined as

$$U(x) = e^{i\theta^a(x)T^a}, \tag{2.4}$$

with $\theta(x)$ being any analytic function of x.

The gauge invariance of $\mathcal{L}_{\text{invariant}}$ makes it difficult to be quantized. This problem is solved by introducing a gauge-fixing term, given by

$$\mathcal{L}_{\text{gauge}} = -\frac{\lambda}{2}(\eta^\mu A^a_\mu)^2, \tag{2.5}$$

which restricts the gluon field by $\eta \cdot A^a = 0$. Common choices of η include the

gradient ∂ (covariant gauge) or a fixed vector n (axial gauge). The axial gauge with $n^2 = 0$ is also called light-cone gauge. Because of the non-Abelian nature of QCD, the gauge fixing term in Eq. (2.5) cannot remove the unphysical gluon polarization completely in covariant gauge. In this gauge, the Faddeev-Popov gauge field $\mathcal{L}_{\text{ghost}}$ is also needed [72],

$$\mathcal{L}_{\text{ghost}} = \eta^{\mu}\bar{c}^{a}(\partial_{\mu}\delta^{ad} - g_s f^{abd}A^{b}_{\mu})c^{d}, \tag{2.6}$$

where c^a is the ghost field. So the general quantized QCD Lagrangian can be written as

$$\mathcal{L}_{\text{QCD}}(\psi_f, A_\mu, \dots) = \mathcal{L}_{\text{invariant}} + \mathcal{L}_{\text{gauge}} + \mathcal{L}_{\text{ghost}}, \tag{2.7}$$

where $\dots$ represents ghost field c, gauge coupling g_s and possible masses.

2.2.2 Renormalization and running coupling

Given the QCD Lagrangian in Eq. (2.7), it is straightforward to derive the Feynman rules for perturbation theory. However, the application of these Feynman rules in calculating cross sections and other physical observables suffers from UV divergence, which is associated with infinitely large loop momenta. With the idea of renormalization, the perturbative UV divergence can be effectively canceled by redefining the fields and parameters in the Lagrangian. Physical predictions of the theory come only after completion of the renormalization.

Renormalization in QCD can be summarized as follows. Starting with the QCD Lagrangian in Eq. (2.7), we define the renormalized Lagrangian as

$$\begin{aligned}\mathcal{L}_{\text{renormalized}}(\psi_R, A_R, \dots, Z's) \equiv{}& \mathcal{L}_{\text{classical}}(\psi_R, A_R, \dots) \\ &+ \mathcal{L}_{\text{counter-term}}(\psi_R, A_R, \dots, Z's) \\ ={}& \mathcal{L}_{\text{bare}}(\psi_0, A_0, \dots),\end{aligned} \tag{2.8}$$

where $\dots$ represents renormalized or bare ghost field c, gauge coupling g_s and possible masses. $\mathcal{L}_{\text{classical}}(\psi_R, A_R, \dots)$ and $\mathcal{L}_{\text{bare}}(\psi_0, A_0, \dots)$ have the same functional form of their variables as $\mathcal{L}_{\text{QCD}}$ in Eq. (2.7). $Z's$ are renormalization constants, which define the relation between the renormalized and bare variables,

$$\psi_{f,0} = Z_{\psi}^{1/2}(\mu_r)\,\psi_{f,R}(\mu_r), \tag{2.9a}$$

$$A^{a}_{\mu,0} = Z_{A}^{1/2}(\mu_r)\,A^{a}_{\mu,R}(\mu_r), \tag{2.9b}$$

$$c^{a}_{0} = Z_{c}^{1/2}(\mu_r)\,c^{a}_{R}(\mu_r), \tag{2.9c}$$

$$g_{s,0} = Z_g(\mu_r)\,g_{s,R}(\mu_r), \tag{2.9d}$$

$$m_{f,0} = Z_m(\mu_r)\, m_{f,R}(\mu_r), \tag{2.9e}$$

where μ_r is the renormalization scale.

Since μ_r is an arbitrary scale in renormalized QCD, a physical observable (e.g. cross section σ) should not depend on μ_r,

$$\mu_r^2 \frac{\mathrm{d}}{\mathrm{d}\mu_r^2}\, \sigma\left(\frac{Q_{ij}^2}{\mu_r^2}, \alpha_s(\mu_r), \mu_r\right) = 0, \tag{2.10}$$

where Q_{ij}^2 are Lorentz invariants constructed from external Lorentz vectors (i.e. momenta and spins), and $\alpha_s = g_s^2/(4\pi)$. We can then obtain a renormalization group equation as

$$\left(\mu_r^2 \frac{\partial}{\partial \mu_r^2} + \beta(\alpha_s)\frac{\partial}{\partial \alpha_s} + \omega\right) \sigma\left(\frac{Q_{ij}^2}{\mu_r^2}, \alpha_s(\mu_r), \mu_r\right) = 0. \tag{2.11}$$

Here $\beta(\alpha_s)$ is defined as

$$\beta(\alpha_s) = \mu_r^2 \frac{\partial \alpha_s}{\partial \mu_r^2}. \tag{2.12}$$

Consequently, the coupling α_s is not a constant, instead it is a function of μ_r with the dependence as in Eq. (2.12). This is where the name "running coupling" comes from. The β-function can be expanded in powers of α_s as

$$\beta(\alpha_s) = -\frac{\beta_0}{4\pi}\alpha_s^2 - \frac{\beta_1}{8\pi^2}\alpha_s^3 - \frac{\beta_2}{128\pi^3}\alpha_s^4 - \cdots, \tag{2.13}$$

where

$$\beta_0 = 11 - \frac{2}{3}n_f, \tag{2.14a}$$

$$\beta_1 = 51 - \frac{19}{3}n_f, \tag{2.14b}$$

$$\beta_2 = 2857 - \frac{5033}{9}n_f + \frac{325}{27}n_f^2, \tag{2.14c}$$

where n_f is the number of quark flavors with masses smaller than μ_r. From Eqs. (2.12) and (2.13), we can solve α_s approximately

$$\begin{aligned}\frac{\alpha_s(\mu_r)}{\pi} =& \frac{12/(33-2n_f)}{\ln(\mu_r^2/\Lambda_{QCD}^2)} + \frac{72(153-19n_f)}{(33-2n_f)^3}\frac{\ln\ln(\mu_r^2/\Lambda_{QCD}^2)}{\ln^2(\mu_r^2/\Lambda_{QCD}^2)} \\ &+ \mathcal{O}\left(\frac{\ln^2[\ln(\mu_r^2/\Lambda_{QCD}^2)]}{\ln^3(\mu_r^2/\Lambda_{QCD}^2)}\right),\end{aligned} \tag{2.15}$$

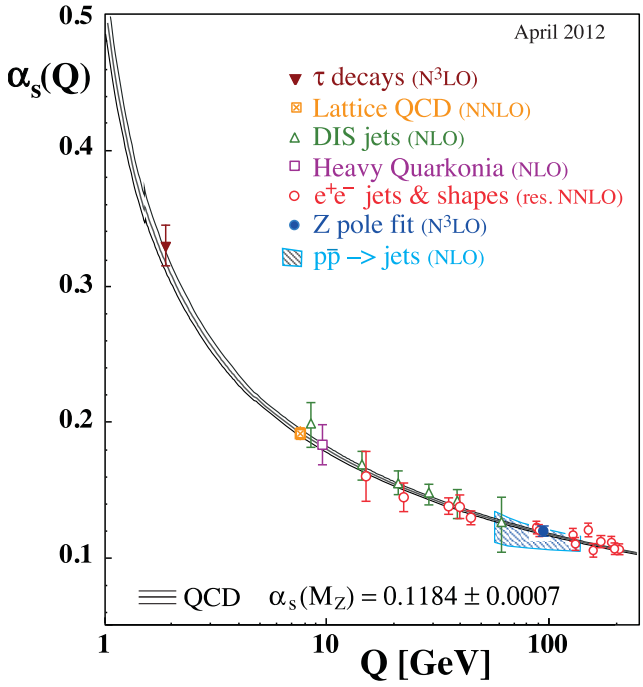

Figure 2.1: The QCD coupling constant as a function of scale. Figure taken from [1].

where $\Lambda_{QCD} \sim 200$ MeV is a scale which needs to be determined from experiments. From Eq. (2.15), with $\mu_r \gg \Lambda_{QCD}$ and increasing, $\alpha_s(\mu_r)$ decreases. In other words, QCD coupling constant is smaller at higher energy. The running of α_s has been verified by many experiments (see Fig. 2.1). This feature of QCD is the asymptotic freedom of the strong interaction. It serves as the basis for applying the perturbative method in high-energy processes.

2.3 Factorization and probability distributions

With renormalization and asymptotic freedom, one could in principle apply QCD perturbation theory to calculate physical observables in high-energy processes, where the gauge coupling α_s is small. However, most of the physical processes involve identified hadrons, and typically, have two or more energy scales:

- the transferred energy Q in the hard scattering, usually larger than a few GeV,

- the scale of hadron binding energies, typically at the order of $\Lambda_{QCD} \sim$ 200 MeV.

Therefore a typical physical observable (e.g. cross section) is also sensitive to the dynamics in soft scales, which disqualify the application of QCD perturbation theory.

A solution is provided by the factorization theorems (refer to Ref. [73] for a good review). According to these theorems, for many processes, physical observables can be factorized into convolutions of short-distance hard parts, which are perturbatively calculable, with non-perturbative but universal long-distance distribution functions (or matrix elements). The interference between the hard part and the soft interaction with scale q_{soft} is suppressed by powers of q_{soft}/Q, typically $q_{\text{soft}} \sim \Lambda_{QCD}$.

A simple application of factorization is in the cross section of inclusive Deep Inelastic Scattering (DIS), where an electron collides and smashes a hadron, usually a proton, as shown in Fig. 2.2(a). By measuring the momentum and the angular distribution of the outgoing electron, the distributions of quarks inside the proton are directly probed. There are two well-separated energy scales in DIS process: the binding energy of proton $\sim \Lambda_{QCD}$ and the transferred energy between the incoming electron and proton $Q^2 = -q^2 \gg \Lambda^2_{QCD}$.

For simplicity, we consider both the incoming electron and proton as unpolarized. With one photon exchange, the inclusive DIS cross section can be written as,

$$E' \frac{\mathrm{d}\sigma}{\mathrm{d}^3 k'} = \frac{1}{2s} \left(\frac{1}{Q^2} \right)^2 L^{\mu\nu}(k, k') W_{\mu\nu}(q, p), \tag{2.16}$$

where $L^{\mu\nu}$ is the QED process of a lepton emitting a hard photon. From known symmetries of strong interaction, the hadronic tensor $W_{\mu\nu}$ can be expressed as

$$\begin{aligned} W_{\mu\nu}(q, P) =& \frac{1}{4\pi} \int \mathrm{d}^4 z \, e^{iq\cdot z} \langle p | J^\dagger_\mu(0) J_\nu(z) | p \rangle \\ =& - \left(g_{\mu\nu} - \frac{q_\mu q_\nu}{q^2} \right) F_1(x_B, Q^2) \\ &+ \frac{1}{p \cdot q} \left(p_\mu - q_\mu \frac{p \cdot q}{q^2} \right) \left(p_\nu - q_\nu \frac{p \cdot q}{q^2} \right) F_2(x_B, Q^2), \end{aligned} \tag{2.17}$$

where F_1 and F_2 are dimensionless structure functions including the information of partons inside the proton, $x_B = Q^2/(2p \cdot q)$ is the Bjorken variable. The dependences of F_1 and F_2 on x_B and Q^2 in Eq. (2.17) can be extracted from experimental data, It is the task of QCD to explain these dependencies.

In the hard collision, the region probed by the virtual photon is of size $1/Q^2$, which is much smaller than the size of the proton ($R \sim 1/\Lambda_{QCD}$). As a result,

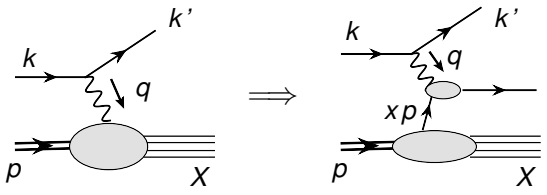

Figure 2.2: Sketch for inclusive DIS process.

the probability of finding two or more physical partons at the probed region is suppressed by powers of $(1/Q)/R$. The interaction between the spectators of incoming hadron and the produced final-state parton is also suppressed after summing over all outgoing hadrons. Moreover, since the virtuality of the scattered parton is of order Λ_{QCD}, at the leading power of $1/Q$, the effect of this non-zero virtuality can be neglected. Therefore, at the leading power of $1/Q$, we have a clean picture of this DIS process as shown in Fig. 2.2(b) and 2.3, where an on-shell parton interacts with a hard virtual photon at energy scale Q. The hadron acts as a "source" of partons with some unknown momentum distributions, which can be fitted from experimental data.

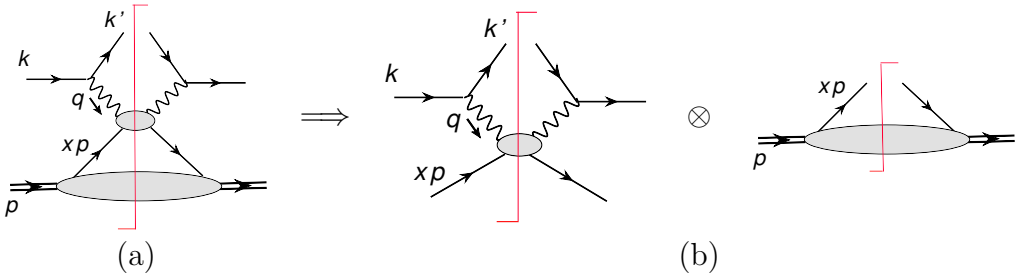

Figure 2.3: Graphical representation of leading power in collinear factorization for inclusive DIS.

If we further assume the transverse components of the scattered parton's momentum are so small compared to the longitudinal component that they can be effectively neglected, we obtain the collinear factorization formalism. As an example, the structure function F_2 in Eq. (2.17) can be factorized in this collinear factorization approach as [74–76],

$$F_2^h(x_B, Q^2) = \sum_f \int_{x_B}^1 \frac{\mathrm{d}y}{y} C_2^f \left(\frac{x_B}{y}, \frac{Q^2}{\mu^2}, \alpha_s \right) \phi_{f/h}(y, \mu^2)$$

$$\equiv \sum_f C_{2f} \otimes \phi_{f/h}, \tag{2.18}$$

where the summation runs over all parton flavors, C_2^f is the short-distance coefficient function which can be calculated perturbatively, μ is the factorization scale, and $\phi_{f/h}(x)$ is the probability of finding parton f with longitudinal momentum fraction x inside hadron h, known as the parton distribution function (PDF).

The PDFs are defined explicitly in collinear factorization formalism. For example, for the unpolarized quark PDF, we have

$$\phi_{q/h}(x,\mu^2) = \int \frac{\mathrm{d}\xi^-}{2\pi} e^{ixp^+\xi^-} \langle h(p)|\bar{\psi}_q(0)\frac{\gamma^+}{2}W(0,\xi^-)\psi_q(\xi^-)|h(p)\rangle, \tag{2.19}$$

where $W(0,\xi^-)$ is the gauge link,

$$W(0,\xi^-) = \mathcal{P}\exp\left[ig\int_0^\infty \mathrm{d}\eta^- A^+(\eta^-)\right]\mathcal{P}\exp\left[ig\int_\infty^{\xi^-} \mathrm{d}\eta^- A^+(\eta^-)\right], \tag{2.20}$$

which sums up the leading power (LP) contribution from the collinear longitudinally polarized gluons to the cross section, and makes the definition gauge invariant. The PDFs include dynamics at energy scale Λ_{QCD}, thus cannot be calculated perturbatively. However, their evolutions with scale μ^2 are determined by DGLAP evolution equations, with perturbatively calculable kernels. Consequently, to apply collinear factorization, a set of PDFs at some input scale μ_0 is required, which can be fitted from a set of experiments or through a global fitting procedure. The predictive power of collinear factorization formalism relies on our ability to calculate the short-distance coefficients and the universality of the long-distance PDFs.

Other important non-perturbative distribution functions include fragmentation functions (FFs), which are interpreted as the probability of finding a specific hadron in the fragments of a energetic parton (or partons). Different from PDFs, which describe strongly-interacting systems in their equilibrium states, FFs provide information about dynamical hadronization processes. The factorization scale dependencies of FFs are also determined by DGLAP evolution equations, thus a set of FFs at an input scale are required to be extracted from experimental data.

Only for a few processes, factorization formalisms are proved to all orders of α_s [74]. In many other processes, factorization is used as an ansatz, based on argument of large space and time separation of different parts in each specific process. One can test this ansatz by calculating the short-distance coefficients

to high orders and check whether all IR divergences are canceled. Another test is the universality of the distribution functions in different processes.

Generally speaking, the LP factorization formalism works very well and serves as a powerful tool for us to understand strong interaction and QCD in both perturbative and non-perturbative aspects, either directly or indirectly. However, for some observables, the LP contribution is found not to be dominant. In some extreme cases, such as single transverse spin asymmetry, LP contribution is zero in collinear factorization formalism. For these observables, considering only the LP is problematic, thus a systematic method to expand the observables to next-to-leading power or even higher powers is necessary [77, 78]. The inclusive heavy quarkonium production, as explained in the rest of this dissertation, is an observable for which the LP contribution is not enough, and power corrections are important.

Chapter 3

Heavy quarkonium and its production

This chapter is organized as follows. In Sec. 3.1, we first review some basic properties of the heavy quarkonium and the measurement of the momentum and polarization in experiments. From Sec. 3.2 to 3.4, we review three historical models: the color singlet model (CSM), the color evaporation model (CEM) and the non-relativistic QCD (NRQCD) factorization approach. Our focus is on the NRQCD factorization since we will use it in our calculation of the fragmentation functions. Finally in Sec. 3.5, we explain the reason for the large high-order correction in the CSM and the NRQCD factorization approach.

3.1 Heavy quarkonium

Heavy quarkonia are mesons made of a valence heavy quark pair $Q\bar{Q}$, where Q is the charm or bottom (the top quark decays before forming bound states). Depending on the flavor of Q, heavy quarkonium are also called charmonium or bottomium. The term *heavy quarkonium* indicates its similarity to positronium in the e^+e^- system, by exhibiting a series of excited states with different principal and angular-momentum quantum numbers, shown for bottomium in Fig. 3.1. In Table 3.1, we list some properties of the most important heavy quarkonia. Notice that S and L are not exact good quantum numbers. Mixings, such as the S-D mixing, are allowed.

In experiments, heavy quarkonia are observed by measuring their decay products. Take charmonia as an example. Table 3.2 lists the important decay channels used to reconstruct each charmonium state in various experiments. By measuring the momenta of the decay products, the momentum of the

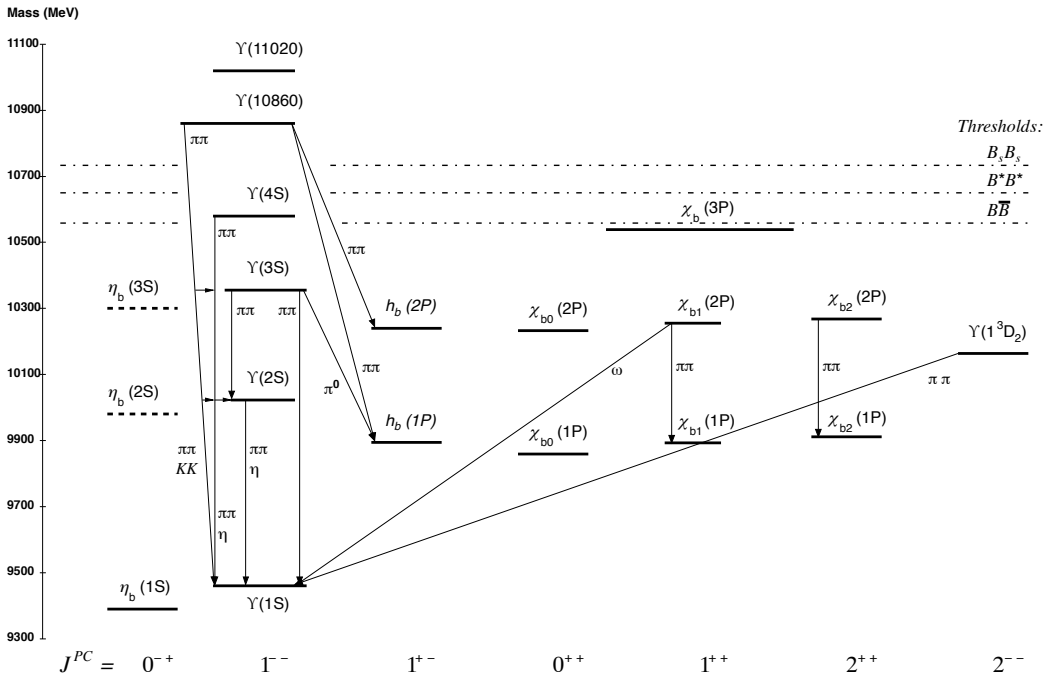

Figure 3.1: The bottomium bound states and their observed transitions. Figure taken from [2].

parent charmonium can be calculated. Information about the polarization of the parent charmonium can be extracted by measuring the angular distribution of the decay products in the parent charmonium rest frame. For example, in the case of J/ψ, the distribution of the di-lepton is parametrized as

$$\frac{\mathrm{d}N}{\mathrm{d}\cos\theta} \propto 1 + \lambda_\theta \cos^2\theta, \tag{3.1}$$

where angle θ is the direction of l^+ relative to a chosen spin-quantization axis. The parameter λ_θ is directly related to the fraction of the cross section that is transverse or longitudinal: $\lambda_\theta = 1$ corresponds to 100% transverse polarization; $\lambda_\theta = -1$ corresponds to 100% longitudinal polarization. The value of λ_θ depends on the choice of the spin-quantization axis. A review of the most commonly-used choices and their relations can be found in Ref. [2].

In general, not all charmonium are produced directly in the hard scattering. Other main contributions are the feeddown of the charmonium at higher energy levels, and the B meson decay. The addition of the direct production and the

Table 3.1: Properties of the most important heavy quarkonia. $m(\eta_b)$ is estimated from Ref. [19–21]. $m(h_b)$ is estimated from Ref. [22]. Other masses are from Particle Data Group [1], with error in the least significant digit. The three masses following $m(\chi_{cJ})$ are for $J = 0, 1, 2$ respectively, similarly for $m(\chi_{bJ})$. For comparison, $m_c(\mu = m_c) = 1.27$ GeV and $m_b(\mu = m_b) = 4.19$ GeV, in $\overline{\text{MS}}$ scheme.

Quarkonium	J^{PC}	$n\ ^{2S+1}L_J$	Mass(MeV)
η_c, η_b	0^{-+}	$1\ ^1S_0$	$m(\eta_c) = 2980$ $m(\eta_b) \approx 9390$
J/ψ, Υ	1^{--}	$1\ ^3S_1$	$m(J/\psi) = 3096.92$ $m(\Upsilon) = 9460.3$
h_c, h_b	1^{+-}	$1\ ^1P_1$	$m(h_c) = 3525.4$ $m(h_b) \approx 9900$
χ_{cJ}, χ_{bJ}	J^{++}	$1\ ^3P_J$	$m(\chi_{cJ}) = 3414.8, 3510.66, 3556.20$ $m(\chi_{bJ}) = 9859.4, 9892.8, 9912.2$
ψ', $\Upsilon(2S)$	1^{--}	$2\ ^3S_1$	$m(\psi') = 3686.09$ $m(\Upsilon(2S)) = 10023.3$

Table 3.2: Important decay channels used to reconstruct the charmonium in experiments. Decay width are estimated from Particle Data Group [1].

Charmonium	Decay channels	Decay width
η_c	$\eta_c \to \gamma\gamma$	1.68 keV
J/ψ	$J/\psi \to l^+l^-$	5.46 keV
h_c	$h_c \to \eta_c\gamma$	357 keV
χ_{cJ}	$\chi_{cJ} \to J/\psi\gamma$	χ_{c0} : 40, χ_{c1} : 1207, χ_{c2} : 693 MeV
ψ'	$\psi' \to J/\psi\pi^+\pi^-$ $\psi' \to l^+l^-$	102 keV 2.34 keV

feeddown contribution is usually referred to as "prompt production", while the production of the charmonium from the B meson decay is called "non-prompt production". In modern high-energy experiments, "prompt production" can be separated from "non-prompt production".

Because the heavy quark's mass is much larger than the binding energy, the motion of the heavy quark pair inside the heavy quarkonium H is effectively non-relativistic in the rest frame of H (e.g. $v^2 \approx 0.3$ for the J/ψ and $v^2 \approx 0.1$ for the Υ). Consequently, there are at least three separated momentum scales in a heavy quarkonium: the heavy-quark mass m_Q; the momentum of the heavy quark or antiquark in heavy quarkonium rest frame mv, and the binding energy mv^2. If a heavy quarkonium is produced in a hard-scattering process, an additional scale p is involved. p is usually set by the typical large momentum scale in the hard scattering, such as p_T in hadron-hadron collision.

Among these scales, the scales p and m_Q are much larger than Λ_{QCD}, thus are perturbative, while other scales are non-perturbative. As a result, the heavy quark pair is produced perturbatively in the hard-scattering process. Its later evolution into a heavy quarkonium is non-perturbative. Different factorization approaches have different treatments of the non-perturbative interactions. In the rest of this section, we review the most important historical models for heavy quarkonium production.

3.2 The color-singlet model

The color-singlet model (CSM) was first proposed shortly after the discovery of J/ψ in 1974, and was developed in subsequent years [28–35]. It has the following assumptions:

1. The heavy quarkonium production process can be factorized into two stages. In the first stage, an on-shell heavy quark pair is produced with relative 3-momentum $\mathbf{q}$. In the second stage, the heavy quark pair evolves into the observed heavy quarkonium H.

2. Because the energy scales p and m_Q in the first stage are much larger than Λ_{QCD}, the expansion in powers of α_s for the production of the heavy quark pair converges quickly.

3. The probability for the heavy quark pair with relative momentum $\mathbf{q}$ to form a heavy quarkonium decreases rapidly when $\mathbf{q}$ increases. Therefore the production of the pair in the first stage can be expanded at $\mathbf{q} = \mathbf{0}$.

4 During the second stage, the heavy quark pair hadronizes into a heavy quarkonium without emitting gluons.

Because of the fourth assumption, the heavy quark pair produced in the first stage must have the same quantum numbers with the observed heavy quarkonium H. Particularly, it must be in a color singlet. This is why the model is called the color-singlet model.

Under these assumptions, the amplitude to produce a S-wave heavy quarkonium is

$$\begin{aligned}\mathcal{A}_H &= \int \mathrm{d}^3\mathbf{q}\mathcal{A}_{[\mathcal{Q}\bar{\mathcal{Q}}]}(\mathbf{q})\widetilde{\Phi}_H(\mathbf{q}) \\ &\approx \mathcal{A}_{[\mathcal{Q}\bar{\mathcal{Q}}]}(\mathbf{0}) \times \int \mathrm{d}^3\mathbf{q}\widetilde{\Phi}_H(\mathbf{q}) \\ &= \mathcal{A}_{[\mathcal{Q}\bar{\mathcal{Q}}]}(\mathbf{0}) \times \Phi_H(\mathbf{0}),\end{aligned} \tag{3.2}$$

where $\mathcal{A}_{[Q\bar{Q}]}$ is the amplitude of producing a $Q\bar{Q}$ pair with the same quantum numbers as H in the hard scattering, $\widetilde{\Phi}_H(\mathbf{q})$ is the wave-function of H in its rest frame. In the second step we have used assumption #3. For P-wave heavy quarkonium, $\Phi_H(\mathbf{0})$ is zero. Then we need to keep the second term when expanding $\mathcal{A}_{[Q\bar{Q}]}$, which results in the derivative of wave-function at the origin.

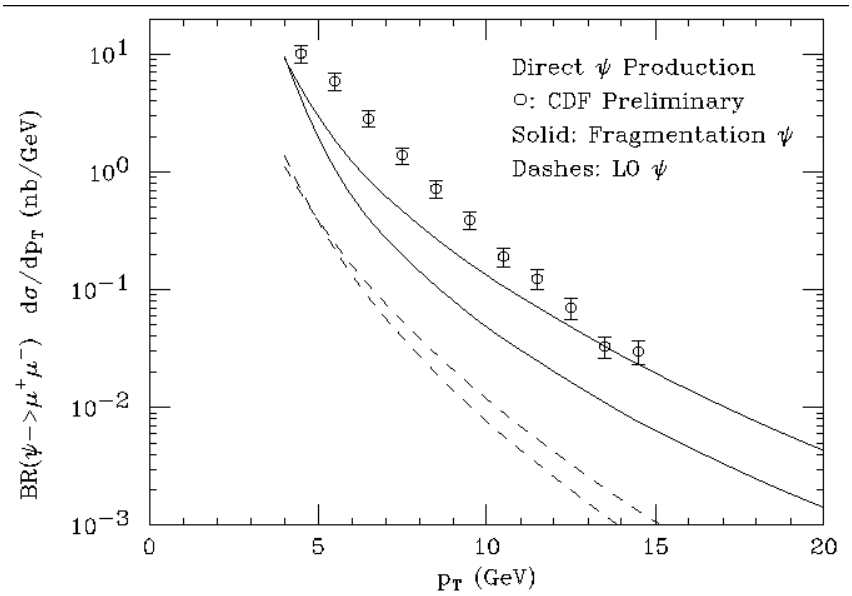

Figure 3.2: Comparison of the CSM prediction on the prompt J/ψ production with the prompt production data measured by the CDF collaboration. The errors of the two bands are from the uncertainties of m_c, as well as various scales (μ_r, μ_f and μ_{frag}). Figure taken from Ref. [3].

The predictive power of the CSM for inclusive production of heavy quarkonium H relies on our ability to calculate $\mathcal{A}_{[Q\bar{Q}]}$ perturbatively, and our knowl-

edge of the wave-function (or its derivative) of H at the origin. The latter can be extracted from the decay process of H, or be calculated from the potential model or lattice QCD. Therefore, the CSM has no free parameter for heavy quarkonium production.

The experiments before 1993 were operated at low energies and were not able to separate the prompt and non-prompt production of J/ψ. At that time, the LO CSM prediction generally agreed with the data. Since 1993, the CDF collaboration managed to separate J/ψ and ψ' prompt production with the silicon vertex detector. It turned out (Fig. 3.2) that the LO CSM prediction underestimates the data by more than an order of magnitude. The difference was once interpreted as the large feeddown contribution from χ_{cJ}. At the same time, the LO CSM prediction for ψ' is smaller than the data by two orders of magnitude (Fig. 3.3). Since there is no known charmonium state which decays to ψ', the large deficiency cannot be explained by the feeddown contribution.

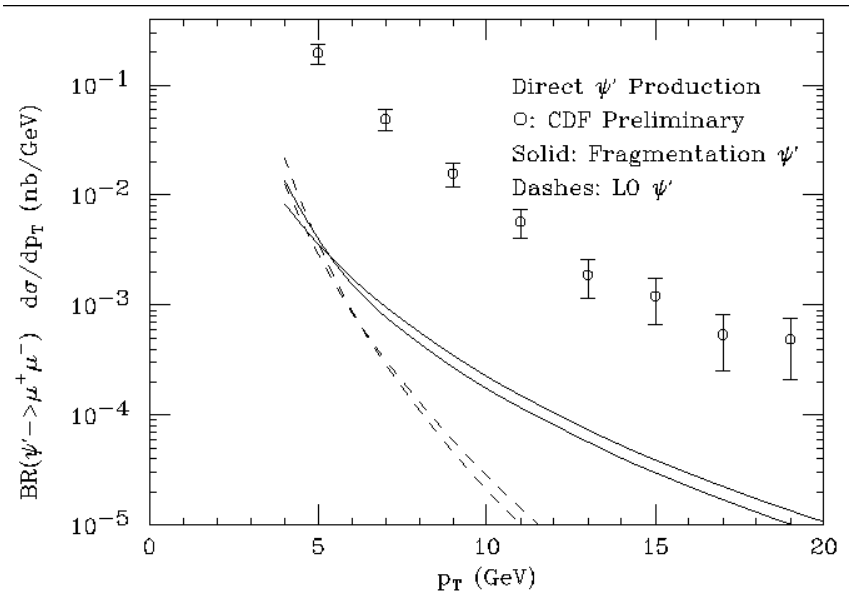

Figure 3.3: Same as Fig. 3.2, but for ψ'. Figure taken from Ref. [3].

To narrow the large gap between the LO CSM prediction and the data, and to correct the wrong p_T-behavior of the LO CSM prediction at large p_T, Eric Braaten and Tzu Chiang Yuan [79] proposed that the single parton fragmentation contribution should be dominant when p_T is large. After a series of work fitting the single parton fragmentation functions [80, 81], it was found that χ_{cJ} production are greatly enhanced by the single parton fragmenting

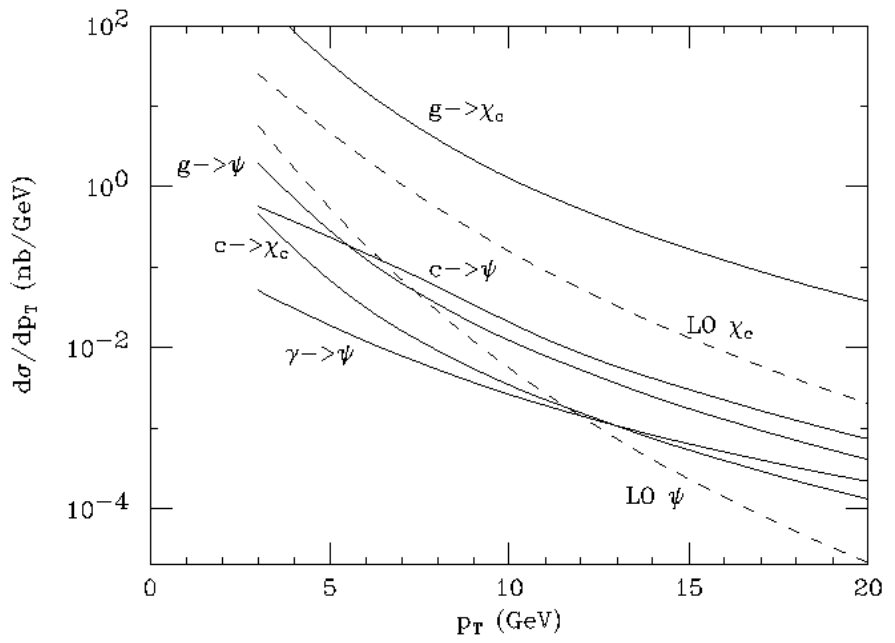

Figure 3.4: Contributions from different channels to the cross section of inclusive prompt J/ψ production at the Tevatron: the fragmentation contribution (solid curves) and the LO CSM contribution (dashed curves). Figure taken from Ref. [3].

(Fig. 3.4). Addition of the corrected feedown contribution from χ_{cJ}, the single parton fragmentation to J/ψ and the LO CSM prediction of J/ψ production is in agreement with the CDF prompt J/ψ production data (see Fig. 3.2). However, even with the single parton fragmentation contribution added, the prediction for prompt ψ' production is still one or two orders of magnitude smaller than the data (see Fig. 3.3), so called "ψ' anomaly".

In 1997, the CDF collaboration updated their measurement of J/ψ production by removing the feeddown contribution from χ_c [82]. The new data were compared with the LO CSM prediction of direct J/ψ production and were found to be larger than the addition of the fragmentation contribution and the LO CSM prediction by a factor of 30 (see Fig. 3.5). Therefore the LO CSM cannot explain the data for both J/ψ and ψ' production.

Recently, NLO correction for J/ψ and Υ direct production in the CSM were accomplished. Surprisingly, it increases the LO prediction by a factor of 100 for J/ψ and a factor of 10 for Υ at $p_T \sim 25$ GeV (see Fig. 3.6). Inclusion

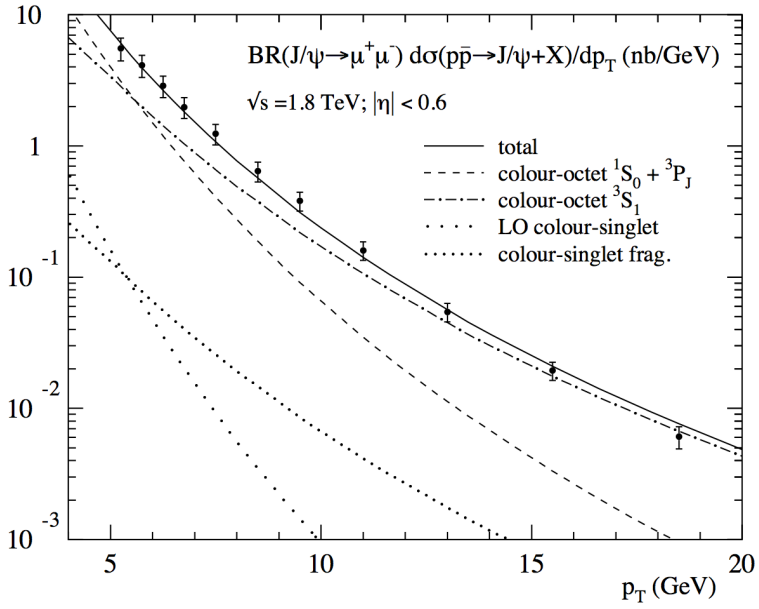

Figure 3.5: Direct J/ψ production with predictions of the LO CSM and the LO NRQCD factorization. Figure taken from Ref. [4].

of the NLO correction also flips the polarization of J/ψ and Υ from almost all transverse to mainly longitudinal (see Fig. 3.7). However, the NLO CSM prediction is still an order of magnitude smaller than the CDF data. Later, the authors of Ref. [83, 84] proposed the NNLO* method. In this method, only tree diagrams of the NNLO CSM correction are considered, and an infrared cutoff (s_{ij}^{min}) is introduced to control the IR divergence. The NNLO* estimate narrows the big gap between the NLO CSM prediction and the CDF data (see Fig. 3.6). However it is still much less than the CDF data for J/ψ. Moreover, the authors of Ref. [48] pointed out that the NNLO* method overestimates the contribution of the NNLO CSM.

It is clear now that the CSM mechanism is not enough to explain the production of S-wave heavy quarkonium, such as J/ψ, ψ' and Υ. For P-wave heavy quarkonium production, the CSM is deficient theoretically by exhibiting uncanceled IR divergence. Therefore, the CSM cannot be the full story of heavy quarkonium production.

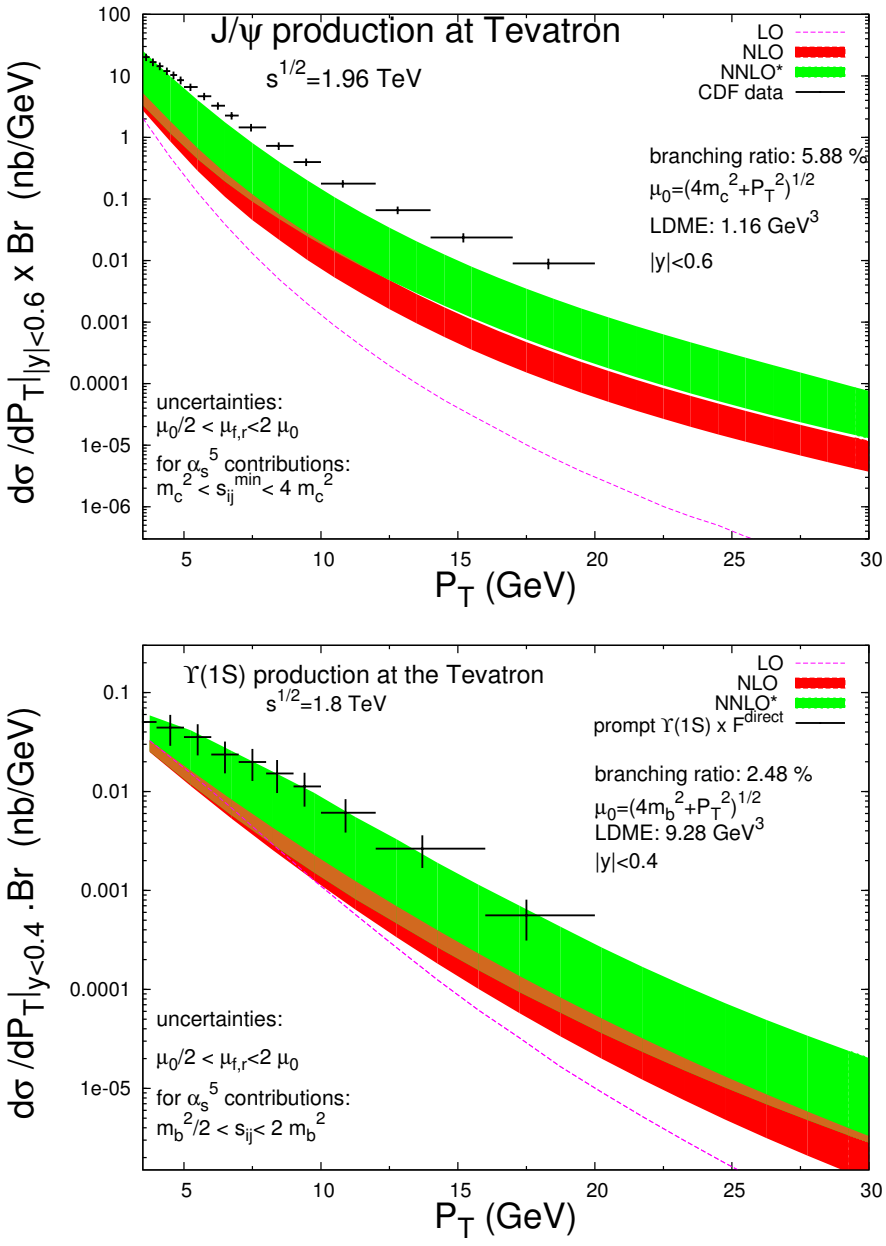

Figure 3.6: Calculations of the J/ψ (Υ) production cross sections in the CSM compared with the CDF Run II data [5] ([6]). Figures taken from [7], based on the calculation in [8].

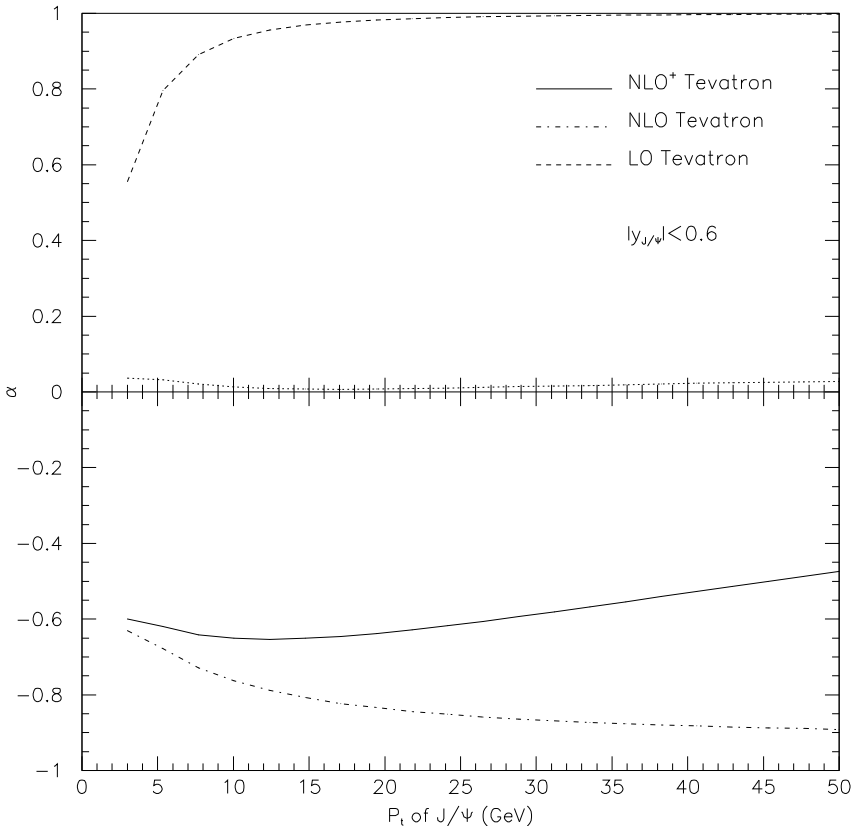

Figure 3.7: Direct J/ψ polarization prediction with the LO and the NLO CSM. The NLO$^+$ denotes NLO CSM prediction including the contribution from $gg \to J/\psi\, c\,\bar{c}$. Figure taken from Ref. [9].

3.3 The color-evaporation model

The color-evaporation model (CEM) was first proposed in 1977 [85–88]. Compared to the CSM, it has the same assumptions #1 and #2, but different assumptions on the non-perturbative interaction in heavy quarkonium production. Specifically, it assumes

3 The heavy quark pairs with different invariant masses have the same probability to evolve into a specific heavy quarkonium, as long as its invariant masses are below the open-charm/bottom threshold. The heavy quark pair with the invariant mass above the open-charm/bottom threshold do not form heavy quarkonium.

4 The gluon emission in the hadronization process completely randomizes

all the quantum numbers, S, L, J and color.

In the CEM, the production of a heavy quarkonium (take J/ψ as an example) can be expressed as

$$\sigma_{J/\psi} = \frac{1}{9}\rho_{J/\psi}\int_{2m_c}^{2m_D} \mathrm{d}m_{c\bar{c}}\frac{\mathrm{d}\sigma_{c\bar{c}}}{\mathrm{d}m_{c\bar{c}}}, \tag{3.3}$$

where $2m_D$ is the open charm threshold, the number $\rho_{J/\psi}$ represents the probability of the heavy quark pair to form J/ψ, 1/9 is the probability of the heavy quark pair to be in color singlet. Notice the CEM has one free parameter ρ in Eq. (3.3) for each heavy quarkonium state.

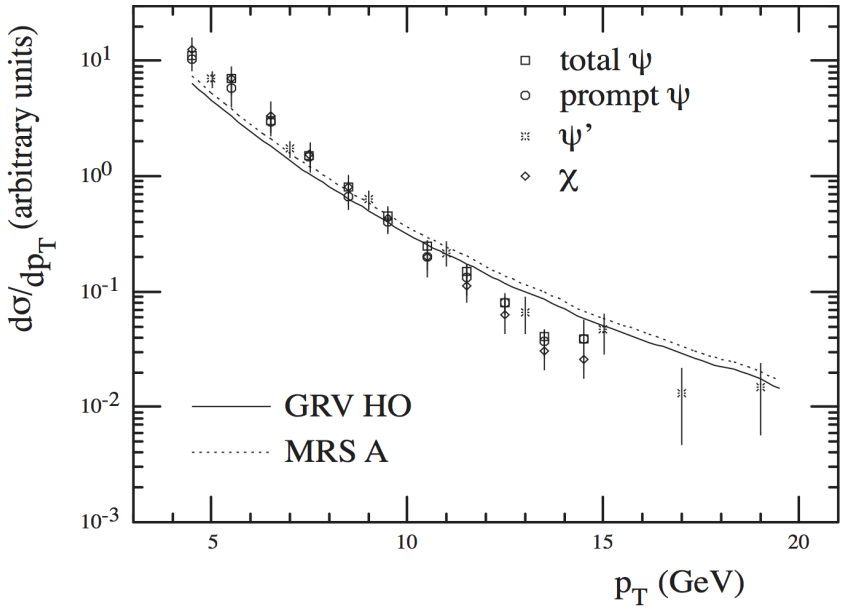

Figure 3.8: The comparison of the LO CEM calculation with the CDF data. Figure taken from Ref. [10].

The CEM is successful in explaining why the energy dependence of the open charm and charmonium production cross section was essentially the same, for both photoproduction and hadroproduction [10]. It also successfully describes the general features of the p_T behaviors for different charmonium states (see Fig. 3.8).

The CEM predicts that the ratio of production rate of any two different heavy quarkonium states is a process-independent constant. However, this prediction contradicts the data from many experiments, for example, the ratio

of the p_T-distribution of J/ψ and χ_{cJ} is very different in the photo-production and in the hadron-production.

3.4 The non-relativistic QCD factorization

In this section, we briefly review the non-relativistic QCD (NRQCD) factorization model. Our focus is on heavy quarkonium production processes. For application of the NRQCD factorization to heavy quarkonium decay processes, either hadronic or electromagnetic, one can refer to Ref. [36]. In Sec. 3.4.1, we first introduce NRQCD effective theory, with the power-counting rule and a brief discussion of symmetries. In section 3.4.2, the NRQCD factorization approach for heavy quarkonium production is reviewed. Some useful relations of NRQCD long-distance matrix elements (LDMEs) are discussed in Sec. 3.4.3. Finally we review the phenomenological application and the unsolved problems of the NRQCD factorization approach in Sec. 3.4.4.

3.4.1 NRQCD effective theory

In the rest frame of the heavy quarkonium, the relative velocity v of the heavy quark pair is much less than one. Consequently, the heavy quark pair production and annihilation scale m_Q, the relative momentum of the heavy quark pair in the heavy quarkonium rest frame $m_Q v$, the binding energy $m_Q v^2$ are well separated. This separation enables us to integrate over the high energy scales and write down an effective field theory, focusing on the low energy interaction.

NRQCD effective theory is such a theory which integrates over the energy scales of m_Q or higher. Its effective Lagrangian has the form

$$\mathcal{L}_{\text{NRQCD}} = \mathcal{L}_{\text{light}} + \mathcal{L}_{\text{heavy}} + \delta\mathcal{L}. \tag{3.4}$$

The motion of the gluon and the light quarks, and their interaction is described by relativistic Lagrangian, which is the same as full QCD in Eq. (2.1)

$$\mathcal{L}_{\text{light}} = -\frac{1}{4} G^a_{\mu\nu} G^{\mu\nu,a} + \sum_{\text{light flavor}} \bar{q}\, i\not{D}\, q. \tag{3.5}$$

The motion of the heavy quark and heavy antiquark with mass m_Q is described by the Schrödinger Lagrangian

$$\mathcal{L}_{\text{heavy}} = \psi^\dagger (iD_t + \frac{\mathbf{D}^2}{2m_Q})\psi + \chi^\dagger (iD_t - \frac{\mathbf{D}^2}{2m_Q})\chi, \tag{3.6}$$

where ψ (χ) is the Pauli spinor which annihilates a heavy quark (creates a heavy antiquark), D_t and $\mathbf{D}$ are the time and space components of the covariant derivative D^μ, respectively. The relativistic correction of heavy quark motion is included in $\delta\mathcal{L}$. In principle, to recover full QCD, $\delta\mathcal{L}$ should include an infinite number of terms. These terms, however, are not equally weighted and can be ordered by powers of v. The power-counting of different fields and coupling was worked out in Ref. [89] and is repeated in Table 3.3. According to the power-counting rule, the most important relativistic corrections are added by the bilinear terms

$$\begin{aligned}
&\delta\mathcal{L}_{\text{bilinear}} \\
=&\frac{c_1}{8m_Q^3}[\psi^\dagger(\mathbf{D}^2)^2\psi - \chi^\dagger(\mathbf{D}^2)^2\chi] \\
+&\frac{c_2}{8m_Q^2}[\psi^\dagger(\mathbf{D}\cdot g\mathbf{E} - \mathbf{E}\cdot g\mathbf{D})\psi + \chi^\dagger(\mathbf{D}\cdot g\mathbf{E} - \mathbf{E}\cdot g\mathbf{D})\chi] \\
+&\frac{c_3}{8m_Q^2}[\psi^\dagger(i\mathbf{D}\times g\mathbf{E} - g\mathbf{E}\times i\mathbf{D})\cdot\boldsymbol{\sigma}\psi + \chi^\dagger(i\mathbf{D}\times g\mathbf{E} - g\mathbf{E}\times i\mathbf{D})\cdot\boldsymbol{\sigma}\chi] \\
+&\frac{c_4}{2m_Q}[\psi^\dagger(g\mathbf{B}\cdot\boldsymbol{\sigma})\psi - \chi^\dagger(g\mathbf{B}\cdot\boldsymbol{\sigma})\chi],
\end{aligned} \tag{3.7}$$

where $E^i = G^{0i}$ and $B^i = \frac{1}{2}\epsilon^{ijk}G^{jk}$ are the electric and magnetic components of the gluon field-strength tensor $G^{\mu\nu}$. Notice that NRQCD effective theory respects the heavy quark spin symmetry approximately, since the first terms violating this symmetry appear in the last row of Eq. (3.7) and are suppressed by v^2.

The production of a heavy quark pair involves interactions with energy of order or larger than m_Q, thus cannot be fully described by NRQCD. However, the production rate, which is the square of the amplitude summed over final states except the heavy quarkonium, can be mimicked in NRQCD by adding four-fermion operators,

$$\delta\mathcal{L}_{\text{4-fermion}} = \sum_n \frac{f_n(\mu_\Lambda)}{m_Q^{d_n-4}}\mathcal{O}_n^H(\mu_\Lambda), \tag{3.8}$$

where n is the state of the heavy quark pair, which will be clear shortly; $\mu_\Lambda \sim m_Q$ is the factorization scale, $\mathcal{O}_n^H(\mu_\Lambda)$ are four-fermion operators with dimension d_n, $f_n(\mu_\Lambda)$ are short-distance coefficients (SDCs). Both $\mathcal{O}_n^H(\mu_\Lambda)$ and $f_n(\mu_\Lambda)$ depend on μ_Λ in a way that their dependencies cancel. The power of m_Q in the denominator ensures that $f_n(\mu_\Lambda)$ is dimensionless. The summation over n has infinite terms, but for a specific heavy quarkonium state H, they can be ordered in powers of v. The most important terms are dimension-6 and

dimension-8 four-fermion terms. Notice that in NRQCD effective theory, the dimension of an operator does not indicate the relative importance because of the mismatching between the dimension and the power-counting of v (see Table. 3.3). The power-counting of each operator also depends on the heavy quarkonium state H, which is explained in Sec. 3.4.2.

There are 4 four-fermion operators with dimension six,

$$\begin{aligned}(\delta\mathcal{L}_{\text{4-fermion}})_{d=6} = &\frac{f(^1S_0^{[1]})}{m_Q^2}\mathcal{O}^H(^1S_0^{[1]}) + \frac{f(^1S_0^{[8]})}{m_Q^2}\mathcal{O}^H(^1S_0^{[8]}) + \frac{f(^3S_1^{[1]})}{m_Q^2}\mathcal{O}^H(^3S_1^{[1]}) \\ &+ \frac{f(^3S_1^{[8]})}{m_Q^2}\mathcal{O}^H(^3S_1^{[8]}),\end{aligned} \tag{3.9}$$

where these operators are defined as

$$\mathcal{O}^H(^1S_0^{[1]}) = \frac{1}{2N_c}\chi^\dagger\psi(a_H^\dagger a_H)\psi^\dagger\chi, \tag{3.10a}$$

$$\mathcal{O}^H(^1S_0^{[8]}) = \chi^\dagger T^a\psi(a_H^\dagger a_H)\psi^\dagger T^a\chi, \tag{3.10b}$$

$$\mathcal{O}^H(^3S_1^{[1]}) = \frac{1}{2N_c}\chi^\dagger\sigma^i\psi(a_H^\dagger a_H)\psi^\dagger\sigma^i\chi, \tag{3.10c}$$

$$\mathcal{O}^H(^3S_1^{[8]}) = \chi^\dagger\sigma^i T^a\psi(a_H^\dagger a_H)\psi^\dagger\sigma^i T^a\chi. \tag{3.10d}$$

Here we use the spectroscopic notation $^{2S+1}L_J$ to label the heavy quarkonium

Table 3.3: The power counting of field and coupling constant

Operator	Estimate	Description
α_s	v	effective quark-gluon coupling constant
ψ	$(m_Q v)^{3/2}$	heavy-quark (annihilation) field
χ	$(m_Q v)^{3/2}$	heavy-antiquark (creation) field
D_t	$m_Q v^2$	gauge-covariant time derivative
$\mathbf{D}$	$m_Q v$	gauge-covariant spatial derivative
$g\mathbf{E}$	$m_Q^2 v^3$	chromoelectric field
$g\mathbf{B}$	$m_Q^2 v^4$	chromomagnetic field
$g\phi$ (in Coulomb gauge)	$m_Q v^2$	scalar potential
$g\mathbf{A}$ (in Coulomb gauge)	$m_Q v^3$	vector potential

state. The subscript 1 or 8 indicates the color state of the heavy quarkonium, singlet or octet respectively. Repeated indices, i.e. $i = 1, 2, 3$ and $a = 1 \dots 8$, are summed.

Some of the dimension-8 four-fermion operators are

$$\begin{aligned}(\delta\mathcal{L}_{4-\text{fermion}})_{d=8} =& \frac{f(^1P_1^{[1]})}{m_Q^4}\mathcal{O}^H(^1P_1^{[1]}) + \frac{f(^1P_1^{[8]})}{m_Q^4}\mathcal{O}^H(^1P_1^{[8]}) \\ &+ \sum_{J=0,1,2}\frac{f(^3P_J^{[1]})}{m_Q^4}\mathcal{O}^H(^3P_J^{[1]}) + \sum_{J=0,1,2}\frac{f(^3P_J^{[8]})}{m_Q^4}\mathcal{O}^H(^3P_J^{[8]}) + \cdots,\end{aligned} \tag{3.11}$$

where the color octet operators are defined as

$$\mathcal{O}^H(^1P_1^{[8]}) = \chi^\dagger T^a(-\frac{i}{2}\overleftrightarrow{\boldsymbol{D}})^j\psi(a_H^\dagger a_H)\psi^\dagger T^a(-\frac{i}{2}\overleftrightarrow{\boldsymbol{D}})^j\chi, \tag{3.12a}$$

$$\mathcal{O}^H(^3P_0^{[8]}) = \frac{1}{3}\chi^\dagger T^a(\frac{-i}{2}\overleftrightarrow{\boldsymbol{D}}\cdot\boldsymbol{\sigma})\psi(a_H^\dagger a_H)\psi^\dagger T^a(\frac{-i}{2}\overleftrightarrow{\boldsymbol{D}}\cdot\boldsymbol{\sigma})\chi, \tag{3.12b}$$

$$\mathcal{O}^H(^3P_1^{[8]}) = \frac{1}{2}\chi^\dagger T^a(\frac{-i}{2}\overleftrightarrow{\boldsymbol{D}}\times\boldsymbol{\sigma})^j\psi(a_H^\dagger a_H)\psi^\dagger T^a(\frac{-i}{2}\overleftrightarrow{\boldsymbol{D}}\times\boldsymbol{\sigma})^j\chi, \tag{3.12c}$$

$$\mathcal{O}^H(^3P_2^{[8]}) = \frac{1}{2}\chi^\dagger T^a(\frac{-i}{2}\overleftrightarrow{\boldsymbol{D}}^{(i}\boldsymbol{\sigma}^{j)})\psi(a_H^\dagger a_H)\psi^\dagger T^a(\frac{-i}{2}\overleftrightarrow{\boldsymbol{D}}^{(i}\boldsymbol{\sigma}^{j)})\chi. \tag{3.12d}$$

Here $\overleftrightarrow{\boldsymbol{D}}$ is the difference of the covariant derivative acting on the spinor to its right and on the spinor to its left, i.e. $\chi^\dagger\overleftrightarrow{\boldsymbol{D}}\psi = \chi^\dagger(\boldsymbol{D}\psi) - (\boldsymbol{D}\chi)^\dagger\psi$. The bracket in the superscript defines a symmetric traceless component of a tensor, $T^{(ij)} = (T^{ij} + T^{ji})/2 - T^{kk}\delta^{ij}/3$. By removing T^a's and multiplying $1/(2N_c)$ to Eq. (3.12), we obtain the definitions of the corresponding color singlet dimension-8 four-fermion operators.

Eq. (3.12) are not all dimension-8 four-fermion operators we can write down. Operators like

$$\mathcal{P}^H(^1S_0^{[8]}) = \frac{1}{2}\left[\chi^\dagger T^a\psi(a_H^\dagger a_H)\psi^\dagger(-\frac{i}{2}\overleftrightarrow{\boldsymbol{D}})^2T^a\chi + \text{H.c}\right], \tag{3.13a}$$

$$\mathcal{P}^H(^3S_1^{[8]}) = \frac{1}{2}\left[\chi^\dagger\sigma^i T^a\psi(a_H^\dagger a_H)\psi^\dagger\sigma^i(-\frac{i}{2}\overleftrightarrow{\boldsymbol{D}})^2T^a\chi + \text{H.c}\right], \tag{3.13b}$$

are also allowed. These operators contribute to the relativistic correction of operators $\mathcal{O}^H(^1S_0^{[8]})$ and $\mathcal{O}^H(^3S_1^{[8]})$ defined in Eq. (3.10).

3.4.2 NRQCD factorization formula for heavy quarkonium production

In 1994, Bodwin, Braaten and Lepage [36] proposed the NRQCD factorization approach for heavy quarkonium production. Compared with the four assumptions of the CSM in Sec. 3.2, the NRQCD factorization approach agrees with the first three, but has a different assumption of the soft interaction:

4 The gluon emission in the hadronization process are described by NRQCD effective theory.

In the NRQCD factorization approach, the cross section of heavy quarkonium production is conjectured to be factorized as

$$\sigma(H) = \sum_n \frac{F_n(\mu_\Lambda)}{m_Q^{d_n-4}} \langle 0|\mathcal{O}_n^H(\mu_\Lambda)|0\rangle, \tag{3.14}$$

where $F_n(\mu_\Lambda)$ is the short-distance coefficient which describes the production of a heavy quark-antiquark pair in the state n in the hard scattering, other notations are the same as in Eq. (3.8). Since $\mu_\Lambda \sim m_Q \gg \Lambda_{QCD}$, $F_n(\mu_\Lambda)$ can be calculated perturbatively. The non-perturbative interaction which evolves the heavy quark pair from state n to heavy quarkonium H is encoded in the NRQCD LDMEs $\langle 0|\mathcal{O}_n^H(\mu_\Lambda)|0\rangle$, some of which are defined in Eqs. (3.10) and (3.12). The summation includes an infinite number of terms, nevertheless, they can be ordered in powers of v. Therefore Eq. (3.14) is a double expansion of α_s and v. For practical use, we can truncate the summation and keep only a finite number of terms.

We can estimate the relative size of α_s and v by employing the Virial theorem. At the limit $m_Q \to \infty$, the potential of the heavy quark pair is effectively $\alpha_s(1/r)/r$, with $r \sim (m_Q v)^{-1}$. From the Virial theorem, we have $m_Q v^2 \sim \alpha_s(m_Q v) \times m_Q v$, or

$$\alpha_s(m_Q v) \sim v. \tag{3.15}$$

This estimate has a very important implication. Since $\alpha_s(\mu)$ decreases with increasing energy, v is larger than $\alpha_s(m_Q)$ with m_Q sufficiently large. Therefore the relativistic corrections are expected to be more important than the corrections from high orders of α_s expansion.

The power counting of the NRQCD LDME $\langle 0|\mathcal{O}_n^H(\mu_\Lambda)|0\rangle$ depends on both n and H. To obtain the power counting of these LDMEs, we need to expand

the meson state $H = {}^{2S+1}L_J$ by NRQCD Fock states

$$|H({}^{2S+1}L_J)\rangle = \mathcal{O}(1)|Q\bar{Q}({}^{2S+1}L_J^{[1]})\rangle + \mathcal{O}(v)|Q\bar{Q}({}^{2S+1}(L\pm 1)_{J'}^{[8]})g\rangle + \mathcal{O}(v^2)|Q\bar{Q}({}^{2S'+1}(L)_{J'}^{[8]})g\rangle + \mathcal{O}(v^2)|Q\bar{Q}({}^{2S+1}(L')_{J'}^{[1,8]})gg\rangle + \cdots , \tag{3.16}$$

where the relative powers of the coefficients are obtained by the non-relativistic perturbation method and the heavy quark-gluon interaction in Eqs. (3.6) and (3.7) [36]. Therefore in the NRQCD factorization approach, the heavy quark pair in any state $n = {}^{2S+1}L_J^{[c]}$ can evolve into a heavy quarkonium with the quantum number $H = {}^{2S'+1}L'_{J'}$, but the process is suppressed by the probability of finding Fock state n in H as well as the power counting of the operator generating state n.

For the production of S-wave heavy quarkonium, if keeping only the operators at the lowest order of v in Eq. (3.14), the NRQCD factorization approach is the same as CSM. However, the NRQCD factorization provides a systematic approach to add the relativistic corrections and to estimate the uncertainties. For P-wave heavy quarkonium production, the advantage of the NRQCD factorization over the CSM is more striking. At the end of Sec. 3.2 we know that the calculation of P-wave heavy quarkonium production in the CSM suffers from uncanceled IR divergence. In the NRQCD factorization, besides the color-singlet channel in the CSM, there is a second channel with n being a color-octet S-wave heavy quark pair in Eq. (3.14). The leftover IR divergence of the color-singlet channel in the CSM is canceled by the additional color-octet channel. For example, the production of χ_{cJ} has two equally-weighted channels: $n = {}^3P_J^{[1]}$ and $n = {}^3S_1^{[8]}$ in the NRQCD factorization. In contrast, only the first channel is considered in the CSM.

3.4.3 NRQCD LDMEs

In Eq. (3.14), for a specific heavy quarkonium state H, there is a finite number of NRQCD LDMEs at a certain order of v. These LDMEs are non-perturbative and serve as free parameters in the NRQCD factorization. With some approximation, we can find relations of these parameters and enhance the predictive power of the NRQCD factorization.

- **Heavy-quark spin symmetry**: from NRQCD Lagrangian in Eq. (3.6) and (3.7), the interaction flipping the heavy quark spin is suppressed by at least v^2. Consequently the difference between spin-singlet and

spin-triplet NRQCD LDMEs is in order of v^2,

$$\langle 0|\mathcal{O}^{J/\psi}({}^3S_1^{[1,8]})|0\rangle = \langle 0|\mathcal{O}^{\eta_c}({}^1S_0^{[1,8]})|0\rangle[1+\mathcal{O}(v^2)], \tag{3.17a}$$

$$\langle 0|\mathcal{O}^{\chi_{cJ}}({}^3P_J^{[1,8]})|0\rangle = \langle 0|\mathcal{O}^{h_c}({}^1P_1^{[1,8]})|0\rangle[1+\mathcal{O}(v^2)]. \tag{3.17b}$$

- **Vacuum-saturation approximation**: for the color-singlet heavy quark pair, we can find the following relation between the NRQCD LDMEs in production and decay process

$$\begin{aligned}&\langle 0|\mathcal{O}_n^H(\mu_\Lambda)|0\rangle \approx \langle 0|\chi^\dagger\mathcal{K}_n\psi(\sum_{m_J}|H\rangle\langle H|)\psi^\dagger\mathcal{K}_n'\chi|0\rangle\\ =&(2J+1)\langle H|\psi^\dagger\mathcal{K}_n'\chi|0\rangle\langle 0|\chi^\dagger\mathcal{K}_n\psi|H\rangle\\ \approx&(2J+1)\langle H|\mathcal{O}_n^{\text{decay}}|H\rangle,\end{aligned} \tag{3.18}$$

where $\mathcal{K}_n$ and $\mathcal{K}_n'$ are products of a color matrix, a spin matrix, and a polynomial in $\mathbf{D}$; $\langle H|\mathcal{O}_n^{\text{decay}}|H\rangle = \langle H|\psi^\dagger\mathcal{K}_n'\chi\cdot\chi^\dagger\mathcal{K}_n\psi|H\rangle$ is the decay four-fermion operator [36]. In the second row of Eq. (3.18), we assume that the heavy quarkonium H is unpolarized. In the last row, because the heavy quark pair is color singlet, the Fock states we neglected start from $|gg\rangle\langle gg|$, which is suppressed by v^4. Therefore the error of this relation is at the order of v^4. With this relation, we can use the NRQCD LDMEs extracted from the decay processes to make predictions for heavy quarkonium production. This relation cannot be applied to the color-octet LDMEs, since the leading Fock state in this case does not have the same color quantum number as the vacuum.

- **Relation to wave-functions**: for the color-singlet heavy quark pair, the NRQCD LDMEs can be expressed in terms of wave-functions, or their derivatives, evaluated at the origin. First we use vacuum-saturation approximation

$$\begin{aligned}&\langle 0|\mathcal{O}_n^H(\mu_\Lambda)|0\rangle \approx \langle 0|\chi^\dagger\mathcal{K}_n\psi(\sum_{m_J}|H\rangle\langle\ H|)\psi^\dagger\mathcal{K}_n'\chi|0\rangle\\ =&(2J+1)\langle\ H|\psi^\dagger\mathcal{K}_n'\chi|0\rangle\langle 0|\chi^\dagger\mathcal{K}_n\psi|H\rangle.\end{aligned} \tag{3.19}$$

Then we can use the non-relativistic wave-functions

$$|\eta_c\rangle \propto \int \mathrm{d}\boldsymbol{r}\Psi(\boldsymbol{r})\chi(-\boldsymbol{r}/2)\psi^\dagger(\boldsymbol{r}/2)|0\rangle, \tag{3.20a}$$

$$|\psi(\boldsymbol{\epsilon})\rangle \propto \int \mathrm{d}\boldsymbol{r}\Psi(\boldsymbol{r})\chi(-\boldsymbol{r}/2)\boldsymbol{\sigma}\psi^\dagger(\boldsymbol{r}/2)|0\rangle, \tag{3.20b}$$

to calculate the matrix element in the second row of Eq. (3.19). In this way, we obtain

$$\langle \mathcal{O}^{\eta_c}_{[c\bar{c}(^1S_0^{[1]})]} \rangle = \frac{1}{4\pi}|R_{\eta_c}(0)|^2, \tag{3.21a}$$

$$\langle \mathcal{O}^{J/\psi}_{[c\bar{c}(^3S_1^{[1]})]} \rangle = \frac{3}{4\pi}|R_{J/\psi}(0)|^2, \tag{3.21b}$$

$$\langle \mathcal{O}^{h_c}_{[c\bar{c}(^1P_1^{[1]})]} \rangle = \frac{9}{4\pi}|R'_{h_c}(0)|^2, \tag{3.21c}$$

$$\langle \mathcal{O}^{\chi_{cJ}}_{[c\bar{c}(^3P_J^{[1]})]} \rangle = \frac{3(2J+1)}{4\pi}|R'_{\chi_{cJ}}(0)|^2, \tag{3.21d}$$

where $R(\mathbf{r}) = \sqrt{4\pi}\Psi(\mathbf{r})$.

- **Factorization scale dependence**: the NRQCD LDMEs with different factorization scales μ_Λ are related by an evolution equation similar to the renormalization group equation,

$$\mu_\Lambda \frac{\mathrm{d}}{\mathrm{d}\mu_\Lambda}\langle 0|\mathcal{O}_n^H(\mu_\Lambda)|0\rangle = \sum_k \frac{\gamma_{nk}(\mu_\Lambda)}{m_Q^{d_k-d_n}}\langle 0|\mathcal{O}_k^H(\mu_\Lambda)|0\rangle, \tag{3.22}$$

where the anomalous-dimension coefficients $\gamma_{nk}(\mu_\Lambda)$ are computable in powers of $\alpha_s(\mu_\Lambda)$. Therefore as long as we know the values of these NRQCD LDMEs in an input scale μ_Λ^{input}, we can solve the evolution equation to obtain the values of the NRQCD LDMEs in other scales.

3.4.4 Application to heavy quarkonium hadron production

Besides its theoretical advantage over the CSM, phenomenologically, the NRQCD factorization approach has also achieved many successes in predicting experimental data from the e^+e^-, ep and pp colliders. Similar to the CSM, the NRQCD factorization suffers from large high-order corrections. After taking into account the QCD radiative correction and/or relativistic correction, NRQCD predictions are in great agreement with many experiments. Nevertheless, there are still many data which NRQCD factorization has difficulties to explain. Next we focus on heavy quarkonium production in hadron colliders. An extensive review of the phenomenological successes and failures of NRQCD factorization in other experiments can be found in Ref. [26].

In hadron colliders, most data are for J/ψ, ψ' and $\Upsilon(nS)$ because of their clean and easy-to-measure decay products (see Table 3.2). Both the QCD

Table 3.4: Essential channels for various heavy quarkonium production, with the relative power-counting of each operator labelled explicitly.

Quarkonium	Essential channels
J/ψ, ψ', $\Upsilon(nS)$	$\mathcal{O}^H(^3S_1^{[1]})[v^0]$, $\mathcal{O}^H(^1S_0^{[8]})[v^4]$, $\mathcal{O}^H(^3S_1^{[8]})[v^4]$, $\mathcal{O}^H(^3P_J^{[8]})[v^4]$
η_c, η_b	$\mathcal{O}^H(^1S_0^{[1]})[v^0]$
h_c, h_b	$\mathcal{O}^H(^1P_1^{[1]})[v^0]$, $\mathcal{O}^H(^1S_0^{[8]})[v^0]$
χ_{cJ}, χ_{bJ}	$\mathcal{O}^H(^3P_J^{[1]})[v^0]$, $\mathcal{O}^H(^3S_1^{[8]})[v^0]$

radiative correction and the relativistic corrections are important for achieving good agreement between the NRQCD factorization prediction and the data from different experiments, such as the Tevatron and the LHC. In Table 3.4, we list the currently-considered essential channels and their power-countings for J/ψ, ψ' and $\Upsilon(nS)$, as well other heavy quarkonium states.

To have a good agreement with the data of J/ψ, ψ' and $\Upsilon(nS)$ production, the state of the art is the extraction of the three color-octet NRQCD LDMEs listed in Table 3.4. Different fitting procedures result in some differences in the prediction [90]. In Ref. [11, 48], after calculating the short-distance coefficients at NLO, the authors noticed that for the production of J/ψ and ψ', the short-distance coefficient of $^3P_J^{[8]}$ channel can be decomposed into a linear combination of the other two color-octet channels within an error of a few percents

$$\mathrm{d}\hat{\sigma}[^3P_J^{[8]}] = r_0 \mathrm{d}\hat{\sigma}[^1S_0^{[8]}] + r_1 \mathrm{d}\hat{\sigma}[^3S_1^{[8]}], \tag{3.23}$$

where $r_0 = 3.9, r_1 = -0.56$ for the Tevatron, and $r_0 = 4.1, r_1 = -0.56$ for the LHC. Therefore they argued that only two linearly combined NRQCD LDMEs can be reasonably fitted from the data,

$$M^H_{0,r_0} = \langle \mathcal{O}^H(^1S_0^{[8]}) \rangle + \frac{r_0}{m_c^2} \langle \mathcal{O}^H(^3P_0^{[8]}) \rangle, \tag{3.24a}$$

$$M^H_{0,r_1} = \langle \mathcal{O}^H(^3S_1^{[8]}) \rangle + \frac{r_1}{m_c^2} \langle \mathcal{O}^H(^3P_0^{[8]}) \rangle, \tag{3.24b}$$

where H is J/ψ or ψ', the difference of the LDMEs for $^3P_J^{[8]}$ with different J-values are at higher powers of v.

After fitting $M^{J/\psi}_{0,r_0}$ and $M^{J/\psi}_{0,r_1}$ from the Tevatron data with $p_T > 7$ GeV, the authors give the prediction for prompt J/ψ and direct ψ' production(see Fig. 3.9). In this figure, we can clearly see that M_0 and M_1 have different p_T-behaviors; M_0 dominates at the low-p_T region and M_1 dominates at the

high-p_T region, while the color-singlet channel, which is at leading power of v (see Table 3.4) contributes less than 1% at $p_T > 20$ GeV. To compare the contributions from different orders of α_s, Fig. 3.10 shows the K factors, which is defined as the ratio of NLO to LO short-distance coefficients, for all four channels. For the ${}^3S_1^{[1]}$ and ${}^3P_J^{[8]}$ channels, the NLO correction dominates from p_T as low as 10 GeV; for the ${}^1S_0^{[8]}$ channel, the NLO correction becomes more important than the LO at $p_T \gtrsim 30$ GeV; for the ${}^3S_1^{[8]}$ channel, the LO is dominant for the whole p_T range plotted.

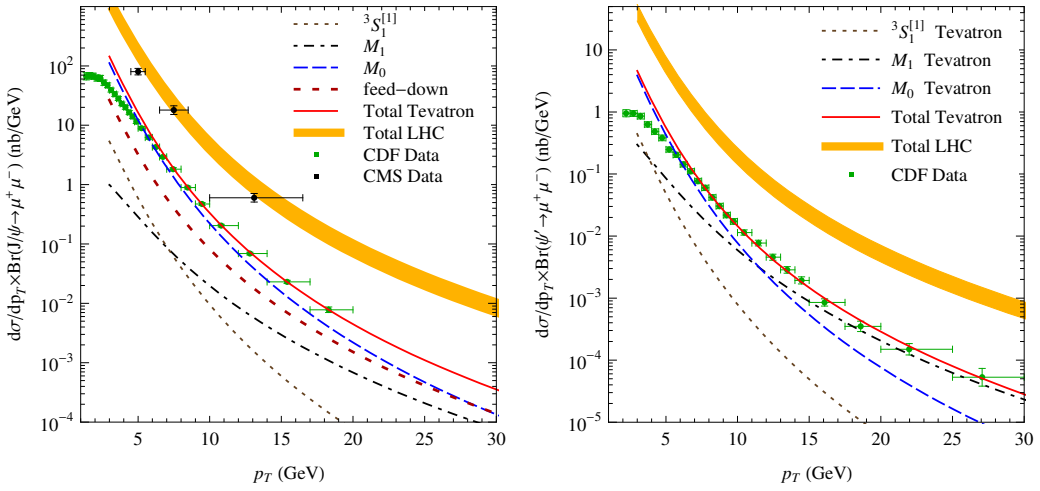

Figure 3.9: The p_T distributions of prompt J/ψ and direct ψ' production at the Tevatron and the LHC. Figures taken from Ref. [11].

Fig. 3.11 shows the comparison of the NLO NRQCD prediction for direct J/ψ production with the data from the Tevatron on prompt J/ψ polarization (feeddown contribution is small, see the left plot of Fig. 3.9) from the same group [12]. The data from CDF Run I and Run II are in different shapes, but recent data from the LHC confirms the CDF Run II. The almost unpolarized J/ψ is due to the cancellation of the ${}^3S_1^{[8]}$ and ${}^3P_J^{[8]}$ channels, which is also implied from the small value of M_{1,r_1} in Eq. (3.24): $M_{1,r_1}^{J/\psi}/M_{0,r_0}^{J/\psi} \approx 0.007$ [11, 48].

Several inconsistencies between the NLO NRQCD calculations and the experimental data have been realized recently. The value of $M_{0,r_0=3.9}^{J/\psi}$ is fitted to be $7.4 \times 10^{-2}\text{GeV}^3$ from the J/ψ hadron production [11, 48], which contradicts its upper limit 2.0×10^{-2} from the e^+e^- data [41]. In 2011, a first attempt of a global fitting all three color-octet NRQCD LDMEs for the J/ψ

production was completed with all available high-quality data from KEKB, LEP II, RHIC, HERA, the Tevatron, and the LHC [13, 38] (see Fig. 3.12 and 3.13). Although the NLO NRQCD predictions agree with the data generally, the minimum χ^2 per degree of freedom of the fitting is as large as 4.42. The NLO NRQCD calculations also have trouble in explaining the prompt heavy quarkonium polarization. By considering the feeddown contribution, the NLO NRQCD calculations are able to explain the polarizations of low energy heavy quarkonium states. However, the same calculation cannot explain the polarization of prompt ψ' and $\Upsilon(3S)$, which do not have feeddown contributions (see Figs. 3.14 and 3.15).

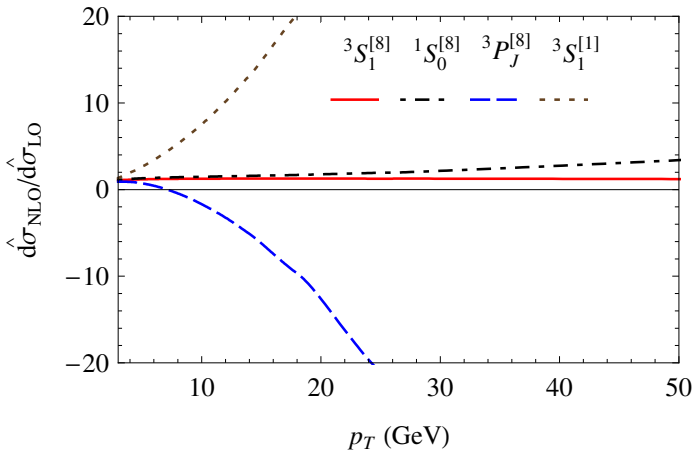

Figure 3.10: The dependence of K factors on p_T for different channels in $J/\psi(\psi')$ direct production at the Tevatron. The negative value of $^3P_J^{[8]}$ channel is because of the $\overline{\text{MS}}$ scheme and do not affect the physical result. Figure taken from Ref. [11].

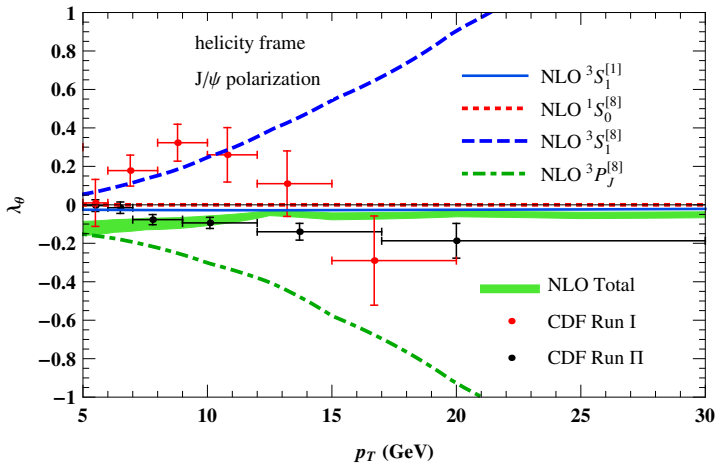

Figure 3.11: NLO NRQCD prediction for the polarization observable λ_θ (defined in Eq. (3.1)) of J/ψ production at the Tevatron. Figure taken from Ref. [12].

3.5 Why are high-order corrections so large?

In this section, we explain the reason for the "counter-intuitive" high-order correction in both the CSM and the NRQCD calculation for heavy quarkonium production at large p_T. In Fig. 3.6, the NLO CSM correction is more than 100 times larger than the LO result, and the NNLO* correction raises the prediction by another factor of 10. Moreover, the LO, NLO and NNLO* results have different p_T behaviors. Similarly for the NRQCD calculation, see Fig. 3.10, the NLO corrections for the $^3S_1^{[1]}$ and $^3P_J^{[8]}$ channels dominate at $p_T \gtrsim 10$ GeV; the NLO corrections for the $^1S_0^{[8]}$ channel dominates at $p_T \gtrsim 50$ GeV. Only for the $^3S_1^{[8]}$ channel the LO is always dominant. Again, the K factors for the $^3S_1^{[1]}$, $^3P_J^{[8]}$ and $^1S_0^{[8]}$ channels increase with p_T, showing that the NLO corrections for these three channels have stronger p_T behaviors than the corresponding LO results.

The reason for this behavior is that the high-order corrections for some channels are enhanced by powers of p_T^2/m_Q^2. When $p_T \gg m_Q$, this power enhancement is more important than the suppression of α_s in the high-order corrections. Next we explain this power enhancement in the CSM calculation in detail, following the argument in Ref. [40]. Since it is the same reason for the NRQCD factorization calculation, we only mention the situation in the NRQCD factorization briefly at the end of this section.

In the CSM, the heavy quark pair produced in the hard scattering must have the same quantum numbers as the observed heavy quarkonium. Espe-

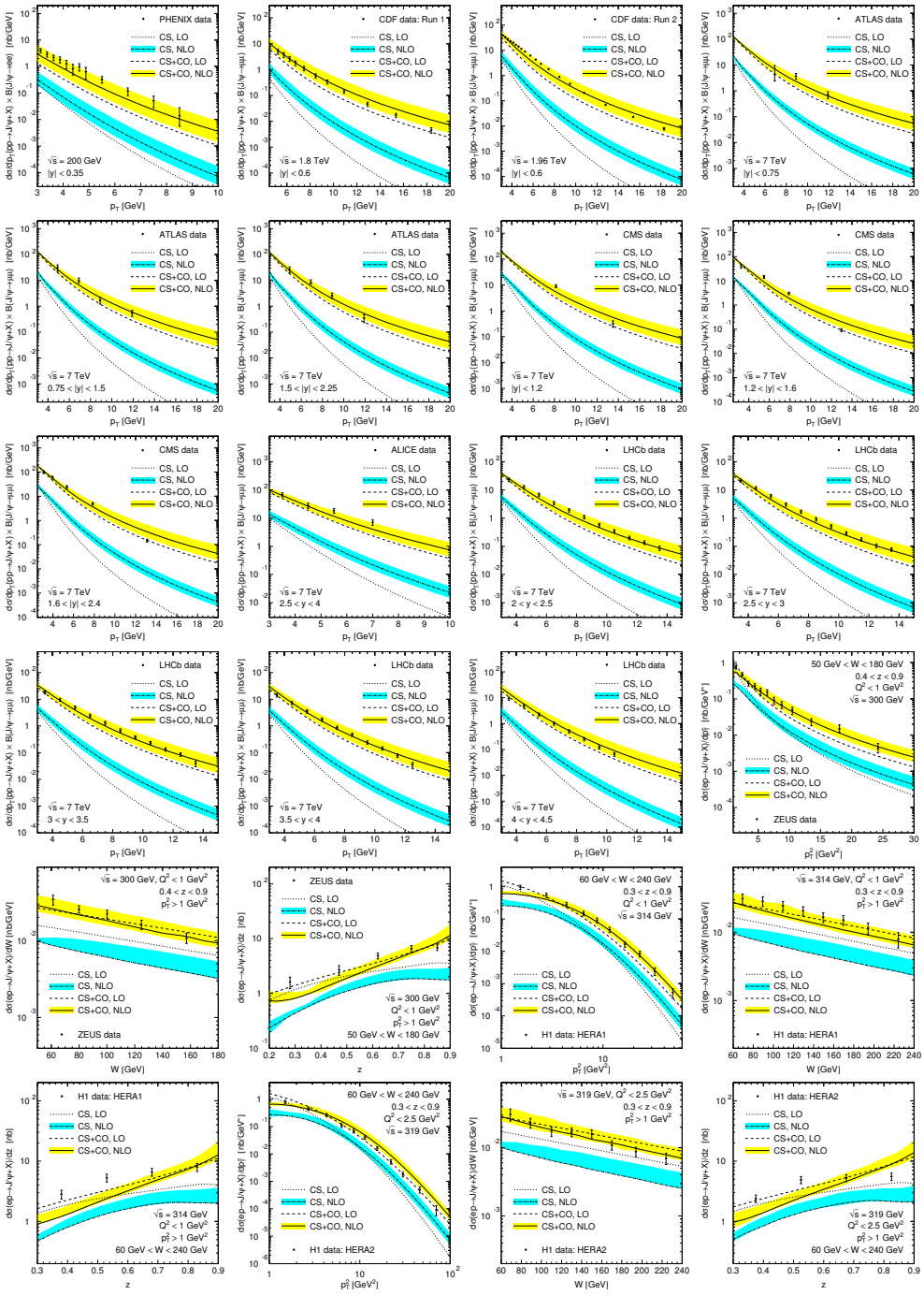

Figure 3.12: NLO NRQCD fit compared to RHIC, Tevatron, LHC, and HERA data for J/ψ production. Figure taken from [13].

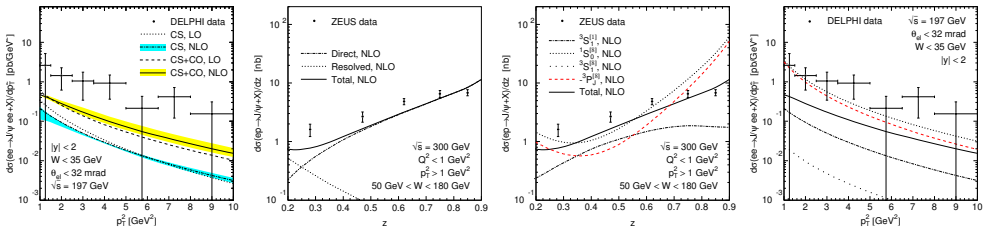

Figure 3.13: NLO NRQCD fit compared to LEP II and HERA I data for J/ψ production. Figure taken from [13].

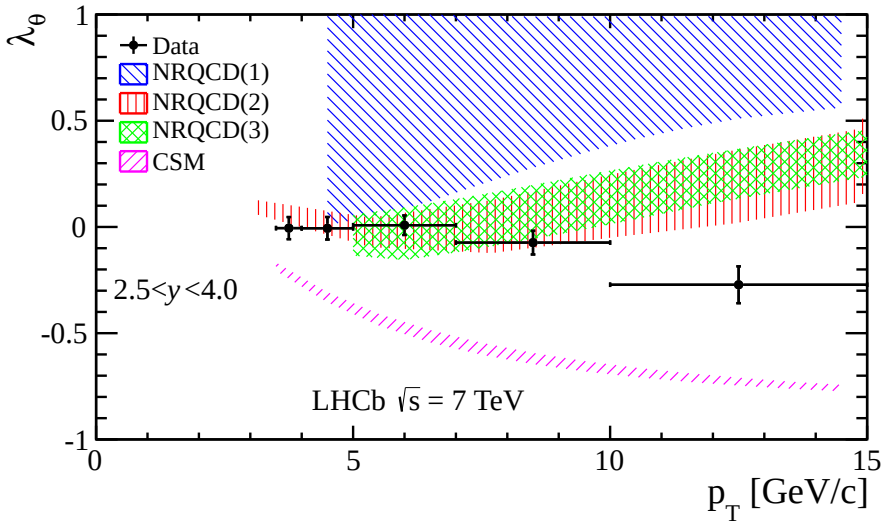

Figure 3.14: Comparison of the CSM calculation and three different NLO NRQCD calculations and the data from LHCb for ψ' polarization. The λ_θ is defined in Eq. (3.1). The CSM calculation and NRQCD(1) are from Ref. [14], NRQCD(2) is from Ref. [15], NRQCD(3) is from Ref. [12]. The difference of the three NRQCD calculations comes from different methods of fitting the color-octet NRQCD LDMEs. Figure taken from Ref [16].

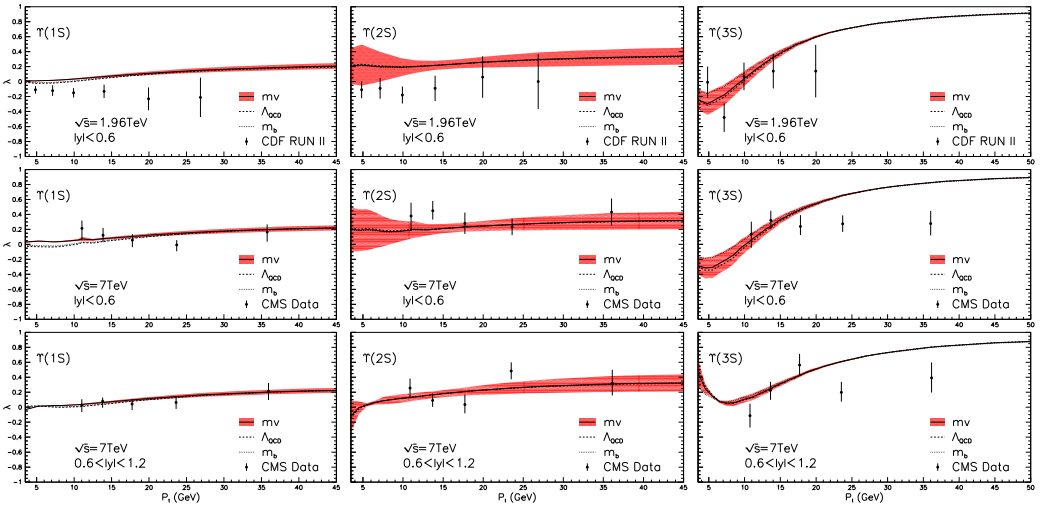

Figure 3.15: Comparison of NLO NRQCD calculation and the data from the CDF, and CMS for prompt $\Upsilon(nS)$ polarization. Figure taken from Ref. [17]

cially, to produce a J/ψ, the heavy quark pair must be in the ${}^3S_1^{[1]}$, color-singlet state. The LO Feynman diagram is showed in Fig. 3.16. Because the final-state gluon has to balance the large p_T of the J/ψ, both the heavy quark propagators are off-shell by the order of p_T. Moreover, the numerator does not give an invariant growing with p_T^2. Therefore, the LO calculation in the CSM behaves as $1/p_T^8$.

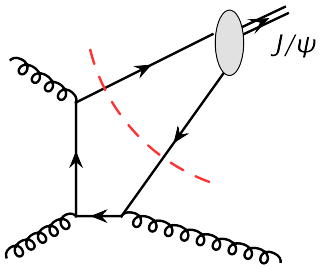

Figure 3.16: A sample Feynman diagram giving the LO contribution to J/ψ production in the CSM.

At NLO, in the real diagrams with another gluon emitted, some of which are shown in Fig. 3.17(a)-(c), the heavy quark pair can emit the additional gluon at a scale softer than p_T. In this case, the heavy quark pair produced at distance $\mathcal{O}(1/p_T)$ is in a relativistic spin state with color octet. When

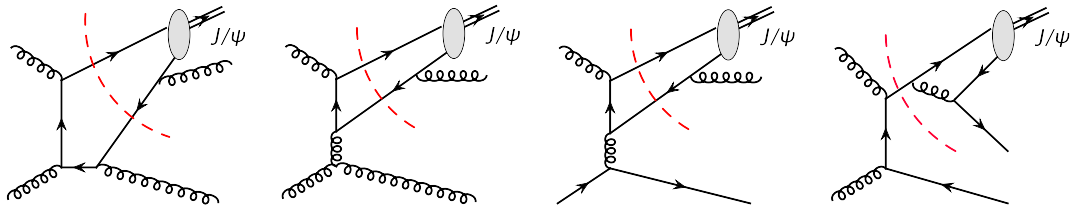

(a) (b) (c) (d)

Figure 3.17: Sample Feynman diagrams giving the NLO contribution to J/ψ production in the CSM.

$p_T \gg m_Q$, there is a large phase space for the pair to emit the gluon to become the non-relativistic ${}^3S_1^{[1]}$ state at the scale $\mathcal{O}(1/m_Q)$. Similar to the LO case, the two off-shell propagators needed to produce a heavy quark pair at large p_T result in a factor $1/p_T^8$. However, at NLO, the numerator can produce a p_T^2 enhancement. Consequently, the NLO contribution is power enhanced by a factor of p_T^2/m_Q^2 compared to the LO. There is another contribution at this order, shown in Fig. 3.17(d). This associated production is power enhanced by two powers of p_T^2/m_Q^2. However, this associated production contribution is very small [91]. Therefore, the NLO CSM behaves as $1/p_T^6$ at current collider energy.

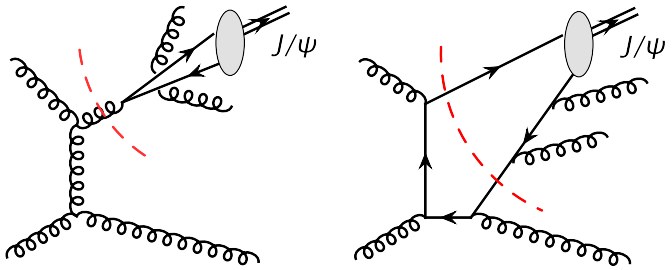

(a) (b)

Figure 3.18: Sample Feynman diagrams giving the NNLO contribution to J/ψ production in the CSM.

The process with the gluon fragmentation is open at NNLO, showed in Fig. 3.18(a). This process behaves as $1/p_T^4$. As a result, the NNLO correction is enhanced by two powers of p_T^2/m_Q^2 compared with the LO result. There are other diagrams at NNLO, such as the one in Fig. 3.18(b), which is in the same power as the NLO correction. Because the strongest p_T behavior is $1/p_T^4$, we

don't expect further power enhancement beyond NNLO.

However, even if we manage to calculate the full NNLO correction in the CSM and have a good control of the power enhancement, there still exist logarithms in forms of $\ln(p_T^2/m_Q^2)$. These logarithms increase with p_T and finally disqualify the truncation of the perturbative series. A systematic resummation procedure is necessary to sum these large logarithms to all orders in α_s.

For the J/ψ production in the NRQCD factorization, we need to consider the power behaviors of all four channels (see Table 3.4). The situation is the same as the CSM for the ${}^3S_1^{[1]}$ channel. In principle we should calculate it to NNLO, where the strongest p_T behavior arises. Nonetheless, it has been shown that the NNLO correction of this channel is negligible compared to the data at current collider energies [3, 48]. For the ${}^3S_1^{[8]}$, ${}^3P_J^{[8]}$ and ${}^1S_0^{[8]}$ channels, the strongest p_T behavior appears at NLO. Therefore, the NRQCD calculation with $\mathcal{O}(\alpha_s v^4)$ correction should include all important power behavior for p_T distribution of J/ψ. However, a systematic resummation procedure is still needed to sum the large logarithms to all orders in α_s.

To summarize, the CSM and the NRQCD factorization approach suffer from large high-order corrections because the power enhancement p_T^2/m_Q^2 is much larger than the suppression of α_s at large p_T. In the NRQCD factorization approach, the NLO calculations of all four channels are expected to have good control of the leading p_T behavior. However, these calculations are very difficult and only numerical results are available so far. Besides, large logarithms $\ln(p_T^2/m_Q^2)$ disqualifies the truncation of the perturbative series at sufficiently large p_T. As a result, although we find inconsistencies between the data and the NLO NRQCD calculation, it is very difficult to determine whether they are from large high-order corrections or from the failure of NRQCD factorization conjecture.

In the next chapter we introduce the QCD factorization formalism. In this formalism, the cross section is first expanded by powers of $1/p_T^2$. The large logarithms $\ln(p_T^2/m_Q^2)$ are resummed to all orders of α_s by solving a closed set of evolution equations. Therefore, QCD factorization has very good control of the p_T behavior at large p_T, and is expected to provide more insight of heavy quarkonium production mechanism.

Chapter 4

QCD Factorization for heavy quarkonium production: Overview

This chapter is organized as follows. In Sec. 4.1, we first argue that the next-to-leading-power (NLP) contribution is important (if not dominant) in heavy quarkonium production processes at current collider energies. In Sec. 4.2, we introduce the QCD factorization formalism for inclusive heavy quarkonium production. Then in Sec. 4.3, we give the definition of the fragmentation functions for both the leading-power (LP) and NLP contributions. In Sec. 4.4, we introduce the evolution equations of these fragmentation functions. Finally, in the last section, we derive a relation between the color-singlet $Q\bar{Q}$ fragmentation functions and the light-cone distribution amplitudes.

4.1 NLP contribution is important

A general inclusive heavy quarkonium production process is

$$A(p_1) + B(p_2) \to H(Q) + X, \tag{4.1}$$

where $A(p_1)$ and $B(p_2)$ are the colliding hadrons with momenta p_1 and p_2, $H(Q)$ denotes the observed heavy quarkonium, and X represents other unobserved particles produced in the collision. The scale Q of the hard-scattering process is usually chosen as p_T, the transverse momentum of the heavy quarkonium H. In modern high-energy experiments, p_T can be as large as 105 GeV [92].

According to the LP collinear factorization theorem, the cross section for

this process can be written as

$$\sigma_{AB\to HX}(p_1,p_2,p_T) = \sum_{a,b,c}\int \mathrm{d}x_1\,\mathrm{d}x_2\,\mathrm{d}z\, f_{a/A}(x_1;\mu_F) f_{b/B}(x_2;\mu_F) \times \hat{\sigma}_{ab\to c}(x_1,x_2,z,p_T;\mu_F) D_{H/c}(z;\mu_F) + \mathcal{O}(q_{soft}/p_T), \tag{4.2}$$

where μ_F is the factorization scale; the indices $a, b = q, \bar{q}, g$ denote parton flavors; $\hat{\sigma}_{ab\to c}$ is the short-distance coefficient function (partonic cross section) for the process $a + b \to c$, which has only the large scale p_T and can be calculated in QCD perturbation theory; $f_{a/A}(x_1)$, $f_{b/B}(x_2)$ and $D_{H/c}(z)$ are non-perturbative, long-distance distribution functions. See Fig. 4.1 for a diagrammatic illustration of this factorization. $f_{a/A}(x_1)$ denotes the probability density to find a parton of flavor a inside the hadron A with longitudinal momentum fraction x_1, similarly for $f_{b/B}(x_2)$. $D_{H/c}(z)$ denotes the probability density to find the observed heavy quarkonium in the outgoing energetic parton c, with the heavy quarkoinium taking a longitudinal momentum fraction z.

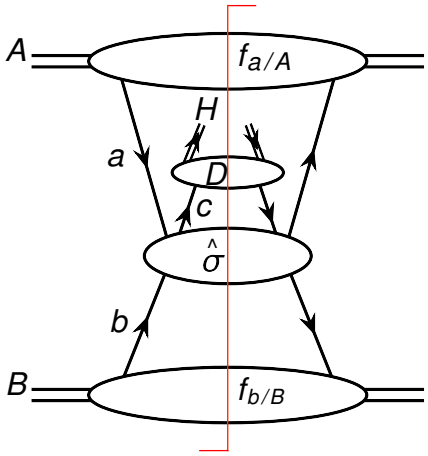

Figure 4.1: Collinear QCD factorization at LP corresponding to Eq. (4.2)

However, the experimental data imply that the LP contribution may not be dominant at current collider energies. Take inclusive J/ψ production as an example. In the LP collinear factorization formula, J/ψ with large p_T are produced mainly from gluon fragmentation. Consequently, if the LP contribution is dominant, the produced J/ψ should be almost all transversely polarized. However, the experimental data show no sign for this transverse polarization (see Figs. 3.11). Moreover, although the LP contribution is dominant for the

${}^3S_1^{[8]}$ and ${}^3P_J^{[8]}$ channels (see Fig. 3.10), recent studies show that their LP contributions almost cancel [11, 18, 48]. Furthermore, Fig. 3.10 also indicates that the LP contribution of the ${}^1S_0^{[8]}$ channel is dominant only for p_T as large as 50 GeV. Finally, it has been shown that the LP of the ${}^3S_1^{[1]}$ channel is negligible compared with the experimental data [3, 48]. All of these imply that the LP contribution might not dominate the production rate at current collider energies. A recent study which combines the NLO NRQCD calculation and the LP contribution confirms this conclusion [18].

The QCD factorization approach, which includes the NLP contribution systematically, was first proposed in Ref. [23]. For unpolarized incoming hadrons, the NLP contributions come from three terms

$$\begin{aligned}\sigma(p_T, q_{\rm soft}) - \sigma^{\rm LP}(p_T, q_{\rm soft}) = & \left(\frac{\Lambda_{QCD}}{p_T}\right)^2 f_A^{(4)} \otimes f_B^{(2)} \otimes \sigma_1 \otimes D^{(2)} \\ & + \left(\frac{\Lambda_{QCD}}{p_T}\right)^2 f_A^{(2)} \otimes f_B^{(4)} \otimes \sigma_2 \otimes D^{(2)} \\ & + \left(\frac{m_Q}{p_T}\right)^2 f_A^{(2)} \otimes f_B^{(2)} \otimes \sigma_3 \otimes D^{(4)} \\ & + \mathcal{O}\left(q_{\rm soft}^4/p_T^4\right), \end{aligned} \tag{4.3}$$

where $\otimes$ is a shorthand notation of convolution, distributions with superscript (2) denote twist-2 functions, which is the same as those in Eq. (4.2) without the superscripts, superscript (4) denotes twist-4 distributions. The diagrammatic illustrations of the three terms on the right-hand side of Eq. (4.3) are shown in Fig. 4.2. For the first two NLP terms $q_{\rm soft} \sim \Lambda_{QCD}$, while for the third NLP term $q_{\rm soft}$ is at the same order as m_Q, the heavy quark mass. Since $m_Q \gg \Lambda_{QCD}$, the third NLP term is more important than the first two NLP terms.

Moreover, $D^{(4)}$ includes the contribution that the fragmenting parton pair are exactly the same heavy quark pair inside the observed heavy quarkonium. This contribution may not be small even compared with the LP contribution at current collider energies. Intuitively, it is more likely to find a heavy quarkonium from the corresponding heavy quark pair than from a single parton, say a gluon in the LP contribution. Therefore, the NLP contribution with fragmenting heavy quark pair receives non-perturbative enhancement and is probably a large correction to the LP term.

LP and NLP contributions together are very promising to cover the full story of heavy quarkonium production. In a physical process, the heavy quark pair, which eventually forms the observed heavy quarkonium, can be produced (1) at a very late time $\mathcal{O}(1/m_Q)$, or (2) in the hard scattering at time $\mathcal{O}(1/p_T)$,

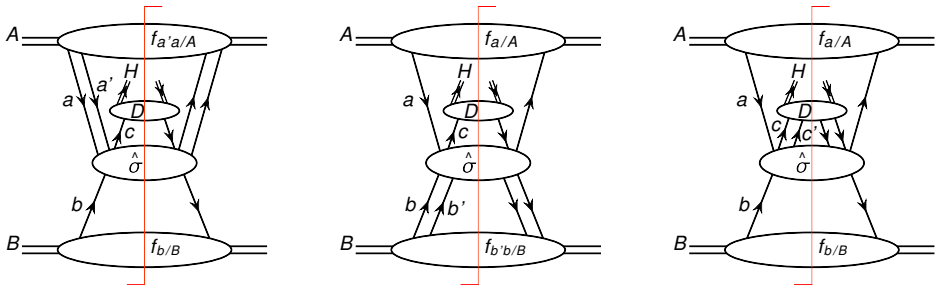

Figure 4.2: Diagrammatic illustration of NLP contributions corresponding to the three terms on the right-hand-side of Eq. (4.3), respectively.

or (3) somewhere between these two scales. The LP contribution with fragmentation functions calculated with the NRQCD factorization only considers the first situation [18]. By taking care of the NLP contribution systematically, the second situation is described as the heavy quark pair fragmenting, while the third situation is included by solving a closed set of evolution equations, which also sums over large logarithms $\ln(p_T^2/m_Q^2)$ to all orders of α_s.

4.2 The QCD factorization formula

In the QCD factorization approach, the production cross section of a heavy quarkonium H with momentum p at a large transverse momentum p_T in the lab frame is expanded in a power series of $1/p_T$ [23, 40]

$$
\begin{aligned}
E_p \frac{d\sigma_{A+B\to H+X}}{d^3p}(p) \approx & \sum_f \int \frac{dz}{z^2} D_{f\to H}(z;m_Q) E_c \frac{d\hat{\sigma}_{A+B\to f(p_c)+X}}{d^3p_c}\left(p_c = \frac{1}{z}\hat{p}\right) \\
& + \sum_{[Q\bar{Q}(\kappa)]} \int \frac{dz}{z^2} \frac{d\zeta_1\, d\zeta_2}{4} \mathcal{D}_{[Q\bar{Q}(\kappa)]\to H}(z,\zeta_1,\zeta_2;m_Q) \\
& \times E_c \frac{d\hat{\sigma}_{A+B\to [Q\bar{Q}(\kappa)](p_c)+X}}{d^3p_c}(P_Q, P_{\bar{Q}}; P'_Q, P'_{\bar{Q}}),
\end{aligned}
\tag{4.4}
$$

where the factorization scale μ_F dependence is suppressed, and the summation over unobserved particles X is understood. In Eq. (4.4), the heavy quarkonium momentum p^μ is defined in the lab frame as $p^\mu = (m_T \cosh y,\ \mathbf{p}_T,\ m_T \sinh y)$ with rapidity y, $m_T = \sqrt{m_H^2 + p_T^2}$ and $p_T = \sqrt{\mathbf{p}_T^2}$. For our calculation of

input FFs, it is more convenient to define the momentum p^μ in a frame in which it has no transverse component as $p^\mu = (p^+,\, p^-\,, 0_\perp)$ with

$$\begin{aligned} p^+ &= \left(m_T\, \cosh y + \sqrt{p_T^2 + m_T^2\, \sinh^2 y}\right)/\sqrt{2}\,, \\ p^- &= \left(m_T\, \cosh y - \sqrt{p_T^2 + m_T^2\, \sinh^2 y}\right)/\sqrt{2}\,, \end{aligned} \tag{4.5}$$

in terms of the rapidity and transverse momentum in the lab frame. The components in the light-cone coordinate in Eq. (4.5) are defined as $p^\pm = (p^0 \pm p^3)/\sqrt{2}$. With the two light-like vectors $\hat{\bar{n}}^\mu = (1^+, 0^-, 0_\perp)$ and $\hat{n}^\mu = (0^+, 1^-, 0_\perp)$, which satisfy $\hat{\bar{n}}^2 = \hat{n}^2 = 0$ and $\hat{\bar{n}}\cdot\hat{n} = 1$, the light-cone components of momentum p^μ can be expressed as $p^+ = p\cdot\hat{n}$ and $p^- = p\cdot\hat{\bar{n}}$. In this frame, we have the momenta of perturbatively produced partons in Eq. (4.4) as $p_c = \hat{p}/z$ with $\hat{p}^\mu = (p^+,\, 0^-, 0_\perp) = p^\mu(m_H = 0)$ (or $z = \hat{p}^+/p_c^+$), and

$$P_Q = \frac{1+\zeta_1}{2}\, p_c,\;\; P_{\bar{Q}} = \frac{1-\zeta_1}{2}\, p_c,\;\; P'_Q = \frac{1+\zeta_2}{2}\, p_c,\;\; P'_{\bar{Q}} = \frac{1-\zeta_2}{2}\, p_c\,, \tag{4.6}$$

where ζ_1 and ζ_2 are relative light-cone momentum fractions between the heavy quark and antiquark in the amplitude and its complex conjugate, respectively. Note that in Eq. (4.4), we used variables ζ_1 and ζ_2 instead of the u and v used in Ref. [40], which are one to one corresponded as $\zeta_1 = 2u - 1$, $\zeta_2 = 2v - 1$, and $d\zeta_1 d\zeta_2/4 = du\, dv$.

The factorization formula in Eq. (4.4) has been argued to be valid in QCD perturbation theory to all orders in α_s [40]. The first term on the right-hand side is the LP contribution to the production cross section in its $1/p_T$ expansion, while the second term is the NLP contribution, or the first power correction. The Feynman diagrams in the cut diagram notation for these two terms are shown in Fig. 4.3. Physically, the first term represents the production of a single parton of flavor f at short distance, followed by its fragmentation into the observed heavy quarkonium H. The $\sum_f$ runs over all parton flavors $f = q, \bar{q}, g$ including heavy quarks with its mass $m_Q \ll p_T$. For collider energies at the LHC, the sum could include charm quark c as well as bottom quark b. The second term describes the production of a heavy $Q\bar{Q}$ pair at the hard collision, and the pair then fragments into an observed heavy quarkonium H. The $\sum_{[Q\bar{Q}(\kappa)]}$ runs over all possible spin and color states of the $Q\bar{Q}$-pair, which could be the vector ($v^{[1,8]}$), axial-vector ($a^{[1,8]}$) or tensor ($t^{[1,8]}$) state, with the superscripts labeling the color state of the pair: singlet ($^{[1]}$) or octet ($^{[8]}$). Projection operators are used to select a specific $Q\bar{Q}$ state, which is the topic of Sec. 5.2. Note that in the diagram on the right in Fig.

4.3, the $Q\bar{Q}$ pair on the left of the cut could have different relative momentum from the $Q\bar{Q}$ pair on the right, which means that ζ_1 is not necessarily equal to ζ_2 in Eq. (4.4).

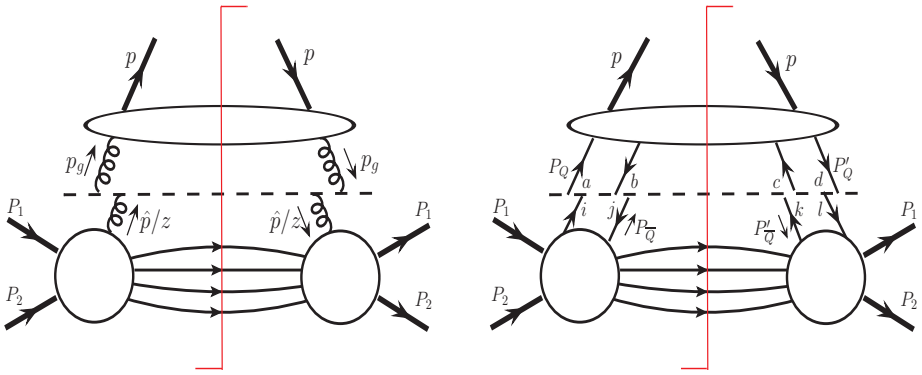

Figure 4.3: QCD factorization diagrams of heavy quarkonium production. Left: single parton (here taking gluon as an example) fragmentation. Right: heavy quark pair fragmentation.

The same factorization formula can be derived from Soft-Collinear Effective Theory (SCET) [44]. In the large p_T limit of heavy quarkonium production, the IR physics is controlled by scale m_Q and the scaling parameter is thus $\lambda = m_Q/p_T$. By assuming the cancellation of Glauber contributions, the authors of Ref. [44] show the soft, collinear and hard region can be factorized.

4.3 Fragmentation Functions

The soft interaction, which is responsible for the formation of heavy quarkonium bound states, is factorized into several fragmentation functions in Eq. (4.4). In this section, we give the definitions of these functions.

The single parton fragmentation functions to heavy quark pair are defined similarly as to light hadrons [93]. The quark fragmentation can be written as

$$D_{q\to H}(z;m_Q,\mu_0) = \frac{z}{4N_c}\sum_X \int \frac{\mathrm{d}x^-}{2\pi} e^{-ik^+x^-} \times \mathrm{Tr}\left[\not{\hat{n}}\ \langle 0|\psi(0)[\Phi^{(F)}_{\hat{n}}(0)]|p,X\rangle\langle p,X|[\Phi^{(F)}_{\hat{n}}(x^-)]^\dagger\bar{\psi}(x^-)|0\rangle\right], \quad (4.7)$$

where $\hat{n}$ is defined below Eq. (4.5), $z = p^+/k^+$, with k^+ (p^+) the light-cone momentum of the outgoing quark (observed hadron), the trace is for both

spinor and color. The gauge link in the matrix element is given by

$$\Phi_{\hat{n}}^{(j)}(y^-) = \mathcal{P}\exp\left[-i\,g\int_{y^-}^{\infty} d\lambda\,\hat{n}\cdot A^{(j)}(\lambda\hat{n})\right], \tag{4.8}$$

where $j = F, A$ represents fundamental or adjoint representation of color $SU(3)$, respectively. By switching ψ and $\bar{\psi}$, we get the definition for the antiquark fragmentation. Similarly, the gluon fragmentation function is defined as

$$\begin{aligned} D_{g\to H}(z; m_Q, \mu_0) = {} & \frac{z}{2k^+(N_c^2-1)}\sum_X \int \frac{\mathrm{d}x^-}{2\pi} e^{-ik^+x^-} \\ & \times (-g_{\lambda\lambda'})\mathrm{Tr}_c\langle 0|G^{+\lambda}(0)[\Phi_{\hat{n}}^{(A)}(0)]|p,X\rangle\langle p,X|[\Phi_{\hat{n}}^{(A)}(x^-)]^\dagger G^{+\lambda'}(x^-)|0\rangle, \end{aligned} \tag{4.9}$$

where Tr_c is the trace for color.

The fragmentation function for a $Q\bar{Q}$ pair in a particular spinor and color state κ to a physical heavy quarkonium H with momentum p is defined as [40]

$$\begin{aligned} & \mathcal{D}_{[Q\bar{Q}(\kappa)]\to H}(z, \zeta_1, \zeta_2; m_Q, \mu_0) \\ & = \int \frac{p^+dy^-}{2\pi}\frac{p^+/z\,dy_1^-}{2\pi}\frac{p^+/z\,dy_2^-}{2\pi} e^{-i(p^+/z)y^-} e^{i(p^+/z)[(1-\zeta_2)/2]\,y_1^-} e^{-i(p^+/z)[(1-\zeta_1)/2]\,y_2^-} \\ & \times \mathcal{P}^{(s)}_{ij,kl}(p_c)\,\mathcal{C}^{[I]}_{ab,cd}\,\langle 0|\bar{\psi}_{c',k}(y_1^-)[\Phi_{\hat{n}}^{(F)}(y_1^-)]^\dagger_{c'c}[\Phi_{\hat{n}}^{(F)}(0)]_{dd'}\,\psi_{d',l}(0)|H(p)\,X\rangle \\ & \times \langle H(p)\,X|\bar{\psi}_{a',i}(y^-)[\Phi_{\hat{n}}^{(F)}(y^-)]^\dagger_{a'a}[\Phi_{\hat{n}}^{(F)}(y^-+y_2^-)]_{bb'}\psi_{b',j}(y^-+y_2^-)|0\rangle, \end{aligned} \tag{4.10}$$

where the subscripts i, j, k, l are the spinor indices of heavy quark and heavy antiquark fields, $a, a', b, b' \ldots$ are color indices of SU(3) color in the fundamental representation, and the summation over repeated indices are understood. $\Phi_{\hat{n}}^{(F)}$ is the gauge link defined in Eq. (4.8). Operators $\mathcal{P}^{(s)}_{ij,kl}(p_c)$ and $\mathcal{C}^{[I]}_{ab,cd}$ project the fragmenting $Q\bar{Q}$ pair to a particular spin and color state κ, which could be a vector ($v^{[1,8]}$), axial-vector ($a^{[1,8]}$), or tensor ($t^{[1,8]}$) state, with the superscript denoting the color. They are defined as [40]

$$\mathcal{P}^{(v)}(p)_{ij,lk} = \frac{1}{4p\cdot\hat{n}}(\gamma\cdot\hat{n})_{ij}\frac{1}{4p\cdot\hat{n}}(\gamma\cdot\hat{n})_{lk}, \tag{4.11a}$$

$$\mathcal{P}^{(a)}(p)_{ij,lk} = \frac{1}{4p\cdot\hat{n}}(\gamma\cdot\hat{n}\gamma_5)_{ij}\frac{1}{4p\cdot\hat{n}}(\gamma\cdot\hat{n}\gamma_5)_{lk}, \tag{4.11b}$$

$$\mathcal{P}^{(t)}(p)_{ij,lk} = \frac{1}{4p\cdot\hat{n}}(\gamma\cdot\hat{n}\gamma_\perp^\beta)_{ij}\frac{1}{4p\cdot\hat{n}}(\gamma\cdot\hat{n}\gamma_\perp^\beta)_{lk}, \tag{4.11c}$$

and

$$\mathcal{C}^{[1]}_{ab,cd} = \left[\frac{\delta_{ab}}{\sqrt{N_c}}\right]\left[\frac{\delta_{cd}}{\sqrt{N_c}}\right], \tag{4.12a}$$

$$\mathcal{C}^{[8]}_{ab,cd} = \frac{1}{N_c^2-1}\sum_B \left[\sqrt{2}\left(t^B\right)_{ab}\right]\left[\sqrt{2}\left(t^B\right)_{cd}\right]. \tag{4.12b}$$

Notice that in Eq. (4.10), the relative momenta of the $Q\bar{Q}$ pairs in the amplitude and its complex conjugate are not necessarily the same, thus ζ_1 and ζ_2 could be different.

4.4 Evolution Equations

In Eq. (4.4), the short-distance partonic hard parts $d\hat{\sigma}$ could be systematically calculated in powers of α_s (needs to convolute with PDFs if A and/or B is a hadron). The fragmentation functions $D_{f\to H}(z; m_Q, \mu_F)$ and $\mathcal{D}_{[Q\bar{Q}(\kappa)]\to H}(z, \zeta_1, \zeta_2; m_Q, \mu_F)$ are unknown, but process independent, universal functions. Their dependence on factorization scale μ_F is determined by a closed set of evolution equations [40],

$$\begin{aligned}\frac{\partial}{\partial \ln \mu_F^2} D_{f\to H}(z; m_Q, \mu_F) &= \sum_{f'}\int_z^1 \frac{dz'}{z'} D_{f'\to H}(z'; m_Q, \mu_F)\ \gamma_{f\to f'}(z/z', \alpha_s) \\ &+ \frac{1}{\mu_F^2}\sum_{[Q\bar{Q}(\kappa')]}\int_z^1\frac{dz'}{z'}\int_{-1}^1\frac{d\zeta_1'}{2}\int_{-1}^1\frac{d\zeta_2'}{2}\,\mathcal{D}_{[Q\bar{Q}(\kappa')]\to H}(z', \zeta_1', \zeta_2'; m_Q, \mu_F) \\ &\times \gamma_{f\to[Q\bar{Q}(\kappa')]}(\frac{z}{z'}, u' = \frac{1+\zeta_1'}{2}, v' = \frac{1+\zeta_2'}{2}),\end{aligned} \tag{4.13}$$

$$\begin{aligned}&\frac{\partial}{\partial \ln \mu_F^2}\mathcal{D}_{[Q\bar{Q}(\kappa)]\to H}(z, \zeta_1, \zeta_2; m_Q, \mu_F) \\ &= \sum_{[Q\bar{Q}(\kappa')]}\int_z^1\frac{dz'}{z'}\int_{-1}^1\frac{d\zeta_1'}{2}\int_{-1}^1\frac{d\zeta_2'}{2}\,\mathcal{D}_{[Q\bar{Q}(\kappa')]\to H}(z', \zeta_1', \zeta_2'; m_Q, \mu_F) \\ &\times \Gamma_{[Q\bar{Q}(\kappa)]\to[Q\bar{Q}(\kappa')]}(\frac{z}{z'}, u = \frac{1+\zeta_1}{2}, v = \frac{1+\zeta_2}{2}; u' = \frac{1+\zeta_1'}{2}, v' = \frac{1+\zeta_2'}{2}),\end{aligned} \tag{4.14}$$

where we explicitly convert the variables u and v to ζ_1 and ζ_2 in the argument of evolution kernels $\gamma_{f\to[Q\bar{Q}(\kappa')]}$ and $\Gamma_{[Q\bar{Q}(\kappa)]\to[Q\bar{Q}(\kappa')]}$ to avoid confusion. The evolution kernels $\gamma's$ and $\Gamma's$ are process independent and perturbatively

calculable. The well-known DGLAP evolution kernels $\gamma_{f\to f'}$ are available to next-to-next-to-leading order in α_s. The power-mixing evolution kernels $\gamma_{f\to[Q\bar{Q}(\kappa')]}$ were calculated in Ref. [40], and the heavy quark pair evolution kernels $\Gamma_{[Q\bar{Q}(\kappa)]\to[Q\bar{Q}(\kappa')]}$ have been recently calculated by two groups independently [40, 94]. If both κ and κ' are color singlet, the kernel $\Gamma_{[Q\bar{Q}(\kappa)]\to[Q\bar{Q}(\kappa')]}$ reduces to the well-known Efremov-Radyushkin-Brodsky-Lepage evolution kernel for exclusive processes [95, 96].

Similar to the FFs for pion or kaon production, a set of single parton and $Q\bar{Q}$ pair fragmentation functions at an input factorization scale μ_0 is required as the boundary conditions (BCs) for solving the evolution equations in Eqs. (4.13) and (4.14). For production of each heavy quarkonium state at high $p_T \gg m_Q$, we need *four* single parton input FFs and *six* $Q\bar{Q}$ pair input FFs as the required BCs. Since these BCs are non-perturbative, in principle, they should be extracted from the data. However, extracting *ten* or more unknown functions for each physical heavy quarkonium is difficult in practice. The extraction is practically feasible if we have some knowledge of these BCs, such as their functional forms.

When the factorization scale $\mu_F \to \mu_0 \gtrsim 2m_Q$, the $\ln(\mu_0^2/m_Q^2)$-type logarithms as well as powers of μ_0^2/m_Q^2 in NRQCD calculations are no longer large. With a clear separation of momentum scales, $\mu_0 \sim O(m_Q) \gg m_Q v$, NRQCD might be the right effective theory for calculating these input FFs by factorizing the dynamics at μ_0 from non-perturbative soft physics at the scale of $m_Q v$ and below. From the next chapter, as a conjecture [23, 24, 43], we apply NRQCD factorization to these input FFs at μ_0, and calculate the corresponding short-distance coefficient functions to the first nontrivial order in α_s for the fragmentation via all S-wave and P-wave NRQCD $Q\bar{Q}$ states.

4.5 Relation with light-cone distribution amplitude

For the hard exclusive processes, the amplitudes can be factorized as a convolutions of the perturbatively calculable hard-kernels and some non-perturbative but universal light-cone distribution amplitudes (LCDA) [97, 98]. Recently, people have applied the NRQCD factorization model to calculate these LCDAs [99–106]. In this section, we show the relation between the twist-2 LCDAs and the color singlet heavy quark pair fragmentation functions defined in Eq. (4.10).

We take the process $[Q\bar{Q}(a^{[1]})] \to \eta_{(c,b)}$ as an example. The LCDA is

defined as [106]

$$\langle\eta_{(c,b)}|\bar{\psi}(\frac{\omega^-}{2})\not{n}\gamma_5\psi(-\frac{\omega^-}{2})|0\rangle = -if_\eta\, p^+\int_0^1 \mathrm{d}x\, e^{i\omega^- p^+(x-1/2)}\hat{\phi}_\eta(x), \tag{4.15}$$

where f_η, p^+ and $\hat{\phi}_\eta$ are the decay constant, light-cone momentum, and the twist-2 LCDA of the outgoing $\eta_{(c,b)}$, respectively. After proper Poincaré translation and Fourier transformation, Eq. (4.15) converts to

$$\int \mathrm{d}\omega^- e^{-i\frac{1-\zeta}{2}p^+\omega^-}\langle\eta_{(c,b)}|\bar{\psi}(\frac{\omega^-}{2})\not{n}\gamma_5\psi(-\frac{\omega^-}{2})|0\rangle = -if_\eta\,\hat{\phi}_\eta(\frac{1+\zeta}{2}). \tag{4.16}$$

On the other hand, for the exclusive process $[Q\bar{Q}(a^{[1]})]\to\eta_{(c,b)}$, the heavy quark fragmentation defined in Eq. (4.10) can be written as

$$\begin{aligned}
&\mathcal{D}_{[Q\bar{Q}(^1S_0^{[1]})]\to\eta_{(c,b)}}(z,\zeta_1,\zeta_2;m_Q,\mu_0)\\
&=\int\frac{p^+dy^-}{2\pi}\frac{p^+\,dy_1^-}{2\pi}\frac{p^+\,dy_2^-}{2\pi}e^{-ip^+y^-}e^{ip^+[(1-\zeta_2)/2]\,y_1^-}e^{-ip^+[(1-\zeta_1)/2]\,y_2^-}\\
&\times\frac{1}{16N_c(p^+)^2}\langle 0|\bar{\psi}(y_1^-)\not{n}\gamma^5\psi(0)|\eta_{(c,b)}(p)\rangle\langle\eta_{(c,b)}(p)|\bar{\psi}(y^-)\not{n}\gamma^5\psi(y^-+y_2^-)|0\rangle,
\end{aligned} \tag{4.17}$$

where we have suppressed the spinor and color indices, as well as the gauge links, and the X in the outgoing states is removed since it is an exclusive process. After proper Poincaré translation and y^--integral, we have

$$\begin{aligned}
&\mathcal{D}_{[Q\bar{Q}(^1S_0^{[1]})]\to\eta_{(c,b)}}(z,\zeta_1,\zeta_2;m_Q,\mu_0)\\
&\quad=\frac{1}{16N_c}\delta(1-z)\int\frac{dy_1^-}{2\pi}\frac{dy_2^-}{2\pi}e^{ip^+[(1-\zeta_2)/2]\,y_1^-}e^{-ip^+[(1-\zeta_1)/2]\,y_2^-}\\
&\quad\times\langle 0|\bar{\psi}(y_1^-)\not{n}\gamma^5\psi(0)|\eta_{(c,b)}(p)\rangle\langle\eta_{(c,b)}(p)|\bar{\psi}(0)\not{n}\gamma^5\psi(y_2^-)|0\rangle.
\end{aligned} \tag{4.18}$$

With this equation and Eq. (4.16), the relation between the heavy quark pair fragmentation functions and the twist-2 LCDAs for process $[Q\bar{Q}(a^{[1]})]\to\eta_{(c,b)}$ is straightforward,

$$\begin{aligned}
&\mathcal{D}_{[Q\bar{Q}(^1S_0^{[1]})]\to\eta_{(c,b)}}(z,\zeta_1,\zeta_2;m_Q,\mu_0)\\
&\quad=\frac{1}{(8\pi)^2N_c}\delta(1-z)f_\eta^2\,\hat{\phi}_\eta(\frac{1+\zeta_1}{2})\,\hat{\phi}_\eta^{\,*}(\frac{1+\zeta_2}{2}).
\end{aligned} \tag{4.19}$$

We can use this relation to cross-check our calculations of color singlet heavy

quark pair fragmentation functions.

Chapter 5

Calculation of Heavy Quark Pair Fragmentation in NRQCD factorization model: General Analysis

As analyzed at the end of Sec. 4.4, the predictive power of QCD factorization theorem depends on our knowledge of the fragmentation functions (FFs) at an input scale μ_0. If choosing $\mu_0 \gtrsim 2m_Q$, we can use the NRQCD factorization approach to further factorize the perturbative part with energy scale $\sim m_Q$ with the non-perturbative part with energy scale much smaller than m_Q. After this calculation, we can express dozens of multi-variable FFs in terms of a few NRQCD long-distance matrix elements (LDMEs), therefore greatly increasing the predictive power of the QCD factorization theorem.

In this chapter, we explain in detail the techniques used in our calculation of these FFs in the NRQCD factorization approach. In Sec. 5.1, we first show how to match the FFs to the NRQCD factorization approach. After the matching, we can calculate these FFs order by order in α_s. We will use the projection method to do this calculation, which is the topic of Sec. 5.2. The result, however, is usually IR divergent. If the NRQCD factorization approach is valid to NLO, the IR divergence should be canceled by the NRQCD LDMEs. In Sec. 5.3, we expand the NRQCD LDMEs to NLO in perturbative NRQCD. In Sec. 5.4, we constrain the structures of the short-distance coefficients with the discrete symmetries. Finally in Sec. 5.5, we prove a very important trick to simplify our calculations.

5.1 Matching to NRQCD factorization

In this section, we overview the method of matching the fragmentation functions onto NRQCD. We first briefly discuss the single parton fragmentation process for completeness. Then we focus on heavy quark pair fragmentation and work out a formula to calculate the short distance coefficients.

5.1.1 Calculation of single-parton FFs

By matching the fragmentation functions defined in Sec. 4.3 onto NRQCD, We can write the NRQCD factorization formalism for heavy quarkonium FFs from a single parton as [23, 24, 43]

$$D_{f\to H}(z;m_Q,\mu_0)=\sum_{[Q\bar{Q}(n)]}\hat{d}_{f\to[Q\bar{Q}(n)]}(z;m_Q,\mu_0,\mu_\Lambda)\langle\mathcal{O}^H_{[Q\bar{Q}(n)]}(\mu_\Lambda)\rangle, \tag{5.1}$$

where H represents a particular physical heavy quarkonium state, $\mu_0\gtrsim 2m_Q$ represents the input QCD factorization scale at which the $\ln(\mu_0/m_Q)$-type logarithmic contributions to the production cross section are comparable with the m_Q/μ_0-type power suppressed contribution, and $\mu_\Lambda\sim m_Q$ is the NRQCD factorization scale and does not have to be equal to μ_0. The summation runs over all intermediate non-relativistic $Q\bar{Q}$ states, which are labeled as $n={}^{2S+1}L_J^{[1,8]}$, with the superscript $^{[1]}$ (or $^{[8]}$) denoting the color singlet (or octet) state. Short-distance coefficients $\hat{d}_{f\to[Q\bar{Q}(n)]}(z;m_Q,\mu_0,\mu_\Lambda)$ describe the dynamics at an energy scale larger than $\mu_\Lambda\gg\Lambda_{QCD}$; thus they could be calculated perturbatively. The LDMEs $\langle\mathcal{O}^H_{[Q\bar{Q}(n)]}(\mu_\Lambda)\rangle$ include all interaction below scale μ_Λ and are intrinsically non-perturbative. These universal LDMEs are scaled in powers of the $Q\bar{Q}$ pair's relative velocity $v\ll 1$ in the rest frame of H, which we have discussed in Sec. 3.4.2. Hence, in practice, the summation could be approximately truncated, with only a few terms left to be considered (see Table 3.4). In Eq. (5.1), the factorization scales μ_0 and μ_Λ, along with the LDMEs, should be determined by fitting the experimental data.

Since the short-distance coefficients $\hat{d}_{f\to[Q\bar{Q}(n)]}(z;m_Q,\mu_0,\mu_\Lambda)$ are not sensitive to long-distance details of the heavy quarkonium state, the same factorization formula in Eq. (5.1) could be applied to an asymptotic partonic state, such as an asymptotic $Q\bar{Q}$ pair state. By replacing the heavy quarkonium state H with an asymptotic $Q\bar{Q}$ pair state, $[Q\bar{Q}(n')]$, we can write

$$D_{f\to[Q\bar{Q}(n')]}(z;m_Q,\mu_0)=\sum_{[Q\bar{Q}(n)]}\hat{d}_{f\to[Q\bar{Q}(n)]}(z;m_Q,\mu_0,\mu_\Lambda)\langle\mathcal{O}^{[Q\bar{Q}(n')]}_{[Q\bar{Q}(n)]}(\mu_\Lambda)\rangle. \tag{5.2}$$

With this form, one could calculate the $D_{f\to[Q\bar{Q}(n')]}(z;m_Q,\mu_0)$ on the left with perturbative QCD and the $\langle\mathcal{O}^{[Q\bar{Q}(n')]}_{[Q\bar{Q}(n)]}(\mu_\Lambda)\rangle$ on the right with perturbative NRQCD. If the NRQCD factorization is valid for these input FFs, the LDMEs on the right should reproduce all infrared (IR) and Coulomb divergences in $D_{f\to[Q\bar{Q}(n')]}(z;m_Q,\mu_0)$, with short-distance coefficients $\hat{d}_{f\to[Q\bar{Q}(n)]}(z;m_Q,\mu_0,\mu_\Lambda)$ IR safe to all orders.

However, there is a major difference between applying the NRQCD factorization to heavy quarkonium production cross sections and to the heavy quarkonium FFs [24]. For the production cross section, all perturbative UV divergences are completely taken care of by the renormalization of QCD. For the input FFs, on the other hand, there are additional perturbative UV divergences associated with the composite operators that define the FFs. Since the NRQCD factorization on the right-hand side (RHS) of Eq. (5.1), so as Eq. (5.2), is a factorization of the soft region corresponding to heavy quark binding, it does not deal with the UV divergence of the composite operators defining the FFs on the left-hand side (LHS) of the same equation. That is, the matching in Eq. (5.1), so as in Eq. (5.2), and similarly, that in Eq. (5.3) below, makes sense only if all perturbative UV divergences associated with the composite operators defining the FFs on the LHS are renormalized and any ambiguity in connection with this renormalization is simply a part of the factorization scheme dependence of the FFs [24].

Although a formal proof for the NRQCD factorization formula in Eq. (5.1) is still lacking, the derivation of the coefficients $\hat{d}_{f\to[Q\bar{Q}(n)]}(z;m_Q,\mu_0,\mu_\Lambda)$ by calculating both sides of Eq. (5.2) perturbatively actually provides an explicit verification of the factorization formalism, order by order in perturbation theory. In the case of single parton FFs, we calculated all the short-distance coefficients up to $\mathcal{O}(\alpha_s^2)$ and no inconsistency was found. Many of these single parton FFs have been calculated before and are available in the literature [79–81, 107–111]. We found that our results agree with almost all of them. Since enough calculation details were presented in those early papers, here we simply list our complete results for single parton FFs in Appendix A and point out any differences from early publications.

5.1.2 Calculation of $Q\bar{Q}$ pair FFs

Assuming that the NRQCD factorization works for the heavy quarkonium FFs, we can factorize the heavy quarkonium FFs from a $Q\bar{Q}$ pair as [24]

$$\begin{aligned}&\mathcal{D}_{[Q\bar{Q}(\kappa)]\to H}(z,\zeta_1,\zeta_2;m_Q,\mu_0)\\&\quad=\sum_{[Q\bar{Q}(n)]}\hat{d}_{[Q\bar{Q}(\kappa)]\to[Q\bar{Q}(n)]}(z,\zeta_1,\zeta_2;m_Q,\mu_0,\mu_\Lambda)\langle\mathcal{O}^H_{[Q\bar{Q}(n)]}(\mu_\Lambda)\rangle,\end{aligned}\tag{5.3}$$

where the symbols have the same meaning as those in Eq. (5.1). Similar to the case of single parton fragmentation, if the factorization formalism in Eq. (5.3) is valid, it should also be valid if we replace the heavy quarkonium state H by any asymptotic partonic state. By replacing the heavy quarkonium state H with an asymptotic $Q\bar{Q}$ pair state, $[Q\bar{Q}(n')]$, we can write

$$\begin{aligned}&\mathcal{D}_{[Q\bar{Q}(\kappa)]\to[Q\bar{Q}(n')]}(z,\zeta_1,\zeta_2;m_Q,\mu_0)\\&\quad=\sum_{[Q\bar{Q}(n)]}\hat{d}_{[Q\bar{Q}(\kappa)]\to[Q\bar{Q}(n)]}(z,\zeta_1,\zeta_2;m_Q,\mu_0,\mu_\Lambda)\langle\mathcal{O}^{[Q\bar{Q}(n')]}_{[Q\bar{Q}(n)]}(\mu_\Lambda)\rangle\,,\end{aligned}\tag{5.4}$$

and derive the short-distance coefficients, $\hat{d}_{[Q\bar{Q}(\kappa)]\to[Q\bar{Q}(n)]}(z,\zeta_1,\zeta_2;m_Q,\mu_0,\mu_\Lambda)$ above by calculating both sides of the equation, perturbatively. If the factorization is valid, any IR sensitivity of the fragmentation function to an asymptotic state of a $Q\bar{Q}$ pair on the LHS of the equation should be systematically absorbed into the NRQCD LDMEs on the RHS, in the same manner as in Eq. (5.2). As explained in the last subsection, the matching in Eq. (5.3), so as Eq. (5.4), is possible only if the UV renormalization of the composite operators defining the FFs on the LHS of the equation is taken care of [24].

In this paper, we use dimensional regularization to regularize various divergences involved in our NLO calculations. With the definition in Eq. (4.10),

we have an explicit D-dimensional expression for the LHS of Eq. (5.4) as

$$\begin{aligned}
&\mathcal{D}_{[Q\bar{Q}(s^{[b]})]\to[Q\bar{Q}(i^{[b']})]}(z,\zeta_1,\zeta_2;m_Q,\mu_0)\\
&=\frac{z^{D-2}}{N_s N_b N_i^{\rm NR} N_{b'}^{\rm NR}}\int\frac{{\rm d}^D p_c}{(2\pi)^D}\left(\prod_X\int\frac{{\rm d}^{D-1}p_X}{(2\pi)^{D-1}2E_X}\right)\delta(z-\frac{p^+}{p_c^+})\\
&\quad\times\mathcal{M}_{[Q\bar{Q}(s^{[b]})]\to[Q\bar{Q}(i^{[b']})]}(p,z,\zeta_1,\zeta_2)(2\pi)^D\delta^D(p_c-p-\sum_X p_X)+{\rm UVCT}(\mu_0)\\
&=\frac{z^{D-2}}{N_s N_b N_i^{\rm NR} N_{b'}^{\rm NR}}\left(\prod_X\int\frac{{\rm d}^{D-1}p_X}{(2\pi)^{D-1}2E_X}\right)\delta(z-\frac{p^+}{p_c^+})\\
&\quad\times\mathcal{M}_{[Q\bar{Q}(s^{[b]})]\to[Q\bar{Q}(i^{[b']})]}(p,z,\zeta_1,\zeta_2)+{\rm UVCT}(\mu_0)\,,
\end{aligned}\tag{5.5}$$

where p is the momentum of the produced heavy quark state $[Q\bar{Q}(i^{[b']})]$, and "UVCT(μ_0)" indicates the UV counter-term needed to remove the UV divergence associated with the composite operators defining the FFs. In Eq. (5.5), we have separated the spinor and color labels for both the initial and final $Q\bar{Q}$ pair. s and b (i and b') denote the spin and color state for the incoming (outgoing) $Q\bar{Q}$ pair. s could be vector (v), axial-vector (a) or tensor (t). i is labeled with the spectroscopic notation $^{2S+1}L_J$. Color state b and b' can be either "1" for color singlet or "8" for color octet. N_s and N_b ($N_i^{\rm NR}$ and $N_{b'}^{\rm NR}$) are the spin and color normalization factors for the incoming (outgoing) $Q\bar{Q}$ pair. Their definitions are listed in Sec. 5.2. The phase space integration for the unobserved particles X is given explicitly.

The function $\mathcal{M}$ in Eq. (5.5) is given by

$$\begin{aligned}
&\mathcal{M}_{[Q\bar{Q}(s^{[b]})]\to[Q\bar{Q}(i^{[b']})]}(p,z,\zeta_1,\zeta_2)\\
&\quad={\rm Tr}\left[\Gamma_s(p_c)\,C_b\,\mathcal{A}_{[Q\bar{Q}(s^{[b]})]\to[Q\bar{Q}(i^{[b']})]}(p,z,\zeta_1)\right]\\
&\quad\times{\rm Tr}\left[\Gamma_s^\dagger(p_c)\,C_b^\dagger\,\mathcal{A}^\dagger_{[Q\bar{Q}(s^{[b]})]\to[Q\bar{Q}(i^{[b']})]}(p,z,\zeta_2)\right]\times P_s(p_c)\,P_i^{\rm NR}(p)\,,
\end{aligned}\tag{5.6}$$

where "Tr" is understood as the trace for both spinor and color. In deriving Eq. (5.6), we explicitly write the spinor (color) projection operator $\mathcal{P}^{(s)}(p_c)$ (and $\mathcal{C}^{[I]}$) in Eq. (4.10) as a product of the corresponding operator in the scattering amplitude and that in its complex conjugate, such that $\mathcal{P}^{(s)}(p_c)\equiv\Gamma_s(p_c)\Gamma_s^\dagger(p_c)P_s/N_s$ (and $\mathcal{C}^{[I]}\equiv C_bC_b^\dagger/N_b$). All of these projection operators and corresponding normalization factors are listed in Sec. 5.2.

The transition amplitude $\mathcal{A}$ in Eq. (5.6) is defined as

$$\mathcal{A}_{[Q\bar{Q}(s^{[b]})]\to[Q\bar{Q}(i^{[b']})]}(p,z,\zeta_1) = \lim_{q_r\to 0}\left(\prod_{j=0}^{L}\frac{\mathrm{d}}{\mathrm{d}q_r^{\alpha_j}}\right)\left\{\int\frac{\mathrm{d}^D q_1}{(2\pi)^D}\times 2\,\delta(\zeta_1-\frac{2q_1^+}{p_c^+})\right.$$
$$\left.\times\,\bar{\mathcal{A}}_{[Q\bar{Q}(s^{[b]})]\to[Q\bar{Q}(i^{[b']})]}(q_1,q_r)\,\Gamma_i^{\mathrm{NR}}(p)\,C_{b'}^{\mathrm{NR}}\right\}, \tag{5.7}$$

where $\bar{\mathcal{A}}$ is the amputated amplitude, and the factor 2 in front of the delta function comes from the integration of y_1^- in Eq. (4.10). Spin projection operators Γ_i^{NR} and color projection operators $C_{b'}^{\mathrm{NR}}$ for outgoing Q and $\bar{Q}$ are defined in Sec. 5.2, which may have Lorentz indexes and color indices, respectively. In Eq. (5.7), q_1 (q_r) is the momentum of the incoming (outgoing) heavy quark relative to the incoming (outgoing) $Q\bar{Q}$ pair's center of mass. The derivative operation, $\prod_{j=0}^{L}\mathrm{d}/\mathrm{d}q_r^{\alpha_j}$, with α_j the Lorentz index of momentum q_r, picks up the contribution to the L^{th} orbital angular momentum state, with $L=1,2,3\ldots$ corresponding to the orbital angular momentum state S, P, $D\ldots$ of the final $Q\bar{Q}$ pair, respectively. For the contribution to a S-wave $Q\bar{Q}$ state, $\prod_{j=0}^{L=0}\mathrm{d}/\mathrm{d}q_r^{\alpha_j}=1$, and there is no need for the derivative operation on q_r. For higher orbital momentum states, $L>0$, we expand the amplitude to the L^{th}-order in q_r.

Note that in Eq. (5.7), $\lim_{q_r\to 0}\left(\prod_{j=0}^{L}\mathrm{d}/\mathrm{d}q_r^{\alpha_j}\right)$, the limit and derivative operation, is outside of the q_1 integration. In principle, we should keep q_r finite in the integration of q_1, which is usually difficult and tedious. In Sec. 5.5, we will show that we are qualified to do the derivative and limit before the q_1-integral. By doing this, the Coulomb region does not appear on the LHS of Eq. (5.4). Since the short distance coefficients on the RHS of Eq. (5.4) is the effect of the hard region only, the ignorance of the Coulomb region has no effect to our results. More details are in Sec. 5.5.

5.2 QCD and NRQCD projection operators

To obtain the short distance coefficients in Eq. (5.2) and (5.4), we can expand a general amplitude by NRQCD LDMEs and pick up the coefficient needed, or we can project the outgoing heavy quark pair to a certain NRQCD state with some projection operators. The former is named "Threshold Expansion" method [109] and the later is usually called "Projection" method [112]. Because the heavy quark is represented by 4-component Dirac spinor in full QCD and 2-component Pauli spinor in NRQCD, to do the matching, we need to

convert one to the other in our calculation. The threshold Expansion method converts the Dirac spinor to Pauli spinor, while the Projection method does the opposite. The two methods can be shown equivalent. In this paper, we will adopt the Projection method. In this section, we give the QCD projection operator for the incoming heavy quark pair, as well as the NRQCD projection operators for all unpolarized S-wave and P-wave outgoing heavy quark pair. Projection operators for polarized outgoing heavy quark pairs are given in chapter 8.

5.2.1 Projection operators in QCD factorization

The heavy quark pair fragmentation function to a physical heavy quarkonium is defined in Eq. (4.10), in which there are two operators $\mathcal{P}^{(s)}_{ij,kl}(p_c)$ and $\mathcal{C}^{[I]}_{ab,cd}$ projecting the fragmenting heavy quark pair to a particular spin and color state. Subscripts i, j, k, l are the spinor indices and a, b, c, d label the color of each field. All of the definitions are given in Eqs. (4.11) and (4.12). Here we generalize them to D-dimension, which are convenient with dimensional regularization.

The definitions of $\mathcal{P}^{(s)}_{ij,kl}(p_c)$ in D dimensions are

$$\mathcal{P}^{(v)}(p_c)_{ij,kl} = \frac{1}{4p_c\cdot\hat{n}}\,(\gamma\cdot\hat{n})_{ij}\,\frac{1}{4p_c\cdot\hat{n}}\,(\gamma\cdot\hat{n})_{kl}, \tag{5.8a}$$

$$\mathcal{P}^{(a)}(p_c)_{ij,kl} = \frac{1}{4p_c\cdot\hat{n}}\,\frac{[\gamma\cdot\hat{n}\,,\gamma_5]_{ij}}{2}\,\frac{1}{4p_c\cdot\hat{n}}\,\frac{[\gamma\cdot\hat{n}\,,\gamma_5]_{kl}}{2}, \tag{5.8b}$$

$$\mathcal{P}^{(t)}(p_c)_{ij,kl} = \frac{1}{D-2}\sum_{\rho=1,2,\cdots,D-2}\frac{1}{4p_c\cdot\hat{n}}\,(\gamma\cdot\hat{n}\,\gamma^{\rho}_{\perp})_{ij}\,\frac{1}{4p_c\cdot\hat{n}}\,(\gamma\cdot\hat{n}\,\gamma^{\rho}_{\perp})_{kl}, \tag{5.8c}$$

where the superscripts (v), (a), or (t) represent that the heavy quark pair is in a vector, axial-vector or tensor state, respectively, and $\hat{n}$ is a light-like vector, defined in Sec. 4.2. To keep the charge conjugation invariance of the axial-vector heavy quark pair fragmentation function in dimensional regularization, we use $[\gamma\cdot\hat{n}\,,\gamma_5]/2 = (\gamma\cdot\hat{n}\,\gamma_5 - \gamma_5\,\gamma\cdot\hat{n})/2$ instead of $\gamma\cdot\hat{n}\,\gamma_5$.

The definitions of color projection operators $\mathcal{C}^{[I]}_{ab,cd}$ are

$$\mathcal{C}^{[1]}_{ab,cd} = \frac{1}{\sqrt{N_c}}\delta_{a,b}\frac{1}{\sqrt{N_c}}\delta_{c,d}, \tag{5.9a}$$

$$\mathcal{C}^{[8]}_{ab,cd} = \frac{2}{N_c^2-1}\sum_f (t^{(F)}_f)_{ab}\,(t^{(F)}_f)_{cd}. \tag{5.9b}$$

In Eqs. (5.5), (5.6) and (5.7), we split $\mathcal{P}^{(s)}(p_c)$ and $\mathcal{C}^b$ into products of

several operators and normalization factors as

$$\mathcal{P}^{(s)} = \frac{\Gamma_s(p_c)\Gamma_s^\dagger(p_c)}{N_s} P_s, \tag{5.10a}$$

$$\mathcal{C}^b = \frac{C_b C_b^\dagger}{N_b}, \tag{5.10b}$$

where the indices are suppressed, and all operators are understood to be inserted in the proper location as they are in Eqs. (5.5) and (5.6). In Eq. (5.10), s could be vector (v), axial-vector (a), or tensor (t), and b could be "1" for color singlet or "8" for color octet. The operators in Eq. (5.10a) are defined in D dimension as

$$\Gamma_v(p_c) = \frac{\gamma \cdot \hat{n}}{4p_c \cdot \hat{n}} \ , \ N_v = 1, \tag{5.11a}$$

$$\Gamma_a(p_c) = \frac{[\gamma \cdot \hat{n}\,, \gamma_5]}{8p_c \cdot \hat{n}} \ , \ N_a = 1, \tag{5.11b}$$

$$\Gamma_t(p_c) = \frac{\gamma \cdot \hat{n}\, \gamma^\rho}{4p_c \cdot \hat{n}} \ , \ N_t = D - 2, \tag{5.11c}$$

and

$$P_v(p_c) = P_a(p_c) = 1, \tag{5.12a}$$

$$P_t(p_c) = -g_{\rho\rho'} + \frac{(p_c)_\rho \hat{n}_{\rho'} + (p_c)_{\rho'} \hat{n}_\rho}{p_c \cdot \hat{n}} - \frac{p_c^2}{(p_c \cdot \hat{n})^2} \hat{n}_\rho \hat{n}_{\rho'}, \tag{5.12b}$$

where Lorentz index ρ' is the counterpart of ρ in $\Gamma_t^\dagger(p_c)$.

The color operators in Eq. (5.10b) are defined as

$$C_1 = \frac{\mathbf{1}}{\sqrt{N_c}} \ , \ N_1 = 1, \tag{5.13a}$$

$$C_8 = \sqrt{2}\, t_a^{(F)} \ , \ N_8 = N_c^2 - 1, \tag{5.13b}$$

where $\mathbf{1}$ is a 3×3 unit matrix, the superscript (F) represents the fundamental representation of SU(3), and subscript a is summed between C_8 and $C_8^\dagger$.

5.2.2 Projection operators in NRQCD factorization

NRQCD projectors $N_{b'}^{\rm NR}$ in Eq. (5.5) and $C_{b'}^{\rm NR}$ in Eq. (5.7) are the same as the color projection operators of QCD factorization in Eq. (5.13), that is

$$C_{b'}^{\rm NR} = C_{b'} \ , \ N_{b'}^{\rm NR} = N_{b'}. \tag{5.14}$$

However, the meaning of $N_8 = N_c^2 - 1$ and that of $N_8^{\rm NR} = N_c^2 - 1$ are significantly different. The former indicates that the $Q\bar{Q}$ pair FFs are defined to average over the color of the fragmenting pair. In contrast, the latter means that we need to average over the color of the NRQCD states in the short-distance coefficients, since the NRQCD LDMEs in Eqs. (3.10) and (3.12) are defined to sum over all possible color states of the heavy quark pair.

The NRQCD spinor projection operators $\Gamma_i^{\rm NR}$ in Eq. (5.7) are given by

$$\Gamma_i^{\rm NR}(p) = \frac{1}{\sqrt{8m_Q^3}}(\frac{\not{p}}{2} - \not{q}_r - m_Q)\gamma_5(\frac{\not{p}}{2} + \not{q}_r + m_Q) \qquad \text{if } i \text{ is spin singlet,} \tag{5.15a}$$

$$\Gamma_i^{\rm NR}(p) = \frac{1}{\sqrt{8m_Q^3}}(\frac{\not{p}}{2} - \not{q}_r - m_Q)\gamma^\beta(\frac{\not{p}}{2} + \not{q}_r + m_Q) \qquad \text{if } i \text{ is spin triplet,} \tag{5.15b}$$

where m_Q is the heavy quark mass. The factor $1/(8m_Q^3)^{1/2}$ is partly caused by different normalizations between the individual heavy quark and the pair, and we refer the interested readers to Ref. [113], for example, for a more detailed discussion.

The normalization factors $N_i^{\rm NR}$ in Eq. (5.5) are defined as the number of states in D dimension (number of color states are not counted here),

$$N_{^1S_0}^{\rm NR} = N_{^3P_0}^{\rm NR} = 1, \tag{5.16a}$$

$$N_{^3S_1}^{\rm NR} = N_{^1P_1}^{\rm NR} = D - 1, \tag{5.16b}$$

$$N_{^3P_1}^{\rm NR} = \frac{1}{2}(D-1)(D-2), \tag{5.16c}$$

$$N_{^3P_2}^{\rm NR} = \frac{1}{2}(D+1)(D-2), \tag{5.16d}$$

$$\sum_{J=0,1,2} N_{^3P_J}^{\rm NR} = (D-1)^2. \tag{5.16e}$$

The $P_i^{\rm NR}$ in Eq. (5.6) are defined as,

$$P_{^1S_0}^{\rm NR} = 1, \tag{5.17a}$$
$$P_{^3S_1}^{\rm NR} = \mathbb{P}^{\beta\beta'}(p), \tag{5.17b}$$
$$P_{^1P_1}^{\rm NR} = \mathbb{P}^{\alpha\alpha'}(p), \tag{5.17c}$$
$$P_{^3P_0}^{\rm NR} = \frac{1}{D-1}\mathbb{P}^{\alpha\beta}(p)\mathbb{P}^{\alpha'\beta'}(p), \tag{5.17d}$$
$$P_{^3P_1}^{\rm NR} = \frac{1}{2}(\mathbb{P}^{\alpha\alpha'}(p)\mathbb{P}^{\beta\beta'}(p) - \mathbb{P}^{\alpha\beta'}(p)\mathbb{P}^{\beta\alpha'}(p)), \tag{5.17e}$$
$$P_{^3P_2}^{\rm NR} = \frac{1}{2}(\mathbb{P}^{\alpha\alpha'}(p)\mathbb{P}^{\beta\beta'}(p) + \mathbb{P}^{\alpha\beta'}(p)\mathbb{P}^{\beta\alpha'}(p)) - \frac{1}{D-1}\mathbb{P}^{\alpha\beta}(p)\mathbb{P}^{\alpha'\beta'}(p), \tag{5.17f}$$

where $\mathbb{P}^{\mu\nu}(p)$ is given by

$$\mathbb{P}^{\alpha\alpha'}(p) = -g^{\alpha\alpha'} + \frac{p^\alpha p^{\alpha'}}{p^2}\,, \tag{5.18}$$

and the Lorentz index α will be contracted with the Lorentz index from the derivative in Eq. (5.7), and the primed Lorentz indices are for the complex conjugate of the amplitude, which are the counterparts of the unprimed ones in the amplitude.

5.3 Expand LDMEs to NLO with perturbative NRQCD

The calculation of the LHS of Eq. (5.2) and (5.4) with the projection operators given in last section is usually IR-divergent. The IR divergence needs to be absorbed in the NRQCD LDMEs on the RHS of these equations. After replacing the final heavy quarkonium by an asymptotic heavy quark pair, we can calculate the NRQCD LDMEs on the RHS of Eqs. (5.2) and (5.4) perturbatively in NRQCD effective theory. These LDMEs with both initial and final state being a heavy quark pair does not depend on the hard process. Therefore they can be calculated once and for all. Here we summarize the results for unpolarized heavy quark pair in the literature [36, 112, 114–117]. The results for polarized NRQCD LDMEs are given in chapter 8.

$$\langle\mathcal{O}^{Q\bar{Q}}(^1S_0^{[1]})\rangle = \langle\mathcal{O}^{Q\bar{Q}}(^1S_0^{[1]})\rangle_{\rm LO} - C_\epsilon\frac{1}{2N_c}\langle\mathcal{O}^{Q\bar{Q}}(^1P_1^{[8]})\rangle_{\rm LO}, \tag{5.19a}$$
$$\langle\mathcal{O}^{Q\bar{Q}}(^1S_0^{[8]})\rangle = \langle\mathcal{O}^{Q\bar{Q}}(^1S_0^{[8]})\rangle_{\rm LO}$$

$$- C_\epsilon \left[C_F \langle \mathcal{O}^{Q\bar{Q}}({}^1P_1^{[1]}) \rangle_{\rm LO} + B_F \langle \mathcal{O}^{Q\bar{Q}}({}^1P_1^{[8]}) \rangle_{\rm LO} \right], \tag{5.19b}$$

$$\langle \mathcal{O}^{Q\bar{Q}}({}^1P_1^{[1]}) \rangle = \langle \mathcal{O}^{Q\bar{Q}}({}^1P_1^{[1]}) \rangle_{\rm LO} - C_\epsilon \frac{1}{2N_c} \langle \mathcal{O}^{Q\bar{Q}}({}^1D_2^{[8]}) \rangle_{\rm LO}, \tag{5.19c}$$

$$\begin{aligned} \langle \mathcal{O}^{Q\bar{Q}}({}^1P_1^{[8]}) \rangle &= \langle \mathcal{O}^{Q\bar{Q}}({}^1P_1^{[8]}) \rangle_{\rm LO} \\ &- C_\epsilon \left[C_F \langle \mathcal{O}^{Q\bar{Q}}({}^1D_2^{[1]}) \rangle_{\rm LO} + B_F \langle \mathcal{O}^{Q\bar{Q}}({}^1D_2^{[8]}) \rangle_{\rm LO} \right], \end{aligned} \tag{5.19d}$$

$$\langle \mathcal{O}^{Q\bar{Q}}({}^3S_1^{[1]}) \rangle = \langle \mathcal{O}^{Q\bar{Q}}({}^3S_1^{[1]}) \rangle_{\rm LO} - C_\epsilon \frac{1}{2N_c} \sum_{J=0}^{2} \langle \mathcal{O}^{Q\bar{Q}}({}^3P_J^{[8]}) \rangle_{\rm LO}, \tag{5.19e}$$

$$\begin{aligned} \langle \mathcal{O}^{Q\bar{Q}}({}^3S_1^{[8]}) \rangle &= \langle \mathcal{O}^{Q\bar{Q}}({}^3S_1^{[8]}) \rangle_{\rm LO} \\ &- C_\epsilon \sum_{J=0}^{2} \left[C_F \langle \mathcal{O}^{Q\bar{Q}}({}^3P_J^{[1]}) \rangle_{\rm LO} + B_F \langle \mathcal{O}^{Q\bar{Q}}({}^3P_J^{[8]}) \rangle_{\rm LO} \right], \end{aligned} \tag{5.19f}$$

$$\langle \mathcal{O}^{Q\bar{Q}}({}^3P_J^{[1]}) \rangle = \langle \mathcal{O}^{Q\bar{Q}}({}^3P_J^{[1]}) \rangle_{\rm LO} - C_\epsilon \frac{1}{2N_c} \sum_{J'=0}^{2} C_{J,J'} \langle \mathcal{O}^{Q\bar{Q}}({}^3D_{J'}^{[8]}) \rangle_{\rm LO}, \tag{5.19g}$$

$$\begin{aligned} \langle \mathcal{O}^{Q\bar{Q}}({}^3P_J^{[8]}) \rangle &= \langle \mathcal{O}^{Q\bar{Q}}({}^3P_J^{[8]}) \rangle_{\rm LO} \\ &- C_\epsilon \sum_{J'=0}^{2} C_{J,J'} \left[C_F \langle \mathcal{O}^{Q\bar{Q}}({}^3D_{J'}^{[1]}) \rangle_{\rm LO} + B_F \langle \mathcal{O}^{Q\bar{Q}}({}^3D_{J'}^{[8]}) \rangle_{\rm LO} \right], \end{aligned} \tag{5.19h}$$

where

$$C_\epsilon = \left(\frac{1}{\epsilon} + \ln 4\pi - \gamma_E\right) \left(\frac{\mu_r}{\mu_\Lambda}\right)^{2\epsilon} \frac{4\alpha_s}{3\pi m_Q^2}, \tag{5.20}$$

and $C_{J,J'}$ is the generalized Clebsch-Gordan coefficient [116]. In D dimensions, when $J' = 1, 2, 3$, we have $C_{0,J'} = \frac{(D-2)(D+1)}{2(D-1)^2}, 0, 0$; $C_{1,J'} = \frac{D+1}{4(D-1)}, \frac{3}{4}, 0$; $C_{2,J'} = \frac{(D-3)^2}{4(D-1)^2}, \frac{1}{4}, 1$. Notice Eq. (5.19) is calculated with dimensional regularization and $\overline{\rm MS}$ scheme. It is straightforward to derive the results in other schemes. With Eq. (5.19) , the only task left is to calculate the LHS of Eqs. (5.2) and (5.4) in perturbative QCD with dimensional regularization and $\overline{\rm MS}$ scheme.

5.4 Symmetries

In this section, we show how fundamental symmetries constrain the structure of the FFs calculated in the NRQCD factorization approach.

5.4.1 Color charge conservation

Color charge conservation could be a serious constraint for partonic contributions to $Q\bar{Q}$ pair FFs to a non-relativistic $Q\bar{Q}$ pair without radiating any additional partons into the final-state. For these FFs, such as LO contribution, $\mathcal{D}^{\rm LO}_{[Q\bar{Q}(s^{[b]})]\to[Q\bar{Q}(i^{[b']})]}$, and the NLO virtual contribution, $\mathcal{D}^{\rm NLO\text{-}V}_{[Q\bar{Q}(s^{[b]})]\to[Q\bar{Q}(i^{[b']})]}$, the color of the fragmenting QCD heavy quark pair $[Q\bar{Q}(s^{[b]})]$ should be the same as that of final-state non-relativistic heavy quark pair $[Q\bar{Q}(i^{[b']})]$, or $b = b'$. Because of the color normalizaiton $N_8^{\rm NR}$ for NRQCD matrix elements, as defined in Eq. (5.14) , the color charge conservation requires $\mathcal{D}^{\rm LO}_{[Q\bar{Q}(s^{[8]})]\to[Q\bar{Q}(i^{[8]})]} = (N_c^2-1)^{-1} \times \mathcal{D}^{\rm LO}_{[Q\bar{Q}(s^{[1]})]\to[Q\bar{Q}(i^{[1]})]}$.

5.4.2 Lorentz invariance

Even if the initial and the final $Q\bar{Q}$ pair are in the same color state, the partonic contributions to $\mathcal{D}_{[Q\bar{Q}(s^{[b]})]\to[Q\bar{Q}(i^{[b]})]}$ without radiating any parton to the final-state may still vanish, due to Lorentz invariance, or more precisely, angular momentum conservation. For initial-state $s = v, a, t$ and final-state $i = {}^1S_0, {}^3S_1, {}^1P_1, {}^3P_0, {}^3P_1, {}^3P_2$, we can have a total of 18 (or 24) channels (if we distinguish the two initial tensor states). By applying Lorentz invariance, 8 out of the 18 partonic fragmentation channels vanish. Once all loop integrations are performed, contributions to all these fragmentation channels can only depend on two momentum vectors, $\hat{n}$ and p, and three polarization vectors: ϵ_α for the $L = 1$ states, ϵ_β for the $S = 1$ states, and ϵ_ρ if the initial $Q\bar{Q}$ pair is in the t state.

If there is one γ^5 in the combined initial- and final-state spin projector: $\Gamma_s\Gamma_i^{\rm NR}$, we need two of three possible polarization vectors (ϵ's discussed above) plus the two linear momenta $\hat{n}$ and p to construct the Levi-Civita tensor. Consequently, the partonic fragmentation channels: $v \to {}^1S_0$, $t \to {}^1S_0$, $a \to {}^3S_1$, and $v \to {}^1P_1$ must vanish.

Since p^α and p^β give zero when contracting with ϵ_α (for $L = 1$ states) and ϵ_β (for $S = 1$ states), respectively, the Lorentz structure of the amplitude of the process $v \to {}^3P_J$ must be a linear combination of $\hat{n}^\alpha\hat{n}^\beta$ and $g^{\alpha\beta}$, which is symmetric under the exchange of α and β. For the amplitude of the process $a \to {}^3P_J$, the Lorentz structure must be $\epsilon^{\alpha\beta\mu\nu}n_\mu p_\nu$, which is anti-symmetric under the exchange of α and β. Therefore, the partonic fragmentation processes: $v \to {}^3P_1$, $a \to {}^3P_0$ and $a \to {}^3P_2$ are not allowed, since the ${}^3P_{0,2}$ are symmetric between the spin and orbital angular momentum while ${}^3P_1$ is antisymmetric between spin and orbital angular momentum.

Finally, the partonic fragmentation channel: $t \to {}^3P_0$ must vanish because p^ρ and $\hat{n}^\rho$ give zero when contracted with the tensor polarization vector ϵ_ρ,

and there is no other Lorentz structure to take the index ρ. Our explicit calculations up to NLO in α_s support our analysis and confirm these constraints.

5.4.3 Reality and symmetries

As both the cross section and the partonic hard part are real, the heavy quark pair FFs defined in Eq. (4.10) is also real, $\mathcal{D}_{[Q\bar{Q}(\kappa)]\to H}(z,\zeta_1,\zeta_2;m_Q,\mu_0)^* = \mathcal{D}_{[Q\bar{Q}(\kappa)]\to H}(z,\zeta_1,\zeta_2;m_Q,\mu_0)$. The reality requires that these FFs are symmetric in ζ_1 and ζ_2.

QCD is invariant under the charge conjugation, parity, and time-reversal transformation, but, it is not easy to apply these symmetry transformations to the FFs directly. However, they could be used to study the symmetry properties of the matrix elements defining the FFs in Eq. (4.10). Since time-reversal transformation is not unitary, its operation connects the matrix elements of the states with and without time-reversal transformation [118, 119]

$$\langle 0|\,\widehat{\mathcal{O}}(\psi,A_\mu)\,|H(p)X\rangle = \left(\langle H(p)X|\mathcal{T}^{-1}\right)\mathcal{T}\widehat{\mathcal{O}}(\psi,A_\mu)^\dagger\mathcal{T}^{-1}\left(\mathcal{T}|0\rangle\right) \tag{5.21}$$

where $\widehat{\mathcal{O}}(\psi,A_\mu)$ is an operator of the quark and gluon field, $\mathcal{T}$ is the time-reversal operator and $(\langle H(p)X|\mathcal{T}^{-1})$ and $(\mathcal{T}|0\rangle)$ are time-reversal transformed states. Since the charge conjugation $\mathcal{C}$ and parity $\mathcal{P}$ transformation are unitary, they can be directly inserted into the matrix element as

$$\begin{aligned}\langle 0|\,\widehat{\mathcal{O}}(\psi,A_\mu)\,|H(p)X\rangle &= \langle 0|\,\widehat{\mathcal{O}}(\psi,A_\mu)\,\mathcal{C}^{-1}\mathcal{C}\,|H(p)X\rangle \\ &= \langle 0|\,\widehat{\mathcal{O}}(\psi,A_\mu)\,\mathcal{P}^{-1}\mathcal{P}\,|H(p)X\rangle\,. \end{aligned}\tag{5.22}$$

For example, by applying the parity and time-reversal invariance to the matrix elements of the FFs to an unpolarized final-state heavy quarkonium, defined in Eq. (4.10), one can derive the same $\zeta_1 \leftrightarrow \zeta_2$ symmetry property of the FFs obtained by applying the reality of the FFs.

Although the charge conjugation operation $\mathcal{C}$ cannot be applied to the FFs directly, because the initial fragmenting $Q\bar{Q}$ pair is not an eigenstate of $\mathcal{C}$ due to its relative momentum, we find that the FFs are actually invariant under a modified charge conjugation $\overline{\mathcal{C}}$, if both the initial and the final heavy quark pairs are color singlet. The modified charge conjugation operation $\overline{\mathcal{C}}$ is defined as the charge conjugation operation $\mathcal{C}$ followed by reversing the direction of the relative light-cone momentum of the pair, i.e. $\zeta_1 \to -\zeta_1$ for the amplitude. More specifically, for the fragmentation from a QCD $Q\bar{Q}$ pair to a non-relativistic $Q\bar{Q}$ pair, the $\overline{\mathcal{C}}$ operation leads to $(-1)^{\delta_{s,a}+1}$ for the initial $Q\bar{Q}$ pair with $s = v,a,t$, and $(-1)^{L+S}$ for a final non-relativistic $Q\bar{Q}$ pair ($^{2S+1}L_J$). By applying $\overline{\mathcal{C}}$ on the amplitude and keeping the complex

conjugate of the amplitude untouched for a FF, one picks up an overall factor $(-1)^{L+S+\delta_{s,a}+1}$. If there is a gluon radiated into the final state, we can still apply the $\overline{\mathcal{C}}$ operation as long as one of the initial and final $Q\bar{Q}$ pairs is in a color singlet state. By applying the $\overline{\mathcal{C}}$ operation on the amplitude of the FFs and keeping the complex conjugate of the amplitude untouched, one picks up an overall factor of $(-1)^{L+S+\delta_{s,a}}$.

More generally, if we apply the $\overline{\mathcal{C}}$ operation to both the amplitude and its complex conjugate for heavy quark pair FFs and combine the reality, we have

$$\mathcal{D}_{[Q\bar{Q}(s^{[b]})]\to[Q\bar{Q}(^{2S+1}L_J^{[b']})]}(z,-\zeta_1,-\zeta_2) = \mathcal{D}_{[Q\bar{Q}(s^{[b]})]\to[Q\bar{Q}(^{2S+1}L_J^{[b']})]}(z,\zeta_1,\zeta_2), \quad (5.23)$$

where $b, b' = [1], [8]$. Combining the symmetry property of the FFs when $\zeta_1 \leftrightarrow \zeta_2$ and that in Eq. (5.23), the FFs also have the following crossing symmetry,

$$\mathcal{D}_{[Q\bar{Q}(s^{[b]})]\to[Q\bar{Q}(^{2S+1}L_J^{[b']})]}(z,-\zeta_1,-\zeta_2) = \mathcal{D}_{[Q\bar{Q}(s^{[b]})]\to[Q\bar{Q}(^{2S+1}L_J^{[b']})]}(z,\zeta_2,\zeta_1). \quad (5.24)$$

All these symmetry properties of the FFs are verified by our explicit calculations below.

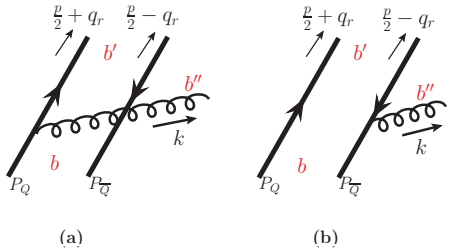

Figure 5.1: Real NLO corrections of the $Q\bar{Q}$ pair FFs in light-cone gauge with the NRQCD factorization approach.

Charge conjugation can also be employed to constrain the delta function structure of real gluon emission subprocess in our NLO calculation, for which the Feynman diagrams in light-cone gauge are shown in Fig. 5.1. The analysis is easier in light-cone gauge $A^+ = 0$, although the conclusion is gauge independent. Before performing the q_r-derivative operations and the limit $q_r \to 0$ as in Eq. (5.7), the amplitude of the Feynman diagram in Fig. 5.1(a) can be written in a general form as $F(z, q_r)G(b, b', b'')\delta(1 - z - \zeta_1 + 2q_r^+/p^+)$, where $G(b, b', b'')$ represents the color structure with color indices b, b', b'' listed in the figure, and $F(z, q_r)$ denotes the rest of the amplitude. Then the amplitude of the diagram in Fig. 5.1(b) can be obtained from that in Fig. 5.1(a) by performing charge

conjugation, as well as the replacements $\zeta_1 \to -\zeta_1$ and $q_r \to -q_r$, which give $(-1)^{S+\delta_{s,a}} F(z,-q_r) G^\dagger(b,b',b'') \delta(1-z+\zeta_1 - 2q_r^+/p^+)$. Therefore, the addition of these two diagrams is given by

$$\begin{aligned} I_{a+b} &= F(z,q_r) G(b,b',b'') \delta\left(1-z-\zeta_1+\frac{2q_r^+}{p^+}\right) \\ &+ (-1)^{S+\delta_{s,a}} F(z,-q_r) G^\dagger(b,b',b'') \delta\left(1-z+\zeta_1-\frac{2q_r^+}{p^+}\right). \end{aligned} \tag{5.25}$$

For producing a S-wave final-state $Q\bar{Q}$ pair, we can set the relative momentum q_r to zero and find

$$I^S_{a+b} = F(z,0) \left[G(b,b',b'') \delta(1-z-\zeta_1) + (-1)^{S+\delta_{s,a}} G^\dagger(b,b',b'') \delta(1-z+\zeta_1) \right], \tag{5.26}$$

which has two general structures depending on the color indices b and b'. If only one of the two indices is color octet, we have $G(b,b',b'') = G^\dagger(b,b',b'')$. Multiplied with the complex conjugate of the amplitude, we obtain the first type of δ-function structure:

$$\left[\delta(1-z-\zeta_1) + (-1)^{S+\delta_{s,a}} \delta(1-z+\zeta_1)\right] \tag{5.27}$$

$$\times \left[\delta(1-z-\zeta_2) + (-1)^{S+\delta_{s,a}} \delta(1-z+\zeta_2)\right]. \tag{5.28}$$

If both b and b' are color octet, we have $G(b,b',b'') = \mathrm{Tr}[t_b^{(F)} t_{b'}^{(F)} t_{b''}^{(F)}]$ with $t_b^{(F)}$ the generator of fundamental representation of SU(3) color. Multiplied with the complex conjugate of the amplitude, we obtain the second type of δ-function structure:

$$\begin{aligned} &(N_c^2-2) \left[\delta(1-z+\zeta_1)\delta(1-z+\zeta_2) + \delta(1-z-\zeta_1)\delta(1-z-\zeta_2)\right] \\ &\quad - (-1)^{S+\delta_{s,a}} 2 \left[\delta(1-z+\zeta_1)\delta(1-z-\zeta_2) + \delta(1-z-\zeta_1)\delta(1-z+\zeta_2)\right]. \end{aligned} \tag{5.29}$$

The δ-function structures in Eqs. (5.27) and (5.29) exhaust all possible δ-function structures of the NLO FFs to a S-wave $Q\bar{Q}$ pair. Our explicit calculations in the next chapter confirm the conclusion of the above analysis.

For producing a P-wave final state $Q\bar{Q}$ pair, we need to take the q_r-derivative before setting q_r to zero. From Eq. (5.25), we find the amplitude is

a linear combination of

$$F'(z,0)\left[G(b,b',b'')\delta(1-z-\zeta_1)+(-1)^{L+S+\delta_{s,a}}G^\dagger(b,b',b'')\delta(1-z+\zeta_1)\right], \tag{5.30}$$

and

$$F(z,0)\left[G(b,b',b'')\delta'(1-z-\zeta_1)+(-1)^{L+S+\delta_{s,a}}G^\dagger(b,b',b'')\delta'(1-z+\zeta_1)\right], \tag{5.31}$$

where we have replaced $-(-1)^{S+\delta_{s,a}}$ by $(-1)^{L+S+\delta_{s,a}}$ since $L=1$. Similar to the S-wave case, multiplying the above amplitude with its complex conjugate, we obtain three δ-function structures for each color combination.

Here we list all δ-function structures allowed by symmetries, as well as their behaviors at threshold $z\to 1$. The threshold behaviors are very important when we cancel the IR divergence between real and virtual diagrams.

$$\Delta_0 = 4\,\delta(\zeta_1)\delta(\zeta_2), \tag{5.32a}$$

$$\Delta_0'' = 4\,z^2\,\delta'(\zeta_1)\delta'(\zeta_2), \tag{5.32b}$$

$$\Delta_\pm^{[1]} = 4\left[\delta(1-z+\zeta_1)\pm\delta(1-z-\zeta_1)\right]\left[\delta(1-z+\zeta_2)\pm\delta(1-z-\zeta_2)\right], \tag{5.32c}$$

$$\begin{aligned}\Delta_\pm^{[1]\prime} = -4\,z\Big\{&\left[\delta'(1-z+\zeta_1)\pm\delta'(1-z-\zeta_1)\right]\left[\delta(1-z+\zeta_2)\pm\delta(1-z-\zeta_2)\right]\\&+\left[\delta(1-z+\zeta_1)\pm\delta(1-z-\zeta_1)\right]\left[\delta'(1-z+\zeta_2)\pm\delta'(1-z-\zeta_2)\right]\Big\},\end{aligned} \tag{5.32d}$$

$$\Delta_\pm^{[1]\prime\prime} = 4\,z^2\,\left[\delta'(1-z+\zeta_1)\pm\delta'(1-z-\zeta_1)\right]\left[\delta'(1-z+\zeta_2)\pm\delta'(1-z-\zeta_2)\right], \tag{5.32e}$$

$$\begin{aligned}\Delta_\pm^{[8]} = 4\Big\{&(N_c^2-2)\left[\delta(1-z+\zeta_1)\delta(1-z+\zeta_2)+\delta(1-z-\zeta_1)\delta(1-z-\zeta_2)\right]\\&\mp 2\left[\delta(1-z+\zeta_1)\delta(1-z-\zeta_2)+\delta(1-z-\zeta_1)\delta(1-z+\zeta_2)\right]\Big\},\end{aligned} \tag{5.32f}$$

$$\begin{aligned}\Delta_\pm^{[8]\prime} = -4\,z\Big\{&(N_c^2-2)\big[\delta'(1-z+\zeta_1)\delta(1-z+\zeta_2)+\delta(1-z+\zeta_1)\delta'(1-z+\zeta_2)\\&+\delta'(1-z-\zeta_1)\delta(1-z-\zeta_2)+\delta(1-z-\zeta_1)\delta'(1-z-\zeta_2)\big]\\&\mp 2\big[\delta'(1-z+\zeta_1)\delta(1-z-\zeta_2)+\delta(1-z+\zeta_1)\delta'(1-z-\zeta_2)\\&+\delta'(1-z-\zeta_1)\delta(1-z+\zeta_2)+\delta(1-z-\zeta_1)\delta'(1-z+\zeta_2)\big]\Big\},\end{aligned} \tag{5.32g}$$

$$\Delta_{\pm}^{[8]''} = 4\,z^2\,\Big\{(N_c^2-2)\,[\delta'(1-z+\zeta_1)\delta'(1-z+\zeta_2)+\delta'(1-z-\zeta_1)\delta'(1-z-\zeta_2)]$$
$$\mp 2\,[\delta'(1-z+\zeta_1)\delta'(1-z-\zeta_2)+\delta'(1-z-\zeta_1)\delta'(1-z+\zeta_2)]\,\Big\}, \tag{5.32h}$$

All these Δ-functions are invariant under the transformation ($\zeta_1 \to -\zeta_1$, $\zeta_2 \to -\zeta_2$) and the exchange $\zeta_1 \leftrightarrow \zeta_2$, including the crossing exchange ($\zeta_1 \to -\zeta_2$, $\zeta_2 \to -\zeta_1$). In addition, Δ_0, $\Delta_+^{[1]}$, $\Delta_+^{[1]'}$ and $\Delta_+^{[1]''}$ are even in both ζ_1 and ζ_2, while Δ_0'', $\Delta_-^{[1]}$, $\Delta_-^{[1]'}$ and $\Delta_-^{[1]''}$ are odd in both ζ_1 and ζ_2. Under the integration of ζ_1 and ζ_2 with a well-behaved test function, the asymptotic behaviors of these Δ-functions at $z \to 1$ are

$$\lim_{z\to 1}\Delta_+^{[1]} = O[1], \qquad \lim_{z\to 1}\Delta_-^{[1]} = O[(1-z)^2],$$
$$\lim_{z\to 1}\Delta_+^{[1]'} = O[(1-z)], \qquad \lim_{z\to 1}\Delta_-^{[1]'} = O[(1-z)],$$
$$\lim_{z\to 1}\Delta_+^{[1]''} = O[(1-z)^2], \qquad \lim_{z\to 1}\Delta_-^{[1]''} = O[1],$$
$$\lim_{z\to 1}\Delta_\pm^{[8]} = O[1], \qquad \lim_{z\to 1}\Delta_\pm^{[8]'} = O[(1-z)],$$
$$\lim_{z\to 1}\Delta_\pm^{[8]''} = O[1],$$

Therefore,

$$\frac{\Delta_-^{[1]}}{(1-z)}, \quad \frac{\Delta_\pm^{[1]'}}{(1-z)}, \quad \frac{\Delta_+^{[1]''}}{(1-z)}, \quad \text{and} \quad \frac{\Delta_\pm^{[8]'}}{(1-z)}$$

do not exhibit any pole at $z = 1$.

5.5 Coulomb divergence and the expansion of heavy quark relative momentum

In this section, we justify our procedure of calculating the S-wave and P-wave contributions by expanding the relative momentum of the final-state non-relativistic heavy quark pair, q_r, before the integration over the relative momentum of the initial-state perturbative heavy quark pair, q_1.

As shown in Eq. (5.7), the general structure of the one-loop amplitude of

the $Q\bar{Q}$ pair FFs is of the following form,

$$A_1(\zeta_1) = \lim_{q_r\to 0}\left(\prod_{j=0}^{L}\frac{\mathrm{d}}{\mathrm{d}q_r^{\alpha_j}}\right)\left\{\int\frac{\mathrm{d}^D q_1}{(2\pi)^D}\,\delta(\zeta_1-\frac{2q_1^+}{p_c^+})\,\bar{A}(q_1,q_r)\right\}, \tag{5.33}$$

where the q_1-integration should be performed before taking the derivatives with respect to q_r and the limit $q_r \to 0$. However, the calculation in this order is often very complicated. On the other hand, a similar calculation,

$$A_2(\zeta_1) = \int\frac{\mathrm{d}^D q_1}{(2\pi)^D}\,\delta(\zeta_1-\frac{2q_1^+}{p_c^+})\lim_{q_r\to 0}\left(\prod_{j=0}^{L}\frac{\mathrm{d}}{\mathrm{d}q_r^{\alpha_j}}\bar{A}(q_1,q_r)\right), \tag{5.34}$$

could be carried out more easily due to the fact that the derivatives and the limit of q_r were taken before performing the q_1-integration. In general, $A_1(\zeta_1)$ and $A_2(\zeta_1)$ are not necessary to be equal, unless the integration region of $q_1 \lesssim q_r \to 0$ is not important, which means that the integrand $\bar{A}(q_1,q_r)$ has no pole as $q_1 \to 0$ and $q_r \to 0$. Unfortunately, this condition is not satisfied by the process that we are considering here.

However, we show in this section that the difference between $A_1(\zeta_1)$ and $A_2(\zeta_1)$ can be exactly absorbed into the NLO expansion of NRQCD LDMEs, and in our NLO calculations, we are justified to switch the order of q_1-integration from the derivatives and the limit of q_r. To achieve this conclusion, we will assume in the following that all distributions of ζ_1 will be convoluted with a function $f(\zeta_1)$, which has a Taylor expansion for the region $-1 < \zeta_1 < 1$. Since applying the derivative and the limit operations for q_r is equivalent to performing the Taylor expansion of q_r, in the following, we just compare the methods of either expanding q_r before or after the q_1-integration.

To be specific, we are working at the NLO in the Feynman gauge. Diagrams (a), (b) and (f)-(i) in Fig. 6.2 do not cause any problem because they are not connected diagrams and the additional energy-momentum conservation $\delta^D(q_r - q_1)$ makes the integration over q_1 trivial. It will be clear later that there is no problem for the diagrams (c), (d), (j), (k) and (l), because these two diagrams do not have Coulomb divergence. After all, we need only to consider carefully the diagram (e), whose amplitude can be written as

$$\bar{A}(q_1,q_r) = \frac{B(q_1,q_r)}{\left[(q_r-q_1)^2+i\varepsilon\right]\left[(p/2+q_1)^2-m_Q^2+i\varepsilon\right]\left[(p/2-q_1)^2-m_Q^2+i\varepsilon\right]}, \tag{5.35}$$

where $B(q_1,q_r)$ is a polynomial of q_1 and q_r. In the rest frame of the $Q\bar{Q}$

pair, $p \sim (2m_Q, \mathbf{0})$, and $q_r \sim (0, m_Q \boldsymbol{v})$. In the Coulomb region where $q_1 \sim (m_Q v^2, m_Q \boldsymbol{v})$, the relevant scaling relations are: $(q_r - q_1)^2 \sim (p/2 + q_1)^2 - m_Q^2 \sim (p/2 - q_1)^2 - m_Q^2 \sim m_Q^2 v^2$ and $d^D q_1 \sim m_Q^D v^{D+1}$. Therefore, the leading contribution in this region behaves as v^{D-5}, which leads to a v^{-1} Coulomb singularity in four dimensions as $v \to 0$. This simple analysis indicates that the integration region of $q_1 <\approx q_r$ is, indeed, very important for the diagram (e).

First, let us consider a simpler case $B(q_1, q_r) = 1$. That is, we need to deal with the following integration,

$$I_1 \equiv \int \frac{\mathrm{d}^D q_1}{(2\pi)^D} \frac{\delta(\zeta_1 - \frac{2q_1^+}{p^+})}{\left[(q_r - q_1)^2 + i\varepsilon\right]\left[(p/2 + q_1)^2 - m_Q^2 + i\varepsilon\right]\left[(p/2 - q_1)^2 - m_Q^2 + i\varepsilon\right]} \,. \tag{5.36}$$

After using the Feynman parametrization to combine the denominators, we have

$$I_1 = \int_0^1 \mathrm{d}x_1 \int_0^{1-x_1} \mathrm{d}y_1 \int \frac{\mathrm{d}^D q_1}{(2\pi)^D} \frac{2\,\delta(\zeta_1 - \frac{2q_1^+}{p^+})}{\left[(q_1 - q_1')^2 - \Delta\right]^3} \,, \tag{5.37}$$

where

$$\begin{aligned} q_1' &= x_1 q_r + (1 - x_1 - 2y_1)\, p/2, \\ \Delta &= (1 - x_1)^2 q_r^2 + (1 - x_1 - 2y_1)^2\, p^2/4 - i\varepsilon. \end{aligned} \tag{5.38}$$

In Eq. (5.37), with a single pole, the integration of q_1^- vanishes unless $q_1^+ = q'^+_1$. In general, the following relation,

$$\int \frac{\mathrm{d}^D q_1}{(2\pi)^D} \frac{\delta(\zeta_1 - \frac{2q_1^+}{p^+})}{\left[(q_1 - q_1')^2 - \Delta\right]^n} = \delta(\zeta_1 - \frac{2q'^+_1}{p^+}) \int \frac{\mathrm{d}^D q_1}{(2\pi)^D} \frac{1}{\left[(q_1 - q_1')^2 - \Delta\right]^n} \,, \tag{5.39}$$

is valid when both sides are convoluted with any smooth function $f(\zeta_1)$ that can be Taylor expanded in the region $-1 < \zeta_1 < 1$. Applying the relation in Eq. (5.39) to the integration in Eq. (5.37), and performing the q_1-integration, we obtain

$$I_1 = -\frac{i}{(4\pi)^{2-\epsilon}} \frac{\Gamma(1+\epsilon)}{(p^2/4)^{1+\epsilon}} \int_0^1 \mathrm{d}x_1 \int_0^{1-x_1} \mathrm{d}y_1 \frac{\delta(\zeta_1 - 2q'^+_1/p^+)}{\Delta^{1+\epsilon}} \,, \tag{5.40}$$

where $\epsilon = (4 - D)/2$. By changing variable $x_1 = 1 - x$ and then letting

$y_1 = x(1-y)/2$, we can rewrite I_1 as

$$I_1 = -\frac{i}{(4\pi)^{2-\epsilon}} \frac{\Gamma(1+\epsilon)}{(p^2/4)^{1+\epsilon}} \frac{1}{2} Z(\zeta_1, q_r), \tag{5.41}$$

with

$$Z(\zeta_1, q_r) = \int_{-1}^{1} \frac{dy}{(y^2 - \beta^2 - i\varepsilon)^{1+\epsilon}} \int_0^1 \frac{dx}{x^{1+2\epsilon}} \delta(\zeta_1 - \tilde{\beta} + xy + x\tilde{\beta}), \tag{5.42}$$

where $\tilde{\beta} = 2q_r^+/p^+$ and $\beta^2 = -4q_r^2/p^2$, and both are small parameters. Since $Z(\zeta_1, q_r)$ will eventually convolute with a non-singular function $f(\zeta_1)$, we can expand the δ-function as

$$\begin{aligned} &\delta(\zeta_1 - \tilde{\beta} + xy + x\tilde{\beta}) \\ =&\delta(\zeta_1) + \delta'(\zeta_1)(-\tilde{\beta} + xy + x\tilde{\beta}) + \cdots \\ =& \sum_{i,j\geq k,k} C_{i,j,k} \tilde{\beta}^i x^j y^k \\ =& \sum_{i,j\geq 2k,k} C_{i,j,2k} \tilde{\beta}^i x^j y^{2k}, \end{aligned} \tag{5.43}$$

where i, j, and k are natural numbers, and the power of x cannot be less than the power of y. The equation in Eq. (5.43) is a result of the fact that the terms odd in y vanish under the integration of y from -1 to 1. Then, the x-integration in $Z(\zeta_1, q_r)$ is trivial,

$$\int_0^1 \frac{dx}{x^{1+2\epsilon}} x^j = \frac{1}{j - 2\epsilon}. \tag{5.44}$$

To perform the y-integration, we introduce a parameter $\Lambda \gg \beta$, and rewrite the y-integration as

$$\begin{aligned} \int_{-1}^{1} \frac{y^{2k} dy}{(y^2 - \beta^2 - i\varepsilon)^{1+\epsilon}} = &\left(\int_{-1}^{-\Lambda} + \int_{\Lambda}^{1} \right) \frac{y^{2k} dy}{(y^2 - \beta^2 - i\varepsilon)^{1+\epsilon}} \\ &+ \int_{-\Lambda}^{\Lambda} \frac{y^{2k} dy}{(y^2 - \beta^2 - i\varepsilon)^{1+\epsilon}}. \end{aligned}$$

Since $y^2 \geq \Lambda^2 \gg \beta^2$ in the first term above, we can expand β^2 before perform-

ing the y-integration, and obtain

$$\frac{y^{2k}}{(y^2-\beta^2-i\varepsilon)^{1+\epsilon}} = \frac{y^{2k}}{y^{2-2\epsilon}} + (1+\epsilon)\frac{y^{2k}}{y^{4+2\epsilon}}\beta^2 + \cdots \equiv E_k(y^2)\,, \tag{5.45}$$

and

$$\int_{-1}^{1} \frac{y^{2k}dy}{(y^2-\beta^2-i\varepsilon)^{1+\epsilon}} = \left(\int_{-1}^{-\Lambda} + \int_{\Lambda}^{1}\right) E_k(y^2)dy + \int_{-\Lambda}^{\Lambda} \frac{y^{2k}dy}{(y^2-\beta^2-i\varepsilon)^{1+\epsilon}}\,. \tag{5.46}$$

This identity can also be written as

$$\begin{aligned}\int_{-1}^{1} \frac{y^{2k}dy}{(y^2-\beta^2-i\varepsilon)^{1+\epsilon}} - \int_{-1}^{1} E_k(y^2)dy \\ = \int_{-\Lambda}^{\Lambda} \frac{y^{2k}dy}{(y^2-\beta^2-i\varepsilon)^{1+\epsilon}} - \int_{-\Lambda}^{\Lambda} E_k(y^2)dy\,.\end{aligned}$$

On the LHS of the above identity, the first term corresponds to the performing y-integration before expanding β^2, while the second term corresponds to expanding β^2 before doing the y-integration. The RHS provides the corrections to the original y-integration caused by expanding β^2 first. Since the corrections on the RHS do not depend on the choice of Λ as long as $\Lambda \gg \beta$, we can choose $\Lambda = \infty$ to simplify the identity as,

$$\begin{aligned}\int_{-1}^{1} \frac{y^{2k}dy}{(y^2-\beta^2-i\varepsilon)^{1+\epsilon}} - \int_{-1}^{1} E_k(y^2)dy = \int_{-\infty}^{+\infty} \frac{y^{2k}dy}{(y^2-\beta^2-i\varepsilon)^{1+\epsilon}} \\ = \beta^{2k-1-2\epsilon}\int_{-\infty}^{+\infty} \frac{y^{2k}dy}{(y^2-1-i\varepsilon)^{1+\epsilon}}.\end{aligned} \tag{5.47}$$

In deriving the above simplified identify, we used

$$\int_{-\infty}^{+\infty} E_k(y^2)dy = \int_{-\infty}^{+\infty} \left[\frac{y^{2k}}{y^{2+2\epsilon}} + (1+\epsilon)\frac{y^{2k}}{y^{4+2\epsilon}}\beta^2 + \cdots\right] dy = 0. \tag{5.48}$$

Note that using dimensional regularization is crucial for deriving the above results. Although the integration on the RHS of Eq. (6.36) can be further carried out, its result is not really relevant for our discussion here. Instead, we need to point out that it is an odd function of β.

In comparison with the situation discussed in Ref. [120], the second term

on the LHS of Eq. (6.36) corresponds to contributions from the hard region, while the term on the RHS of the equation corresponds to contributions from the potential region, which can be exactly reproduced by the NLO calculation of the NRQCD LDMEs. Note also that deriving Eq. (5.41) from Eq. (5.36) by performing the Feynman parametrization and integrating out q_1, we did not miss anything. Therefore, we conclude that, if we are not interested in the contributions from the potential region, then we can calculate Eq. (5.36) by expanding the q_r before doing the q_1-integration.

When $B(q_1, q_r)$ is a general polynomial of q_1 and q_r, we can carry out essentially all steps in our arguments above for the situation when $B(q_1, q_r) = 1$. We can still expand the δ-function, use the Feynman parametrization to reorganize the q_1-integral, and perform the integration of q_1 before the integration over the Feynman parameters. The key difference is that we get a slightly different y-integral,

$$\int_{-1}^{1} \frac{y^{2k} dy}{(y^2 + \beta^2 - i\varepsilon)^{d+1+\epsilon}}, \tag{5.49}$$

where d is an integer. The trick of introducing a $\Lambda \gg \beta$ is still valid for showing that expanding the q_r before doing the q_1-integration is effectively neglecting the Coulomb region. Since the Coulomb region is canceled exactly by the NLO calculation of the NRQCD LDMEs, we conclude that we can get correct short-distance coefficients at NLO if we expand q_r before the integration of q_1.

Chapter 6

Calculation of Heavy Quark Pair Fragmentation in NRQCD factorization model: S wave unpolarized

In the last chapter, we explained the techniques and tricks used in our calculations of the fragmentation functions (FFs) in the NRQCD factorization approach. In this and the next chapters, we show how to calculate the short-distance coefficients (SDCs) with S-wave and P-wave final-state $Q\bar{Q}$ pair, by explaining some examples in detail. Specifically, in this chapter we take process $[Q\bar{Q}(a^{[8]})] \to [Q\bar{Q}(^1S_0^{[8]})]$ as an example to present the calculation of the SDCs in Eq. (5.3)

6.1 LO matching coefficients

The heavy quark pair FFs to a heavy quarkonium are defined in terms of heavy quark field operators in QCD, see Eq. (4.10) for example, while the heavy quark states in NRQCD factorization are defined as non-relativistic. Therefore, there are matching coefficients between a fragmenting QCD heavy quark pair and a NRQCD heavy quark pair, defining the LDMEs. We derive the LO matching coefficients for all heavy quark fragmentation channels in this section.

A general cut-diagram representation for $\mathcal{D}_{[Q\bar{Q}(s^{[b]})]\to[Q\bar{Q}(i^{[b']})]}(z, \zeta_1, \zeta_2; m_Q, \mu_0)$ at zeroth order in the power of α_s is given in Fig. 6.1, where the momenta of

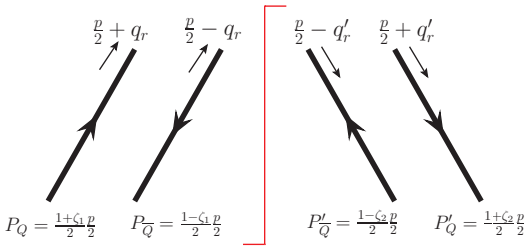

Figure 6.1: Cut-diagram representation of $\mathcal{D}_{[Q\bar{Q}(s^{[b]})]\to[Q\bar{Q}(i^{[b']})]}(z,\zeta_1,\zeta_2;m_Q,\mu_0)$ at zeroth order.

the incoming heavy quark and heavy antiquark are defined as

$$\begin{aligned} P_Q &= \frac{p_c}{2}+q_1, \qquad & P_{\bar{Q}} &= \frac{p_c}{2}-q_1, \\ P'_Q &= \frac{p_c}{2}+q_2, \qquad & P'_{\bar{Q}} &= \frac{p_c}{2}-q_2. \end{aligned} \tag{6.1}$$

At the zeroth order, the LDME in Eq. (5.4) is proportional to the delta function $\delta_{n,n'}$. Thus, Eq. (5.4) is simplified to

$$\mathcal{D}^{\rm LO}_{[Q\bar{Q}(s^{[b]})]\to[Q\bar{Q}(i^{[b']})]}(z,\zeta_1,\zeta_2;m_Q,\mu_0) = \hat{d}^{\rm LO}_{[Q\bar{Q}(s^{[b]})]\to[Q\bar{Q}(i^{[b']})]}(z,\zeta_1,\zeta_2;m_Q,\mu_0)\,. \tag{6.2}$$

Eqs. (5.5) and (5.7) are reduced, respectively, to

$$\begin{aligned} &\mathcal{D}^{\rm LO}_{[Q\bar{Q}(s^{[b]})]\to[Q\bar{Q}(i^{[b']})]}(z,\zeta_1,\zeta_2;m_Q,\mu_0) \\ &\qquad = \frac{\delta(1-z)}{N_s N_b N_i^{\rm NR} N_{b'}^{\rm NR}}\,\mathcal{M}^{\rm LO}_{[Q\bar{Q}(s^{[b]})]\to[Q\bar{Q}(i^{[b']})]}(p,z,\zeta_1,\zeta_2)\,, \end{aligned} \tag{6.3}$$

$$\begin{aligned} \mathcal{A}^{\rm LO}_{[Q\bar{Q}(s^{[b]})]\to[Q\bar{Q}(i^{[b']})]}(p,z,\zeta_1) = \lim_{q_r\to 0}\Bigg\{ & 2\,\delta(\zeta_1-\frac{2q_r^+}{p_c^+}) \\ & \times \bar{\mathcal{A}}^{\rm LO}_{[Q\bar{Q}(s^{[b]})]\to[Q\bar{Q}(i^{[b']})]}(q_1=q_r)\Gamma_i^{\rm NR}(p)\,C_{b'}^{\rm NR}\Bigg\}\,. \end{aligned} \tag{6.4}$$

In Eq. (7.2), the delta function is expected because all momenta flow from the incoming $Q\bar{Q}$-pair into the final $Q\bar{Q}$-pair.

One can further simplify the calculation by noting that at LO, the initial and final heavy quark pair must have the same quantum numbers, i.e., (1) color label b and b' must be the same; (2) spinor label s and i must have the same parity. The parity of the outgoing $Q\bar{Q}$ state, $i = {}^{2S+1}L_J$ with

$L=0$, is $(-1)^S$, while the parity for the incoming $Q\bar{Q}$ state is -1 for $s=v,t$, and $+1$ for $s=a$. Processes violating either of these two rules, such as $\mathcal{D}_{[Q\bar{Q}(s^{[1]})]\to[Q\bar{Q}(i^{[8]})]}(z,\zeta_1,\zeta_2;m_Q,\mu_0)$ and $\mathcal{D}_{[Q\bar{Q}(v^{[b]})]\to[Q\bar{Q}({}^1S_0^{[b']})]}(z,\zeta_1,\zeta_2;m_Q,\mu_0)$, must vanish at this order.

For our example $[Q\bar{Q}(a^{[8]})]\to[Q\bar{Q}({}^1S_0^{[8]})]$, there is no derivative of q_r in Eq. (7.3). From Eqs. (5.6) and (7.3), we have

$$\begin{aligned}
&\mathrm{Tr}\left[\Gamma_a(p_c)\,C_8\,\mathcal{A}^{\mathrm{LO}}_{[Q\bar{Q}(a^{[8]})]\to[Q\bar{Q}({}^1S_0^{[8]})]}(p,z,\zeta_1)\right]\\
=&\mathrm{Tr}_c\left[\sqrt{2}t^{(F)}_{c_{in}}\sqrt{2}t^{(F)}_{c_{out}}\right]\mathrm{Tr}_\gamma\left[\frac{\gamma\cdot\hat{n}\,\gamma_5-\gamma_5\,\gamma\cdot\hat{n}}{8p\cdot\hat{n}}\frac{1}{\sqrt{8m_Q^3}}(\frac{\not{p}}{2}-m_Q)\gamma_5(\frac{\not{p}}{2}+m_Q)\right]\\
&\times 2\,\delta(\zeta_1)\\
=&-\frac{1}{\sqrt{2m_Q}}\,\delta_{c_i,c_f}\,\delta(\zeta_1),
\end{aligned}\tag{6.5}$$

where "Tr_c" is the trace for color, "Tr_γ" is the trace of γ-matrices, and $c_{in}(c_{out})$ is the color for the incoming (outgoing) $Q\bar{Q}$-pair. In Eq. (6.5), we used the operator definitions given in Sec. 5.2 and the fact that $p_c=p$ for deriving the right-hand-side (RHS) of the equation. For carrying out the trace of γ-matrices in Eq. (6.5), we need to specify the definition of γ_5 in d-dimension. Details of our prescription of γ_5 in d-dimension is the topic of the next section. The delta function $\delta(\zeta_1)$ indicates that the momenta of the initial heavy quark and heavy antiquark must be the same, since we have set the relative momentum of the final-state heavy quark and antiquark to zero. Finally, combining the result Eq. (6.5) with Eqs. (5.6), (7.1) and (7.2), we obtain

$$\hat{d}^{\,\mathrm{LO}}_{[Q\bar{Q}(a^{[8]})]\to[Q\bar{Q}({}^1S_0^{[8]})]}(z,\zeta_1,\zeta_2;m_Q,\mu_0)=\frac{1}{N_c^2-1}\frac{1}{2m_Q}\,\delta(1-z)\,\delta(\zeta_1)\,\delta(\zeta_2).\tag{6.6}$$

A complete list of finite LO matching coefficients is given in Appendix B.

6.2 Mathematical issues

Before calculating the NLO corrections, we deviate to explain some mathematical issues which are important in NLO calculation.

6.2.1 γ_5 in dimensional regularization

The inconsistency between the following two properties of γ_5 in d-dimension

$$\mathrm{Tr}[\gamma_5\gamma_\mu\gamma_\nu\gamma_\rho\gamma_\sigma] = -4i\,\epsilon_{\mu\nu\rho\sigma}, \tag{6.7a}$$

$$[\gamma_5, \gamma_\alpha] = 0, \tag{6.7b}$$

is well known [121]. Many γ_5 schemes in d dimensions have been proposed, such as the 't Hooft-Veltman scheme [121, 122] and Kreimer scheme [123–125]. In principle, we can use any scheme as long as it is self-consistent. Although the resulted short-distance coefficients can differ by using different schemes, the difference is IR and UV finite at NLO calculation. Thus, one can perform a finite renormalization to relate the results of different schemes. In our present work, we use a Kreimer-like scheme. In the Kreimer scheme, one needs to choose a "reading point". As in our calculation all traces have zero, one or two γ_5's, and we adopt the following choice.

For traces with only one γ_5, we "read" or start the spinor trace in the amplitude from the γ_5, then use [126]

$$\mathrm{Tr}[\gamma_5\gamma_{\alpha_1}\cdots\gamma_{\alpha_n}] = \frac{2}{n-4}\sum_{i=2}^{n}\sum_{j=1}^{i-1}(-1)^{i+j+1}g_{\alpha_i\alpha_j}\mathrm{Tr}[\gamma_5\prod_{\substack{k=1,\\k\neq i,j}}^{n}\gamma_{\alpha_k}], \tag{6.8}$$

recursively until the trace involves only four γ_α's. For $n = 4$, we use

$$\mathrm{Tr}[\gamma_5\gamma_\mu\gamma_\nu\gamma_\rho\gamma_\sigma]\mathrm{Tr}[\gamma_5\gamma^\mu\gamma^\nu\gamma^\rho\gamma^\sigma] = 16D(D-1)(D-2)(D-3). \tag{6.9}$$

For traces with an even number of γ_5's, the reading point is, in fact, irrelevant because we can always remove the γ_5's by using Eq. (6.7b) and

$$\gamma_5\,\gamma_5 = 1. \tag{6.10}$$

6.2.2 Generalized Plus/Minus-distributions

We define generalized plus and minus distributions to regularize the singularities at $\zeta_1 = 0$ and $\zeta_2 = 0$. They are collectively defined as

$$\Big(g(\zeta_1)\Big)_{m\pm} \equiv \int_{-1}^{1}[\theta(x) \pm \theta(-x)]\,g(|x|) \times \left(\delta(x-\zeta_1) - \sum_{i=0}^{m-1}\frac{\delta^{(i)}(\zeta_1)}{i\,!}(-x)^{\,i}\right)dx\,, \tag{6.11}$$

where $\delta^{(i)}(\zeta_1)$ represents the i-th derivative of the δ-function. More explicitly, the plus and minus distributions have the following relation under the integration with a test function,

$$\int \Big(g(\zeta_1)\Big)_{m\pm} f(\zeta_1)\, d\zeta_1 \\ \equiv \int_{-1}^{1} \left[\theta(\zeta_1) \pm \theta(-\zeta_1)\right] g(|\zeta_1|) \times \left(f(\zeta_1) - \sum_{i=0}^{m-1} \frac{f^{(i)}(0)}{i\,!} \zeta_1^{\,i} \right) d\zeta_1. \tag{6.12}$$

From the above definition, we find,

$$\begin{aligned} &\Big(g(-\zeta_1)\Big)_{m\pm} \\ &\quad = \int_{-1}^{1} \left[\theta(x) \pm \theta(-x)\right] g(|x|) \times \left(\delta(x+\zeta_1) - \sum_{i=0}^{m-1} \frac{\delta^{(i)}(-\zeta_1)}{i\,!} (-x)^{\,i} \right) dx \\ &\quad = \int_{-1}^{1} \left[\theta(-x) \pm \theta(x)\right] g(|x|) \times \left(\delta(-x+\zeta_1) - \sum_{i=0}^{m-1} \frac{\delta^{(i)}(-\zeta_1)}{i\,!} (x)^{\,i} \right) dx \\ &\quad = \int_{-1}^{1} \pm \left[\theta(x) \pm \theta(-x)\right] g(|x|) \times \left(\delta(x-\zeta_1) - \sum_{i=0}^{m-1} \frac{\delta^{(i)}(\zeta_1)}{i\,!} (-x)^{\,i} \right) dx \\ &\quad = \pm \Big(g(\zeta_1)\Big)_{m\pm}. \end{aligned} \tag{6.13}$$

That is, plus function is an even function with respect to ζ_1, and minus is an odd function with respect to ζ_1. For $m \geq 0$, we have

$$\begin{aligned} &\Big(g(\zeta_1)\Big)_{(2m+2)+} \\ &\quad = \int_{-1}^{1} \left[\theta(x) + \theta(-x)\right] g(|x|) \times \left(\delta(x-\zeta_1) - \sum_{i=0}^{2m+1} \frac{\delta^{(i)}(\zeta_1)}{i\,!} (-x)^{\,i} \right) dx \\ &\quad = \Big(g(\zeta_1)\Big)_{(2m+1)+} - \int_{-1}^{1} \left[\theta(x) + \theta(-x)\right] g(|x|) \times \frac{\delta^{(2m+1)}(\zeta_1)}{(2m+1)\,!} (-x)^{\,2m+1} dx \\ &\quad = \Big(g(\zeta_1)\Big)_{(2m+1)+}, \end{aligned} \tag{6.14}$$

and

$$\begin{aligned}
&\Big(g(\zeta_1)\Big)_{(2m+1)-} \\
&\quad = \int_{-1}^{1} [\theta(x)-\theta(-x)]\, g(|x|) \times \left(\delta(x-\zeta_1) - \sum_{i=0}^{2m} \frac{\delta^{(i)}(\zeta_1)}{i\,!}(-x)^{\,i}\right) dx \\
&\quad = \Big(g(\zeta_1)\Big)_{(2m)-} - \int_{-1}^{1} [\theta(x)-\theta(-x)]\, g(|x|) \times \frac{\delta^{(2m)}(\zeta_1)}{(2m)\,!}(-x)^{\,2m} dx \\
&\quad = \Big(g(\zeta_1)\Big)_{(2m)-}.
\end{aligned} \tag{6.15}$$

With the definition of the generalized plus/minus distributions, we can extract the IR divergence from functions which are divergent at $\zeta_1 = 0$,

$$\frac{1}{(\zeta_1)^{3+2\epsilon}} = 2(1-2\epsilon)\delta'(\zeta_1) + \left(\frac{1}{\zeta_1^3}\right)_{3-} - \epsilon \left(\frac{\ln(\zeta_1^2)}{\zeta_1^3}\right)_{3-}. \tag{6.16a}$$

$$\frac{\mathrm{Sgn}(\zeta_1)}{(\zeta_1)^{2+2\epsilon}} = \frac{1}{\epsilon_{IR}}\delta'(\zeta_1) + \left(\frac{1}{\zeta_1^2}\right)_{2-} - \epsilon \left(\frac{\ln(\zeta_1^2)}{\zeta_1^2}\right)_{2-}. \tag{6.16b}$$

$$\frac{1}{(\zeta_1)^{2+2\epsilon}} = -2(1-2\epsilon)\delta(\zeta_1) + \left(\frac{1}{\zeta_1^2}\right)_{2+} - \epsilon \left(\frac{\ln(\zeta_1^2)}{\zeta_1^2}\right)_{2+}. \tag{6.16c}$$

$$\frac{\mathrm{Sgn}(\zeta_1)}{(\zeta_1)^{1+2\epsilon}} = -\frac{1}{\epsilon_{\mathrm{IR}}}\delta(\zeta_1) + \left(\frac{1}{\zeta_1}\right)_{1+} - \epsilon \left(\frac{\ln(\zeta_1^2)}{\zeta_1}\right)_{1+}, \tag{6.16d}$$

$$\frac{1}{(\zeta_1)^{1+2\epsilon}} = \left(\frac{1}{\zeta_1}\right)_{1-} - \epsilon \left(\frac{\ln(\zeta_1^2)}{\zeta_1}\right)_{1-}. \tag{6.16e}$$

In the same manner, we also write some non-singular functions in terms of these distributions,

$$\mathrm{Sgn}(\zeta_1)\,\zeta_1^{-2\epsilon} = (1)_{0-} - \epsilon\,(\ln(\zeta_1^2))_{0-}, \tag{6.17a}$$

$$\zeta_1^{-2\epsilon} = (1)_{0+} - \epsilon\,(\ln(\zeta_1^2))_{0+}, \tag{6.17b}$$

$$\mathrm{Sgn}(\zeta_1)\,\zeta_1^{1-2\epsilon} = (\zeta_1)_{0+} - \epsilon\,(\zeta_1 \ln(\zeta_1^2))_{0+}, \tag{6.17c}$$

$$\zeta_1^{1-2\epsilon} = (\zeta_1)_{0-} - \epsilon\,(\zeta_1 \ln(\zeta_1^2))_{0-}. \tag{6.17d}$$

6.3 NLO matching coefficients

The NLO short-distance coefficients in Eq. (5.4) can be derived by expanding both sides of the factorized formula to NLO as

$$\mathcal{D}^{\rm NLO}_{[Q\bar{Q}(\kappa)]\to[Q\bar{Q}(n')]}(z,\zeta_1,\zeta_2;m_Q,\mu_0) = \hat{d}^{\rm NLO}_{[Q\bar{Q}(\kappa)\to[Q\bar{Q}(n')]}(z,\zeta_1,\zeta_2;m_Q,\mu_0,\mu_\Lambda) + \sum_{[Q\bar{Q}(n)]} \hat{d}^{\rm LO}_{[Q\bar{Q}(\kappa)]\to[Q\bar{Q}(n)]}(z,\zeta_1,\zeta_2;m_Q,\mu_0)\langle\mathcal{O}^{[Q\bar{Q}(n')]}_{[Q\bar{Q}(n)]}(\mu_\Lambda)\rangle^{\rm NLO}. \tag{6.18}$$

If NRQCD factorization is valid to this order, the second term on the RHS should have the same IR divergence as that of the LHS, so that $\hat{d}^{\rm NLO}_{[Q\bar{Q}(\kappa)\to[Q\bar{Q}(n')]}(z,\zeta_1,\zeta_2;m_Q,\mu_0,\mu_\Lambda)$ is IR finite.

$\mathcal{D}^{\rm NLO}_{[Q\bar{Q}(\kappa)]\to[Q\bar{Q}(n')]}(z,\zeta_1,\zeta_2;m_Q,\mu_0)$ could be calculated directly from Eqs. (5.5)-(5.7) with a proper UV counter term to remove the UV divergence of the composite operators defining the $Q\bar{Q}$-pair FFs. A general NLO correction includes both virtual and real corrections. In the Feynman gauge, these two parts could be represented in terms of the Feynman diagrams in Figs. 6.2 and 6.3, respectively. Note that the diagrams (c), (d) and (e) in Fig. 6.2 are loop diagrams, in the sense that they have also imaginary contribution, because of the q_1-integral in Eq. (5.7).

We use dimensional regularization to regularize all kinds of divergences in this paper. These divergences include ultra-violet (UV) divergence, infrared (IR) divergence, rapidity divergence, and Coulomb divergence. Because of heavy quark mass, there is no collinear divergence. The UV divergence of these diagrams will be canceled by the pQCD renormalization of the composite operators defining the $Q\bar{Q}$-pair FFs, where evolution kernels derived in Ref. [40] are needed. In general, the summation of all diagrams (real and virtual) could still have leftover IR divergence, which should be the same as the IR divergence of LDMEs at NLO. This must be the case if NRQCD factorization is valid, at least up to this order in α_s. Rapidity divergence is characterized as $k\cdot\hat{n}\to 0$, with k the momentum of the gluon. Such divergence could overlap with UV divergence and produce a double pole. Eventually, we find the rapidity divergences are canceled once we sum over all diagrams.

In the rest of this section, we illustrate the detailed NLO calculation with an example: $[Q\bar{Q}(a^{[8]})]\to[Q\bar{Q}(^1S_0^{[8]})]$. For this channel, the second term on the RHS of Eq. (7.8) vanishes, because for any intermediate state $Q\bar{Q}(n)$, either the LO short-distance coefficient or the NLO LDME is equal to zero

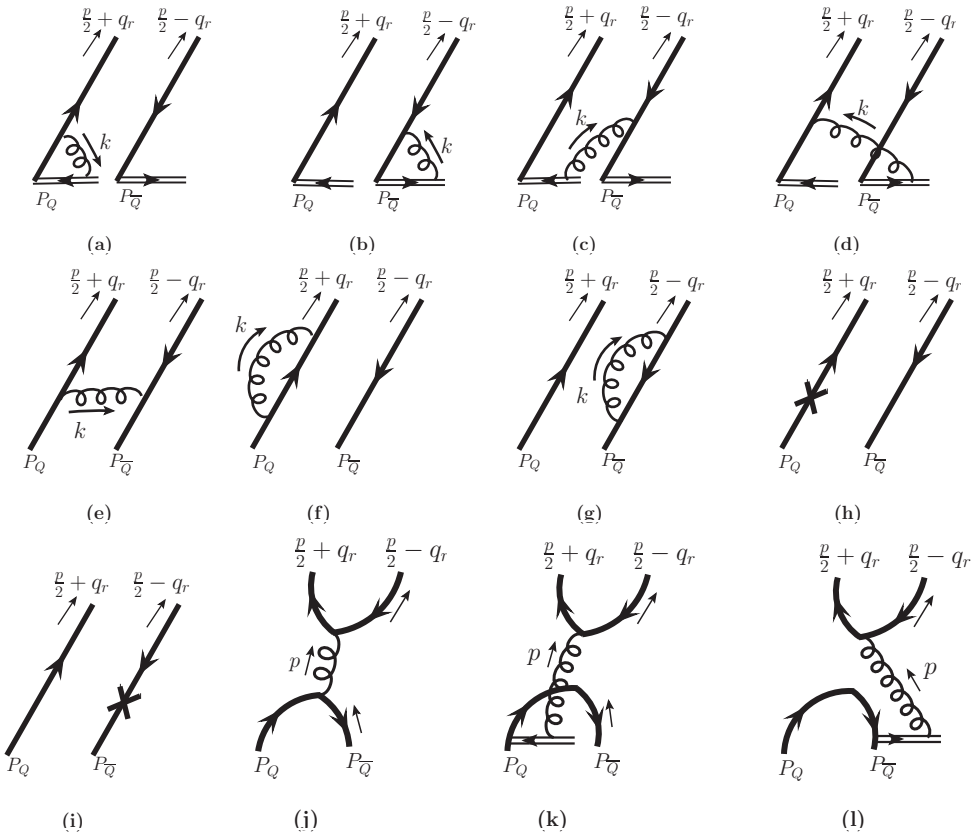

Figure 6.2: Feynman diagrams for virtual correction at NLO.

(after taking the trick proved in section 5.5). Therefore, we have

$$\mathcal{D}^{\rm NLO}_{[Q\bar{Q}(a^{[8]})]\to[Q\bar{Q}(^1S_0^{[8]})]}(z,\zeta_1,\zeta_2;m_Q,\mu_0)=\hat{d}^{\,\rm NLO}_{[Q\bar{Q}(a^{[8]})]\to[Q\bar{Q}(^1S_0^{[8]})]}(z,\zeta_1,\zeta_2;m_Q,\mu_0). \tag{6.19}$$

To calculate the LHS of the above equation, we need to calculate both the real and virtual contributions.

6.3.1 Real contribution

The Feynman diagrams for the real correction are shown in Fig. 6.3. We calculate these diagrams in both Feynman gauge and light-cone gauge, and the results are the same. After some algebra, we derive the real contribution

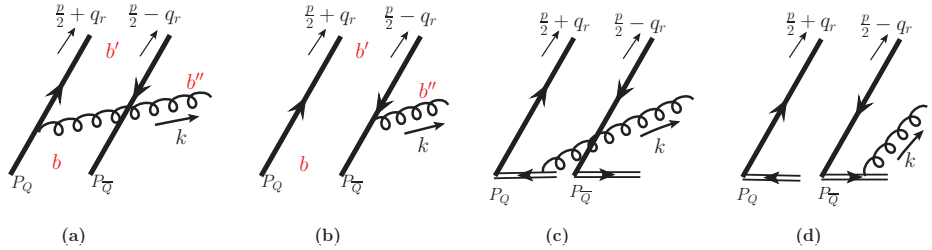

Figure 6.3: Feynman diagrams for real correction at NLO.

as

$$\begin{aligned}
&\mathcal{D}^{\mathrm{NLO},real}_{[Q\bar{Q}(a^{[8]})]\to[Q\bar{Q}(^1S_0^{[8]})]}(z,\zeta_1,\zeta_2;m_Q,\mu_0) \\
&\qquad = \frac{\alpha_s}{4\pi m_Q N_c(N_c^2-1)}\left(\frac{4\pi\mu^2}{(2m_Q)^2}\right)^{\epsilon}\Gamma(1+\epsilon) \\
&\qquad \times\left\{-N_c^2\delta(\zeta_1)\delta(\zeta_2)\delta(1-z)\left(\frac{1}{\epsilon_{\mathrm{UV}}\epsilon_{\mathrm{IR}}}-\frac{1}{\epsilon_{\mathrm{IR}}}\right)+\frac{1}{\epsilon_{\mathrm{UV}}}\frac{z}{(1-z)_+}\frac{\Delta_-^{[8]}}{4}\right. \\
&\qquad \left.+\frac{\Delta_-^{[8]}}{4}\left[-\frac{1}{(1-z)_+}-2\left(\frac{\ln(1-z)}{1-z}\right)_+ +2\ln(1-z)+1\right]\right\},
\end{aligned} \tag{6.20}$$

where $(2m_Q)^2 = p^2$ in the first line is the invariant mass squared of the produced heavy quark pair, $\Delta_-^{[8]}$ is defined in Eq. (5.32).

The origin of each pole is labelled by subscript "UV" or "IR". Infrared divergence at $z\to 1$ is extracted with plus prescription

$$\frac{1}{(1-z)^{1+2\epsilon}} = -\frac{1}{2\,\epsilon_{\mathrm{IR}}}\delta(1-z)+\frac{1}{(1-z)_+}-2\,\epsilon_{\mathrm{IR}}\left(\frac{\ln(1-z)}{1-z}\right)_+. \tag{6.21}$$

The double pole is from the region $k\cdot\hat{n}\to 0, k_\perp\to\infty$. The function is even for both ζ_1 and ζ_2, which is required by charge conjugation symmetry as analyzed in Sec. 5.4.3.

In Eq. (6.20), the multiplicative factor, $(4\pi\mu^2/p^2)^\epsilon$ with $p^2=(2m_Q)^2$, is a generic feature of the one loop calculation using the dimensional regularization, where for the real contribution, p^2 is the invariant mass squared of the produced heavy quark pair. On the other hand, for the virtual contribution, which will be derived in the next subsection, the corresponding multiplicative factor will be $(4\pi\mu^2/(p/2)^2)^\epsilon = (4\pi\mu^2/m_Q^2)^\epsilon$ with the invariant mass of pro-

duced heavy quark or antiquark $(p/2)^2 = m_Q^2$. To prepare for the sum with the virtual correction from the next subsection, we rewrite the multiplicative factor of the real contribution, $(4\pi\mu^2/(2m_Q)^2)^\epsilon$ as $(4\pi\mu^2/m_Q^2)^\epsilon \times 4^{-\epsilon}$, so that the real contribution in Eq.(6.20) can be expressed as

$$
\begin{aligned}
&\mathcal{D}^{\mathrm{NLO},real}_{[Q\bar{Q}(a^{[8]})]\to[Q\bar{Q}(^1S_0^{[8]})]}(z,\zeta_1,\zeta_2;m_Q,\mu_0) \\
&\qquad = \frac{\alpha_s}{4\,\pi m_Q N_c(N_c^2-1)}\left(\frac{4\pi\mu^2}{m_Q^2}\right)^\epsilon \Gamma(1+\epsilon) \\
&\qquad \times \left\{ -N_c^2\delta(\zeta_1)\delta(\zeta_2)\delta(1-z)\left(\frac{1}{\epsilon_{\mathrm{UV}}\epsilon_{\mathrm{IR}}}-\frac{1}{\epsilon_{\mathrm{IR}}}\right)+\frac{1}{\epsilon_{\mathrm{UV}}}\frac{z}{(1-z)_+}\frac{\Delta_-^{[8]}}{4}\right. \\
&\qquad + 2\,(\ln 2)\,N_c^2\,\delta(\zeta_1)\,\delta(\zeta_2)\,\delta(1-z)\frac{1}{\epsilon_{\mathrm{UV}}} \\
&\qquad - 2\left[(\ln 2)^2+\ln 2\right]N_c^2\,\delta(\zeta_1)\,\delta(\zeta_2)\,\delta(1-z) - (2\ln 2)\frac{z}{(1-z)_+}\frac{\Delta_-^{[8]}}{4} \\
&\qquad \left. +\frac{\Delta_-^{[8]}}{4}\left[-\frac{z}{(1-z)_+}-2\,z\left(\frac{\ln(1-z)}{1-z}\right)_+\right]\right\},
\end{aligned}
\tag{6.22}
$$

where terms with $\ln 2$ dependence are due to the multiplication of the $4^{-\epsilon}$ with the poles, and the terms vanishing at $D = 4$ are neglected. Note that since the $4^{-\epsilon}$ originates from infra-red region, its $\mathcal{O}(\epsilon)$ term should first cancel with the $1/\epsilon_{\mathrm{IR}}$ pole before it cancels the $1/\epsilon_{\mathrm{UV}}$ pole. The mismatch between p^2 of the real contribution and the $(p/2)^2$ of the virtual contribution is similar to the phase space mismatch between the real and virtual contributions to the evolution kernels of heavy quark fragmentation functions, which led to the $\ln(u\bar{u}v\bar{v})$ term in the kernels [40]. Actually, such mismatch originates from the difference of the gluon's maximum allowed light-cone momentum between the real and the virtual diagrams [40].

6.3.2 Virtual contribution

In the Feynman gauge, the Feynman diagrams for virtual correction are shown in Fig. 6.2. Note that diagrams (j), (k) and (l) in Fig. 6.2 have no contributions for $[Q\bar{Q}(a^{[8]})] \to [Q\bar{Q}(^1S_0^{[8]})]$ kernel. The full virtual contribution could be thus

written as

$$\begin{aligned}
&\mathcal{D}^{\text{NLO},virtual}_{[Q\bar{Q}(a^{[8]})]\to[Q\bar{Q}(^1S_0^{[8]})]}(z,\zeta_1,\zeta_2;m_Q,\mu_0)\\
&\qquad=2\delta(1-z)\delta(\zeta_2)\left\{\Lambda(\zeta_1)+\Sigma(\zeta_1)+\Pi(\zeta_1)+W(\zeta_1)\right\}\\
&\qquad\quad+2\delta(1-z)\delta(\zeta_1)\left\{\Lambda^\dagger(\zeta_2)+\Sigma^\dagger(\zeta_2)+\Pi^\dagger(\zeta_2)+W^\dagger(\zeta_2)\right\},
\end{aligned}\tag{6.23}$$

where the first (second) line is from the cut-notation diagrams with NLO diagrams in Fig. 6.2 on the left (right) and LO diagrams on the right (left). Each line is further separated into four terms corresponding to different diagrams in Fig. 6.2: Λ for diagrams (a) and (b), Σ for diagrams (c) and (d), Π for diagram (e), and W for diagrams (f), (g), (h) and (i). ζ_1 and ζ_2 could be any number between -1 and 1. From charge conjugation symmetry (Sec. 5.4.3), we find that $\mathcal{D}^{\text{NLO},virtual}_{[Q\bar{Q}(a^{[8]})]\to[Q\bar{Q}(^1S_0^{[8]})]}(z,\zeta_1,\zeta_2;m_Q,\mu_0)$ is an even function of ζ_1 and ζ_2, and therefore, $\Lambda(\zeta_1)$, $\Sigma(\zeta_1)$, $\Pi(\zeta_1)$ and $W(\zeta_1)$ must be even functions of ζ_1 for this process, which is manifested in our results below.

In the calculation of this virtual contribution, we encounter $\zeta_1^{-1-2\epsilon}\,\text{Sgn}(\zeta_1)$ and $\zeta_1^{-2-2\epsilon}$ type terms, which are divergent as $\zeta_1\to 0$. We regularize these singular terms with the generalized plus-distributions defined in Sec. 6.2.2.

After a considerable amount of algebra, we derive the four terms contributing to the virtual contribution in Eq. (6.23),

$$\Lambda(\zeta_1)=\frac{\alpha_s C_F}{8\pi m_Q(N_c^2-1)}\delta(\zeta_1)\left(\frac{4\pi\mu^2}{m_Q^2}\right)^\epsilon\Gamma(1+\epsilon)\left(\frac{1}{\epsilon_{\text{UV}}\epsilon_{\text{IR}}}+\frac{2}{\epsilon_{\text{UV}}}+4\right),\tag{6.24a}$$

$$\begin{aligned}
\Sigma(\zeta_1)=&\frac{\alpha_s}{8\pi m_Q}\frac{1}{2N_c(N_c^2-1)}\left(\frac{4\pi\mu^2}{m_Q^2}\right)^\epsilon\Gamma(1+\epsilon)\left\{\frac{1}{\epsilon_{\text{UV}}\epsilon_{\text{IR}}}\delta(\zeta_1)\right.\\
&\left.+\frac{1}{\epsilon_{\text{UV}}}\left[(1)_{0+}-\left(\frac{1}{\zeta_1}\right)_{1+}\right]+\left(\frac{\ln(\zeta_1^2)}{\zeta_1}\right)_{1+}-\left(\ln(\zeta_1^2)\right)_{0+}\right\},
\end{aligned}\tag{6.24b}$$

$$\begin{aligned}
\Pi(\zeta_1)=&\frac{\alpha_s}{16\pi m_Q}\frac{1}{2N_c(N_c^2-1)}\left(\frac{4\pi\mu^2}{m_Q^2}\right)^\epsilon\Gamma(1+\epsilon)\left\{\frac{1}{\epsilon_{\text{UV}}}\left[(\zeta_1)_{0+}-(1)_{0+}\right]\right.\\
&-\frac{2}{\epsilon_{\text{IR}}}\delta(\zeta_1)+4\,\delta(\zeta_1)-\left(\zeta_1\ln(\zeta_1^2)+\zeta_1\right)_{0+}+2\left(\frac{1}{\zeta_1}\right)_{1+}\\
&\left.-2\left(\frac{1}{\zeta_1^2}\right)_{2+}+\left(\ln(\zeta_1^2)+1\right)_{0+}\right\},
\end{aligned}\tag{6.24c}$$

$$W(\zeta_1) = -\frac{\alpha_s C_F}{16\pi m_Q (N_c^2-1)}\delta(\zeta_1)\left(\frac{4\pi\mu^2}{m_Q^2}\right)^{\epsilon}\Gamma(1+\epsilon)\left(\frac{1}{\epsilon_{\rm UV}}+\frac{2}{\epsilon_{\rm IR}}+4\right), \tag{6.24d}$$

where $C_F = (N_c^2-1)/(2N_c)$. It is straightforward to verify that every function above is even for ζ_1. Substituting these expressions into Eq. (6.23), we obtain the NLO virtual correction

$$\begin{aligned}
&\mathcal{D}^{\rm NLO,\mathit{virtual}}_{[Q\bar{Q}(a^{[8]})]\to[Q\bar{Q}(^1S_0^{[8]})]}(z,\zeta_1,\zeta_2;m_Q,\mu_0)\\
&\quad=\frac{\alpha_s}{8\pi m_Q}\frac{1}{2N_c(N_c^2-1)}\delta(1-z)\delta(\zeta_2)\left(\frac{4\pi\mu^2}{m_Q^2}\right)^{\epsilon}\Gamma(1+\epsilon)\\
&\qquad\times\Bigg\{2\,N_c^2\delta(\zeta_1)\left[\frac{1}{\epsilon_{\rm UV}\epsilon_{\rm IR}}-\frac{1}{\epsilon_{\rm IR}}+2\right]+\frac{1}{\epsilon_{\rm UV}}\left[3(N_c^2-1)\delta(\zeta_1)-2\left(\frac{1}{\zeta_1}\right)_{1+}\right.\\
&\qquad\left.+(\zeta_1+1)_{0+}\right]+2\left[\left(\frac{1}{\zeta_1}\right)_{1+}-\left(\frac{1}{\zeta_1^2}\right)_{2+}+\left(\frac{\ln(\zeta_1^2)}{\zeta_1}\right)_{1+}\right]\\
&\qquad-\Big((\zeta_1+1)\ln(\zeta_1^2)\Big)_{0+}-(\zeta_1-1)_{0+}\Bigg\}+(\zeta_1\longleftrightarrow\zeta_2).
\end{aligned} \tag{6.25}$$

We also derive the same result by using the light-cone gauge. As noted in the last subsection, there is a mismatch between the $(4\pi\mu^2/(2m_Q)^2)^{\epsilon}$ of the real correction in Eq. (6.20) and the $\left(4\pi\mu^2/m_Q^2\right)^{\epsilon}$ of the virtual correction in Eq. (6.25), which led to the extra logarithms in Eq. (6.22).

Comparing Eq. (6.22) with Eq. (6.25), all infrared poles cancel between the real and virtual contributions. However, the sum of Eq. (6.22) and Eq. (6.25) still contains ultraviolet divergence, which should be taken care of by the renormalization of the nonlocal operators defining the fragmentation functions in Eq. (4.10).

6.3.3 Renormalization of composite operators defining FFs

As defined in Eq. (5.5), the heavy quark-pair FF is defined with an UV counter-term, which is a result of the UV renormalization of the composite operators defining the FFs. The UV counter-term removes the perturbative UV divergence of the FFs order by order in powers of α_s. In general, UV divergence of FFs calculated by using the NRQCD factorization should be different from that defined by QCD factorization. The reason is as follows. The heavy quark mass in QCD factorization is a small scale and is set to be zero at the be-

ginning, while the heavy quark mass in NRQCD factorization is a large scale and is always kept to be finite. Because of the finite quark mass, there are helicity flip contribution in NRQCD calculation, which is forbidden in QCD factorization. Therefore, extra UV divergence for the helicity flip contribution may emerge in NRQCD calculation. An example of this kind of UV divergence is the contribution of the diagram (j) in Fig. 6.2 in the NLO calculation of $\mathcal{D}_{[Q\bar{Q}(t^{[8]})]\to[Q\bar{Q}(^3S_1^{[8]})]}$. Thus, the correct way to renormalize the input FFs calculated by using the NRQCD factorization is:

$$\mathcal{D}_{[Q\bar{Q}(\kappa)]\to[Q\bar{Q}(n)]} = \Gamma_{[Q\bar{Q}(\kappa)]\to[Q\bar{Q}(\kappa')]} \otimes \mathcal{Z}_{[Q\bar{Q}(\kappa')]\to[Q\bar{Q}(\kappa'')]} \otimes \mathcal{D}^{bare}_{[Q\bar{Q}(\kappa'')]\to[Q\bar{Q}(n)]}, \tag{6.26}$$

where Γ is the evolution kernel defined in QCD factorization, and $\mathcal{Z}$ is used to take care of the extra UV divergence discussed above. Expanding Eq. (6.26) to NLO, we find

$$\mathcal{D}^{\rm NLO}_{[Q\bar{Q}(\kappa)]\to[Q\bar{Q}(n)]} = \mathcal{D}^{{\rm NLO},bare}_{[Q\bar{Q}(\kappa)]\to[Q\bar{Q}(n)]} + \mathcal{D}^{{\rm NLO},ren,1}_{[Q\bar{Q}(\kappa)]\to[Q\bar{Q}(n)]} + \mathcal{D}^{{\rm NLO},ren,2}_{[Q\bar{Q}(\kappa)]\to[Q\bar{Q}(n)]}, \tag{6.27}$$

where

$$\begin{aligned}
\mathcal{D}^{{\rm NLO},ren,1}_{[Q\bar{Q}(\kappa)]\to[Q\bar{Q}(n)]}(z,\zeta_1,\zeta_2;m_Q) &= \Gamma^{\rm NLO}_{[Q\bar{Q}(\kappa)]\to[Q\bar{Q}(\kappa')]} \otimes \mathcal{D}^{{\rm LO},bare}_{[Q\bar{Q}(\kappa')]\to[Q\bar{Q}(n)]} \\
&= -\frac{A}{\epsilon_{\rm UV}} \sum_{[Q\bar{Q}(\kappa')]} \int_z^1 \frac{dz'}{z'} \int_{-1}^1 \frac{d\zeta_1'\, d\zeta_2'}{4} \\
&\times \Gamma_{[Q\bar{Q}(\kappa)]\to[Q\bar{Q}(\kappa')]}(z', u=\frac{1+\zeta_1}{2}, v=\frac{1+\zeta_2}{2}; u'=\frac{1+\zeta_1'}{2}, v'=\frac{1+\zeta_2'}{2}) \\
&\times \mathcal{D}^{{\rm LO},bare}_{[Q\bar{Q}(\kappa')]\to[Q\bar{Q}(n)]}(z/z', \zeta_1', \zeta_2', m_Q)\,,
\end{aligned} \tag{6.28}$$

the summation runs over all possible perturbative intermediate $Q\bar{Q}$-pair states κ', and $\Gamma_{[Q\bar{Q}(\kappa)]\to[Q\bar{Q}(\kappa')]}$ is the evolution kernel for a heavy quark pair to evolve into another heavy quark pair perturbatively, which is process-independent and has been derived in Refs. [40, 94]. In this paper, we will use the results obtained in Ref. [40]. In Eq. (6.28), LO short-distance coefficient $\mathcal{D}^{{\rm LO},bare}_{[Q\bar{Q}(\kappa')]\to[Q\bar{Q}(n)]} = \mathcal{D}^{\rm LO}_{[Q\bar{Q}(\kappa')]\to[Q\bar{Q}(n)]}$ could be similarly derived as the example in the last section, but, it must be evaluated and kept in d-dimension in the dimensional regularization. The proportional factor, $A = 1 + \mathcal{O}(\epsilon)$ in Eq. (6.28), is a constant whose choice determines the renormalization scheme.

$\mathcal{D}^{\rm NLO,ren,2}_{[Q\bar{Q}(\kappa)]\to[Q\bar{Q}(n)]}$ in Eq. (6.27) is defined as

$$\mathcal{D}^{\rm NLO,ren,2}_{[Q\bar{Q}(\kappa)]\to[Q\bar{Q}(n)]} = \mathcal{Z}^{\rm NLO}_{[Q\bar{Q}(\kappa)]\to[Q\bar{Q}(\kappa')]} \otimes \mathcal{D}^{\rm LO,bare}_{[Q\bar{Q}(\kappa')]\to[Q\bar{Q}(n)]}, \tag{6.29}$$

and can be similarly written in the integration form as Eq. (6.28). $\mathcal{D}^{\rm NLO,ren,2}_{[Q\bar{Q}(\kappa)]\to[Q\bar{Q}(n)]}$ is scheme dependent, and we will use the same scheme as that in Eq. (6.28). Then, in our calculation, $\mathcal{D}^{\rm NLO,ren,2}_{[Q\bar{Q}(\kappa')]\to[Q\bar{Q}(n)]}$ equals to zero for all processes except $[Q\bar{Q}(t^{[8]})] \to [Q\bar{Q}(^3S_1^{[8]})]$, where

$$\mathcal{D}^{\rm NLO,ren,2}_{[Q\bar{Q}(t^{[8]})]\to[Q\bar{Q}(^3S_1^{[8]})]} = \frac{\alpha_s\,\delta(1-z)}{48\,\pi\,m_Q(N_c^2-1)}\frac{A}{\epsilon_{UV}}\left[\delta(\zeta_1)(1)_{0+} + \delta(\zeta_2)(1)_{0+}\right]. \tag{6.30}$$

In the following, we use $\mathcal{D}^{\rm NLO,ren}_{[Q\bar{Q}(\kappa)]\to[Q\bar{Q}(n)]}$ to represent the addition of the two counter-terms in Eq (6.27).

For our example $[Q\bar{Q}(a^{[8]})] \to [Q\bar{Q}(^1S_0^{[8]})]$, from Eq. (6.28), one could conclude that the LO short-distance coefficients vanish unless $[Q\bar{Q}(\kappa)]$ is $a^{[8]}$. Therefore, Eq. (6.28) could be reduced to

$$\begin{aligned}\mathcal{D}^{\rm NLO,ren}_{[Q\bar{Q}(a^{[8]})]\to[Q\bar{Q}(^1S_0^{[8]})]}(z,\zeta_1,\zeta_2;m_Q) = &-\frac{A}{\epsilon_{\rm UV}}\frac{1}{8m_Q(N_c^2-1)}\\ &\times\Gamma_{[Q\bar{Q}(a^{[8]})]\to[Q\bar{Q}(a^{(8)})]}(z,u=\frac{1+\zeta_1}{2},v=\frac{1+\zeta_2}{2};u'=\frac{1}{2},v'=\frac{1}{2}),\end{aligned} \tag{6.31}$$

where we have used the result of LO short-distance coefficient in Eq. (6.6) and performed the integration with the δ-functions. The evolution kernel has been calculated in Ref. [40] as

$$\begin{aligned}&\Gamma_{[Q\bar{Q}(a^{[8]})]\to[Q\bar{Q}(a^{(8)})]}(z,u=\frac{1+\zeta_1}{2},v=\frac{1+\zeta_2}{2};u'=\frac{1}{2},v'=\frac{1}{2})\\ &\quad=\left(\frac{\alpha_s}{2\pi}\right)\frac{1}{N_c}\Big\{\frac{z}{(1-z)_+}\Delta_-^{[8]} + 8\,(\ln 2)\,N_c^2\,\delta(\zeta_1)\,\delta(\zeta_2)\delta(1-z)\\ &\qquad\qquad+\delta(1-z)[\delta(\zeta_2)F(\zeta_1)+\delta(\zeta_1)F(\zeta_2)]\Big\},\end{aligned} \tag{6.32}$$

where $\Delta_-^{[8]}$ is given by Eq. (5.32) and

$$F(\zeta_1) \equiv 3\,(N_c^2-1)\,\delta(\zeta_1) - 2\left(\frac{1}{\zeta_1}\right)_{1+} + (\zeta_1+1)_{0+}. \tag{6.33}$$

By substituting Eq. (6.32) into Eq. (6.31), we obtain the contribution to the

UV counter-term as

$$\mathcal{D}^{\text{NLO},ren}_{[Q\bar{Q}(a^{[8]})]\to[Q\bar{Q}(^1S_0^{[8]})]}(z,\zeta_1,\zeta_2;m_Q)$$
$$= -\frac{\alpha_s}{\pi}(4\pi e^{-\gamma_E})^\epsilon \frac{1}{\epsilon_{\text{UV}}}\frac{1}{16\,m_Q N_c(N_c^2-1)}\times\Big\{\frac{z}{(1-z)_+}\Delta_-^{[8]}$$
$$+ 8(\ln 2)\,N_c^2\,\delta(\zeta_1)\,\delta(\zeta_2)\,\delta(1-z)+\delta(1-z)\big[\delta(\zeta_2)F(\zeta_1)+\delta(\zeta_1)F(\zeta_2)\big]\Big\}, \tag{6.34}$$

where the "A" in Eq. (6.31) was chosen to be $(4\pi e^{-\gamma_E})^\epsilon$ for the $\overline{\text{MS}}$ scheme. It is straightforward to verify the cancellation of the UV divergence by adding up Eqs. (6.22), (6.25) and (6.34).

From Eq. (6.19), we obtain the NLO short-distance coefficient,

$$\hat{d}^{\text{NLO}}_{[Q\bar{Q}(a^{[8]})]\to[Q\bar{Q}(^1S_0^{[8]})]}(z,\zeta_1,\zeta_2;m_Q,\mu_0) = \frac{\alpha_s}{16\,\pi m_Q(N_c^2-1)}$$
$$\times\Big\{\left(\frac{2\pi}{\alpha_s}\right)\Gamma_{[Q\bar{Q}(a^{[8]})]\to[Q\bar{Q}(a^{[8]})]}(z,\frac{1+\zeta_1}{2},\frac{1+\zeta_2}{2};\frac{1}{2},\frac{1}{2})\,\ln\big[\frac{\mu_0^2}{m_Q^2}\big]$$
$$+R(z,\zeta_1,\zeta_2)+\delta(1-z)[V(\zeta_1)\delta(\zeta_2)+V(\zeta_2)\delta(\zeta_1)]\Big\}, \tag{6.35}$$

where R and V are finite contributions from real and virtual diagrams, respectively, which are defined as

$$V(\zeta_1)=\frac{1}{N_c}\left\{2\left[-\left(\frac{1}{\zeta_1^2}\right)_{2+}+\left(\frac{1}{\zeta_1}\right)_{1+}+\left(\frac{\ln(\zeta_1^2)}{\zeta_1}\right)_{1+}\right]-\big((\zeta_1+1)\ln(\zeta_1^2)\big)_{0+}\right.$$
$$\left.-(\zeta_1-1)_{0+}+4N_c^2\delta(\zeta_1)\right\}, \tag{6.36a}$$
$$R(z,\zeta_1,\zeta_2)=\frac{1}{N_c}\left\{\Delta_-^{[8]}\left[-2z\left(\frac{\ln(2-2z)}{1-z}\right)_+-\frac{z}{(1-z)_+}\right]\right.$$
$$\left.-8\left[(\ln 2)^2+\ln 2\right]N_c^2\,\delta(\zeta_1)\,\delta(\zeta_2)\,\delta(1-z)\right\}, \tag{6.36b}$$

where $\Delta_-^{(8)}$ is defined in Eq. (5.32). Although this expression is not in the same compact form as what is shown in Appendix B, it is trivial to verify the equivalence.

We found that all NLO short-distance coefficients for heavy quarkonium FFs from a perturbatively produced heavy quark pair, calculated in NRQCD factorization formulism, are IR safe. A complete list of our results is given in

Appendix B.

Chapter 7

Calculation of Heavy Quark Pair Fragmentation in NRQCD factorization model: P wave unpolarized

In this chapter, we show detailed calculation of some examples to illustrate the IR divergence cancellation in NRQCD factorization for P-wave heavy quarkonium production. Such cancellation is considered to be a strong support of NRQCD factorization approach.

7.1 LO coefficients

A general cut-diagram representation for $\mathcal{D}^{\rm LO}_{[Q\bar{Q}(s^{[b]})]\to Q\bar{Q}(i^{[b']})}$ is shown in Fig. (6.1), with all momenta labeled explicitly. At this order, the LDME in Eq. (5.4) is proportional to $\delta_{n,n'}$, which leads to

$$\mathcal{D}^{\rm LO}_{[Q\bar{Q}(s^{[b]})]\to[Q\bar{Q}(i^{[b']})]}(z,\zeta_1,\zeta_2;m_Q,\mu_0)=\hat{d}^{\rm LO}_{[Q\bar{Q}(s^{[b]})]\to[Q\bar{Q}(i^{[b']})]}(z,\zeta_1,\zeta_2;m_Q,\mu_0). \tag{7.1}$$

For our purpose of producing a P-wave non-relativistic $Q\bar{Q}$-pair, Eqs. (5.5) and (5.7) can be reduced to,

$$\begin{aligned}&\mathcal{D}^{\rm LO}_{[Q\bar{Q}(s^{[b]})]\to[Q\bar{Q}(i^{[b']})]}(z,\zeta_1,\zeta_2;m_Q,\mu_0)\\&\qquad=\frac{\delta(1-z)}{N_sN_bN_i^{\rm NR}N_{b'}^{\rm NR}}\mathcal{M}^{\rm LO}_{[Q\bar{Q}(s^{[b]})]\to[Q\bar{Q}(i^{[b']})]}(p,z,\zeta_1,\zeta_2)\,,\end{aligned} \tag{7.2}$$

and

$$\mathcal{A}^{\rm LO}_{[Q\bar{Q}(s^{[b]})]\to[Q\bar{Q}(i^{[b']})]}(p,z,\zeta_1) = \lim_{q_r\to 0}\frac{\mathrm{d}}{\mathrm{d}q_r^\alpha}\Big\{2\,\delta(\zeta_1-\frac{2q_r^+}{p_c^+}) \times \bar{\mathcal{A}}^{\rm LO}_{[Q\bar{Q}(s^{[b]})]\to[Q\bar{Q}(i^{[b']})]}(q_1=q_r)\Gamma_i^{\rm NR}(p)\,C_{b'}^{\rm NR}\Big\}, \tag{7.3}$$

respectively. The above three equations, plus Eq. (5.6), form the basis of our calculation for $\hat{d}^{\rm LO}_{[Q\bar{Q}(s^{[b]})]\to[Q\bar{Q}(i^{[b']})]}(z,\zeta_1,\zeta_2;m_Q,\mu_0)$. Based on the discussion in Sec. 5.4.1, we find that only independent FFs at LO are those with both the initial and final $Q\bar{Q}$-pair being color singlet. In the following, we show the detailed calculations of two examples, while presenting all nonzero results in Appendix B.3.1.

First, we consider the LO contribution to fragmentation process: $[Q\bar{Q}(v^{[1]})]\to[Q\bar{Q}({}^3P_J^{[1]})]$. From Eqs. (5.6) and (7.3), we have

$$\begin{aligned}
&\mathrm{Tr}\left[\Gamma_v(p_c)\,C_1\,\mathcal{A}^{\rm LO}_{[Q\bar{Q}(v^{[1]})]\to[Q\bar{Q}({}^3P_J^{[1]})]}(p,z,\zeta_1)\right]\\
&\quad=\lim_{q_r\to 0}\frac{\mathrm{d}}{\mathrm{d}q_r^\alpha}\int\frac{d^Dq_1}{(2\pi)^D}\delta^D(q_1-q_r)\Big\{2\,\delta(\zeta_1-\frac{2q_1^+}{p^+})\,\mathrm{Tr}_c\left[\frac{1}{\sqrt{N_c}}\frac{1}{\sqrt{N_c}}\right]\\
&\quad\times\mathrm{Tr}_\gamma\left[\frac{\gamma\cdot\hat{n}}{4p\cdot\hat{n}}\frac{1}{\sqrt{8m_Q^3}}\left(\frac{\not{p}}{2}-\not{q}_r-m_Q\right)\gamma^\beta\left(\frac{\not{p}}{2}+\not{q}_r+m_Q\right)\right]\Big\}\\
&\quad=\frac{\delta'(\zeta_1)}{\sqrt{2m_Q^3}(p^+)^2}n^\alpha(4\,m_Q^2n^\beta-p^+p^\beta),
\end{aligned}\tag{7.4}$$

where "Tr_c" ("Tr_γ") denotes the trace of color matrices (γ-matrices). In deriving Eq. (7.4), we used the projection operators defined in Sec. 5.2.2 as well as the fact that $p_c=p$. Substituting our result in Eq. (7.4) into Eq. (5.6), and then Eq. (7.2), and using Eq. (7.1), we obtain

$$\hat{d}^{\rm LO}_{[Q\bar{Q}(v^{[1]})]\to[Q\bar{Q}({}^3P_0^{[1]})]}(z,\zeta_1,\zeta_2;m_Q,\mu_0)=\frac{1}{D-1}\frac{1}{2m_Q^3}\,\delta(1-z)\,\delta'(\zeta_1)\,\delta'(\zeta_2), \tag{7.5a}$$

$$\hat{d}^{\rm LO}_{[Q\bar{Q}(v^{[1]})]\to[Q\bar{Q}({}^3P_1^{[1]})]}(z,\zeta_1,\zeta_2;m_Q,\mu_0)=0, \tag{7.5b}$$

$$\hat{d}^{\,\mathrm{LO}}_{[Q\bar{Q}(v^{[1]})]\to[Q\bar{Q}(^3P_2^{[1]})]}(z,\zeta_1,\zeta_2;m_Q,\mu_0)=\frac{1}{(D-1)(D+1)}\frac{1}{m_Q^3}\,\delta(1-z)\,\delta'(\zeta_1)\,\delta'(\zeta_2), \tag{7.5c}$$

where $D=4-2\epsilon$. The zero result in the second equation is expected from the Lorentz invariance, as explained in Sec. 5.4.2. The fact that the right-hand side (RHS) of the first and third equations in Eq. (7.5) are odd in both ζ_1 and ζ_2 is consistent with our analysis above the Eq. (5.23).

For the second example, we consider the LO contribution to fragmentation process: $[Q\bar{Q}(a^{[1]})]\to[Q\bar{Q}(^3P_1^{[1]})]$. Similar to Eq. (7.4), the corresponding trace is

$$\begin{aligned}
&\mathrm{Tr}\left[\Gamma_a(p_c)\,C_1\,\mathcal{A}^{\mathrm{LO}}_{[Q\bar{Q}(a^{[1]})]\to[Q\bar{Q}(^3P_1^{[1]})]}(p,z,\zeta_1)\right]\\
&\quad=\lim_{q_r\to 0}\frac{\mathrm{d}}{\mathrm{d}q_r^\alpha}\Bigg\{2\,\delta(\zeta_1-\frac{2q_r^+}{p^+})\,\mathrm{Tr}_c\left[\frac{1}{\sqrt{N_c}}\frac{1}{\sqrt{N_c}}\right]\\
&\qquad\times\mathrm{Tr}\left[\frac{\gamma\cdot\hat{n}\,\gamma_5-\gamma_5\,\gamma\cdot\hat{n}}{8p\cdot\hat{n}}\frac{1}{\sqrt{8m_Q^3}}\left(\frac{\not{p}}{2}-\not{q}_r-m_Q\right)\gamma^\beta\left(\frac{\not{p}}{2}+\not{q}_r+m_Q\right)\right]\Bigg\}\\
&\quad=\frac{\delta(\zeta_1)}{4p^+\sqrt{2m_Q^3}}\mathrm{Tr}\left[\gamma_5\,\gamma^\alpha\,\gamma^\beta\,\not{\hat{n}}\,\not{p}\right].
\end{aligned} \tag{7.6}$$

The Lorentz structure is exactly the same as our analysis in Sec. 5.4.2. Finally, by substituting our result in Eq. (7.6) into Eq. (5.6), and then Eq. (7.2), and using Eq. (7.1), we obtain

$$\hat{d}^{\,\mathrm{LO}}_{[Q\bar{Q}(a^{[1]})]\to[Q\bar{Q}(^3P_1^{[1]})]}(z,\zeta_1,\zeta_2;m_Q)=\frac{D-3}{m_Q^3(D-1)}\delta(\zeta_1)\delta(\zeta_2)\delta(1-z). \tag{7.7}$$

As expected from our discussion above the equation (5.23), this result is even in both ζ_1 and ζ_2.

7.2 NLO coefficients

In this section, we calculate the short-distance coefficients in Eq. (5.4) at NLO in α_s. We first expand both sides of Eq. (5.4) to NLO,

$$\mathcal{D}^{\rm NLO}_{[Q\bar{Q}(\kappa)]\to[Q\bar{Q}(n')]}(z,\zeta_1,\zeta_2;m_Q,\mu_0) = \hat{d}^{\rm NLO}_{[Q\bar{Q}(\kappa)]\to[Q\bar{Q}(n')]}(z,\zeta_1,\zeta_2;m_Q,\mu_0,\mu_\Lambda) + \sum_{[Q\bar{Q}(n)]} \hat{d}^{\rm LO}_{[Q\bar{Q}(\kappa)]\to[Q\bar{Q}(n)]}(z,\zeta_1,\zeta_2;m_Q,\mu_0)\langle\mathcal{O}^{Q\bar{Q}[n']}_{Q\bar{Q}[n]}(\mu_\Lambda)\rangle^{\rm NLO}, \tag{7.8}$$

Generally, the LHS of Eq. (7.8) has both virtual and real contributions, which are represented by Feynman diagrams in Figs. 6.2 and 6.3, respectively. For any specific subprocess, we can use the symmetry constraints derived in Sec. 5.4.2 to simplify our calculations.

We use dimensional regularization to regularize all kinds of divergences, including the ultra-violet (UV) divergence, infrared (IR) divergence, rapidity divergence, and Coulomb divergence. We apply the technical trick discussed below Eq. (5.7) to our calculations. Consequently, the Coulomb divergence does not appear in our derivations. As shown in Sec. 5.5, the Coulomb divergence in our calculations is effectively absorbed into the NRQCD LDMEs. The rapidity divergence comes from the region $k\cdot\hat{n}\to 0$, with k the momentum of the radiated gluon and $\hat{n}$ the light-cone vector. This region overlaps with the UV region and could lead to a double pole. By adding up all diagrams, the rapidity divergence cancels.

After summing over all diagrams in Figs. 6.2 and 6.3, there are still leftover UV and IR divergences in $\mathcal{D}^{\rm NLO}_{[Q\bar{Q}(\kappa)]\to[Q\bar{Q}(n')]}(z,\zeta_1,\zeta_2;m_Q)$ for producing a P-wave NRQCD $Q\bar{Q}$-pair with the spin-color state $[Q\bar{Q}(n')]$. The UV divergence is canceled by pQCD renormalization of the operator defining the FFs in the same manner as the calculation of FFs to produce S-wave $Q\bar{Q}$-pairs. If NRQCD factorization is valid to NLO, the leftover IR divergence should be exactly the same as the IR divergence in the NLO LDMEs on the RHS of Eq. (7.8), leaving NLO short-distance coefficient IR safe.

In this paper, we calculated all short-distance coefficients of FFs through a P-wave NRQCD $Q\bar{Q}$-pair up to NLO in α_s. From our explicit calculations, we find that the leftover IR divergence cancels for all fragmentation channels at this order.

In the rest of this section, we present the calculation of the short-distance coefficient for the fragmentation channel: $[Q\bar{Q}(a^{[1]})]\to[Q\bar{Q}(^1P_1^{[8]})]$ to demonstrate the cancellation of infrared divergence in NRQCD factorization formalism. From Eq. (7.8), the NLO short-distance coefficient for this channel is

given by

$$\hat{d}^{\,\mathrm{NLO}}_{[Q\bar{Q}(a^{[1]})]\to[Q\bar{Q}(^1P_1^{[8]})]}(z,\zeta_1,\zeta_2;m_Q,\mu_0,\mu_\Lambda)$$
$$=\mathcal{D}^{\mathrm{NLO}}_{[Q\bar{Q}(a^{[1]})]\to[Q\bar{Q}(^1P_1^{[8]})]}(z,\zeta_1,\zeta_2;m_Q,\mu_0)$$
$$-\hat{d}^{\,\mathrm{LO}}_{[Q\bar{Q}(a^{[1]})]\to[Q\bar{Q}(^1S_0^{[1]})]}(z,\zeta_1,\zeta_2;m_Q,\mu_0)\left\langle\mathcal{O}^{[Q\bar{Q}(^1P_1^{[8]})]}_{[Q\bar{Q}(^1S_0^{[1]})]}(\mu_\Lambda)\right\rangle^{\mathrm{NLO}},\tag{7.9}$$

For this channel, the calculation of $\mathcal{D}^{\mathrm{NLO}}_{[Q\bar{Q}(a^{[1]})]\to[Q\bar{Q}(^1P_1^{[8]})]}(z,\zeta_1,\zeta_2;m_Q,\mu_0)$ involves only real correction from Feynman diagrams shown in Fig. 6.3. The calculation of these diagrams is complicated by both UV and IR divergences. We remove the UV divergence by the UV counter-term in the $\overline{\mathrm{MS}}$ scheme, which is associated with pQCD renormalization of the operator defining $[Q\bar{Q}(a^{[1]})]$. This is just like what we did in our calculation of $Q\bar{Q}$ FFs to S-wave $Q\bar{Q}$-pairs. After this $\overline{\mathrm{MS}}$ renormalization procedure, the calculated fragmentation function $\mathcal{D}^{\mathrm{NLO}}_{[Q\bar{Q}(a^{[1]})]\to[Q\bar{Q}(^1P_1^{[8]})]}(z,\zeta_1,\zeta_2;m_Q,\mu_0)$ has only IR divergence left,

$$\mathcal{D}^{\mathrm{NLO}}_{[Q\bar{Q}(a^{[1]})]\to[Q\bar{Q}(^1P_1^{[8]})]}$$
$$=\frac{\alpha_s z\,C_F}{24\pi\,m_Q^3(N_c^2-1)}\left\{(1-z)\Delta_+^{[1]}+\Delta_+^{[1]\prime}+\frac{1}{(1-z)}\Delta_+^{[1]\prime\prime}\right\}\left(\ln[\frac{\mu_0^2}{4m_Q^2}]-\frac{2}{3}\right)$$
$$+\frac{\alpha_s\,C_F}{18\pi\,m_Q^3(N_c^2-1)}\left(\frac{\pi\mu^2}{m_Q^2}\right)^{\epsilon}\Gamma(1+\epsilon)\left\{\left(-\frac{3}{\epsilon_{\mathrm{IR}}}+1\right)\Delta_0\,\delta(1-z)\right.$$
$$-\frac{\Delta_+^{[1]}}{4}\left[-6\left(\frac{1}{1-z}\right)_+ +5z^2+7z-6(z-1)z\ln(1-z)+6\right]$$
$$\left.+\frac{\Delta_+^{[1]\prime}}{4}\frac{z}{(1-z)}[z+6(z-1)\ln(1-z)-4]+\frac{\Delta_+^{[1]\prime\prime}}{4}\frac{z}{(1-z)}[-6\ln(1-z)-1]\right\},\tag{7.10}$$

where μ is the renormalization scale, μ_0 is the QCD factorization scale for input FFs, and the 2/3 along with $\ln(\mu_0^2/4m_Q^2)$ came from the ϵ-dependence of $\hat{d}^{\,\mathrm{LO}}_{[Q\bar{Q}(a^{[8]})]\to[Q\bar{Q}(^1P_1^{[8]})]}$, which is a part of the UV counter-term. As expected from the general symmetry analysis in Sec. 5.4.3, and as shown in Eq. (7.10), only possible structures of ζ_1 and ζ_2 dependence for $\mathcal{D}^{\mathrm{NLO}}_{[Q\bar{Q}(a^{[1]})]\to[Q\bar{Q}(^1P_1^{[8]})]}(z,\zeta_1,\zeta_2;m_Q,\mu_0)$ are given by those Δ-functions: $\Delta_+^{[1]}$, $\Delta_+^{[1]\prime}$ and $\Delta_+^{[1]\prime\prime}$, defined in Eq. (5.32).

Note that since both $\Delta_+^{[1]\prime}$ and $\Delta_+^{[1]\prime\prime}$ vanish at $z \to 1$, the denominator $(1-z)$ in Eq. (7.10), so as that in Eq. (7.14) below, does not exhibit a pole as $z \to 1$. However, the partonic fragmentation function in Eq. (7.10) still shows IR divergence, as indicated by $1/\epsilon_{\rm IR}$, which is expected to be canceled by the second term on the RHS of Eq. (7.9).

For the second term on the RHS of the Eq. (7.9), the NLO LDME can be read from Eq. (5.19)

$$\left\langle \mathcal{O}^{[Q\bar{Q}(^1P_1^{[1]})]}_{[Q\bar{Q}(^1S_0^{[1]})]}(\mu_\Lambda) \right\rangle^{\rm NLO} = \frac{2\alpha_s}{3\,\pi\, m_Q^2 N_c}(4\pi e^{-\gamma_E})^\epsilon \left(\frac{\mu^2}{\mu_\Lambda^2}\right)^\epsilon \frac{1}{\epsilon_{\rm IR}}, \tag{7.11}$$

where we have chosen the $\overline{\rm MS}$ renormalization scheme, and μ (μ_Λ) is the renormalization (NRQCD factorization) scale. The LO short-distance coefficient in Eq. (7.9) can be calculated similarly as in Sec. 6.1,

$$\hat{d}^{\rm LO}_{[Q\bar{Q}(a^{[1]})]\to Q\bar{Q}[(^1S_0^{[1]})]}(z,\zeta_1,\zeta_2;m_Q) = \frac{1}{2\,m_Q}\delta(1-z)\delta(\zeta_1)\delta(\zeta_2). \tag{7.12}$$

Therefore the second term of Eq. (7.9) is

$$\begin{aligned}
&\hat{d}^{\rm LO}_{[Q\bar{Q}(a^{[1]})]\to[Q\bar{Q}(^1S_0^{[1]})]}(z,\zeta_1,\zeta_2;m_Q)\left\langle \mathcal{O}^{[Q\bar{Q}(^1P_1^{[1]})]}_{[Q\bar{Q}(^1S_0^{[1]})]}(\mu_\Lambda) \right\rangle^{\rm NLO} \\
&\qquad = \frac{\alpha_s}{4\,\pi\, m_Q^3 N_c}(4\pi e^{-\gamma_E})^\epsilon \left(\frac{\mu^2}{\mu_\Lambda^2}\right)^\epsilon \frac{1}{\epsilon_{\rm IR}}\delta(1-z)\delta(\zeta_1)\delta(\zeta_2).
\end{aligned} \tag{7.13}$$

By substituting Eqs. (7.10) and (7.13) into Eq. (7.9), we find that the IR divergence is canceled exactly between the first and second terms in Eq. (7.9), and the finite remainder after the IR cancellation is effectively the NLO short-distance coefficient,

$$\begin{aligned}
&\hat{d}^{\rm NLO}_{[Q\bar{Q}(a^{[1]})]\to Q\bar{Q}[(^1P_1^{[8]})]}(z,\zeta_1,\zeta_2;m_Q,\mu_0,\mu_\Lambda) \\
&\qquad = \frac{\alpha_s z}{24\pi\, m_Q^3 N_c}\Big\{2\,\Delta_0\,\delta(1-z)(-\ln\big[\frac{\mu_\Lambda^2}{m_Q^2}\big] + 2\ln 2 + \frac{1}{3}) \\
&\qquad + \big[\frac{\Delta_+^{[1]\prime\prime}}{(1-z)} + \Delta_+^{[1]\prime} + \Delta_+^{[1]}(1-z)\big](\frac{1}{2}\ln\big[\frac{\mu_0^2}{m_Q^2}\big] - \frac{1}{3}) \\
&\qquad - \frac{\Delta_+^{[1]\prime\prime}}{(1-z)}R_1(z) - \frac{\Delta_+^{[1]\prime}}{(1-z)}R_2(z) - \Delta_+^{[1]}\,R_3(z)\Big\},
\end{aligned} \tag{7.14}$$

The R-functions in Eq. (7.14) are defined as

$$R_1(z) = \ln(2-2z) + \frac{1}{6}, \tag{7.15}$$

$$R_2(z) = (1-z)\ln(2-2z) - \frac{1}{6}z + \frac{2}{3}, \tag{7.16}$$

$$R_3(z) = -\frac{1}{(1-z)_+} + (1-z)\ln(2-2z) + \frac{5}{6}z + \frac{7}{6}. \tag{7.17}$$

A complete list of our results is given in Appendix B.3.

Chapter 8

Calculation of Heavy Quark Pair Fragmentation in NRQCD factorization approach: Polarized

In this chapter, we explain the calculation of polarized heavy quarkonium fragmentation functions (FFs) in the NRQCD factorization approach. In Sec. 8.1, we first analyze the operators needed for our calculation. Then in Sec. 8.2, we generalize the definitions of polarized NRQCD long-distance matrix elements (LDMEs) to d dimensions. The factorized forms of the polarized FFs in the NRQCD factorization are given in Sec. 8.3. In Sec. 8.4, we obtain the projection operators from our definitions of the polarized NRQCD LDMEs. Finally in Sec. 8.5, we expand the polarized LDMEs to the next-to-leading order, which is important for the IR divergence cancellation. In this chapter, we do not show the calculation since it is very similar to the calculations of unpolarized FFs, which are explained in detail in the last two chapters. We simply list the results for polarized FFs in Appendixes C and D.

8.1 Essential NRQCD four-fermion operators

The polarization of the heavy quarkonium is encoded in the angular distribution of its decay products (see Sec. 3.1). For the cases of J/ψ, ψ' and their counterparts in the bottom sector, the parameter λ_θ in Eq. (3.1) can be written as [12]

$$\lambda_\theta = \frac{\mathrm{d}\sigma_{11} - \mathrm{d}\sigma_{00}}{\mathrm{d}\sigma_{11} + \mathrm{d}\sigma_{00}}, \tag{8.1}$$

where $\mathrm{d}\sigma_{ij}$ $(i,j = 0,\pm 1)$ represents the ij component in the spin density matrix of the heavy quarkonium, with respect to a specified z-axis. For χ_{cJ} and χ_{bJ}, the expression is more complicated [127]. Nonetheless, in all these expressions, λ_θ is only related to the diagonal entries of the spin density matrix of the heavy quarkonium.

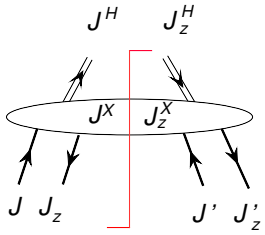

Figure 8.1: Interference term with $Q\bar{Q}$ pair in different polarization.

However, the spin density matrix of the produced heavy quark pair may not be diagonalized. Recall that the NRQCD factorization separates the production of a heavy quarkonium H in two stages: (1) the production of the heavy quark pair $Q\bar{Q}$ at energy scale $\mathcal{O}(m_Q)$ or higher; (2) the hadronization process from $Q\bar{Q}$ to H. Because of the gluon emission, the polarization of $Q\bar{Q}$ pair cannot be uniquely fixed by the polarization of H. Consequently, interference terms also contribute. Fig. 8.1 shows a diagrammatic illustration, where J^X and J_z^X represent the total angular momentum and its z-component of all particles except H, as well as possible orbital angular momentum due to the relative motion between H and X. Consider this process as a forward scattering amplitude from $|J, J_z\rangle$ to $|J', J'_z\rangle$. At the moment the J^H and J_z^H are measured, the wave function collapses to one of the eigenfunctions of J^H and J_z^H. Mathematically, the projection of the collapsed wave function onto the final state $|J', J'_z\rangle$ is expressed as

$$\langle J', J'_z| \sum_{J^X} \Big(|J^H, J_z^H\rangle \; |J^X, J_z - J_z^H\rangle\langle J^X, J_z - J_z^H| \; \langle J^H, J_z^H| \Big) |J, J_z\rangle. \tag{8.2}$$

Requiring Eq. (8.2) to be nonzero gives $J_z = J'_z$, but J and J' can be different. Consequently, off-diagonal terms with the same J_z but different J's in the amplitude and the complex conjugate contribute. To be strict, we still need to consider the L-S coupling in hadron H because S^H and L^H are also measured, besides J^H and J_z^H. Nonetheless, it does not change the conclusion.

The above analysis is valid for any underlying theory which conserves angular momentum. Specifically for NRQCD, for each final state H, we can use the power counting rule in Sec. 3.4.2 to order the possible combinations of

Table 8.1: Essential channels for various polarized heavy quarkonium production, with relative power-counting of each operator explicitly. See text for details.

Quarkonium	Polarization	Essential channels
$J/\psi, \psi',$ $\Upsilon(nS)$	λ	$\mathcal{O}^H({}^3S^{[1]}_{1,\lambda})[v^0], \mathcal{O}^H({}^1S^{[8]}_0)[v^4], \mathcal{O}^H({}^3S^{[8]}_{1,\lambda})[v^4],$ $\mathcal{O}^H({}^3P^{[8]}_0)[v^4], \mathcal{O}^H({}^3P^{[8]}_{1,T})[v^4], \mathcal{O}^H({}^3P^{[8]}_{1,L})[v^4],$ $\mathcal{O}^H({}^3P^{[8]}_{2,T2})[v^4], \mathcal{O}^H({}^3P^{[8]}_{2,T1})[v^4], \mathcal{O}^H({}^3P^{[8]}_{2,L})[v^4]$ $\mathcal{O}^H({}^3P^{[8]}_{2,L}, {}^3P^{[8]}_0)[v^4], \mathcal{O}^H({}^3P^{[8]}_{1,T}, {}^3P^{[8]}_{2,T1})[v^4]$ or $\mathcal{O}^H({}^3S^{[1]}_{1,\lambda})[v^0], \mathcal{O}^H({}^1S^{[8]}_0)[v^4], \mathcal{O}^H({}^3S^{[8]}_{1,\lambda})[v^4],$ $\mathcal{O}^H({}^3P^{[8]}_{J,\lambda})[v^4]$
h_c, h_b	λ	$\mathcal{O}^H({}^1P^{[1]}_{1,\lambda})[v^0]$, $\mathcal{O}^H({}^1S^{[8]}_0)[v^0]$
χ_{c2}, χ_{b2}	λ'	$\mathcal{O}^H({}^3P^{[1]}_{2,\lambda'})[v^0]$, $\mathcal{O}^H({}^3S^{[8]}_{1,T})[v^0]$, $\mathcal{O}^H({}^3S^{[8]}_{1,L})[v^0]$
χ_{cJ}, χ_{bJ} $(J = 0, 1)$	λ	$\mathcal{O}^H({}^3P^{[1]}_{J=0,1;\lambda})[v^0], \mathcal{O}^H({}^3S^{[8]}_{1,T})[v^0], \mathcal{O}^H({}^3S^{[8]}_{1,L})[v^0]$

(J, J', J_z). From the operators for unpolarized heavy quarkonium shown in Table 3.4, we can work out the important operators for the polarized case. These operators are listed in Table 8.1, where the non-relativistic $Q\bar{Q}$ pair polarization $\lambda = T, L$ ($\lambda' = T2, T1, L$) corresponds to $|J_z| = 1, 0$ ($|J_z| = 2, 1, 0$), respectively.

The contribution of the *eight* P-wave operators for the polarized heavy quarkonium $H = J/\psi$, ψ' or $\Upsilon(nS)$ can be effectively combined into *one* operator, by noticing that the polarization of H is determined by the spin of the non-relativistic $Q\bar{Q}$ pair at low orders of v, since the flipping of spin is suppressed by v^4. Performing the L-S coupling mixes the spin and orbital angular momentum, thus conceals this relation. In fact, it is much easier to leave the spin and orbital angular momentum separated. Since the latter does not affect the polarization of H, it can be summed over. As a result, contributions from the eight P-wave operators in the first row of Table 8.1 are described by only one operator $\mathcal{O}^H({}^3P^{[8]}_{J,\lambda})$, where $\lambda = T, L$ represents the polarization of the S-wave heavy quarkonium H, not the non-relativistic $Q\bar{Q}$ pair. Definitions of all these operators are given in the next section.

8.2 Polarized NRQCD four-fermion operators in d dimensions

In previous chapters, we calculated both the single and double parton fragmentation functions (FFs) for an unpolarized heavy quarkonium. We used conventional dimensional regularization (CDR) to regularize all the UV and IR divergences. By doing this, we implicitly generalized the NRQCD four-fermion operators defined in Eqs. (3.10) and (3.12) to $(d-1)$ space dimensions. This generalization is simple, in the sense that with J_z summed over, there is no special direction in the heavy quarkonium rest frame. In this case, $(d-4)$-dimensional space is a simple copy of that in 3 dimensions.

The situation is more complicated with the polarization, where a specific direction $\hat{z}$ needs to be specified. In this chapter, we work in the helicity frame, with $\hat{z}$ chosen to be along the moving direction of the heavy quarkonium in Laboratory frame. To separate contributions with the same J but different $|J_z|$, we need to know the detailed structure of the $(d-4)$-dimensional space. The situation is more severe with angular momentum couplings, such as the L-S coupling, which is exactly what we have in the NRQCD factorization.

First consider the coupling of the spin angular momenta of the $Q\bar{Q}$ pair. For $d \neq 4$, the product of two sponsorial representations gives rise to other representations, in addition to the scalar and vector representations in $d = 4$ case. In principle, we should deal with an infinite set of states. However, the projectors defined in Eq. (5.15) are still correct for the scalar and vector representations. The ignorance of the higher-spin states are allowed because the mix of them with scalar and vector representations is forbidden by heavy quark spin symmetry at low orders of v [112].

Next consider the L-S coupling for P-wave heavy quark pair. The contributions with the same J but different $|J_z|$ have different symmetries in operations such as rotation and parity transformation, which can be applied to separate the contribution of different $|J_z|$. Specifically, we apply the following rules,

- Rule 1: for ${}^3S_1$ and ${}^1P_1$, the wave functions of the heavy quark pair with $|J_z| = 1$ (or $J_z = 0$) in its rest frame are anti-symmetric (or symmetric) when flipping the directions of all axes except $\hat{z}$.

- Rule 2: for ${}^3P_J$, the wave function with $J = 0$ has $SO(d-1)$ symmetry. Wave functions with $J = 2$ (or $J = 1$) are symmetric (or anti-symmetric) in its orbital and spin indices and are constructed to be traceless.

- Rule 3: for ${}^3P_2$, the wave functions with $|J_z| = 1$ are separated from those with $|J_z| = 0, 2$ by flipping the direction of all axes except $\hat{z}$, similarly

as in Rule 1. The wave functions with $J_z = 0$ and $|J_z| = 2$ are further separated by requiring the invariance of the wave function with $J_z = 0$ under the rotation about z-axis.

- Rule 4: for ${}^3P_1$, in d dimensions, there exist wave functions with $|J_z| = 0, 1, 2$. Wave functions with different $|J_z|$ can be separated similarly as in Rule 3. Wave functions with $|J_z| = 1$ are transversely polarized at $d = 4$. Wave functions with $|J_z| = 2$ vanish at $d = 4$ and they have different parity with $|J_z| = 1$ wave functions, so it is natural to consider $|J_z| = 2$ wave functions as longitudinal.

Notice that in d dimensions, there is no unique way to group states into categories with different J and $|J_z|$. Different grouping methods are equally good as long as they are consistent and give the correct decomposition at $d = 4$. They serve as different schemes in dimensional regularization.

With the four rules above, we give our definition of NRQCD four-fermion operators for polarized quarkonium production in arbitrary dimension d,

$$\mathcal{O}^H({}^3S^{[8]}_{1,T}) = \chi^\dagger \sigma^{j_\perp} T^a \psi (a_H^\dagger a_H) \psi^\dagger \sigma^{j_\perp} T^a \chi, \tag{8.3a}$$

$$\mathcal{O}^H({}^3S^{[8]}_{1,L}) = \chi^\dagger \sigma^z T^a \psi (a_H^\dagger a_H) \psi^\dagger \sigma^z T^a \chi, \tag{8.3b}$$

$$\mathcal{O}^H({}^1P^{[8]}_{1,T}) = \chi^\dagger (-\frac{i}{2} \overleftrightarrow{D}^{j_\perp}) T^a \psi (a_H^\dagger a_H) \psi^\dagger (-\frac{i}{2} \overleftrightarrow{D}^{j_\perp}) T^a \chi, \tag{8.3c}$$

$$\mathcal{O}^H({}^1P^{[8]}_{1,L}) = \chi^\dagger (-\frac{i}{2} \overleftrightarrow{D}^{z}) T^a \psi (a_H^\dagger a_H) \psi^\dagger (-\frac{i}{2} \overleftrightarrow{D}^{z}) T^a \chi, \tag{8.3d}$$

$$\mathcal{O}^H({}^3P^{[8]}_{1,T}) = \frac{1}{2} \chi^\dagger (-\frac{i}{2} \overleftrightarrow{D}^{\,[j_\perp} \sigma^{z]}) T^a \psi (a_H^\dagger a_H) \psi^\dagger (-\frac{i}{2} \overleftrightarrow{D}^{\,[j_\perp} \sigma^{z]}) T^a \chi, \tag{8.3e}$$

$$\mathcal{O}^H({}^3P^{[8]}_{1,L}) = \frac{1}{4} \chi^\dagger (-\frac{i}{2} \overleftrightarrow{D}^{\,[j_\perp} \sigma^{k_\perp]}) T^a \psi (a_H^\dagger a_H) \psi^\dagger (-\frac{i}{2} \overleftrightarrow{D}^{\,[j_\perp} \sigma^{k_\perp]}) T^a \chi, \tag{8.3f}$$

$$\begin{aligned} \mathcal{O}^H({}^3P^{[8]}_{2,T2}) = \chi^\dagger (-\frac{i}{2} (\frac{1}{2} \overleftrightarrow{D}^{\,\{j_\perp} \sigma^{k_\perp\}} - \frac{\delta^{j_\perp k_\perp}}{d-2} \overleftrightarrow{\boldsymbol{D}}_T \cdot \boldsymbol{\sigma}_T)) T^a \psi \\ (a_H^\dagger a_H) \psi^\dagger (-\frac{i}{2} (\frac{1}{2} \overleftrightarrow{D}^{\,\{j_\perp} \sigma^{k_\perp\}} - \frac{\delta^{j_\perp k_\perp}}{d-2} \overleftrightarrow{\boldsymbol{D}}_T \cdot \boldsymbol{\sigma}_T)) T^a \chi, \end{aligned} \tag{8.3g}$$

$$\mathcal{O}^H({}^3P^{[8]}_{2,T1}) = \frac{1}{2} \chi^\dagger (-\frac{i}{2} \overleftrightarrow{D}^{\,\{j_\perp} \sigma^{z\}}) T^a \psi (a_H^\dagger a_H) \psi^\dagger (-\frac{i}{2} \overleftrightarrow{D}^{\,\{j_\perp} \sigma^{z\}}) T^a \chi, \tag{8.3h}$$

$$\begin{aligned} \mathcal{O}^H({}^3P^{[8]}_{2,L}) = \frac{d-2}{d-1} \chi^\dagger (-\frac{i}{2} (\overleftrightarrow{D}^{z} \sigma^z - \frac{1}{d-2} \overleftrightarrow{\boldsymbol{D}}_T \cdot \boldsymbol{\sigma}_T)) T^a \psi \\ (a_H^\dagger a_H) \psi^\dagger (-\frac{i}{2} (\overleftrightarrow{D}^{z} \sigma^z - \frac{1}{d-2} \overleftrightarrow{\boldsymbol{D}}_T \cdot \boldsymbol{\sigma}_T)) T^a \chi, \end{aligned} \tag{8.3i}$$

$$\mathcal{O}^H({}^3P^{[8]}_{J,T}) = \chi^\dagger (-\frac{i}{2} \overleftrightarrow{D}^{j} \sigma^{k_\perp}) T^a \psi (a_H^\dagger a_H) \psi^\dagger (-\frac{i}{2} \overleftrightarrow{D}^{j} \sigma^{k_\perp}) T^a \chi, \tag{8.3j}$$

$$\mathcal{O}^H({}^3P_{J,L}^{[8]}) = \chi^\dagger(-\frac{i}{2}\overleftrightarrow{D}^j\sigma^z)\,T^a\psi(a_H^\dagger a_H)\psi^\dagger(-\frac{i}{2}\overleftrightarrow{D}^j\sigma^z)\,T^a\chi, \tag{8.3k}$$

$$\mathcal{O}^H({}^3P_0^{[8]}) = \frac{1}{d-1}\,\chi^\dagger(-\frac{i}{2}\overleftrightarrow{\boldsymbol{D}}\cdot\boldsymbol{\sigma})\,T^a\psi(a_H^\dagger a_H)\psi^\dagger(-\frac{i}{2}\overleftrightarrow{\boldsymbol{D}}\cdot\boldsymbol{\sigma})\,T^a\chi, \tag{8.3l}$$

$$\mathcal{O}^H({}^1S_0^{[8]}) = \chi^\dagger\,T^a\psi(a_H^\dagger a_H)\psi^\dagger\,T^a\chi, \tag{8.3m}$$

where the summations of $j_\perp$ and $k_\perp$ run over all directions perpendicular to $\hat{z}$-axis, and

$$\psi^\dagger\overleftrightarrow{\boldsymbol{D}}\chi \equiv \psi^\dagger(\boldsymbol{D}\chi) - (\boldsymbol{D}\psi)^\dagger\chi, \tag{8.4a}$$

$$\overleftrightarrow{\boldsymbol{D}}_T\cdot\boldsymbol{\sigma}_T \equiv \overleftrightarrow{\boldsymbol{D}}\cdot\boldsymbol{\sigma} - \overleftrightarrow{D}^z\sigma^z, \tag{8.4b}$$

$$\overleftrightarrow{D}^{\,[j_\perp}\,\sigma^{k_\perp]} \equiv \overleftrightarrow{D}^{j_\perp}\,\sigma^{k_\perp} - \overleftrightarrow{D}^{k_\perp}\,\sigma^{j_\perp}, \tag{8.4c}$$

$$\overleftrightarrow{D}^{\,\{j_\perp}\,\sigma^{k_\perp\}} \equiv \overleftrightarrow{D}^{j_\perp}\,\sigma^{k_\perp} + \overleftrightarrow{D}^{k_\perp}\,\sigma^{j_\perp}. \tag{8.4d}$$

For the states ${}^3S_1$, ${}^1P_1$ and ${}^3P_1$, the subscript T (or L) represents the non-relativistic $Q\bar{Q}$ pair with $|J_z| = 1$ (or $J_z = 0$). For the state ${}^3P_2$, the subscripts $T2$, $T1$, and L represent the non-relativistic $Q\bar{Q}$ pair with $|J_z| = 2$, $|J_z| = 1$ and $J_z = 0$, respectively. Notice that T and L in operators $\mathcal{O}^H({}^3P_{J,T}^{[8]})$ and $\mathcal{O}^H({}^3P_{J,L}^{[8]})$ are the polarization of the outgoing S-wave heavy quarkonium, not the non-relativistic P-wave $Q\bar{Q}$ pair, as explained at the end of Sec. 8.1. For completeness, we also list the operators for states ${}^3P_0$ and ${}^1S_0$, which are unpolarized. By removing the two T^a's and multiplying the factor $1/(2N_c)$, we obtain the definitions for the color singlet operators.

In addition to these diagonal operators above, we also need off-diagonal ones

$$\begin{aligned}\mathcal{O}^H[{}^3P_{1,T}^{[8]}, {}^3P_{2,T1}^{[8]}] = \frac{1}{4}\Big[&\chi^\dagger(-\frac{i}{2}\overleftrightarrow{D}^{\,[j_\perp}\,\sigma^{z]})\,T^a\psi(a_H^\dagger a_H)\\ &\psi^\dagger(-\frac{i}{2}\overleftrightarrow{D}^{\,\{j_\perp}\,\sigma^{z\}})\,T^a\chi + \text{H.c.}\Big],\end{aligned} \tag{8.5a}$$

$$\begin{aligned}\mathcal{O}^H[{}^3P_0^{[8]}, {}^3P_{2,L}^{[8]}] = \frac{1}{2}\Big[&\frac{d-2}{d-1}\chi^\dagger(-\frac{i}{2}\overleftrightarrow{\boldsymbol{D}}\cdot\boldsymbol{\sigma})\,T^a\psi(a_H^\dagger a_H)\\ &\psi^\dagger(-\frac{i}{2}(\overleftrightarrow{D}^z\sigma^z - \frac{1}{d-2}\overleftrightarrow{\boldsymbol{D}}_T\cdot\boldsymbol{\sigma}_T))\,T^a\chi + \text{H.c.}\Big].\end{aligned} \tag{8.5b}$$

With the definitions above, it is straightforward to check that by adding up operators with the same J but different $|J_z|$ and choose $d = 4$, the definitions in Eqs. (3.10) and (3.12) can be retrieved.

8.3 NRQCD Factorization for polarized FFs

In the NRQCD factorization approach, the fragmentation functions for polarized heavy quarkonium H can be written into the form

$$\mathcal{D}_{f\to H_{pol_1}}(z;m_Q) = \sum_{[Q\bar{Q}(n,pol_2)]} \pi\alpha_s \Big\{ \hat{d}^{(0)}_{f\to[Q\bar{Q}(n,pol_2)]}(z;m_Q) + \left(\frac{\alpha_s}{\pi}\right) \hat{d}^{(1)}_{f\to[Q\bar{Q}(n,pol_2)]}(z;m_Q) + O(\alpha_s^2) \Big\} \frac{\langle \mathcal{O}^{H_{pol_1}}_{[Q\bar{Q}(n,pol_2)]} \rangle}{m_Q^{2L+3}}, \tag{8.6}$$

and

$$\mathcal{D}_{[Q\bar{Q}(\kappa)]\to H_{pol_1}}(z,\zeta_1,\zeta_2;m_Q) = \sum_{[Q\bar{Q}(n,pol_2)]} \Big\{ \hat{d}^{(0)}_{[Q\bar{Q}(\kappa)]\to[Q\bar{Q}(n,pol_2)]}(z,\zeta_1,\zeta_2;m_Q) + \left(\frac{\alpha_s}{\pi}\right) \hat{d}^{(1)}_{[Q\bar{Q}(\kappa)]\to[Q\bar{Q}(n,pol_2)]}(z,\zeta_1,\zeta_2;m_Q) + O(\alpha_s^2) \Big\} \frac{\langle \mathcal{O}^{H_{pol_1}}_{[Q\bar{Q}(n,pol_2)]} \rangle}{m_Q^{2L+1}}, \tag{8.7}$$

where the QCD factorization and NRQCD factorization scales are suppressed, pol_1 (pol_2) labels the polarization of the heavy quarkonium H (non-relativistic $Q\bar{Q}$-pair). For the states ${}^3S_1$, ${}^1P_1$ and ${}^3P_1$, the labels pol_1 and pol_2 could be transverse (T) or longitudinal (L), while for the state ${}^3P_2$, they could be $T2$, $T1$, or L. In the calculation of λ_θ in helicity frame, $\hat{z}$ can be expressed as a linear combination of the heavy quarkonium momentum p^μ and the light-cone vector $\hat{n}$, thus no additional 4-vector is introduced in the polarized FFs. As a result, the argument that the mixed fragmentation function in Fig 8.2 is absorbed into the heavy quark fragmentation term for the unpolarized FFs [40] also applies to our calculation of polarized FFs.

To a relative accuracy of the order v^4, the polarized NRQCD LDMEs are related to the unpolarized ones as

$$\langle \mathcal{O}^{H_{pol_1}}_{[Q\bar{Q}(n,pol_2)]}(\mu_\Lambda)\rangle = \frac{N^{\rm NR}_{n,pol}}{N^{\rm NR}_n} \delta_{pol_1,pol_2} \langle \mathcal{O}^{H}_{[Q\bar{Q}(n)]}(\mu_\Lambda)\rangle + O(v^4), \tag{8.8}$$

where $N^{\rm NR}_{n,pol}$ and $N^{\rm NR}_n$ are defined in Eqs. (8.17) and (5.16), respectively.

Replacing the hadron by a heavy quark pair in Eqs. (8.6) and (8.7) as in

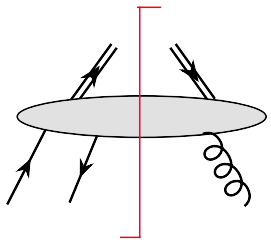

Figure 8.2: Interference term with $Q\bar{Q}$ pair and a single gluon state.

the unpolarized case, we have

$$\mathcal{D}_{f\to[Q\bar{Q}(n',pol_1)]}(z;m_Q) = \sum_{[Q\bar{Q}(n,pol_2)]} \pi\alpha_s \Big\{ \hat{d}^{(0)}_{f\to[Q\bar{Q}(n,pol_2)]}(z;m_Q) + \left(\frac{\alpha_s}{\pi}\right) \hat{d}^{(1)}_{f\to[Q\bar{Q}(n,pol_2)]}(z;m_Q) + O(\alpha_s^2) \Big\} \frac{\langle \mathcal{O}^{[Q\bar{Q}(n',pol_1]}_{[Q\bar{Q}(n,pol_2)]} \rangle}{m_Q^{2L+3}}, \tag{8.9}$$

and

$$\mathcal{D}_{[Q\bar{Q}(\kappa)]\to[Q\bar{Q}(n',pol_1)]}(z,\zeta_1,\zeta_2;m_Q) = \sum_{[Q\bar{Q}(n,pol_2)]} \Big\{ \hat{d}^{(0)}_{[Q\bar{Q}(\kappa)]\to[Q\bar{Q}(n,pol_2)]}(z,\zeta_1,\zeta_2;m_Q) + \left(\frac{\alpha_s}{\pi}\right) \hat{d}^{(1)}_{[Q\bar{Q}(\kappa)]\to[Q\bar{Q}(n,pol_2)]}(z,\zeta_1,\zeta_2;m_Q) + O(\alpha_s^2) \Big\} \frac{\langle \mathcal{O}^{[Q\bar{Q}(n',pol_1]}_{[Q\bar{Q}(n,pol_2)]} \rangle}{m_Q^{2L+1}}, \tag{8.10}$$

where the QCD factorization and the NRQCD factorization scales are suppressed.

Summing over the polarizations, the FFs above should give the unpolarized FFs calculated in previous chapters. With the definition of unpolarized NRQCD matrix elements in Eqs. (3.10) and (3.12), as well as our definition of polarized NRQCD matrix elements above in Eq. (8.3), we have the relation

$$N_n^{\rm NR} \cdot \hat{d}^{(0\ or\ 1)}_{f\to[Q\bar{Q}(n)]} = \sum_{pol} N^{\rm NR}_{n,pol} \cdot \hat{d}^{(0\ or\ 1)}_{f\to[Q\bar{Q}(n,pol)]} + O(v^4), \tag{8.11a}$$

$$N_n^{\rm NR} \cdot \hat{d}^{(0\ or\ 1)}_{[Q\bar{Q}(\kappa)]\to[Q\bar{Q}(n)]} = \sum_{pol} N^{\rm NR}_{n,pol} \cdot \hat{d}^{(0\ or\ 1)}_{[Q\bar{Q}(\kappa)]\to[Q\bar{Q}(n,pol)]} + O(v^4), \tag{8.11b}$$

to a relative accuracy of order v^4, where $\hat{d}^{(0\ or\ 1)}_{f\to[Q\bar{Q}(n)]}$ and $\hat{d}^{(0\ or\ 1)}_{[Q\bar{Q}(\kappa)]\to[Q\bar{Q}(n)]}$ are the short-distance coefficients for unpolarized heavy-quark pair. The summation

runs over all polarization states of n. In Appendix C and D, we only list the $\hat{d}^{(0\ or\ 1)}_{f\to[Q\bar{Q}(n)]}$ and $\hat{d}^{(0\ or\ 1)}_{[Q\bar{Q}(\kappa)]\to[Q\bar{Q}(n,pol)]}$ for one polarization state (two polarization states)for ${}^3S_1$, ${}^1P_1$, and ${}^3P_1$ (${}^3P_2$). The other one can be calculated with Eq. (8.11) and the results in Appendixes. A and B.

8.4 Projection Operators

All four-fermion operators defined in Sec. 8.2 can be written into a product of spin-sumed 4-fermion operator and a projection operator which picks the polarization in consideration. For example,

$$\mathcal{O}^H({}^3S^{[1]}_{1,T}) = \frac{1}{2N_c}\chi^\dagger\sigma^j\,\psi(a_H^\dagger a_H)\psi^\dagger\sigma^k\,\chi\times(\delta^{j,k}-\delta^{j,z}\delta^{k,z}). \tag{8.12}$$

Compared to the unpolarized case, the only difference is the projection operator in the last bracket. If boosting the heavy quarkonium along $\hat{z}$-direction so that it has d-momentum $p^\mu=(p^0,\mathbf{0}_\perp,p^z)$, the boosted projection operator is

$$P^{\rm NR}_{{}^3S_1,T}(p) = (-g_{\beta\beta'}+\frac{p_\beta\hat{n}_{\beta'}+p_{\beta'}\hat{n}_\beta}{p\cdot\hat{n}}-\frac{p^2}{(p\cdot\hat{n})^2}\hat{n}_\beta\hat{n}_{\beta'}), \tag{8.13}$$

where $\hat{n}^\mu=\frac{1}{\sqrt{2}}(1,0,0,-1)$ is a light-like vector.

In this way, we can write down the projection operators for all diagonal NRQCD four-fermion operators defined in Eq. (8.3).

$$P^{\rm NR}_{{}^3S_1,T} = P^{\rm NR}_{{}^1P_1,T} = \mathbb{P}_\perp^{\beta\beta'}(p), \tag{8.14a}$$

$$P^{\rm NR}_{{}^3S_1,L} = P^{\rm NR}_{{}^1P_1,L} = \mathbb{P}_\parallel^{\beta\beta'}(p), \tag{8.14b}$$

$$P^{\rm NR}_{{}^3P_1,T} = \frac{1}{2}\Big(\mathbb{P}_\perp^{\alpha\alpha'}(p)\mathbb{P}_\parallel^{\beta\beta'}(p)+\mathbb{P}_\perp^{\beta\beta'}(p)\mathbb{P}_\parallel^{\alpha\alpha'}(p)-\mathbb{P}_\perp^{\alpha\beta'}(p)\mathbb{P}_\parallel^{\beta\alpha'}(p) -\mathbb{P}_\perp^{\beta\alpha'}(p)\mathbb{P}_\parallel^{\alpha\beta'}(p)\Big), \tag{8.14c}$$

$$P^{\rm NR}_{{}^3P_1,L} = \frac{1}{2}\Big(\mathbb{P}_\perp^{\alpha\alpha'}(p)\mathbb{P}_\perp^{\beta\beta'}(p)-\mathbb{P}_\perp^{\alpha\beta'}(p)\mathbb{P}_\perp^{\beta\alpha'}(p)\Big), \tag{8.14d}$$

$$P^{\rm NR}_{{}^3P_2,T2} = \frac{1}{2}\Big(\mathbb{P}_\perp^{\alpha\alpha'}(p)\mathbb{P}_\perp^{\beta\beta'}(p)+\mathbb{P}_\perp^{\alpha\beta'}(p)\mathbb{P}_\perp^{\alpha'\beta}(p)\Big)-\frac{1}{d-2}\mathbb{P}_\perp^{\alpha\beta}(p)\mathbb{P}_\perp^{\alpha'\beta'}(p), \tag{8.14e}$$

$$P^{\rm NR}_{{}^3P_2,T1} = \frac{1}{2}\Big(\mathbb{P}_\perp^{\alpha\alpha'}(p)\mathbb{P}_\parallel^{\beta\beta'}(p)+\mathbb{P}_\perp^{\beta\beta'}(p)\mathbb{P}_\parallel^{\alpha\alpha'}(p)+\mathbb{P}_\perp^{\alpha\beta'}(p)\mathbb{P}_\parallel^{\beta\alpha'}(p) +\mathbb{P}_\perp^{\beta\alpha'}(p)\mathbb{P}_\parallel^{\alpha\beta'}(p)\Big), \tag{8.14f}$$

$$P^{\rm NR}_{^3P_2,L} = \frac{d-2}{d-1}(\mathbb{P}_\parallel^{\alpha\beta}(p) - \frac{1}{d-2}\mathbb{P}_\perp^{\alpha\beta}(p))(\mathbb{P}_\parallel^{\alpha'\beta'}(p) - \frac{1}{d-2}\mathbb{P}_\perp^{\alpha'\beta'}(p)), \tag{8.14g}$$

$$P^{\rm NR}_{^3P_0} = \frac{1}{d-1}\mathbb{P}^{\alpha\beta}(p)\mathbb{P}^{\alpha'\beta'}(p), \tag{8.14h}$$

$$P^{\rm NR}_{^1S_0} = 1, \tag{8.14i}$$

$$P^{\rm NR}_{^3P_J,T} = \mathbb{P}^{\alpha\alpha'}(p)\mathbb{P}_\perp^{\beta\beta'}(p), \tag{8.14j}$$

$$P^{\rm NR}_{^3P_J,L} = \mathbb{P}^{\alpha\alpha'}(p)\mathbb{P}_\parallel^{\beta\beta'}(p), \tag{8.14k}$$

where

$$\mathbb{P}_\perp^{\alpha\alpha'}(p) = -g^{\alpha\alpha'} + \frac{p^\alpha \hat{n}^{\alpha'} + p^{\alpha'}\hat{n}^\alpha}{p\cdot\hat{n}} - \frac{p^2}{(p\cdot\hat{n})^2}\hat{n}^\alpha\hat{n}^{\alpha'}, \tag{8.15a}$$

$$\mathbb{P}_\parallel^{\alpha\alpha'}(p) = \frac{p^\alpha p^{\alpha'}}{p^2} - \frac{p^\alpha \hat{n}^{\alpha'} + p^{\alpha'}\hat{n}^\alpha}{p\cdot\hat{n}} + \frac{p^2}{(p\cdot\hat{n})^2}\hat{n}^\alpha\hat{n}^{\alpha'}, \tag{8.15b}$$

$$\mathbb{P}^{\alpha\alpha'}(p) = \mathbb{P}_\parallel^{\alpha\alpha'}(p) + \mathbb{P}_\perp^{\alpha\alpha'}(p) = -g^{\alpha\alpha'} + \frac{p^\alpha p^{\alpha'}}{p^2}. \tag{8.15c}$$

α and β (α' and β') are the indices for the orbital angular momentum and spin of the heavy quark pair in the amplitude (complex conjugate of the amplitude), respectively.

Making use of the identity

$$\mathbb{P}_\parallel^{\alpha\alpha'}\mathbb{P}_\parallel^{\beta\beta'} = \mathbb{P}_\parallel^{\alpha\beta'}\mathbb{P}_\parallel^{\beta\alpha'} \tag{8.16}$$

and adding up the projection operators with different $|J_z|$ but the same J, we can get the same results in Eq. (5.17). Choosing $d = 4$ in the $P^{\rm NR}_{^3P_2}$, we retrieve the results in Ref. [128].

We normalize these projection operators by the number of states, since the four-fermion operators in Eq. (8.3) are defined to sum over the number of states with the specific polarization. The normalization factors are

$$N^{\rm NR}_{^3S_1,T} = N^{\rm NR}_{^1P_1,T} = N^{\rm NR}_{^3P_1,T} = N^{\rm NR}_{^3P_2,T1} = d-2, \tag{8.17a}$$

$$N^{\rm NR}_{^3S_1,L} = N^{\rm NR}_{^1P_1,L} = N^{\rm NR}_{^3P_2,L} = 1, \tag{8.17b}$$

$$N^{\rm NR}_{^3P_1,L} = \frac{1}{2}(d-2)(d-3), \tag{8.17c}$$

$$N^{\rm NR}_{^3P_2,T2} = \frac{1}{2}(d-1)(d-2) - 1, \tag{8.17d}$$

$$N^{\rm NR}_{^3P_J,T} = (d-1)(d-2), \tag{8.17e}$$

$$N^{\rm NR}_{^3P_J,L} = (d-1). \tag{8.17f}$$

To get these results, we have used

$$(-g_{\alpha\alpha'})\mathbb{P}_{\perp}^{\alpha\alpha'} = d-2, \tag{8.18a}$$

$$(-g_{\alpha\alpha'})\mathbb{P}_{\parallel}^{\alpha\alpha'} = 1, \tag{8.18b}$$

$$(-g_{\alpha\alpha'})(-g_{\beta\beta'})\mathbb{P}_{\perp}^{\alpha\beta'}\mathbb{P}_{\perp}^{\beta\alpha'} = d-2, \tag{8.18c}$$

$$(-g_{\alpha\alpha'})(-g_{\beta\beta'})\mathbb{P}_{\parallel}^{\alpha\beta'}\mathbb{P}_{\parallel}^{\beta\alpha'} = 1, \tag{8.18d}$$

$$(-g_{\alpha\alpha'})(-g_{\beta\beta'})\mathbb{P}_{\parallel}^{\alpha\beta'}\mathbb{P}_{\perp}^{\beta\alpha'} = 0, \tag{8.18e}$$

By adding the number of states with the same J but different J_z, we can retrieve the normalization factor for unpolarized heavy-quark-pair in Eq. (5.16). By choosing $d=4$, we obtain the familiar L-S coupling results.

8.5 Expand polarized LDMEs to NLO with perturbative NRQCD

To cancel the IR divergence from the NLO full QCD calculation, we need to expand the polarized NRQCD LDMEs to NLO, as for the unpolarized case in Sec. 5.3. We can calculate the NLO NRQCD corrections for these four-fermion operators using the same method as Ref. [117]. For our purpose, we only calculate the NLO correction of S-wave 4-fermion operators,

$$\langle \mathcal{O}^{Q\bar{Q}}({}^1S_0^{[1]})\rangle = \langle \mathcal{O}^{Q\bar{Q}}({}^1S_0^{[1]})\rangle^{\mathrm{LO}} - C_\epsilon \frac{1}{2N_c}\Big\{\langle \mathcal{O}_T^{Q\bar{Q}}({}^1P_1^{[8]})\rangle^{\mathrm{LO}} + \langle \mathcal{O}_L^{Q\bar{Q}}({}^1P_1^{[8]})\rangle^{\mathrm{LO}}\Big\}, \tag{8.19a}$$

$$\begin{aligned}\langle \mathcal{O}^{Q\bar{Q}}({}^1S_0^{[8]})\rangle = \langle \mathcal{O}^{Q\bar{Q}}({}^1S_0^{[8]})\rangle^{\mathrm{LO}} - C_\epsilon\Big\{ & C_F\left(\langle \mathcal{O}_T^{Q\bar{Q}}({}^1P_1^{[1]})\rangle^{\mathrm{LO}} + \langle \mathcal{O}_L^{Q\bar{Q}}({}^1P_1^{[1]})\rangle^{\mathrm{LO}}\right) \\ & + B_F\left(\langle \mathcal{O}_T^{Q\bar{Q}}({}^1P_1^{[8]})\rangle^{\mathrm{LO}} + \langle \mathcal{O}_L^{Q\bar{Q}}({}^1P_1^{[8]})\rangle^{\mathrm{LO}}\right)\Big\},\end{aligned} \tag{8.19b}$$

$$\langle \mathcal{O}_T^{Q\bar{Q}}({}^3S_1^{[1]})\rangle = \langle \mathcal{O}_T^{Q\bar{Q}}({}^3S_1^{[1]})\rangle^{\mathrm{LO}} - C_\epsilon \frac{1}{2N_c} CO_T, \tag{8.19c}$$

$$\langle \mathcal{O}_L^{Q\bar{Q}}({}^3S_1^{[1]})\rangle = \langle \mathcal{O}_L^{Q\bar{Q}}({}^3S_1^{[1]})\rangle^{\mathrm{LO}} - C_\epsilon \frac{1}{2N_c} CO_L, \tag{8.19d}$$

$$\langle \mathcal{O}_T^{Q\bar{Q}}({}^3S_1^{[8]})\rangle = \langle \mathcal{O}_T^{Q\bar{Q}}({}^3S_1^{[8]})\rangle^{\mathrm{LO}} - C_\epsilon\Big\{C_F\cdot CS_T + B_F\cdot CO_T\Big\}, \tag{8.19e}$$

$$\langle \mathcal{O}_L^{Q\bar{Q}}({}^3S_1^{[8]})\rangle = \langle \mathcal{O}_L^{Q\bar{Q}}({}^3S_1^{[8]})\rangle^{\mathrm{LO}} - C_\epsilon\Big\{C_F\cdot CS_L + B_F\cdot CO_L\Big\}, \tag{8.19f}$$

where

$$\begin{aligned} CS_T =& \frac{d-2}{d-1}\langle \mathcal{O}^{Q\bar{Q}}({}^3P_0^{[1]})\rangle^{\rm LO} + \frac{1}{2}\langle \mathcal{O}_T^{Q\bar{Q}}({}^3P_1^{[1]})\rangle^{\rm LO} + \langle \mathcal{O}_L^{Q\bar{Q}}({}^3P_1^{[1]})\rangle^{\rm LO} \\ &+ \langle \mathcal{O}_{T2}^{Q\bar{Q}}({}^3P_2^{[1]})\rangle + \frac{1}{2}\langle \mathcal{O}_{T1}^{Q\bar{Q}}({}^3P_2^{[1]})\rangle^{\rm LO} + \frac{1}{d-1}\langle \mathcal{O}_L^{Q\bar{Q}}({}^3P_2^{[1]})\rangle^{\rm LO} \\ &- \frac{2}{d-1}\langle \mathcal{O}[({}^3P_0^{[1]}), ({}^3P_2^{[1]})_L]\rangle^{\rm LO} - \langle \mathcal{O}[({}^3P_1^{[1]})_T, ({}^3P_2^{[1]})_{T1}]\rangle^{\rm LO}, \end{aligned} \tag{8.20a}$$

$$\begin{aligned} CS_L =& \frac{1}{d-1}\langle \mathcal{O}^{Q\bar{Q}}({}^3P_0^{[1]})\rangle^{\rm LO} + \frac{1}{2}\langle \mathcal{O}_T^{Q\bar{Q}}({}^3P_1^{[1]})\rangle^{\rm LO} + \frac{1}{2}\langle \mathcal{O}_{T1}^{Q\bar{Q}}({}^3P_2^{[1]})\rangle^{\rm LO} \\ &+ \frac{d-2}{d-1}\langle \mathcal{O}_L^{Q\bar{Q}}({}^3P_2^{[1]})\rangle^{\rm LO} + \frac{2}{d-1}\langle \mathcal{O}[({}^3P_0^{[1]}), ({}^3P_2^{[1]})_L]\rangle^{\rm LO} \\ &+ \langle \mathcal{O}[({}^3P_2^{[1]})_{T1}, ({}^3P_1^{[1]})_T]\rangle^{\rm LO}, \end{aligned} \tag{8.20b}$$

$$C_\epsilon = \frac{4\alpha_s}{3\pi m_Q^2}\frac{1}{\epsilon_{IR}}(4\pi e^{-\gamma_E})\left(\frac{\mu_r}{\mu_\Lambda}\right)^\epsilon, \tag{8.20c}$$

$$B_F = \frac{N_c^2-4}{4N_c}, \tag{8.20d}$$

and CO_T (CO_L) is the same as CS_T (CS_L) except that all matrix elements are in color octet state.

8.6 Compare with NLO NRQCD calculation

The complicated, numerical NLO NRQCD calculation for J/ψ polarization can be easily understood with the result of LO polarized fragmentation functions. In the following, we only give a qualitative analysis, while leaving the numerical study in the future work.

The NLO NRQCD result for direct J/ψ production is shown in Fig. 3.11. In Fig. 8.3, we also show the p_T dependence of λ_θ for all four important channels of J/ψ production. Recall that in the NRQCD factorization, the LO results for the ${}^3S_1^{[8]}$, ${}^3P_J^{[8]}$, and ${}^1S_0^{[8]}$ are dominated by the next-to-leading-power (NLP) contribution, while the NLO results are dominated by the leading-power (LP) contribution, both at large p_T. For the ${}^3S_1^{[1]}$ channel in the NRQCD factorization, the LO result is dominated by the next-to-next-to-leading-power (NNLP) contribution, while the NLO result is dominated by the NLP contribution, both at large p_T. (More details in Sec. 3.5)

The results of polarized fragmentation functions are listed in Appendixes C and D. In Table 8.2, we show the LO contributions from different channels to

the J/ψ polarization. The single-quark fragmentations are not important since they are suppressed at large z. The contribution with a fragmenting $Q\bar{Q}$ pair in a tensor state is suppressed by the hard part [24]. These suppressed channels are not showed in Table 8.2. For completeness, we also list the ${}^1S_0^{[8]}$ channel, which contributes to unpolarized J/ψ production.

Table 8.2: The contributions of LO FFs to the J/ψ polarization. The labels "T", "L", and "Un" represent transversely polarized, longitudinally polarized, and unpolarized, respectively.

	${}^3S_1^{[1]}$	${}^3S_1^{[8]}$	${}^3P_J^{[8]}$	${}^1S_0^{[8]}$
g		T		
$v^{[1]}$	L			
$v^{[8]}$		L	L	
$a^{[1]}$				
$a^{[8]}$			T	Un

For the ${}^3S_1^{[1]}$ channel, the LO NRQCD result is dominated by the NNLP contribution, which is not included in the QCD factorization approach in Eq. (4.4). The NLO NRQCD result is dominated by NLP contribution. From Table 8.2, the dominant NLP contribution is from a fragmenting $Q\bar{Q}$ pair in $v^{[1]}$ state, which gives longitudinally polarized J/ψ. This conclusion agrees with the NLO NRQCD calculation in Fig. 8.3.

For the ${}^3S_1^{[8]}$ channel, both the LO and NLO NRQCD calculation are dominated by LP contribution, which produces transversely polarized J/ψ. The NRQCD calculation in Fig. 8.3 also shows the transverse polarization.

For the ${}^3P_J^{[8]}$ channel, the LO NRQCD calculation is dominated by the NLP contribution. At NLP, the fragmenting $Q\bar{Q}$ pair can be in either $v^{[8]}$ or $a^{[8]}$ states, and these two states give opposite J/ψ polarization. Since the hard part of $v^{[8]}$ is larger than that of $a^{[8]}$ [24], the produced J/ψ is longitudinally polarized.

The NLO NRQCD calculation for the ${}^3P_J^{[8]}$ channel is dominated by LP contribution. In the QCD factorization, this contribution comes from the NLO FFs from a single gluon to the ${}^3P_J^{[8]}$ $Q\bar{Q}$ pair. Eq. (C.21) shows that the longitudinally polarized J/ψ produced from the LP ${}^3P_J^{[8]}$ contribution is suppressed at large z region. However, the unpolarized FF in Eq. (A.14) shows that the contribution of LP ${}^3P_J^{[8]}$ channel to the polarization-summed J/ψ production is, surprisingly, negative. Consequently, the LP ${}^3P_J^{[8]}$ channel

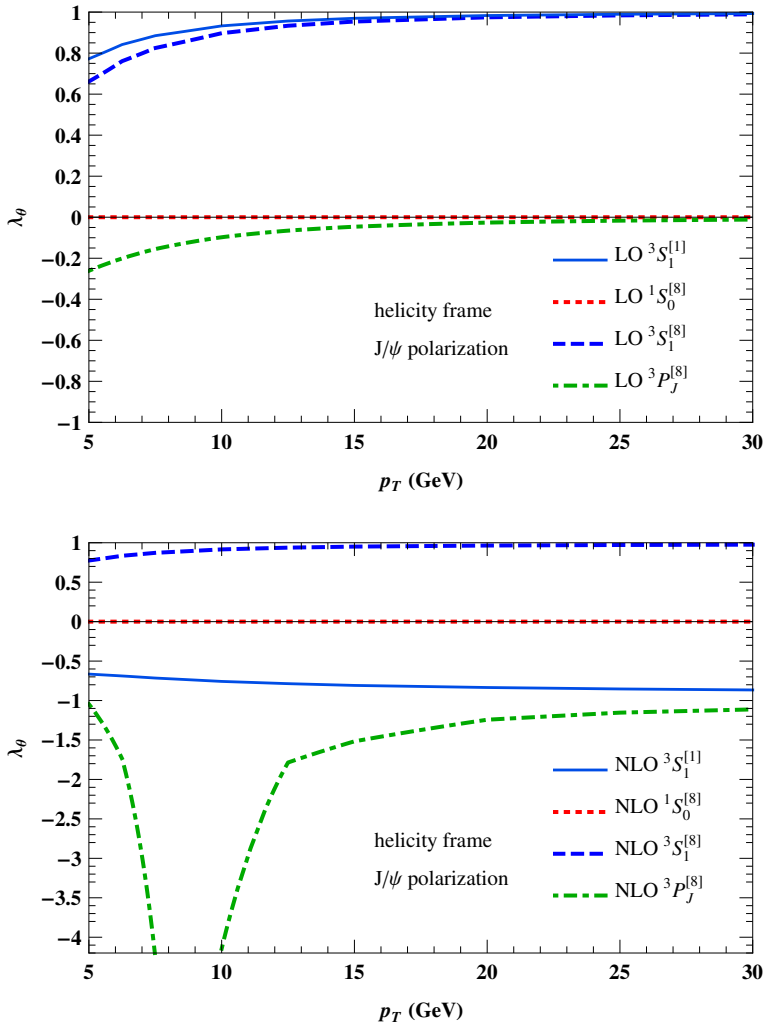

Figure 8.3: The p_T dependence of λ_θ for ${}^3S_1^{[1]}$, ${}^1S_0^{[8]}$, ${}^3S_1^{[8]}$, and ${}^3P_J^{[8]}$ channels. For the NLO ${}^3P_J^{[8]}$ channel, the dot-dashed curve means the value of $(\mathrm{d}\hat{\sigma}_{11} - \mathrm{d}\hat{\sigma}_{00})/|\mathrm{d}\hat{\sigma}_{11}+\mathrm{d}\hat{\sigma}_{00}|$. For other curves, the definition of λ_θ is in Eq. (8.1). Figure taken from Ref. [12]

has a negative contribution to the transversely polarized J/ψ. Therefore, at large p_T,

$$\frac{\mathrm{d}\hat{\sigma}_{11} - \mathrm{d}\hat{\sigma}_{00}}{|\mathrm{d}\hat{\sigma}_{11} + \mathrm{d}\hat{\sigma}_{00}|} \approx \frac{\mathrm{d}\hat{\sigma}_{11}}{|\mathrm{d}\hat{\sigma}_{11}|} = -1. \tag{8.21}$$

This is exactly the behavior of the ${}^3P_J^{[8]}$ channel in the NLO NRQCD calcula-

tion shown in Fig. 8.3.

Recall that ψ' is produced as almost unpolarized at current collider energies, which is called the polarization puzzle (see Sec. 3.4.4). A possible explanation comes from the observation that the LP terms and the NLP terms contribute to opposite polarization of ψ' (Table 8.2 also works for the ψ' production). At the p_T region where LP terms and NLP terms are approximately equal, the cancellation of LP and NLP contributions may lead to unpolarized ψ' production. At relatively large p_T, it is necessary to evolve the polarized FFs at an input scale $\mu_0 \gtrsim 2m_Q$ to the scale p_T by solving the evolution equations in Eqs. (4.13) and (4.14). Notice the mixed kernel in Eq. (4.13) may "smear" the contribution of the LP terms to the transversely polarized ψ'. If this smearing effect is strong enough, the produced ψ' could be unpolarized even at relatively large p_T. Detailed numerical study is needed to check this conjecture. However it is fair to say that the QCD factorization has the potential to solve the polarization puzzle.

To summarize, as a qualitative analysis, the polarized FFs can explain the p_T dependence of λ_θ in the NLO NRQCD calculation, for all important channels of J/ψ polarization. Depending on the effect of the mixed kernel in the single-parton evolution equation, the QCD factorization has the potential to solve the polarization puzzle.

Chapter 9

Phenomenological study of QCD factorization

The predictive power of QCD factorization approach relies on our ability to calculate the short-distance coefficients perturbatively, to solve the evolution equations in Eqs. (4.13) and (4.14), and our knowledge of a large set of multi-variable input fragmentation functions (FFs). In previous chapters, we have calculated these fragmentation functions to heavy quarkonium with input scale $\mu_0 \gtrsim 2m_Q$ in the NRQCD factorization and further factorized the non-perturbative contribution into a few NRQCD long-distance matrix elements (LDMEs). In this chapter, with these input FFs at hand, we apply the QCD factorization to unpolarized J/ψ production. We compare the QCD factorization prediction, including the leading (LP) and the first next-to-leading power (NLP) in p_T, to the next-to-leading-order (NLO) NRQCD calculation.

Specifically, we compare leading-order (LO) result of QCD factorization without resuming large logarithms, to NLO NRQCD calculation (some modifications are required, which will be clear later). Recall that the NLO NRQCD calculation is extremely difficult and are only accomplished numerically (see Sec. 3.4). If our simple analytical LO calculation can reproduce NLO NRQCD, it will be a direct evidence of the power of QCD factorization.

To be self-contained, we repeat the QCD factorization formula in Eq. (4.4) below,

$$\begin{aligned} & d\sigma_{A+B\to H+X}(p) \\ & \approx \sum_f \int_0^1 \frac{dz}{z^2} D_{f\to H}(z)\, d\hat{\sigma}_{A+B\to f(p_c)+X}(p/z) \\ & \quad + \sum_\kappa \int_0^1 \frac{dz}{z^2} \int_{-1}^1 \frac{d\zeta_1 d\zeta_2}{4}\, \mathcal{D}_{[Q\bar{Q}(\kappa)]\to H}(z,\zeta_1,\zeta_2) \end{aligned} \tag{9.1}$$

$$\times d\hat{\sigma}_{A+B\to[Q\bar{Q}(\kappa)](p_c)+X}(p(1\pm\zeta_1)/2z, p(1\pm\zeta_2)/2z),$$

where $D_{f\to H}$ ($\mathcal{D}_{[Q\bar{Q}(\kappa)]\to H}$) are single (double) parton FFs, which give the LP (NLP) contribution, $\sum_f$ runs over all parton flavor $f = q, \bar{q}, g$, and $\sum_\kappa$ includes all spin and color states of fragmenting heavy quark-antiquark pairs: $v^{[1,8]}$, $a^{[1,8]}$, or $t^{[1,8]}$, where v, a and t refer to the vector, axial-vector, and tensor states of the pair's spin. In Eq. (9.1), the $d\hat{\sigma}$ are short-distance coefficients (SDCs) to produce on-shell fragmenting parton(s), and contain all information about the initial colliding state, including convolutions with parton distribution functions (PDFs) if A and B are hadrons. Longitudinal momentum fractions are defined as $z = p^+/p_c^+$, $\zeta_1 = 2q_1^+/p_c^+$ and $\zeta_2 = 2q_2^+/p_c^+$, where p^+, p_c^+, and q_1^+ (q_2^+) are the light-cone "+" components of, respectively, the momenta of the quarkonium, the fragmenting single parton or heavy quark-antiquark pair, and half the relative momentum of the heavy quark and antiquark in the amplitude (complex conjugate amplitude).

For numerical predictions, we need to use the SDCs and evolution kernels of FFs and PDFs at the same order in their perturbative expansion to provide a fully consistent factorized cross section. For example, for the LO contribution to the cross section, we should use LO PDFs and FFs (evaluated with LO kernels) and LO SDCs. It is important to note, however, that the order of the factorized cross section should be distinguished from the order at which we calculate the input FFs in NRQCD. To have the best model predictions for the FFs, we should always use the input FFs calculated in NRQCD at the highest order available in α_s evaluated at the NRQCD factorization scale, regardless the order at which we evaluate the perturbative contribution to the factorized cross section.

However, the factorized power expansion in Eq. (9.1) and NRQCD factorization organize the order of perturbative contributions to heavy quarkonium production differently. NRQCD factorization calculation for large p_T J/ψ production starts at the order α_s^3 (see Fig. 3.16). For those heavy quark pair with even charge parity, such as ${}^1S_0^{[8]}$ and ${}^3P_J^{[8]}$, LP Feynman diagrams first appear at NLO. In Fig. 9.1, we show one of these Feynman diagrams and its decomposition in the QCD factorization. This diagram is NLO in the NRQCD factorization and should convolute with the NLO parton distribution functions (PDFs). However, it has the LO SDC in the QCD factorization and should convolute with the LO PDFs in principle. To compare with the NLO NRQCD calculation, we also use the NLO PDFs for such diagrams in the QCD factorization calculation.

In particular, in the power expansion we must independently specify the order of evolution for parton distributions and the order at which we compute

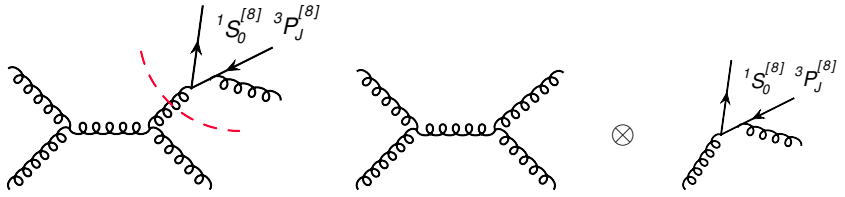

(a) (b)

Figure 9.1: A typical Feynman diagram in NRQCD factorization calculation and its factorized form in QCD factorization.

FFs as well as SDCs. Our choices for this numerical comparison are listed in Table 9.1. To compare our LO predictions with NLO NRQCD calculations, we in general evaluate Eq. (9.1) for both the LP and NLP contributions with the LO hard parts [24], LO PDFs (CTEQ6L1 [129]), and FFs from Refs. [45, 46] without including the evolution. We use, however, NLO PDFs for the $^1S_0^{[8]}$ and $^3P_J^{[8]}$ channels at LP for the reason explained above.

Table 9.1: The choices for our LO QCD factorization calculations in Eq. (9.1) for comparison with NLO NRQCD calculations. Explicit formulas for the SDCs in Ref. [23, 24] for NLP and Ref. [25] for LP.

Channel	$^3S_1^{[1]}$	$^3S_1^{[1]}$	$^3S_1^{[8]}$	$^3S_1^{[8]}$	$^1S_0^{[8]}$	$^1S_0^{[8]}$	$^3P_J^{[8]}$	$^3P_J^{[8]}$
Power	LP	NLP	LP	NLP	LP	NLP	LP	NLP
PDFs	-	LO	LO	LO	NLO	LO	NLO	LO
FFs	-	α_s^1	α_s^1	α_s^0	α_s^2	α_s^0	α_s^2	α_s^0
SDCs	-	α_s^3	α_s^2	α_s^3	α_s^2	α_s^3	α_s^2	α_s^3

In Fig. 9.2, we show the ratios of our analytic LO predictions with the PDFs and parameter choices in Table 9.1 to the numerical results of NLO NRQCD calculations in various leading NRQCD channels. Note that the values of the NRQCD matrix elements cancel in these ratios. The tilde of $d\tilde{\sigma}_{\rm LO}^{\rm QCD}$ indicates the slightly modified LO contribution, with the choices specified in Table 9.1, to better match the NLO NRQCD calculations. We choose $\sqrt{S} = 7$ TeV and $|y| < 0.9$ for a typical kinematic regime at the LHC. We take charm quark mass $m_c = 1.5$ GeV, $\Lambda_{\rm QCD}^{(5)} = 165$ MeV ($\Lambda_{\rm QCD}^{(5)} = 226$ MeV) for LO (NLO) α_s with quark active flavors $n_f = 5$, and CTEQ6M when NLO PDFs are needed

[129], and set the renormalization, factorization, and the NRQCD scales to $\mu_r = \mu_f = p_T$ and $\mu_\Lambda = m_c$, respectively.

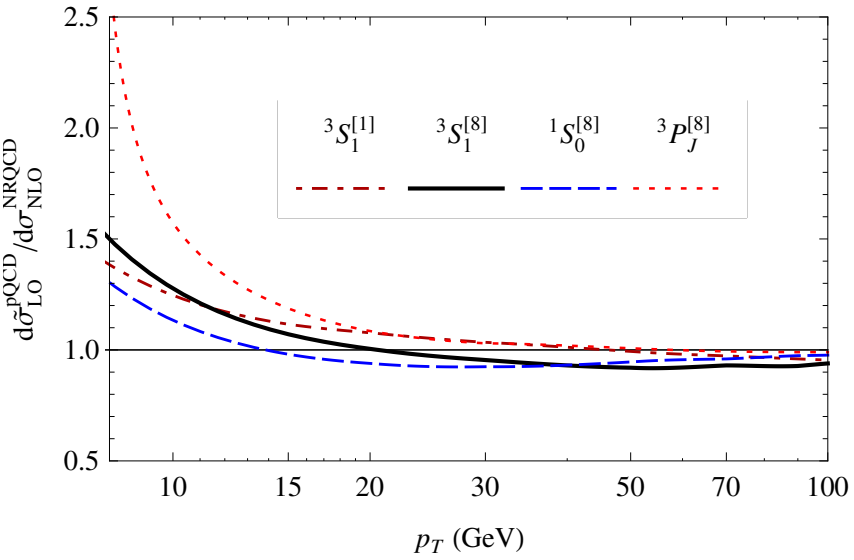

Figure 9.2: Ratio of J/ψ production rate from LO QCD factorization over that of NLO NRQCD calculation for four leading NRQCD channels. See the text for details.

As shown in Fig. 9.2, our slightly modified LO QCD calculation can almost reproduce the NLO NRQCD calculation channel-by-channel for $p_T > 10 - 15$ GeV, depending on the channel. The comparison in Fig. 9.2 demonstrates that the very complicated results of NLO NRQCD calculations can be reproduced by the simple and fully analytic LO calculation of the QCD factorization approach for $p_T > 10$ GeV, and clearly indicates that perturbative organization of the factorized power expansion is well suited to heavy quarkonium production at high p_T. It also shows the importance of the NLP contribution. For comparison, Fig 9.3 shows the weight of LP contribution in the NLO NRQCD calculations [18]. In this figure, the ratio for the $^3S_1^{[1]}$ channel is strictly zero. With NLP contributions, not only can we reproduce the NLO NRQCD results for the $^3S_1^{[1]}$ and $^1S_0^{[8]}$ channels, the $^3S_1^{[8]}$ and $^3P_J^{[8]}$ channels also converge faster to the NLO NRQCD results.

To further illustrate the importance of NLP contributions, we plot the ratio of the NLP contribution to the total LO QCD contribution in Fig. 9.4 for each channel. Figure 9.4 clearly shows that NLP contributions are negligible for the $^3S_1^{[8]}$ channel over the full p_T range, and are small for the $^3P_J^{[8]}$ channel when $p_T > 20$ GeV, beyond which it below 10 percent. However, the NLP

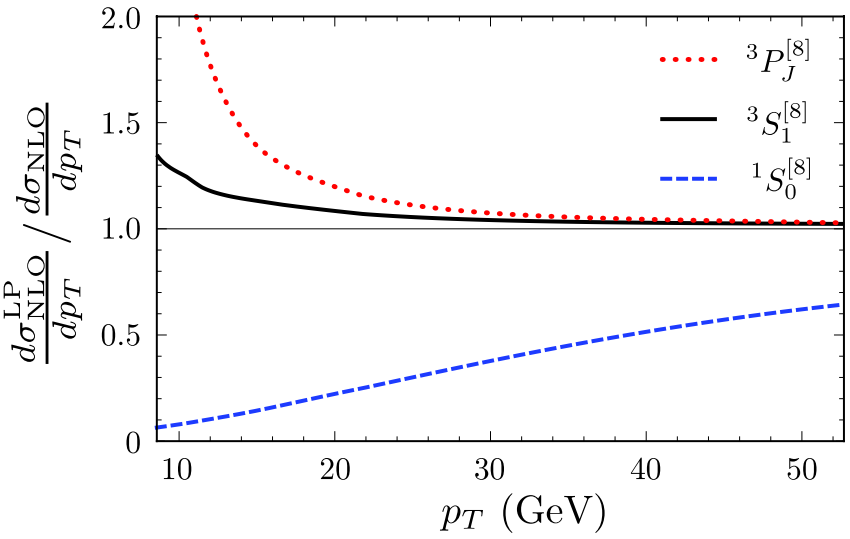

Figure 9.3: Weight of LP contributions in NLO NRQCD calculation for J/ψ production for four leading NRQCD channels. The weight for $^3S_1^{[1]}$ channel is strictly zero. Figure taken from [18].

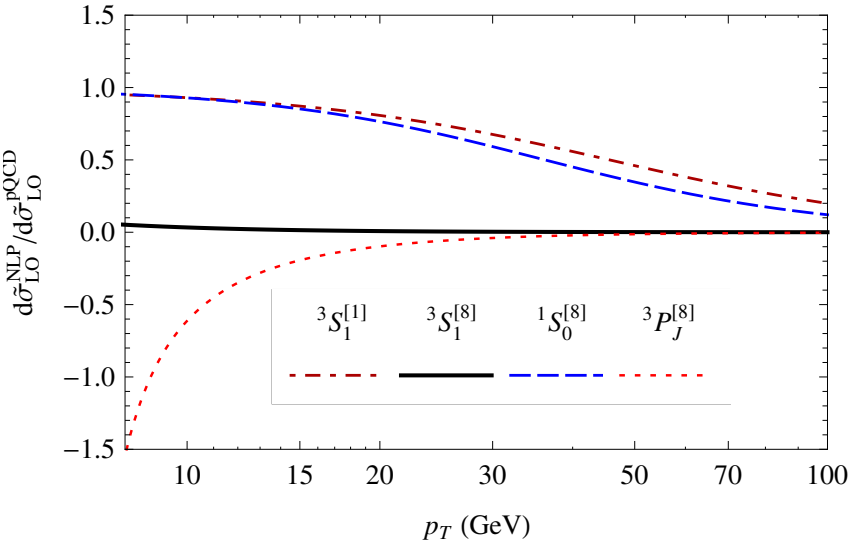

Figure 9.4: Ratio of NLP contributions to total contribution in LO QCD for each channel. $d\tilde{\sigma}$ means we have a special choice for PDFs. See text for details.

contributions are crucial for ${}^1S_0^{[8]}$ and ${}^3S_1^{[1]}$ channels even if p_T approaches 100 GeV. Since the FFs for a single active parton to fragment into a ${}^3S_1^{[1]}$ heavy quark pair, calculated in NRQCD, vanish for both LO and NLO, as indicated in Table 9.1 the two-loop gluon FF derived in Refs. [79, 130] was used for the LP contribution to the ${}^3S_1^{[1]}$ channel in Fig. 9.4.

In above comparision with NLO NRQCD calculations, we did not include the evolution of FFs. A complete LO QCD calculation should include the evolution of FFs using the LO evolution kernels given in Ref. [40] and input FFs calculated in NRQCD factorization at NLO [45, 46], and a set of updated NRQCD LDMEs by fitting the data. From its consistency with the existing NLO NRQCD results, and the control through evolution of its higher order corrections, we expect such a LO QCD factorized power expansion to clarify existing data on heavy quarkonium production at collider energies. Also, because the LP ${}^3S_1^{[8]}$ and ${}^3P_J^{[8]}$ channels, which produce predominantly transversely polarized heavy quarkonia, appear not to be dominant [12, 18, 131], heavy quarkonium production at current collider energies is strongly influenced by the ${}^1S_0^{[8]}$ channel, and is more likely to be unpolarized.

In summary, we have shown that the LO contribution to hadronic J/ψ production, calculated in a factorized expansion at LP and NLP, naturally reproduces all NLO results calculated in the NRQCD factorization for $p_T \gtrsim 10$ GeV. With the FFs calculated assuming the NRQCD factorization at an input scale of the order of m_Q, NLP contributions are important, and potentially dominant in the production of heavy quarkonia at the current collider energies, at least for the ${}^3S_1^{[1]}$ and ${}^1S_0^{[8]}$ channels. The NLP contribution to the ${}^1S_0^{[8]}$ channel may dominate the total production rate if, as indicated by recent studies [11, 18, 48], the sum of LP contributions from ${}^3S_1^{[8]}$ and ${}^3P_J^{[8]}$ is relatively small. If this is indeed the case, the asymptotic transverse polarization of J/ψ [26] will require even higher p_T to set in, and the theory will naturally accommodate unpolarized or slightly longitudinally polarized cross sections over a wide range of p_T.

Chapter 10

Summary and outlook

The heavy quarkonium production has been serving as an important process to test our understanding of the strong interaction and QCD, both in perturbative and non-perturbative aspects. With the Non-relativistic QCD (NRQCD) factorization approach, tremendous progress has been made in the last twenty years. Nonetheless, there are still many problems unsolved, such as the polarization puzzle and the non-universality of NRQCD long-distance matrix elements (LDMEs). The recently proposed QCD factorization approach provides us new insight of this process and is expected to eventually solve these puzzles. However, the application of this new approach is impeded by the lack of knowledge of a large set of multi-variable input fragmentation functions (FFs).

In this dissertation, we calculated the heavy quarkonium FFs at the input scale $\mu_0 \gtrsim 2m_Q$ in terms of the NRQCD factorization formalism. We evaluated all short-distance coefficients for a perturbatively produced relativistic heavy quark pair to evolve into either S-wave or P-wave non-relativistic heavy quark pair to the first non-trivial order in α_s. With our calculation, we effectively expressed all the non-perturbative heavy quarkonium FFs (at least *ten* unknown multi-variable functions for each heavy quarkonium state produced) in terms of a few of NRQCD LDMEs per quarkonium state with perturbatively calculated coefficients for their dependence on momentum fractions, z, ζ_1 and ζ_2.

Although there is no formal proof of the NRQCD factorization approach to evaluate the heavy quarkonium FFs, we found that all infrared divergences of the FFs at this first non-trivial order are exactly the same as the next-leading-order (NLO) expansion of NRQCD LDMEs, which ensures that the calculated short-distance coefficients are infrared safe. In addition, we found that due to the underlying symmetries of QCD, in particular, the charge conjugation symmetry, the structure (or the dependence on the momentum fractions) of

all short-distance coefficients/contributions to the FFs are very compact, with only a few distinctive structures. Just like any perturbative calculation of short-distance coefficients in a factorization approach, there is factorization scheme dependence for the calculated coefficients at NLO and beyond. In this dissertation, we used the dimensional regularization and the $\overline{\rm MS}$ factorization scheme. It is straightforward to convert our results into any other regularization and factorization schemes.

In this dissertation, we also calculated the polarized heavy quarkonium FFs at the input scale $\mu_0 \gtrsim 2m_Q$ in the NRQCD factorization formalism. In the QCD factorization approach, these universal input FFs determine the polarization of the observed heavy quarkonium. Consequently, these polarized heavy quarkonium FFs are essential for the eventual answer to the polarization puzzle. By general symmetry arguments of $SO(d-1)$ group, we generalized the definitions of polarized NRQCD LDMEs to d dimensions. We found it is necessary to introduce off-diagonal LDMEs. From these d-dimensional definitions, we worked out the projection operators to project the outgoing non-relativistic heavy quark pair into a specific polarized state. We also calculated these d-dimensional LDMEs to NLO in NRQCD effective theory, which are important for the IR divergence cancellation in the calculation of P-wave short-distance coefficients. With conventional dimensional regularization and the $\overline{\rm MS}$ factorization scheme, we evaluated all short-distance coefficients for a perturbatively produced relativistic heavy quark pair to evolve into either S-wave or P-wave polarized non-relativistic heavy quark pair to the first nontrivial order in α_s. We found that all IR divergences are canceled and the calculated short-distance coefficients are infrared safe for the polarized heavy quarkonium FFs.

In the first application of the QCD factorization approach with the calculated LO FFs, we showed that the LO contribution to hadronic J/ψ production, calculated in a factorized expansion at LP and NLP, naturally reproduces all NLO results calculated in the NRQCD factorization for $p_T \gtrsim 10$ GeV. We found that the large NLO contributions to the ${}^3S_1^{[1]}$ and ${}^1S_0^{[8]}$ channels in the NRQCD factorization are due primarily to leading-order (LO) NLP corrections in the factorized power expansion. Specifically, with the heavy quark pair FFs we calculated in the NRQCD factorization formalism, the LO contribution at NLP nicely reproduces NLO NRQCD results for both the ${}^3S_1^{[1]}$ and ${}^1S_0^{[8]}$ channels for a wide p_T range. We also found that although the ${}^3S_1^{[8]}$ and ${}^3P_J^{[8]}$ channels are dominated by LP contribution at $p_T > 25$ GeV within an error of 10%, combination of LP and NLP contributions converges to NLO NRQCD result from $p_T \gtrsim 20$ GeV.

The QCD factorization approach requires the short-distance coefficients

and evolution kernels of FFs and PDFs at the same order in their perturbative expansion to provide a fully consistent factorized cross section. In this first application of the QCD factorization approach, in order to compare to the NLO NRQCD results, we didn't use the LO parton distribution functions (PDFs) for LP ${}^1S_0^{[8]}$ and ${}^3P_J^{[8]}$ channels at leading order of α_s.

By applying the QCD factorization approach in a consistent manner and resuming the large logarithms to all orders with the NLO input FFs we calculated, the results of all essential channels will undoubtedly be improved. Based on the new calculations in the QCD factorization approach, a more detailed global study and refitting of NRQCD LDMEs for J/ψ cross sections and polarization is clearly necessary. At the same time, the exploding data from the LHC and other colliders definitely help to constrain these LDMEs in an unprecedented precision. Moreover, with more data accumulated, new observables will be measured and studied. This theoretical and experimental progress will eventually lead us to the full picture for heavy quarkonium production in the near future.

A good understanding of the conventional quarkonium production is also necessary for the research on the exotic quarkonium [132]. Recently, many narrow exotic quarkonium resonances, some of which have electric charges, have been observed in the e^+e^- and hadron-hadron colliders. The discovery of the charged heavy quarkonium states is the first definitive evidence of the exotic hadrons. Research on the production mechanism of these exotic quarkonium states, and its comparison to the mechanism of conventional quarkonium production will definitely provide us deeper insight of the strong interaction and QCD.

Appendix A

Single-Parton Fragmentation Functions to Unpolarized Heavy Quarkonium

In terms of the NRQCD factorization, the heavy quarkonium fragmentation functions from a single-parton are factorized in the form

$$D_{f\to H}(z;m_Q,\mu_0) = \sum_{[Q\bar{Q}(n)]} \pi\alpha_s \Big\{ \hat{d}^{(1)}_{f\to[Q\bar{Q}(n)]}(z;m_Q,\mu_0,\mu_\Lambda) + \left(\frac{\alpha_s}{\pi}\right) \hat{d}^{(2)}_{f\to[Q\bar{Q}(n)]}(z;m_Q,\mu_0,\mu_\Lambda) + O(\alpha_s^2) \Big\} \times \frac{\langle \mathcal{O}^H_{[Q\bar{Q}(n)]}(\mu_\Lambda)\rangle}{m_Q^{2L+3}}, \tag{A.1}$$

where μ_0 (or μ_Λ) is pQCD (or NRQCD) factorization scale, f could be gluon (g), light quark (q), charm quark (c), bottom quark (b), or their anti-particles, $[Q\bar{Q}(n)]$ is an intermediate NRQCD $Q\bar{Q}$ state with quantum number $n = {}^{(2S+1)}L_J^{[1,8]}$, H could be η_c, J/ψ, ψ', h_c, χ_{cJ}, or their bottomonia counterparts, and LDME $\langle \mathcal{O}^H_{Q\bar{Q}[n]}\rangle$ summarizes the nonperturbative physics for the $[Q\bar{Q}(n)]$-pair to evolve into a heavy quarkonium H at the energy scale below μ_Λ. The denominator $m_Q^{-(2L+3)}$ is introduced so that $\hat{d}^{(1)}$ and $\hat{d}^{(2)}$ are dimensionless.

Color singlet NRQCD LDMEs could be related to the value of (or the derivative of) heavy quarkonium wave functions at the origin. The relation is showed in Eq. (3.21) and we repeat it here,

$$\langle \mathcal{O}^{\eta_c}_{[c\bar{c}(^1S_0^{[1]})]}\rangle = \frac{1}{4\pi}|R_{\eta_c}(0)|^2, \tag{A.2}$$

$$\langle \mathcal{O}^{J/\psi}_{[c\bar{c}(^3S_1^{[1]})]} \rangle = \frac{3}{4\pi}|R_{J/\psi}(0)|^2, \tag{A.3}$$

$$\langle \mathcal{O}^{h_c}_{[c\bar{c}(^1P_1^{[1]})]} \rangle = \frac{9}{4\pi}|R'_{h_c}(0)|^2, \tag{A.4}$$

$$\langle \mathcal{O}^{\chi_{cJ}}_{[c\bar{c}(^3P_J^{[1]})]} \rangle = \frac{3(2J+1)}{4\pi}|R'_{\chi_{cJ}}(0)|^2. \tag{A.5}$$

Similar relations are existed for LDMEs of producing bottomonia. Values of these wave functions at the origin could be either calculated from potential model, or fixed by data on heavy quakonium decay. In contrast, color octet NRQCD LDMEs could only be extracted from data of heavy quakonium production at present.

In the rest of this appendix we list short-distance coefficients for all single-parton fragmentation functions to S-wave and P-wave $Q\bar{Q}$-pair up to order $O(\alpha_s^2)$. At $\mathcal{O}(\alpha_s)$, we have

$$\hat{d}^{(1)}_{g\to{}^3S_1^{[8]}} = \frac{\delta(1-z)}{(3-2\epsilon)(N_c^2-1)}, \tag{A.6}$$

while all other channels vanish. Results at $O(\alpha_s^2)$ are given in the following.

A.1 Gluon Fragmentation Functions

$$\hat{d}^{(2)}_{g\to{}^1S_0^{[1]}} = \frac{1}{N_c}\Big\{(1-z)\ln[1-z] - z^2 + \frac{3}{2}z\Big\}, \tag{A.7}$$

$$\hat{d}^{(2)}_{g\to{}^3S_1^{[1]}} = 0, \tag{A.8}$$

$$\hat{d}^{(2)}_{g\to{}^1P_1^{[1]}} = 0, \tag{A.9}$$

$$\hat{d}^{(2)}_{g\to{}^3P_J^{[1]}} = \frac{4}{9N_c}\Big\{\Big[\frac{Q_J}{2J+1} - \frac{1}{2}\ln\big(\frac{\mu_\Lambda^2}{4m_Q^2}\big)\Big]\delta(1-z) + \frac{z}{(1-z)_+} + \frac{P_J(z)}{2J+1}\Big\}, \tag{A.10}$$

$$\begin{aligned}\hat{d}^{(2)}_{g\to{}^3S_1^{[8]}} = \frac{1}{12C_F}\Big[&A(\mu_0)\delta(1-z) + \frac{1}{N_c}P_{gg}(z)\Big(\ln(\frac{\mu_0^2}{4m_Q^2}) - 1\Big) \\ &+ \frac{2(1-z)}{z} - \frac{4(1-z+z^2)^2}{z}\left(\frac{\ln(1-z)}{1-z}\right)_+\Big],\end{aligned} \tag{A.11}$$

$$\hat{d}^{(2)}_{g\to{}^1P_1^{[8]}} = \frac{1}{12C_F}\,[(1-z)\ln(1-z) - z^2 + \frac{3}{2}z], \tag{A.12}$$

$$\hat{d}^{(2)}_{g\to{}^1S_0^{[8]}} = \frac{B_F}{C_F} \times \hat{d}^{(2)}_{g\to{}^1S_0^{[1]}}\,, \tag{A.13}$$

$$\hat{d}^{(2)}_{g\to{}^3P_J^{[8]}} = \frac{B_F}{C_F} \times \hat{d}^{(2)}_{g\to{}^3P_J^{[1]}}\,, \tag{A.14}$$

where

$$B_F = \frac{N_c^2-4}{4N_c}, \tag{A.15}$$

$$Q_0 = \frac{1}{4}, \qquad Q_1 = \frac{3}{8}, \qquad Q_2 = \frac{7}{8}, \tag{A.16}$$

$$P_0(z) = \frac{z(85-26z)}{8} + \frac{9(5-3z)}{4}\ln(1-z), \tag{A.17}$$

$$P_1(z) = -\frac{3z(1+4z)}{4}, \tag{A.18}$$

$$P_2(z) = \frac{5z(11-4z)}{4} + 9(2-z)\ln(1-z), \tag{A.19}$$

$$A(\mu) = \frac{\beta_0}{N_c}\big[\ln\big(\frac{\mu^2}{4m_Q^2}\big) + \frac{13}{3}\big] + \frac{4}{N_c^2} - \frac{\pi^2}{3} + \frac{16}{3}\ln 2, \tag{A.20}$$

$$P_{gg}(z) = 2N_c\Big[\frac{z}{(1-z)_+} + \frac{1-z}{z} + z(1-z) + \frac{\beta_0}{2N_c}\delta(1-z)\Big], \tag{A.21}$$

$$\beta_0 = \frac{11N_c - 2n_f}{6}. \tag{A.22}$$

A.2 Same Flavor Heavy (Anti-)Quark Fragmentation Functions

Heavy quark Q has the same flavor as the outgoing $Q\bar{Q}$-pair.

$$\hat{d}^{(2)}_{Q\to{}^1S_0^{[1]}} = \frac{2}{3}\frac{C_F^2}{N_c}\frac{(z-1)^2}{(z-2)^6}\; z(3z^4-8z^3+8z^2+48), \tag{A.23}$$

$$\hat{d}^{(2)}_{Q\to{}^3S_1^{[1]}} = \frac{2}{3}\frac{C_F^2}{N_c}\frac{(z-1)^2}{(z-2)^6}\; z(5z^4-32z^3+72z^2-32z+16), \tag{A.24}$$

$$\hat{d}^{(2)}_{Q\to{}^1P_1^{[1]}} = \frac{2}{3}\frac{C_F^2}{N_c}\frac{(z-1)^2}{(z-2)^8}\; z(9z^6-56z^5+140z^4-160z^3+176z^2-128z+64), \tag{A.25}$$

$$\hat{d}^{(2)}_{Q\to{}^3P_0^{[1]}} = \frac{2}{9}\frac{C_F^2}{N_c}\frac{(z-1)^2}{(z-2)^8}\; z(59z^6-376z^5+1060z^4-1376z^3+528z^2 + 384z+192), \tag{A.26}$$

$$\hat{d}^{(2)}_{Q\to{}^3P_1^{[1]}} = \frac{8}{9}\frac{C_F^2}{N_c}\frac{(z-1)^2}{(z-2)^8}\, z(7z^6-54z^5+202z^4-408z^3+496z^2-288z+96), \tag{A.27}$$

$$\hat{d}^{(2)}_{Q\to{}^3P_2^{[1]}} = \frac{16}{45}\frac{C_F^2}{N_c}\frac{(z-1)^2}{(z-2)^8}\, z(23z^6-184z^5+541z^4-668z^3+480z^2 - 192z+48), \tag{A.28}$$

$$\begin{aligned}\hat{d}^{(2)}_{Q\to{}^3S_1^{[8]}} = \frac{1}{12}\frac{1}{N_c^3}\frac{1}{(z-2)^6\, z}\Big\{ & N_c^2(z^2-2z+2)(z-2)^6\ln\Big(\frac{\mu_0^2}{(z-2)^2 m_Q^2}\Big) \\ & - N_c^2\,(z-2)^4 z^2(z^2-10z+10) - 16\,N_c\, z(z-2)^2(z^4-7z^3+12z^2-8z+2) \\ & + 2(z-1)^2 z^2(5z^4-32z^3+72z^2-32z+16)\Big\},\end{aligned} \tag{A.29}$$

$$\hat{d}^{(2)}_{Q\to{}^1S_0^{[8]}} = \frac{1}{(N_c^2-1)^2}\times \hat{d}^{(2)}_{Q\to{}^1S_0^{[1]}}\,, \tag{A.30}$$

$$\hat{d}^{(2)}_{Q\to{}^1P_1^{[8]}} = \frac{1}{(N_c^2-1)^2}\times \hat{d}^{(2)}_{Q\to{}^1P_1^{[8]}}\,, \tag{A.31}$$

$$\hat{d}^{(2)}_{Q\to{}^3P_J^{[8]}} = \frac{1}{(N_c^2-1)^2}\times \hat{d}^{(2)}_{Q\to{}^3P_J^{[1]}}\,, \tag{A.32}$$

$$\hat{d}^{(2)}_{\bar{Q}\to n} = \hat{d}^{(2)}_{Q\to n}, \qquad \text{for any } n = {}^{2S+1}L_J^{[1,8]}. \tag{A.33}$$

A.3 Light (Anti-)Quark Fragmentation Functions

Light quark q could be u, d or s.

$$\hat{d}^{(2)}_{q\to{}^3S_1^{[8]}} = \frac{1}{12N_c}\frac{1}{z}\Big\{(z^2-2z+2)\ln\Big[\frac{\mu_0^2}{4m_Q^2(1-z)}\Big] - 2z^2\Big\}, \tag{A.34}$$

$$\hat{d}^{(2)}_{q\to n} = 0, \qquad \text{for } n \neq {}^3S_1^{[8]}, \tag{A.35}$$

$$\hat{d}^{(2)}_{\bar{q}\to n} = \hat{d}^{(2)}_{q\to n}, \qquad \text{for any } n = {}^{2S+1}L_J^{[1,8]}. \tag{A.36}$$

A.4 Different Flavor Heavy (Anti-)Quark Fragmentation Functions

Heavy quark Q' has a different flavor with outgoing $Q\bar{Q}$-pair.

$$\hat{d}^{(2)}_{Q'\to{}^3S_1^{[8]}} = \frac{1}{12N_c}\frac{1}{z}\left\{(z^2-2z+2)\ln\left[\frac{\mu_0^2}{4m_Q^2(1-z+\frac{z^2\eta}{4})}\right] -2z^2\left(1+\frac{1-z-\frac{z^2}{2}}{4-4z+z^2\eta}\eta\right)\right\}, \tag{A.37}$$

$$\hat{d}^{(2)}_{Q'\to n} = 0, \qquad \text{for } n \neq {}^3S_1^{[8]}, \tag{A.38}$$

$$\hat{d}^{(2)}_{\bar{Q}'\to n} = \hat{d}^{(2)}_{Q'\to n}, \qquad \text{for any } n = {}^{2S+1}L_J^{[1,8]}, \tag{A.39}$$

where $\eta = m_{Q'}^2/m_Q^2$, with m_Q the mass of the heavy quark in the outgoing $Q\bar{Q}$-pair.

A.5 Comparison with Previous Results

Many of the above results have been calculated and are available in the literature. We present here a brief comparison with previous results.

For gluon fragmentation into a heavy quark pair, Eq. (A.7) and Eq. (A.13) confirm the results in Refs. [79] and [110], respectively. Eq. (A.10) verifies the result of Ref. [109] using the dimensional regularization, which is consistent with the earlier work in Ref. [81] evaluated in a cutoff regularization scheme. Summing over all J, Eq. (A.10) is also consistent with the result in Ref. [130]. Eq. (A.11) seems to have a very minor difference from the previous calculation of $g \to [Q\bar{Q}({}^3S_1^{[8]})] + X$ fragmentation [107]. The minor difference seems to be caused by the derivation of I_{ACD} in Eq. (A.11) of Ref. [107]. Our result for I_{ACD} can be obtained by replacing $-6\ln^2 2$ in Eq. (A.11) of Ref. [107] with $-2\ln^2 2$.

For light-quark fragmentation into a $Q\bar{Q}$ pair, Eq. (A.34) confirms the result in Ref. [108].

For heavy quark fragmentation into a $Q\bar{Q}$ pair, Eqs. (A.23) and (A.24) confirm the results in Ref. [80]. Eqs. (A.25)-(A.28) and Eq. (A.30) are the same as the results in Ref. [133]. But, our result in Eq. (A.29) is slightly different from both the result in Ref. [133] and that in Ref. [108], while the results from these two authors are slightly different from each other for this $Q \to [Q\bar{Q}({}^3S_1^{[8]})] + Q$ channel.

Appendix B

Double-Parton Fragmentation Functions to Unpolarized Heavy Quarkonium

B.1 Definitions and Notations

Similar to Eq. (A.1), in terms of NRQCD factorization, the $Q\bar{Q}$ pair fragmentation functions could be factorized as

$$\mathcal{D}_{[Q\bar{Q}(\kappa)]\to H}(z,\zeta_1,\zeta_2,\mu_0;m_Q) = \sum_{[Q\bar{Q}(n)]} \left\{ \hat{d}^{(0)}_{[Q\bar{Q}(\kappa)]\to[Q\bar{Q}(n)]}(z,\zeta_1,\zeta_2,\mu_0;m_Q,\mu_\Lambda) + \left(\frac{\alpha_s}{\pi}\right) \hat{d}^{(1)}_{[Q\bar{Q}(\kappa)]\to[Q\bar{Q}(n)]}(z,\zeta_1,\zeta_2,\mu_0;m_Q,\mu_\Lambda) + O(\alpha_s^2) \right\} \times \frac{\langle \mathcal{O}^H_{[Q\bar{Q}(n)]}(\mu_\Lambda)\rangle}{m_Q^{2L+1}}, \tag{B.1}$$

where $[Q\bar{Q}(\kappa)]$ is a perturbatively produced fragmenting heavy quark pair in a particular spin and color state κ, which could be vector (v), axial-vector (a) or tensor (t), with either color singlet or octet. Again, the denominator $m_Q^{-(2L+1)}$ is used so that $\hat{d}^{(0)}$ and $\hat{d}^{(1)}$ are dimensionless.

In the rest of this appendix we list our results of the short-distance coefficients for all $Q\bar{Q}$-pair fragmentation functions into S-wave NRQCD $Q\bar{Q}$-pair up to NLO. In the following, we omit the subscript $Q\bar{Q}$ to use the notation, $\hat{d}^{(j)}_{\kappa\to n}$ $(j=0,1)$ instead of $\hat{d}^{(j)}_{[Q\bar{Q}(\kappa)]\to[Q\bar{Q}(n)]}(z,\zeta_1,\zeta_2,\mu_0;m_Q,\mu_\Lambda)$. Note that we do not list any results that vanish except $\hat{d}^{(1)}_{t^{[1]}\to{}^1S_0^{[8]}}$, which is equal to zero only in our present γ_5 scheme.

B.2 Results of fragmentation functions to S-wave heavy quark pair

B.2.1 LO results

$$\hat{d}^{(0)}_{v^{[1]}\to{}^3S_1^{[1]}} = \frac{1}{2(3-2\epsilon)}\delta(\zeta_1)\delta(\zeta_2)\delta(1-z), \tag{B.2}$$

$$\hat{d}^{(0)}_{a^{[1]}\to{}^1S_0^{[1]}} = \frac{1}{2}\delta(\zeta_1)\delta(\zeta_2)\delta(1-z), \tag{B.3}$$

$$\hat{d}^{(0)}_{t^{[1]}\to{}^3S_1^{[1]}} = \frac{1}{2(3-2\epsilon)}\delta(\zeta_1)\delta(\zeta_2)\delta(1-z), \tag{B.4}$$

$$\hat{d}^{(0)}_{s^{[8]}\to{}^{2S+1}L_J^{[8]}} = \frac{1}{N_c^2-1}\hat{d}^{(0)}_{s^{[1]}\to{}^{2S+1}L_J^{[1]}}(\zeta_1,\zeta_2,z), \tag{B.5}$$

where s could be v, a or t, and $\epsilon = (D-4)/2$.

B.2.2 NLO results

$$\begin{aligned}\hat{d}^{(1)}_{v^{[1]}\to{}^3S_1^{[1]}} = \frac{1}{12}C_F\delta(1-z)\Big\{&\frac{3}{4}\,\Delta_0\times\,\ln\big[\frac{\mu_0^2}{m_Q^2}\big]\\ &+\tilde{V}_{va}(\zeta_1,\zeta_2)\,\big(\ln\big[\frac{\mu_0^2}{m_Q^2}\big]-\frac{2}{3}\big)+V_1(\zeta_1,\zeta_2)\Big\},\end{aligned} \tag{B.6}$$

$$\hat{d}^{(1)}_{v^{[1]}\to{}^1S_0^{[8]}} = \frac{1}{8}\frac{C_F}{(N_c^2-1)}\Delta_+^{[1]}\,z(1-z)\Big\{\ln\big[\frac{\mu_0^2}{m_Q^2}\big]-2\ln(2-2z)-3\Big\}, \tag{B.7}$$

$$\begin{aligned}\hat{d}^{(1)}_{v^{[1]}\to{}^3S_1^{[8]}} = \frac{1}{24}\frac{C_F}{(N_c^2-1)}\Delta_-^{[1]}\,\frac{z}{(1-z)}\Big\{&(\ln\big[\frac{\mu_0^2}{m_Q^2}\big]-\frac{2}{3})-2\ln(2-2z)\\ &+2z^2-4z+\frac{5}{3}\Big\},\end{aligned} \tag{B.8}$$

$$\hat{d}^{(1)}_{v^{[8]}\to{}^1S_0^{[8]}} = \frac{1}{8}\frac{C_F}{(N_c^2-1)^2}\,\Delta_+^{[8]}\,z(1-z)\Big\{\ln\big[\frac{\mu_0^2}{m_Q^2}\big]-2\ln(2-2z)-3\Big\}, \tag{B.9}$$

$$\hat{d}^{(1)}_{v^{[8]}\to{}^3S_1^{[8]}} = -\frac{z}{12}\frac{C_F}{(N_c^2-1)^2}\Big\{\delta(1-z)\Big[\frac{3}{4}\Delta_0\Big(\tilde{c}\times\ \ln\big[\frac{\mu_0^2}{m_Q^2}\big]+c_0\Big) + \big(\tilde{V}_{va}(\zeta_1,\zeta_2)+\frac{N_c}{2}\,\tilde{V}_g(\zeta_1,\zeta_2)\big)\big(\ln\big[\frac{\mu_0^2}{m_Q^2}\big]-\frac{2}{3}\big)+V_1(\zeta_1,\zeta_2) + \frac{N_c}{2}\,V_g(\zeta_1,\zeta_2)\Big]-\frac{\Delta_-^{[8]}}{2\,(1-z)_+}\big(\ln\big[\frac{\mu_0^2}{m_Q^2}\big]-\frac{2}{3}\big)+\Delta_-^{[8]}\,R_1(z)\Big\}, \tag{B.10}$$

$$\hat{d}^{(1)}_{a^{[1]}\to{}^1S_0^{[1]}} = \frac{1}{4}C_F\delta(1-z)\Big\{\big[\,\frac{3}{4}\,\Delta_0+\tilde{V}_{va}(\zeta_1,\zeta_2)\big]\ln\big[\frac{\mu_0^2}{m_Q^2}\big]+V_2(\zeta_1,\zeta_2)\Big\}, \tag{B.11}$$

$$\hat{d}^{(1)}_{a^{[1]}\to{}^1S_0^{[8]}} = \frac{1}{8}\frac{C_F}{(N_c^2-1)}\Delta_-^{[1]}\frac{z}{(1-z)}\Big\{\ln\big[\frac{\mu_0^2}{m_Q^2}\big]-2\ln(2-2z)-1\Big\}, \tag{B.12}$$

$$\hat{d}^{(1)}_{a^{[1]}\to{}^3S_1^{[8]}} = \frac{1}{24}\frac{C_F}{(N_c^2-1)}\Delta_+^{[1]}\,z(1-z)\Big\{(\ln\big[\frac{\mu_0^2}{m_Q^2}\big]-\frac{2}{3})-2\ln(2-2z)-\frac{1}{3}\Big\}, \tag{B.13}$$

$$\hat{d}^{(1)}_{a^{[8]}\to{}^1S_0^{[8]}} = -\frac{z}{4}\frac{C_F}{(N_c^2-1)^2}\Big\{\delta(1-z)\Big[\frac{3}{4}\Delta_0\Big(\tilde{c}\times\ \ln\big[\frac{\mu_0^2}{m_Q^2}\big]+c_0\Big) + \tilde{V}_{va}(\zeta_1,\zeta_2)\ln\big[\frac{\mu_0^2}{m_Q^2}\big]+V_2(\zeta_1,\zeta_2)\Big]-\frac{\Delta_-^{[8]}}{2\,(1-z)_+}\ln\big[\frac{\mu_0^2}{m_Q^2}\big]+\Delta_-^{[8]}\,R_2(z)\Big\}, \tag{B.14}$$

$$\hat{d}^{(1)}_{a^{[8]}\to{}^3S_1^{[8]}} = \frac{1}{24}\frac{C_F}{(N_c^2-1)^2}\Delta_+^{[8]}\,z(1-z)\Big\{(\ln\big[\frac{\mu_0^2}{m_Q^2}\big]-\frac{2}{3})-2\ln(2-2z)-\frac{1}{3}\Big\}, \tag{B.15}$$

$$\hat{d}^{(1)}_{t^{[1]}\to{}^3S_1^{[1]}} = \frac{1}{12}C_F\delta(1-z)\Big\{\frac{3}{4}\,\Delta_0\times\ \ln\big[\frac{\mu_0^2}{m_Q^2}\big]+\tilde{V}_t(\zeta_1,\zeta_2)\,\big(\ln\big[\frac{\mu_0^2}{m_Q^2}\big]-\frac{2}{3}\big) + V_3(\zeta_1,\zeta_2)\Big\}, \tag{B.16}$$

$$\hat{d}^{(1)}_{t^{[1]}\to{}^1S_0^{[8]}} = 0, \tag{B.17}$$

$$\hat{d}^{(1)}_{t^{[1]}\to{}^3S_1^{[8]}} = \frac{1}{24}\frac{C_F}{(N_c^2-1)}\Delta_-^{[1]}\,\frac{z(z^2-2z+2)}{(1-z)}\Big\{(\ln\big[\frac{\mu_0^2}{m_Q^2}\big]-\frac{2}{3})-2\ln(2-2z)-\frac{1}{3}\Big\}, \tag{B.18}$$

$$\hat{d}^{(1)}_{t^{[8]}\to{}^3S_1^{[8]}} = -\frac{z}{12}\frac{C_F}{(N_c^2-1)^2}\Big\{\delta(1-z)\Big[\frac{3}{4}\Delta_0\Big(\tilde{c}\times\ln\big[\frac{\mu_0^2}{m_Q^2}\big]+c_0\Big) + (\tilde{V}_t(\zeta_1,\zeta_2)+\frac{N_c}{2}\tilde{V}_{tg}(\zeta_1,\zeta_2))\big(\ln\big[\frac{\mu_0^2}{m_Q^2}\big]-\frac{2}{3}\big)+V_3(\zeta_1,\zeta_2) + \frac{N_c}{2}V_{tg}(\zeta_1,\zeta_2)\Big]-\Delta_-^{[8]}\frac{(z^2-2z+2)}{2\,(1-z)_+}\big(\ln\big[\frac{\mu_0^2}{m_Q^2}\big]-\frac{2}{3}\big)+\Delta_-^{[8]}R_3(z)\Big\}, \tag{B.19}$$

$$\hat{d}^{(1)}_{s^{[8]}\to{}^{2S+1}L_J^{[1]}} = \hat{d}^{(1)}_{s^{[1]}\to{}^{2S+1}L_J^{[8]}}, \tag{B.20}$$

where the zero result in Eq. (B.17) depends on the γ^5 scheme, the $2/3$ in factor $(\ln[\mu_0^2/m_Q^2]-2/3)$ comes from the ϵ-dependence of LO results, s could be v, a or t. $\tilde{V}$, V, R and c are defined as

$$\tilde{V}_{va}(\zeta_1,\zeta_2) = \delta(\zeta_2)\Big\{\Big(\frac{1}{\zeta_1}\Big)_{1+}-\frac{1}{2}(\zeta_1+1)_{0+}\Big\}+(\zeta_1\leftrightarrow\zeta_2), \tag{B.21}$$

$$\tilde{V}_g(\zeta_1,\zeta_2) = \delta(\zeta_2)\Big\{\big(1-\zeta_1^2\big)_{0+}\Big\}+(\zeta_1\leftrightarrow\zeta_2), \tag{B.22}$$

$$\tilde{V}_t(\zeta_1,\zeta_2) = \delta(\zeta_2)\Big\{\Big(\frac{1}{\zeta_1}\Big)_{1+}-(1)_{0+}\Big\}+(\zeta_1\leftrightarrow\zeta_2), \tag{B.23}$$

$$\tilde{V}_{tg}(\zeta_1,\zeta_2) = \delta(\zeta_2)\ (1)_{0+}+(\zeta_1\leftrightarrow\zeta_2), \tag{B.24}$$

$$V_1(\zeta_1,\zeta_2) = \delta(\zeta_2)\Big\{\Big(\frac{1}{\zeta_1^2}\Big)_{2+}-\Big(\frac{\ln(\zeta_1^2)}{\zeta_1}\Big)_{1+}-\frac{1}{3}\Big(\frac{1}{\zeta_1}\Big)_{1+}+\frac{1}{2}\big(\zeta_1\ln(\zeta_1^2)\big)_{0+} + \frac{7}{6}(\zeta_1)_{0+}+\frac{1}{2}\big(\ln(\zeta_1^2)\big)_{0+}-\frac{11}{6}(1)_{0+}\Big\}+(\zeta_1\leftrightarrow\zeta_2), \tag{B.25}$$

$$V_2(\zeta_1,\zeta_2) = \delta(\zeta_2)\Big\{\Big(\frac{1}{\zeta_1^2}\Big)_{2+}-\Big(\frac{\ln(\zeta_1^2)}{\zeta_1}\Big)_{1+}-\Big(\frac{1}{\zeta_1}\Big)_{1+}+\frac{1}{2}\big(\zeta_1\ln(\zeta_1^2)\big)_{0+} + \frac{1}{2}(\zeta_1)_{0+}+\frac{1}{2}\big(\ln(\zeta_1^2)\big)_{0+}-\frac{1}{2}(1)_{0+}\Big\}+(\zeta_1\leftrightarrow\zeta_2), \tag{B.26}$$

$$V_3(\zeta_1,\zeta_2) = \delta(\zeta_2)\Big\{\Big(\frac{1}{\zeta_1^2}\Big)_{2+}-\Big(\frac{\ln(\zeta_1^2)}{\zeta_1}\Big)_{1+}-\frac{1}{3}\Big(\frac{1}{\zeta_1}\Big)_{1+}+\big(\ln(\zeta_1^2)\big)_{0+} - \frac{2}{3}(1)_{0+}\Big\}+(\zeta_1\leftrightarrow\zeta_2), \tag{B.27}$$

$$V_g(\zeta_1,\zeta_2) = \delta(\zeta_2)\Big\{\big(\zeta_1^2\ln(\zeta_1^2)\big)_{0+}-\big(\ln(\zeta_1^2)\big)_{0+}+\frac{2}{3}\big(1-\zeta_1^2\big)_{0+}\Big\}+(\zeta_1\leftrightarrow\zeta_2), \tag{B.28}$$

$$V_{tg}(\zeta_1,\zeta_2)=\delta(\zeta_2)\Big\{\frac{2}{3}(1)_{0+}-\big(\ln(\zeta_1^2)\big)_{0+}\Big\}+(\zeta_1\leftrightarrow\zeta_2), \tag{B.29}$$

$$R_1(z)=\left(\frac{\ln(2-2z)}{1-z}\right)_+ +\frac{1}{6}\frac{1}{(1-z)_+}-(1-z)\,, \tag{B.30}$$

$$R_2(z)=\left(\frac{\ln(2-2z)}{1-z}\right)_+ +\frac{1}{2}\frac{1}{(1-z)_+}\,, \tag{B.31}$$

$$R_3(z)=(z^2-2z+2)\Big\{\left(\frac{\ln(2-2z)}{1-z}\right)_+ +\frac{1}{6}\frac{1}{(1-z)_+}\Big\}, \tag{B.32}$$

$$\tilde{c}=1-N_c^2(1+\frac{4}{3}\ln 2), \tag{B.33}$$

$$c_0=\frac{4}{3}N_c^2\big[(\ln 2)^2+\ln 2-1\big]. \tag{B.34}$$

B.2.3 Comparison with Other Calculations

A similar calculation for the color singlet process $[Q\bar{Q}(a^{[1]})]\to[Q\bar{Q}(^1S_0^{[1]})]$, in the terminology of distribution amplitude, was completed by two groups previously [102, 103], but, their results disagree with each other. Our result in Eq. (B.11) confirms the calculation of Ref. [103]. For process $[Q\bar{Q}(v^{[1]})]\to[Q\bar{Q}(^3S_1^{[1]})]$, our result in Eq. (B.6) disagree with the result obtained in [102]. Finally, we note that, soon after our paper was submitted, an independent calculation for $[Q\bar{Q}(a^{[1]})]\to[Q\bar{Q}(^1S_0^{[1]})]$, $[Q\bar{Q}(v^{[1]})]\to[Q\bar{Q}(^3S_1^{[1]})]$ and $[Q\bar{Q}(t^{[1]})]\to[Q\bar{Q}(^3S_1^{[1]})]$ was also reported in Ref. [106] in the terminology of distribution amplitude. Our results for these three channels agree with that calculated in Ref. [106].

B.3 Results of fragmentation functions to P-wave heavy quark pair

In this Appendix, we summarize our results of short-distance coefficients for NRQCD factorization expansion of heavy quark-pair FFs to a heavy quarkonium through all possible P-wave states of a non-relativistic heavy quark pair.

B.3.1 LO results

In this part we list all non-vanishing LO short-distance coefficents.

$$\hat{d}^{(0)}_{v^{[1]}\to{}^3P_0^{[1]}}(\zeta_1,\zeta_2,z)=\frac{1}{2(3-2\epsilon)}\delta'(\zeta_1)\delta'(\zeta_2)\delta(1-z), \tag{B.35}$$

$$\hat{d}^{(0)}_{v^{[1]}\to{}^3P_2^{[1]}}(\zeta_1,\zeta_2,z)=\frac{1}{(3-2\epsilon)(5-2\epsilon)}\delta'(\zeta_1)\delta'(\zeta_2)\delta(1-z), \tag{B.36}$$

$$\hat{d}^{(0)}_{a^{[1]}\to{}^1P_1^{[1]}}(\zeta_1,\zeta_2,z)=\frac{1}{2(3-2\epsilon)}\delta'(\zeta_1)\delta'(\zeta_2)\delta(1-z), \tag{B.37}$$

$$\hat{d}^{(0)}_{a^{[1]}\to{}^3P_1^{[1]}}(\zeta_1,\zeta_2,z)=\frac{(1-2\epsilon)}{(3-2\epsilon)}\delta(\zeta_1)\delta(\zeta_2)\delta(1-z), \tag{B.38}$$

$$\hat{d}^{(0)}_{t^{[1]}\to{}^1P_1^{[1]}}(\zeta_1,\zeta_2,z)=\frac{(1-2\epsilon)}{2(3-2\epsilon)}\delta(\zeta_1)\delta(\zeta_2)\delta(1-z), \tag{B.39}$$

$$\hat{d}^{(0)}_{t^{[1]}\to{}^3P_1^{[1]}}(\zeta_1,\zeta_2,z)=\frac{1}{2(3-2\epsilon)(2-2\epsilon)}\delta'(\zeta_1)\delta'(\zeta_2)\delta(1-z), \tag{B.40}$$

$$\hat{d}^{(0)}_{t^{[1]}\to{}^3P_2^{[1]}}(\zeta_1,\zeta_2,z)=\frac{1}{2(5-2\epsilon)(2-2\epsilon)}\delta'(\zeta_1)\delta'(\zeta_2)\delta(1-z), \tag{B.41}$$

$$\hat{d}^{(0)}_{s^{[8]}\to{}^{2S+1}P_J^{[8]}}(\zeta_1,\zeta_2,z)=\frac{1}{N_c^2-1}\hat{d}^{(0)}_{s^{[1]}\to{}^{2S+1}P_J^{[1]}}(\zeta_1,\zeta_2,z), \tag{B.42}$$

where s in the last equation could be v, a or t, and the dimension is defined as $D=4-2\epsilon$.

B.3.2 P-wave NLO results with an initial vector $Q\bar{Q}$-state

In this subsection, we list results of NLO short-distance coefficients to the fragmentation functions for a vector pQCD $Q\bar{Q}$-state to fragment into a P-wave NRQCD $Q\bar{Q}$-state. Fragmentation channels that are equal to zero at this order are not listed.

$$\hat{d}^{(1)}_{v^{[1]}\to{}^3P_0^{[1]}} = -\frac{1}{12}C_F\delta(1-z)\Big\{\frac{\Delta_0''}{4}(\ln\big[\frac{\mu_0^2}{m_Q^2}\big]-4) + \tilde{V}'_{va}(\zeta_1,\zeta_2)(\ln\big[\frac{\mu_0^2}{m_Q^2}\big]-\frac{2}{3})+V'_{v1}(\zeta_1,\zeta_2)\Big\}, \tag{B.43}$$

$$\hat{d}^{(1)}_{v^{[1]}\to{}^3P_2^{[1]}} = -\frac{1}{30}C_F\delta(1-z)\Big\{\frac{\Delta_0''}{4}(\ln\big[\frac{\mu_0^2}{m_Q^2}\big]-4) + \tilde{V}'_{va}(\zeta_1,\zeta_2)(\ln\big[\frac{\mu_0^2}{m_Q^2}\big]-\frac{16}{15})+V'_{v2}(\zeta_1,\zeta_2)\Big\}, \tag{B.44}$$

$$\begin{aligned}\hat{d}^{(1)}_{v^{[1]}\to{}^1P_1^{[8]}} = \frac{1}{12}\frac{C_F}{(N_c^2-1)}z(1-z)\Big\{&\big[\Delta_-^{[1]\prime\prime}+\Delta_-^{[1]\prime}+\Delta_-^{[1]}\big](\frac{1}{2}\ln\big[\frac{\mu_0^2}{m_Q^2}\big]-\frac{1}{3})\\ &-\Delta_-^{[1]\prime\prime}\big(\ln(2-2z)+\frac{7}{6}\big)-\Delta_-^{[1]\prime}\big(\ln(2-2z)+\frac{5}{3}\big)\\ &-\Delta_-^{[1]}\big(\ln(2-2z)+\frac{7}{6}\big)\Big\},\end{aligned} \tag{B.45}$$

$$\begin{aligned}\hat{d}^{(1)}_{v^{[1]}\to{}^3P_0^{[8]}} = \frac{z}{12}\frac{C_F}{(N_c^2-1)}\Big\{&\frac{2}{3}\Delta_0\,\delta(1-z)(-\ln\big[\frac{\mu_\Lambda^2}{m_Q^2}\big]+2\ln 2)\\ &+\big[\frac{\Delta_+^{[1]\prime\prime}}{(1-z)}+\Delta_+^{[1]\prime}+\Delta_+^{[1]}(1-z)\big](\frac{1}{2}\ln\big[\frac{\mu_0^2}{m_Q^2}\big]-\frac{1}{3})\\ &-\frac{\Delta_+^{[1]\prime\prime}}{(1-z)}R_{v1}(z)-\frac{\Delta_+^{[1]\prime}}{(1-z)}R_{v2}(z)-\Delta_+^{[1]}R_{v3}(z)\Big\},\end{aligned} \tag{B.46}$$

$$\begin{aligned}\hat{d}^{(1)}_{v^{[1]}\to{}^3P_1^{[8]}} = \frac{z}{12}\frac{C_F}{(N_c^2-1)}\Big\{&\frac{2}{3}\Delta_0\,\delta(1-z)(-\ln\big[\frac{\mu_\Lambda^2}{m_Q^2}\big]+2\ln 2+\frac{1}{2})\\ &+\Delta_+^{[1]}(1-z)(\ln\big[\frac{\mu_0^2}{m_Q^2}\big]+\frac{4}{3})+\frac{\Delta_+^{[1]\prime\prime}}{2}(1-z)+\frac{\Delta_+^{[1]\prime}}{2}(\frac{3}{2}-z)\\ &+\Delta_+^{[1]}\big[\frac{1}{3}\frac{1}{(1-z)_+}-2(1-z)\ln(2-2z)+\frac{3}{2}z-\frac{7}{6}\big]\Big\},\end{aligned} \tag{B.47}$$

$$\hat{d}^{(1)}_{v^{[1]}\to{}^3P_2^{[8]}} = \frac{z}{30}\frac{C_F}{(N_c^2-1)}\Big\{\frac{5}{3}\Delta_0\,\delta(1-z)(-\ln\big[\frac{\mu_\Lambda^2}{m_Q^2}\big]+2\ln 2+\frac{3}{10})$$
$$+\big[\frac{\Delta_+^{[1]\prime\prime}}{(1-z)}+\Delta_+^{[1]\prime}+\Delta_+^{[1]}(1-z)\big](\frac{1}{2}\ln\big[\frac{\mu_0^2}{m_Q^2}\big]-\frac{8}{15}) \tag{B.48}$$
$$-\frac{\Delta_+^{[1]\prime\prime}}{(1-z)}R_{v4}(z)-\frac{\Delta_+^{[1]\prime}}{(1-z)}R_{v5}(z)-\Delta_+^{[1]}\,R_{v6}(z)\Big\},$$

$$\hat{d}^{(1)}_{v^{[8]}\to{}^1P_1^{[8]}} = \frac{1}{12}\frac{C_F}{(N_c^2-1)^2}z(1-z)\Big\{\big[\Delta_-^{[8]\prime\prime}+\Delta_-^{[8]\prime}+\Delta_-^{[8]}\big](\frac{1}{2}\ln\big[\frac{\mu_0^2}{m_Q^2}\big]-\frac{1}{3})$$
$$-\Delta_-^{[8]\prime\prime}\big(\ln(2-2z)+\frac{7}{6}\big)-\Delta_-^{[8]\prime}\big(\ln(2-2z)+\frac{5}{3}\big)$$
$$-\Delta_-^{[8]}\big(\ln(2-2z)+\frac{7}{6}\big)\Big\}, \tag{B.49}$$

$$\hat{d}^{(1)}_{v^{[8]}\to{}^3P_0^{[8]}} = \frac{z}{12}\frac{C_F}{(N_c^2-1)^2}\Big\{\delta(1-z)\Big[\frac{1}{3}(N_c^2-4)\Delta_0\Big(-\ln\big[\frac{\mu_\Lambda^2}{m_Q^2}\big]+2\ln 2\Big)$$
$$+\frac{1}{4}\Delta_0''\Big(c\times\ln\big[\frac{\mu_0^2}{m_Q^2}\big]+c_1\Big)+\tilde{V}'_{va}(\zeta_1,\zeta_2)\big(\ln\big[\frac{\mu_0^2}{m_Q^2}\big]-\frac{2}{3}\big)$$
$$+V'_{v1}(\zeta_1,\zeta_2)\Big]+\Big[\frac{\Delta_+^{[8]\prime\prime}}{(1-z)_+}+\Delta_+^{[8]\prime}+\Delta_+^{[8]}(1-z)\Big]\big(\frac{1}{2}\ln\big[\frac{\mu_0^2}{m_Q^2}\big]-\frac{1}{3}\big)$$
$$-\Delta_+^{[8]\prime\prime}\,R_{v7}(z)-\frac{\Delta_+^{[8]\prime}}{(1-z)}R_{v2}(z)-\Delta_+^{[8]}R_{v3}(z)\Big\}, \tag{B.50}$$

$$\hat{d}^{(1)}_{v^{[8]}\to{}^3P_1^{[8]}} = \frac{z}{12}\frac{C_F}{(N_c^2-1)^2}\Big\{\frac{1}{3}(N_c^2-4)\Delta_0\,\delta(1-z)(-\ln\big[\frac{\mu_\Lambda^2}{m_Q^2}\big]+2\ln 2+\frac{1}{2})$$
$$+\Delta_+^{[8]}(1-z)(\ln\big[\frac{\mu_0^2}{m_Q^2}\big]+\frac{4}{3})+\frac{\Delta_+^{[8]\prime\prime}}{2}(1-z)+\frac{\Delta_+^{[8]\prime}}{2}(\frac{3}{2}-z)$$
$$+\Delta_+^{[8]}\big[\frac{1}{3}\frac{1}{(1-z)_+}-2(1-z)\ln(2-2z)+\frac{3}{2}z-\frac{7}{6}\big]\Big\}, \tag{B.51}$$

$$\hat{d}^{(1)}_{v^{[8]}\to{}^3P_2^{[8]}} = \frac{z}{30}\frac{C_F}{(N_c^2-1)^2}\Big\{\delta(1-z)\Big[\frac{5}{6}(N_c^2-4)\Delta_0\Big(-\ln\big[\frac{\mu_\Lambda^2}{m_Q^2}\big]+2\ln 2+\frac{3}{10}\Big) + \frac{1}{4}\Delta_0''\Big(c\times\ln\big[\frac{\mu_0^2}{m_Q^2}\big]+c_1\Big)+\tilde{V}'_{va}(\zeta_1,\zeta_2)\big(\ln\big[\frac{\mu_0^2}{m_Q^2}\big]-\frac{16}{15}\big) + V'_{v2}(\zeta_1,\zeta_2)\Big]+\Big[\frac{\Delta_+^{[8]\prime\prime}}{(1-z)_+}+\Delta_+^{[8]\prime}+\Delta_+^{[8]}(1-z)\Big]\big(\frac{1}{2}\ln\big[\frac{\mu_0^2}{m_Q^2}\big]-\frac{8}{15}\big) - \Delta_+^{[8]\prime\prime}R_{v8}(z)-\frac{\Delta_+^{[8]\prime}}{(1-z)}R_{v5}(z)-\Delta_+^{[8]}R_{v6}(z)\Big\}, \tag{B.52}$$

$$\hat{d}^{(1)}_{v^{[8]}\to{}^{2S+1}L_J^{[1]}} = \hat{d}^{(1)}_{v^{[1]}\to{}^{2S+1}L_J^{[8]}}, \tag{B.53}$$

where the dependence on z, ζ_1, ζ_2, and μ_F in the last equation is suppressed. $\tilde{V}$, V, R and c functions in above equations are defined as

$$\tilde{V}'_{va}(\zeta_1,\zeta_2)=\delta'(\zeta_2)\Big\{\Big(\frac{1}{\zeta_1^2}\Big)_{2-}-\frac{1}{2}(\zeta_1+1)_{0-}\Big\}+(\zeta_1\leftrightarrow\zeta_2), \tag{B.54}$$

$$V_{v1}{}'(\zeta_1,\zeta_2)=\delta'(\zeta_2)\Big\{\Big(\frac{1}{\zeta_1^3}\Big)_{3-}-\Big(\frac{\ln(\zeta_1^2)}{\zeta_1^2}\Big)_{2-}+\frac{5}{3}\Big(\frac{1}{\zeta_1^2}\Big)_{2-}+\Big(\frac{1}{\zeta_1}\Big)_{1-} + \frac{1}{2}\big((\zeta_1+1)\ln(\zeta_1^2)\big)_{0-}+\frac{1}{6}(\zeta_1-23)_{0-}\Big\}+(\zeta_1\leftrightarrow\zeta_2), \tag{B.55}$$

$$V_{v2}{}'(\zeta_1,\zeta_2)=\delta'(\zeta_2)\Big\{\Big(\frac{1}{\zeta_1^3}\Big)_{3-}-\Big(\frac{\ln(\zeta_1^2)}{\zeta_1^2}\Big)_{2-}+\frac{31}{15}\Big(\frac{1}{\zeta_1^2}\Big)_{2-}-\frac{7}{2}\Big(\frac{1}{\zeta_1}\Big)_{1-} + \frac{1}{2}\big((\zeta_1+1)\ln(\zeta_1^2)\big)_{0-}+\frac{22}{15}\Big(\zeta_1-\frac{31}{44}\Big)_{0-}\Big\}+(\zeta_1\leftrightarrow\zeta_2), \tag{B.56}$$

$$R_{v1}(z)=\ln(2-2z)+\frac{1}{6}, \tag{B.57}$$

$$R_{v2}(z)=(1-z)\ln(2-2z)+\frac{1}{3}z+\frac{1}{6}, \tag{B.58}$$

$$R_{v3}(z)=-\frac{1}{3}\frac{1}{(1-z)_+}+(1-z)\ln(2-2z)+\frac{7}{6}z+\frac{1}{2}, \tag{B.59}$$

$$R_{v4}(z)=\ln(2-2z)-\frac{3}{4}z^2+\frac{3}{2}z-\frac{47}{60}, \tag{B.60}$$

$$R_{v5}(z)=(1-z)\ln(2-2z)-\frac{3}{4}z^2+\frac{109}{120}z+\frac{41}{120}, \tag{B.61}$$

$$R_{v6}(z)=-\frac{5}{6}\frac{1}{(1-z)_+}+(1-z)\ln(2-2z)+\frac{67}{60}z+\frac{1}{20}, \tag{B.62}$$

$$R_{v7}(z) = \left(\frac{\ln(2-2z)}{1-z}\right)_+ + \frac{1}{6}\frac{1}{(1-z)_+}\,, \tag{B.63}$$

$$R_{v8}(z) = \left(\frac{\ln(2-2z)}{1-z}\right)_+ - \frac{1}{30}\frac{1}{(1-z)_+} - \frac{3}{4}(1-z)\,, \tag{B.64}$$

$$c = N_c^2(3+4\ln 2)+1, \tag{B.65}$$

$$c_1 = -4\,N_c^2\big[(\ln 2)^2 + \ln 2 - 1\big] - 4, \tag{B.66}$$

B.3.3 P-wave NLO results with an initial axial-vector $Q\bar{Q}$-state

Here, we list results of NLO short-distance contributions to the FFs from an axial-vector pQCD $Q\bar{Q}$-state.

$$\begin{aligned}\hat{d}^{(1)}_{a^{[1]}\to{}^1P_1^{[1]}} = &-\frac{1}{12}C_F\delta(1-z)\Big\{\frac{\Delta_0''}{4}(\ln\big[\frac{\mu_0^2}{m_Q^2}\big]-4)\\ &+\tilde{V}'_{va}(\zeta_1,\zeta_2)(\ln\big[\frac{\mu_0^2}{m_Q^2}\big]-\frac{2}{3})+V'_{a1}(\zeta_1,\zeta_2)\Big\},\end{aligned} \tag{B.67}$$

$$\begin{aligned}\hat{d}^{(1)}_{a^{[1]}\to{}^3P_1^{[1]}} = &\frac{1}{6}C_F\delta(1-z)\Big\{\frac{3}{4}\,\Delta_0(\ln\big[\frac{\mu_0^2}{m_Q^2}\big]+\frac{2}{3})\\ &+\tilde{V}_{va}(\zeta_1,\zeta_2)(\ln\big[\frac{\mu_0^2}{m_Q^2}\big]+\frac{4}{3})+V_{a2}(\zeta_1,\zeta_2)\Big\},\end{aligned} \tag{B.68}$$

$$\begin{aligned}\hat{d}^{(1)}_{a^{[1]}\to{}^1P_1^{[8]}} = &\frac{z}{12}\frac{C_F}{(N_c^2-1)}\Big\{2\,\Delta_0\,\delta(1-z)(-\ln\big[\frac{\mu_\Lambda^2}{m_Q^2}\big]+2\ln 2+\frac{1}{3})\\ &+\big[\frac{\Delta_+^{[1]\prime\prime}}{(1-z)}+\Delta_+^{[1]\prime}+\Delta_+^{[1]}(1-z)\big](\frac{1}{2}\ln\big[\frac{\mu_0^2}{m_Q^2}\big]-\frac{1}{3})\\ &-\frac{\Delta_+^{[1]\prime\prime}}{(1-z)}R_{a1}(z)-\frac{\Delta_+^{[1]\prime}}{(1-z)}R_{a2}(z)-\Delta_+^{[1]}\,R_{a3}(z)\Big\},\end{aligned} \tag{B.69}$$

$$\begin{aligned}\hat{d}^{(1)}_{a^{[1]}\to{}^3P_0^{[8]}} = &\frac{1}{24}\frac{C_F}{(N_c^2-1)}z(1-z)\big[\Delta_-^{[1]\prime\prime}+\Delta_-^{[1]\prime}+\Delta_-^{[1]}\big]\\ &\times(\ln\big[\frac{\mu_0^2}{m_Q^2}\big]-2\ln(2-2z)-3),\end{aligned} \tag{B.70}$$

$$\hat{d}^{(1)}_{a^{[1]}\to{}^3P_1^{[8]}} = \frac{z}{6}\frac{C_F}{(N_c^2-1)}\Big\{\frac{\Delta_-^{[1]}}{(1-z)}\big(\frac{1}{2}\ln\big[\frac{\mu_0^2}{m_Q^2}\big]+\frac{2}{3}\big) - \Delta_-^{[1]\prime\prime}R_{a4}(z) - \Delta_-^{[1]\prime}R_{a5}(z) - \frac{\Delta_-^{[1]}}{(1-z)}R_{a6}(z)\Big\}, \tag{B.71}$$

$$\hat{d}^{(1)}_{a^{[1]}\to{}^3P_2^{[8]}} = \frac{1}{30}\frac{C_F}{(N_c^2-1)}z\,(1-z)\Big\{\big[\Delta_-^{[1]\prime\prime}+\Delta_-^{[1]\prime}+\Delta_-^{[1]}\big]\big(\frac{1}{2}\ln\big[\frac{\mu_0^2}{m_Q^2}\big]-\frac{8}{15}\big) - \Delta_-^{[1]\prime\prime}\big[\ln(2-2z)+\frac{13}{60}\big] - \Delta_-^{[1]\prime}\big[\ln(2-2z)+\frac{161}{120}\big] - \Delta_-^{[1]}\big[\ln(2-2z)+\frac{13}{60}\big]\Big\}, \tag{B.72}$$

$$\hat{d}^{(1)}_{a^{[8]}\to{}^1P_1^{[8]}} = \frac{z}{12}\frac{C_F}{(N_c^2-1)^2}\Big\{\delta(1-z)\Big[(N_c^2-4)\Delta_0\Big(-\ln\big[\frac{\mu_\Lambda^2}{m_Q^2}\big]+2\ln 2+\frac{1}{3}\Big) + \frac{1}{4}\Delta_0''\Big(c\times\ln\big[\frac{\mu_0^2}{m_Q^2}\big]+c_1\Big)+\tilde{V}'_{va}(\zeta_1,\zeta_2)\big(\ln\big[\frac{\mu_0^2}{m_Q^2}\big]-\frac{2}{3}\big)+V'_{a1}(\zeta_1,\zeta_2)\Big] + \Big[\frac{\Delta_+^{[8]\prime\prime}}{(1-z)_+}+\Delta_+^{[8]\prime}+\Delta_+^{[8]}(1-z)\Big]\big(\frac{1}{2}\ln\big[\frac{\mu_0^2}{m_Q^2}\big]-\frac{1}{3}\big) - \Delta_+^{[8]\prime\prime}R_{a7}(z) - \frac{\Delta_+^{[8]\prime}}{(1-z)}R_{a2}(z) - \Delta_+^{[8]}R_{a3}(z)\Big\}, \tag{B.73}$$

$$\hat{d}^{(1)}_{a^{[8]}\to{}^3P_0^{[8]}} = \frac{1}{24}\frac{C_F}{(N_c^2-1)^2}z(1-z)\big[\Delta_-^{[8]\prime\prime}+\Delta_-^{[8]\prime}+\Delta_-^{[8]}\big] \times\big(\ln\big[\frac{\mu_0^2}{m_Q^2}\big]-2\ln(2-2z)-3\big), \tag{B.74}$$

$$\hat{d}^{(1)}_{a^{[8]}\to{}^3P_1^{[8]}} = -\frac{z}{6}\frac{C_F}{(N_c^2-1)^2}\Big\{\delta(1-z)\Big[\frac{3}{4}\Delta_0\Big(\tilde{c}\times\ln\big[\frac{\mu_0^2}{m_Q^2}\big]+c_2\Big) + \tilde{V}_{va}(\zeta_1,\zeta_2)\big(\ln\big[\frac{\mu_0^2}{m_Q^2}\big]+\frac{4}{3}\big)+V_{a2}(\zeta_1,\zeta_2)\Big] - \frac{\Delta_-^{[8]}}{(1-z)_+}\big(\frac{1}{2}\ln\big[\frac{\mu_0^2}{m_Q^2}\big]+\frac{2}{3}\big) + \Delta_-^{[8]\prime\prime}R_{a4}(z)+\Delta_-^{[8]\prime}R_{a5}(z)+\Delta_-^{[8]}R_{a8}(z)\Big\}, \tag{B.75}$$

$$\hat{d}^{(1)}_{a^{[8]}\to{}^3P_2^{[8]}} = \frac{1}{30}\frac{C_F}{(N_c^2-1)^2} z\,(1-z)\Big\{\big[\Delta_-^{[8]\prime\prime}+\Delta_-^{[8]\prime}+\Delta_-^{[8]}\big](\frac{1}{2}\ln\big[\frac{\mu_0^2}{m_Q^2}\big]-\frac{8}{15}) - \Delta_-^{[8]\prime\prime}\big[\ln(2-2z)+\frac{13}{60}\big] - \Delta_-^{[8]\prime}\big[\ln(2-2z)+\frac{161}{120}\big] - \Delta_-^{[8]}\big[\ln(2-2z)+\frac{13}{60}\big]\Big\}, \tag{B.76}$$

$$\hat{d}^{(1)}_{a^{[8]}\to{}^{2S+1}L_J^{[1]}} = \hat{d}^{(1)}_{a^{[1]}\to{}^{2S+1}L_J^{[8]}}, \tag{B.77}$$

where, again, the dependence on z, ζ_1, ζ_2 and μ_F in the last equation is suppressed. $\tilde{V}$, V, R and c above are defined as

$$\tilde{V}_{va}(\zeta_1,\zeta_2) = \delta(\zeta_2)\Big\{\left(\frac{1}{\zeta_1}\right)_{1+} - \frac{1}{2}(\zeta_1+1)_{0+}\Big\} + (\zeta_1\leftrightarrow\zeta_2), \tag{B.78}$$

$$V'_{a1}(\zeta_1,\zeta_2) = \delta'(\zeta_2)\Big\{\left(\frac{1}{\zeta_1^3}\right)_{3-} - \left(\frac{\ln(\zeta_1^2)}{\zeta_1^2}\right)_{2-} + \frac{5}{3}\left(\frac{1}{\zeta_1^2}\right)_{2-} - 3\left(\frac{1}{\zeta_1}\right)_{1-} + \frac{1}{2}\big((\zeta_1+1)\ln(\zeta_1^2)\big)_{0-} + \frac{7}{6}\left(\zeta_1-\frac{5}{7}\right)_{0-}\Big\} + (\zeta_1\leftrightarrow\zeta_2), \tag{B.79}$$

$$V_{a2}(\zeta_1,\zeta_2) = \delta(\zeta_2)\Big\{\frac{1}{2}\left(\frac{1}{\zeta_1^2}\right)_{2+} - \left(\frac{\ln(\zeta_1^2)}{\zeta_1}\right)_{1+} - \frac{7}{3}\left(\frac{1}{\zeta_1}\right)_{1+} + \frac{1}{2}\big((\zeta_1+1)\ln(\zeta_1^2)\big)_{0+} + \frac{1}{6}(\zeta_1+10)_{0+}\Big\} + (\zeta_1\leftrightarrow\zeta_2), \tag{B.80}$$

$$R_{a1}(z) = \ln(2-2z)+\frac{1}{6}, \tag{B.81}$$

$$R_{a2}(z) = (1-z)\ln(2-2z) - \frac{1}{6}z + \frac{2}{3}, \tag{B.82}$$

$$R_{a3}(z) = -\frac{1}{(1-z)_+} + (1-z)\ln(2-2z) + \frac{5}{6}z + \frac{7}{6}, \tag{B.83}$$

$$R_{a4}(z) = -\frac{1}{4}(1-z), \tag{B.84}$$

$$R_{a5}(z) = -\frac{3}{8}(1-z), \tag{B.85}$$

$$R_{a6}(z) = \ln(2-2z) + \frac{5}{4}z^2 - 3z + \frac{35}{12}, \tag{B.86}$$

$$R_{a7}(z) = \left(\frac{\ln(2-2z)}{1-z}\right)_+ + \frac{1}{6}\frac{1}{(1-z)_+}, \tag{B.87}$$

$$R_{a8}(z) = \left(\frac{\ln(2-2z)}{1-z}\right)_+ + \frac{7}{6}\frac{1}{(1-z)_+} - \frac{5}{4}z + \frac{7}{4}, \tag{B.88}$$

$$\tilde{c} = 1 - N_c^2(1 + \frac{4}{3}\ln 2), \tag{B.89}$$

$$c_2 = \frac{4}{3}N_c^2\big[(\ln 2)^2 + \ln 2 - 1\big] + \frac{2}{3}, \tag{B.90}$$

B.3.4 P-wave NLO results with an initial tensor $Q\bar{Q}$-state

Here, we list results of NLO short-distance contributions to the FFs for a tensor pQCD $Q\bar{Q}$-state to a non-relativistic P-wave $Q\bar{Q}$-state.

$$\begin{aligned}\hat{d}^{(1)}_{t^{[1]}\to{}^1P_1^{[1]}} = \frac{1}{12}C_F\delta(1-z)\Big\{&\frac{3}{4}\Delta_0(\ln\big[\frac{\mu_0^2}{m_Q^2}\big] + \frac{2}{3}) \\ &+ \tilde{V}_t(\zeta_1,\zeta_2)(\ln\big[\frac{\mu_0^2}{m_Q^2}\big] + \frac{4}{3}) + V_{t1}(\zeta_1,\zeta_2)\Big\},\end{aligned} \tag{B.91}$$

$$\begin{aligned}\hat{d}^{(1)}_{t^{[1]}\to{}^3P_1^{[1]}} = -\frac{1}{24}C_F\delta(1-z)\Big\{&\frac{\Delta_0''}{4}(\ln\big[\frac{\mu_0^2}{m_Q^2}\big] - 4) \\ &+ \tilde{V}_t'(\zeta_1,\zeta_2)(\ln\big[\frac{\mu_0^2}{m_Q^2}\big] - \frac{5}{3}) + V_{t2}'(\zeta_1,\zeta_2)\Big\},\end{aligned} \tag{B.92}$$

$$\begin{aligned}\hat{d}^{(1)}_{t^{[1]}\to{}^3P_2^{[1]}} = -\frac{1}{40}C_F\delta(1-z)\Big\{&\frac{\Delta_0''}{4}(\ln\big[\frac{\mu_0^2}{m_Q^2}\big] - 4) \\ &+ \tilde{V}_t'(\zeta_1,\zeta_2)(\ln\big[\frac{\mu_0^2}{m_Q^2}\big] - \frac{7}{5}) + V_{t3}'(\zeta_1,\zeta_2)\Big\},\end{aligned} \tag{B.93}$$

$$\hat{d}^{(1)}_{t^{[1]}\to{}^1P_1^{[8]}} = \frac{1}{12}\frac{C_F}{(N_c^2-1)}\frac{z}{(1-z)}\Delta_-^{[1]}\Big\{(z^2-2z+2)(\frac{1}{2}\ln\big[\frac{\mu_0^2}{m_Q^2}\big] + \frac{2}{3}) - R_{t1}(z)\Big\}, \tag{B.94}$$

$$\begin{aligned}\hat{d}^{(1)}_{t^{[1]}\to{}^3P_0^{[8]}} = \frac{z}{24}\frac{C_F}{(N_c^2-1)}\Big\{&\frac{4}{3}\Delta_0\,\delta(1-z)(-\ln\big[\frac{\mu_\Lambda^2}{m_Q^2}\big] + 2\ln 2 + \frac{1}{2}) \\ &+ \Delta_+^{[1]\prime\prime}(1-z) + \frac{1}{2}\Delta_+^{[1]\prime}(4-3z) + \frac{2}{3}\Delta_+^{[1]}\big(\frac{1}{(1-z)_+} - 4z + 5\big)\Big\},\end{aligned} \tag{B.95}$$

$$\hat{d}^{(1)}_{t^{[1]}\to{}^3P_1^{[8]}} = \frac{z}{24}\frac{C_F}{(N_c^2-1)}\Big\{\frac{4}{3}\Delta_0\,\delta(1-z)(-\ln\big[\frac{\mu_\Lambda^2}{m_Q^2}\big]+2\ln 2+\frac{1}{4})$$
$$+\big[\frac{\Delta_+^{[1]\prime\prime}}{2(1-z)}(z^2-2z+2)+\frac{\Delta_+^{[1]\prime}}{2}(2-z)+\Delta_+^{[1]}(1-z)\big](\ln\big[\frac{\mu_0^2}{m_Q^2}\big]-\frac{5}{3})$$
$$-\frac{\Delta_+^{[1]\prime\prime}}{(1-z)}R_{t2}(z)-\frac{\Delta_+^{[1]\prime}}{(1-z)}R_{t3}(z)-\Delta_+^{[1]}\,R_{t4}(z)\Big]\Big\}, \tag{B.96}$$

$$\hat{d}^{(1)}_{t^{[1]}\to{}^3P_2^{[8]}} = \frac{z}{40}\frac{C_F}{(N_c^2-1)}\Big\{\frac{20}{9}\Delta_0\,\delta(1-z)(-\ln\big[\frac{\mu_\Lambda^2}{m_Q^2}\big]+2\ln 2+\frac{7}{20})$$
$$+\big[\frac{\Delta_+^{[1]\prime\prime}}{2(1-z)}(z^2-2z+2)+\frac{\Delta_+^{[1]\prime}}{2}(2-z)+\Delta_+^{[1]}(1-z)\big](\ln\big[\frac{\mu_0^2}{m_Q^2}\big]-\frac{7}{5})$$
$$-\frac{\Delta_+^{[1]\prime\prime}}{(1-z)}R_{t5}(z)-\frac{\Delta_+^{[1]\prime}}{(1-z)}R_{t6}(z)-\Delta_+^{[1]}\,R_{t7}(z)\Big]\Big\}, \tag{B.97}$$

$$\hat{d}^{(1)}_{t^{[8]}\to{}^1P_1^{[8]}} = -\frac{z}{12}\frac{C_F}{(N_c^2-1)^2}\Big\{\delta(1-z)\Big[\frac{3}{4}\Delta_0\Big(\tilde{c}\times\ln\big[\frac{\mu_0^2}{m_Q^2}\big]+c_2\Big)$$
$$+\tilde{V}_t(\zeta_1,\zeta_2)\big(\ln\big[\frac{\mu_0^2}{m_Q^2}\big]+\frac{4}{3}\big)+V_{t1}(\zeta_1,\zeta_2)\Big] \tag{B.98}$$
$$-\Delta_-^{[8]}\frac{(z^2-2z+2)}{(1-z)_+}\big(\frac{1}{2}\ln\big[\frac{\mu_0^2}{m_Q^2}\big]+\frac{2}{3}\big)+\Delta_-^{[8]}\,R_{t8}(z)\Big\},$$

$$\hat{d}^{(1)}_{t^{[8]}\to{}^3P_0^{[8]}} = \frac{z}{24}\frac{C_F}{(N_c^2-1)^2}\Big\{\frac{2(N_c^2-4)}{3}\Delta_0\,\delta(1-z)(-\ln\big[\frac{\mu_\Lambda^2}{m_Q^2}\big]+2\ln 2+\frac{1}{2})$$
$$+\Delta_+^{[8]\prime\prime}(1-z)+\frac{1}{2}\Delta_+^{[8]\prime}(4-3z)+\frac{2}{3}\Delta_+^{[8]}\big(\frac{1}{(1-z)_+}-4z+5\big)\Big\}, \tag{B.99}$$

$$\hat{d}^{(1)}_{t^{[8]}\to{}^3P_1^{[8]}} = \frac{z}{24}\frac{C_F}{(N_c^2-1)^2}\Big\{\delta(1-z)\Big[\frac{2}{3}(N_c^2-4)\Delta_0\Big(-\ln\big[\frac{\mu_\Lambda^2}{m_Q^2}\big]+2\ln 2+\frac{1}{4}\Big)$$
$$+\frac{1}{4}\Delta_0''\Big(c\times\ln\big[\frac{\mu_0^2}{m_Q^2}\big]+c_1\Big)+\tilde{V}_t'(\zeta_1,\zeta_2)\big(\ln\big[\frac{\mu_0^2}{m_Q^2}\big]-\frac{5}{3}\big)+V_{t2}'(\zeta_1,\zeta_2)\Big]$$
$$+\Big[\Delta_+^{[8]\prime\prime}\frac{(z^2-2z+2)}{2(1-z)_+}+\frac{\Delta_+^{[8]\prime}}{2}(2-z)+\Delta_+^{[8]}(1-z)\Big]\big(\ln\big[\frac{\mu_0^2}{m_Q^2}\big]-\frac{5}{3}\big)$$
$$-\Delta_+^{[8]\prime\prime}\,R_{t9}(z)-\frac{\Delta_+^{[8]\prime}}{(1-z)}R_{t3}(z)-\Delta_+^{[8]}R_{t4}(z)\Big\}, \tag{B.100}$$

$$\hat{d}^{(1)}_{t^{[8]}\to{}^3P_2^{[8]}} = \frac{z}{40}\frac{C_F}{(N_c^2-1)^2}\Big\{\delta(1-z)\Big[\frac{10}{9}(N_c^2-4)\Delta_0\Big(-\ln\big[\frac{\mu_\Lambda^2}{m_Q^2}\big]+2\ln 2+\frac{7}{20}\Big)$$
$$+\frac{1}{4}\Delta_0''\Big(c\times\ln\big[\frac{\mu_0^2}{m_Q^2}\big]+c_1\Big)+\tilde{V}_t'(\zeta_1,\zeta_2)\big(\ln\big[\frac{\mu_0^2}{m_Q^2}\big]-\frac{7}{5}\big)+V_{t3}'(\zeta_1,\zeta_2)\Big]$$
$$+\Big[\Delta_+^{[8]\prime\prime}\frac{(z^2-2z+2)}{2(1-z)_+}+\frac{\Delta_+^{[8]\prime}}{2}(2-z)+\Delta_+^{[8]}(1-z)\Big]\big(\ln\big[\frac{\mu_0^2}{m_Q^2}\big]-\frac{7}{5}\big)$$
$$-\Delta_+^{[8]\prime\prime}R_{t10}(z)-\frac{\Delta_+^{[8]\prime}}{(1-z)}R_{t6}(z)-\Delta_+^{[8]}R_{t7}(z)\Big\}, \tag{B.101}$$

$$\hat{d}^{(1)}_{t^{[8]}\to{}^{2S+1}L_J^{[1]}} = \hat{d}^{(1)}_{t^{[1]}\to{}^{2S+1}L_J^{[8]}}, \tag{B.102}$$

where the dependence on z, ζ_1, ζ_2, and μ_F in the last equation is suppressed. $\tilde{V}$, V, R and c above are defined as

$$\tilde{V}_t(\zeta_1,\zeta_2) = \delta(\zeta_2)\Big\{\Big(\frac{1}{\zeta_1}\Big)_{1+}-(1)_{0+}\Big\}+(\zeta_1\leftrightarrow\zeta_2), \tag{B.103}$$

$$\tilde{V}_t'(\zeta_1,\zeta_2) = \delta'(\zeta_2)\Big\{\Big(\frac{1}{\zeta_1^2}\Big)_{2-}-(1)_{0-}\Big\}+(\zeta_1\leftrightarrow\zeta_2), \tag{B.104}$$

$$V_{t1}(\zeta_1,\zeta_2) = \delta(\zeta_2)\Big\{\frac{1}{2}\Big(\frac{1}{\zeta_1^2}\Big)_{2+}-\Big(\frac{\ln(\zeta_1^2)}{\zeta_1}\Big)_{1+}-\frac{7}{3}\Big(\frac{1}{\zeta_1}\Big)_{1+}+\big(\ln(\zeta_1^2)\big)_{0+}$$
$$+\frac{11}{6}(1)_{0+}\Big\}+(\zeta_1\leftrightarrow\zeta_2), \tag{B.105}$$

$$V_{t2}'(\zeta_1,\zeta_2) = \delta'(\zeta_2)\Big\{\Big(\frac{1}{\zeta_1^3}\Big)_{3-}-\Big(\frac{\ln(\zeta_1^2)}{\zeta_1^2}\Big)_{2-}+\frac{8}{3}\Big(\frac{1}{\zeta_1^2}\Big)_{2-}-2\Big(\frac{1}{\zeta_1}\Big)_{1-}$$
$$+\big(\ln(\zeta_1^2)\big)_{0-}-\frac{5}{3}(1)_{0-}\Big\}+(\zeta_1\leftrightarrow\zeta_2), \tag{B.106}$$

$$V_{t3}'(\zeta_1,\zeta_2) = \delta'(\zeta_2)\Big\{\Big(\frac{1}{\zeta_1^3}\Big)_{3-}-\Big(\frac{\ln(\zeta_1^2)}{\zeta_1^2}\Big)_{2-}+\frac{12}{5}\Big(\frac{1}{\zeta_1^2}\Big)_{2-}-4\Big(\frac{1}{\zeta_1}\Big)_{1-}$$
$$+\big(\ln(\zeta_1^2)\big)_{0-}+\frac{3}{5}(1)_{0-}\Big\}+(\zeta_1\leftrightarrow\zeta_2), \tag{B.107}$$

$$R_{t1}(z) = (z^2-2z+2)\ln(2-2z)+\frac{5}{3}z^2-\frac{23}{6}z+\frac{10}{3}, \tag{B.108}$$

$$R_{t2}(z) = (z^2-2z+2)\ln(2-2z)+\frac{1}{6}z^2-\frac{1}{3}z-\frac{1}{6}, \tag{B.109}$$

$$R_{t3}(z) = (z^2 - 3z + 2)\ln(2-2z) + \frac{5}{12}z^2 - \frac{1}{4}z + \frac{1}{3}\,, \tag{B.110}$$

$$R_{t4}(z) = -\frac{2}{3}\frac{1}{(1-z)_+}z^2 + \frac{7}{6}z + 2(1-z)\ln(2-2z) - \frac{1}{6}\,, \tag{B.111}$$

$$R_{t5}(z) = (z^2 - 2z + 2)\ln(2-2z) - \frac{11}{30}z^2 + \frac{22}{30}z - \frac{17}{30}\,, \tag{B.112}$$

$$R_{t6}(z) = (z^2 - 3z + 2)\ln(2-2z) + \frac{11}{20}z^2 - \frac{79}{60}z + \frac{76}{60} \tag{B.113}$$

$$R_{t7}(z) = -\frac{10}{9}\frac{1}{(1-z)_+} + \frac{31}{90}z + 2(1-z)\ln(2-2z) + \frac{49}{90}\,, \tag{B.114}$$

$$R_{t8}(z) = \left(\frac{\ln(2-2z)}{1-z}\right)_+ + \frac{7}{6}\frac{1}{(1-z)_+} + (1-z)\ln(2-2z) - \frac{5}{3}z + \frac{13}{6}\,, \tag{B.115}$$

$$R_{t9}(z) = \left(\frac{\ln(2-2z)}{1-z}\right)_+ - \frac{1}{3}\frac{1}{(1-z)_+} + (1-z)\ln(2-2z) + \frac{1}{6}(1-z)\,, \tag{B.116}$$

$$R_{t10}(z) = \left(\frac{\ln(2-2z)}{1-z}\right)_+ - \frac{1}{5}\frac{1}{(1-z)_+} + (1-z)\ln(2-2z) - \frac{11}{30}(1-z)\,. \tag{B.117}$$

Note, finally, that all these short-distance contributions to the FFs, so as the FFs, are invariant under the transformation ($\zeta_1 \to -\zeta_1$, $\zeta_2 \to -\zeta_2$) and the exchange $\zeta_1 \leftrightarrow \zeta_2$, including the crossing exchange ($\zeta_1 \to -\zeta_2$, $\zeta_2 \to -\zeta_1$), which are the features derived from the general symmetries of QCD in section 5.4.

B.3.5 Comparison with Other Calculations

Almost at the same time, color singlet to color singlet processes, means Eqs. (B.43, B.44, B.67, B.68, B.91, B.92, B.93), were also calculated independently in Ref. [106] in the terminology of distribution amplitude. We find that Eq. (B.43, B.44, B.67, B.93) are consistent with their results. Eq. (B.68) cannot be compared with their result due to we use a different γ_5 scheme from theirs. By using their γ_5 scheme, we can indeed reproduce their results. The γ_5 scheme used in our calculation is discussed in section 6.2.1. Eqs. (B.91, B.92) cannot be compared directly with the corresponding results in Ref. [106] because the two calculations use different projection operators. By adopting the projection operators used in Ref. [106] for these two processes, we can reproduce their results.

Appendix C

Single-Parton Fragmentation Functions to Polarized Heavy Quarkonium

In this appendix we list the short-distance coefficients for all single-parton fragmentation functions to S-wave and P-wave polarized $Q\bar{Q}$-pair up to order $O(\alpha_s^2)$. In terms of the NRQCD factorization, the heavy quarkonium fragmentation functions from a single-parton are factorized in the form in Eq. (8.6). The polarized FFs and unpolarized FFs are related by Eq. (8.11). Therefore for outgoing $Q\bar{Q}$ with $n+1$ polarizations, we only give n polarized FFs below. The other one can then be calculated with Eq. (8.11) and unpolarized FFs.Those channels with all polarized FFs vanishing are not listed. The Δ-functions below are defined in Eq. (5.32).

C.1 gluon FFs

Leading order

$$\hat{d}^{(1)}_{g\to[Q\bar{Q}(^3S_1^{[8]},L)]} = 0. \tag{C.1}$$

Next-to-leading order

$$\hat{d}^{(2)}_{g\to[Q\bar{Q}(^3P_1^{[1]},L)]} = \frac{1}{3N_c}\Big\{\delta(1-z)\Big[-\ln\big[\frac{\mu_\Lambda^2}{m_Q^2}\big]+2\ln 2+\frac{1}{2}\Big] + z(2z^2-z+1)\frac{1}{(1-z)_+}\Big\}, \tag{C.2}$$

$$\hat{d}^{(2)}_{g\to[Q\bar{Q}(^3P_2^{[1]},L)]} = \frac{1}{9N_c z^4}\Big\{\delta(1-z)\Big[-\ln\big[\frac{\mu_\Lambda^2}{m_Q^2}\big]+2\ln 2+\frac{1}{2}\Big] + 2z^4\frac{1}{(1-z)_+} - 216(z-2)(z-1)^2\ln(1-z) - z(2z^5+5z^4+38z^3-468z^2+864z-432)\Big\}, \tag{C.3}$$

$$\hat{d}^{(2)}_{g\to[Q\bar{Q}(^3P_2^{[1]},T1)]} = \frac{1}{6N_c z^4}\Big\{\delta(1-z)\Big[-\ln\big[\frac{\mu_\Lambda^2}{m_Q^2}\big]+2\ln 2\Big] + 2z^4\frac{1}{(1-z)_+} - 48(z^4-5z^3+10z^2-10z+4)\ln(1-z) - 2z(z^5+4z^4-55z^3+152z^2-192z+96)\Big\}, \tag{C.4}$$

$$\hat{d}^{(2)}_{g\to[Q\bar{Q}(^3S_1^{[8]},L)]} = \frac{N_c}{(N_c^2-1)}\frac{1-z}{z}, \tag{C.5}$$

$$\hat{d}^{(2)}_{g\to[Q\bar{Q}(^1P_1^{[8]},T)]} = \frac{N_c}{6(N_c^2-1)}\frac{1-z}{z^2}\big[z^3+3z^2-12z+3(3z-4)\ln(1-z)\big], \tag{C.6}$$

$$\hat{d}^{(2)}_{g\to[Q\bar{Q}(^3P_1^{[8]},L)]} = \frac{B_F}{C_F}\times\hat{d}^{(2)}_{g\to[Q\bar{Q}(^3P_1^{[1]},L)]}, \tag{C.7}$$

$$\hat{d}^{(2)}_{g\to[Q\bar{Q}(^3P_2^{[8]},L\text{ or }T1)]} = \frac{B_F}{C_F}\times\hat{d}^{(2)}_{g\to[Q\bar{Q}(^3P_2^{[1]},L\text{ or }T1)]}, \tag{C.8}$$

$$\tag{C.9}$$

C.2 different quark FFs

$$\hat{d}^{(2)}_{q\to[Q\bar{Q}(^3S_1^{[8]},L)]} = \frac{2(1-z)^2}{3N_c z(\eta^2z^2-4z+4)}, \tag{C.10}$$

where $\eta = m_q^2/m_Q^2$.

C.3 same quark FFs

$$\hat{d}^{(2)}_{Q\to[Q\bar{Q}(^3S_1^{[1]},L)]} = \frac{(N_c^2-1)^2}{6N_c^3}\frac{z(1-z)^2}{(z-2)^6}(3z^4-24z^3+64z^2-32z+16), \tag{C.11}$$

$$\hat{d}^{(2)}_{Q\to[Q\bar{Q}(^1P_1^{[1]},L)]} = \frac{(N_c^2-1)^2}{30N_c^3}\frac{z(1-z)^2}{(z-2)^8}(55z^6-232z^5+236z^4+224z^3$$

$$+ 592z^2 - 640z + 320), \tag{C.12}$$

$$\hat{d}^{(2)}_{Q\to[Q\bar{Q}(^3P_1^{[1]},L)]} = \frac{(N_c^2-1)^2}{15N_c^3}\frac{z(1-z)^2}{(z-2)^8}(35z^6 - 312z^5 + 1136z^4 - 2016z^3 + 1872z^2 - 960z + 320), \tag{C.13}$$

$$\hat{d}^{(2)}_{Q\to[Q\bar{Q}(^3P_2^{[1]},T1)]} = \frac{(N_c^2-1)^2}{30N_c^3}\frac{z(1-z)^2}{(z-2)^8}(75z^6 - 580z^5 + 1628z^4 - 1872z^3 + 1328z^2 - 512z + 128), \tag{C.14}$$

$$\hat{d}^{(2)}_{Q\to[Q\bar{Q}(^3P_2^{[1]},T2)]} = \frac{4(N_c^2-1)^2}{15N_c^3}\frac{z(1-z)^4}{(z-2)^8}(5z^4 - 32z^3 + 68z^2 - 32z + 16), \tag{C.15}$$

$$\hat{d}^{(2)}_{Q\to[Q\bar{Q}(^3S_1^{[8]},L)]} = \frac{1}{6N_c^3}\frac{(1-z)^2}{z(z-2)^6}\Big[12N_c^2(z-2)^4 - 12N_c z^2(z-4)(z-2)^2 + z^2(3z^4 - 24z^3 + 64z^2 - 32z + 16)\Big], \tag{C.16}$$

$$\hat{d}^{(2)}_{Q\to[Q\bar{Q}(^1P_1^{[8]},L)]} = \frac{1}{(N_c^2-1)^2}\hat{d}^{(2)}_{Q\to[Q\bar{Q}(^1P_1^{[1]},L)]}, \tag{C.17}$$

$$\hat{d}^{(2)}_{Q\to[Q\bar{Q}(^3P_1^{[8]},L)]} = \frac{1}{(N_c^2-1)^2}\hat{d}^{(2)}_{Q\to[Q\bar{Q}(^3P_1^{[1]},L)]}, \tag{C.18}$$

$$\hat{d}^{(2)}_{Q\to[Q\bar{Q}(^3P_2^{[8]},T1\text{ or }T2)]} = \frac{1}{(N_c^2-1)^2}\hat{d}^{(2)}_{Q\to[Q\bar{Q}(^3P_2^{[1]},T1\text{ or }T2)]}. \tag{C.19}$$

C.4 ^3P_J operators with orbital angular momentum summed

Notice the T or L for $^3P_J^{[1]}$ and $^3P_J^{[8]}$ are the polarization of final S-wave heavy quarkonium, as explained at the end of Sec. 8.1.

$$\hat{d}^{(2)}_{g\to[Q\bar{Q}(^3P_J^{[1]},L)]} = -\frac{1}{2N_c z^2}\Big[2(z-1)(z^2+8z-12)\ln(1-z) + z(2z^3 + z^2 - 28z + 24)\Big], \tag{C.20}$$

$$\hat{d}^{(2)}_{g\to[Q\bar{Q}(^3P_J^{[8]},L)]} = \frac{B_F}{C_F}\times\hat{d}^{(2)}_{g\to[Q\bar{Q}(^3P_J^{[1]},L)]} \tag{C.21}$$

$$\hat{d}^{(2)}_{Q\to[Q\bar{Q}(^3P_J^{[1]},L)]} = \frac{(N_c^2-1)^2}{6N_c^3}\frac{z(1-z)^2}{(z-2)^8}(23z^6 - 192z^5 + 676z^4 - 1120z^3 + 1104z^2 - 512z + 192), \tag{C.22}$$

$$\hat{d}^{(2)}_{Q\to[Q\bar{Q}(^3P_J^{[8]},L)]} = \frac{1}{(N_c^2-1)^2}\hat{d}^{(2)}_{Q\to[Q\bar{Q}(^3P_J^{[1]},L)]}. \tag{C.23}$$

Appendix D

Double-Parton Fragmentation Functions to Polarized Heavy Quarkonium

In this appendix we list the short-distance coefficients for all $Q\bar{Q}$ pair fragmentation functions to S-wave and P-wave polarized $Q\bar{Q}$-pair up to order $O(\alpha_s)$. In terms of the NRQCD factorization, the heavy quarkonium fragmentation functions from a $Q\bar{Q}$ pair are factorized in the form in Eq. (8.7). The polarized FFs and unpolarized FFs are related by Eq. (8.11). Therefore for outgoing $Q\bar{Q}$ with $n+1$ polarizations, we only give n polarized FFs below. The other one can then be calculated with Eq. (8.11) and unpolarized FFs.Those channels with all polarized FFs vanishing are not listed. The Δ-functions below are defined in Eq. (5.32).

D.1 Leading Order

Those channels in which the unpolarized $\hat{d}$ vanish are not listed below.

$$\hat{d}^{(0)}_{[Q\bar{Q}(v^{[1]})]\to[Q\bar{Q}(^3S_1^{[1]},T)]} = 0, \tag{D.1}$$

$$\hat{d}^{(0)}_{[Q\bar{Q}(v^{[1]})]\to[Q\bar{Q}(^3P_2^{[1]},T2)]} = 0, \tag{D.2}$$

$$\hat{d}^{(0)}_{[Q\bar{Q}(v^{[1]})]\to[Q\bar{Q}(^3P_2^{[1]},T1)]} = 0, \tag{D.3}$$

$$\hat{d}^{(0)}_{[Q\bar{Q}(a^{[1]})]\to[Q\bar{Q}(^1P_1^{[1]},T)]} = 0, \tag{D.4}$$

$$\hat{d}^{(0)}_{[Q\bar{Q}(a^{[1]})]\to[Q\bar{Q}(^3P_1^{[1]},T)]} = 0, \tag{D.5}$$

$$\hat{d}^{(0)}_{[Q\bar{Q}(t^{[1]})]\to[Q\bar{Q}(^3S_1^{[1]},L)]} = 0, \tag{D.6}$$

$$\hat{d}^{(0)}_{[Q\bar{Q}(t^{[1]})]\to[Q\bar{Q}(^1P_1^{[1]},L)]} = 0, \tag{D.7}$$

$$\hat{d}^{(0)}_{[Q\bar{Q}(t^{[1]})]\to[Q\bar{Q}(^3P_1^{[1]},L)]} = 0, \tag{D.8}$$

$$\hat{d}^{(0)}_{[Q\bar{Q}(t^{[1]})]\to[Q\bar{Q}(^3P_2^{[1]},T2)]} = 0, \tag{D.9}$$

$$\hat{d}^{(0)}_{[Q\bar{Q}(t^{[1]})]\to[Q\bar{Q}(^3P_2^{[1]},L)]} = 0. \tag{D.10}$$

The corresponding color octet channels also vanish.

D.2 NLO - Vector

$$\hat{d}^{(1)}_{[Q\bar{Q}(v^{[1]})]\to[Q\bar{Q}(^3S_1^{[1]},T)]} = 0, \tag{D.11}$$

$$\hat{d}^{(1)}_{[Q\bar{Q}(v^{[1]})]\to[Q\bar{Q}(^3P_2^{[1]},T1)]} = 0, \tag{D.12}$$

$$\hat{d}^{(1)}_{[Q\bar{Q}(v^{[1]})]\to[Q\bar{Q}(^3P_2^{[1]},T2)]} = 0, \tag{D.13}$$

$$\hat{d}^{(1)}_{[Q\bar{Q}(v^{[1]})]\to[Q\bar{Q}(^3S_1^{[8]},T)]} = \frac{1}{16N_c}(1-z)z\Delta_-^{[1]}, \tag{D.14}$$

$$\hat{d}^{(1)}_{[Q\bar{Q}(v^{[1]})]\to[Q\bar{Q}(^1P_1^{[8]},T)]} = \frac{1}{24N_c}(1-z)z\Delta_-^{[1]}, \tag{D.15}$$

$$\begin{aligned}\hat{d}^{(1)}_{[Q\bar{Q}(v^{[1]})]\to[Q\bar{Q}(^3P_1^{[8]},T)]} &= \frac{1}{192N_c}\Big\{8\Delta_0\delta(1-z)\Big(-\ln\big[\frac{\mu_\Lambda^2}{m_Q^2}\big]+2\ln 2+\frac{1}{2}\Big)\\ &+6\Delta_+^{[1]\prime\prime}\,z\,(1-z)-3\Delta_+^{[1]\prime}\,z\,(2z-3)\\ &+4\,z\,\Delta_+^{[1]}\Big[\frac{1}{(1-z)_+}-2z+3\Big]\Big\},\end{aligned} \tag{D.16}$$

$$\begin{aligned}\hat{d}^{(1)}_{[Q\bar{Q}(v^{[1]})]\to[Q\bar{Q}(^3P_2^{[8]},T1)]} &= \frac{1}{192N_c}\Big\{8\Delta_0\delta(1-z)\Big(-\ln\big[\frac{\mu_\Lambda^2}{m_Q^2}\big]+2\ln 2+\frac{1}{2}\Big)\\ &+6\Delta_+^{[1]\prime\prime}\,z\,(1-z)-3\Delta_+^{[1]\prime}\,z\,(2z-1)\\ &+4\,z\,\Delta_+^{[1]}\Big[\frac{1}{(1-z)_+}-2z+1\Big]\Big\},\end{aligned} \tag{D.17}$$

$$\hat{d}^{(1)}_{[Q\bar{Q}(v^{[1]})]\to[Q\bar{Q}(^3P_2^{[8]},T2)]} = \frac{1}{48N_c}z(1-z)\Delta_+^{[1]}, \tag{D.18}$$

$$\hat{d}^{(1)}_{[Q\bar{Q}(v^{[8]})]\to[Q\bar{Q}(^3S_1^{[8]},T)]} = \frac{1}{16N_c(N_c^2-1)}(1-z)z\Delta_-^{[8]}, \tag{D.19}$$

$$\hat{d}^{(1)}_{[Q\bar{Q}(v^{[8]})]\to[Q\bar{Q}(^1P_1^{[8]},T)]} = \frac{1}{24N_c(N_c^2-1)}(1-z)z\Delta_-^{[8]}, \tag{D.20}$$

$$\begin{aligned}\hat{d}^{(1)}_{[Q\bar{Q}(v^{[8]})]\to[Q\bar{Q}(^3P_1^{[8]},T)]} &= \frac{1}{192N_c(N_c^2-1)}\Big\{4(N_c^2-4)\Delta_0\delta(1-z)\Big(-\ln\big[\frac{\mu_\Lambda^2}{m_Q^2}\big] \\ &\quad + 2\ln 2 + \frac{1}{2}\Big) + 6\Delta_+^{[8]\prime\prime}\,z\,(1-z) - 3\Delta_+^{[8]\prime}\,z\,(2z-3) \\ &\quad + 4\,z\,\Delta_+^{[8]}\Big[\frac{1}{(1-z)_+} - 2z + 3\Big]\Big\},\end{aligned} \tag{D.21}$$

$$\begin{aligned}\hat{d}^{(1)}_{[Q\bar{Q}(v^{[8]})]\to[Q\bar{Q}(^3P_2^{[8]},T1)]} &= \frac{1}{192N_c(N_c^2-1)}\Big\{4(N_c^2-4)\Delta_0\delta(1-z)\Big(-\ln\big[\frac{\mu_\Lambda^2}{m_Q^2}\big] \\ &\quad + 2\ln 2 + \frac{1}{2}\Big) + 6\Delta_+^{[8]\prime\prime}\,z\,(1-z) - 3\Delta_+^{[8]\prime}\,z\,(2z-1) \\ &\quad + 4\,z\,\Delta_+^{[8]}\Big[\frac{1}{(1-z)_+} - 2z + 1\Big]\Big\},\end{aligned} \tag{D.22}$$

$$\hat{d}^{(1)}_{[Q\bar{Q}(v^{[8]})]\to[Q\bar{Q}(^3P_2^{[8]},T2)]} = \frac{1}{48N_c(N_c^2-1)}z(1-z)\Delta_+^{[8]}, \tag{D.23}$$

$$\hat{d}^{(1)}_{[Q\bar{Q}(v^{[8]})]\to[Q\bar{Q}(^{2S+1}L_J^{[1]},pol)]} = \hat{d}^{(1)}_{[Q\bar{Q}(v^{[1]})]\to[Q\bar{Q}(^{2S+1}L_J^{[8]},pol)]}, \tag{D.24}$$

where *pol* is the polarization of the outgoing heavy quark pair.

D.3 NLO - Axial-vector

$$\hat{d}^{(1)}_{[Q\bar{Q}(a^{[1]})]\to[Q\bar{Q}(^1P_1^{[1]},T)]} = 0, \tag{D.25}$$

$$\hat{d}^{(1)}_{[Q\bar{Q}(a^{[1]})]\to[Q\bar{Q}(^3P_1^{[1]},T)]} = 0, \tag{D.26}$$

$$\hat{d}^{(1)}_{[Q\bar{Q}(a^{[1]})]\to[Q\bar{Q}(^3S_1^{[8]},T)]} = \frac{1}{16N_c}z(1-z)\Delta_+^{[1]}, \tag{D.27}$$

$$\begin{aligned}\hat{d}^{(1)}_{[Q\bar{Q}(a^{[1]})]\to[Q\bar{Q}(^1P_1^{[8]},T)]} &= \frac{1}{48N_c}\Big\{4\Delta_0\delta(1-z)\Big(-\ln\big[\frac{\mu_\Lambda^2}{m_Q^2}\big] + 2\ln 2 + \frac{1}{2}\Big) \\ &\quad + 2\,z\,\Delta_+^{[1]}\Big[\frac{1}{(1-z)_+} - \frac{3}{2}z\Big]\Big\},\end{aligned} \tag{D.28}$$

$$\hat{d}^{(1)}_{[Q\bar{Q}(a^{[1]})]\to[Q\bar{Q}(^3P_1^{[8]},T)]} = \frac{1}{192N_c}z(1-z)\big(6\Delta_-^{[1]\prime\prime} + 9\Delta_-^{[1]\prime} + 16\Delta_-^{[1]}\big), \tag{D.29}$$

$$\hat{d}^{(1)}_{[Q\bar{Q}(a^{[1]})]\to[Q\bar{Q}(^3P_2^{[8]},T1)]} = \frac{1}{192N_c}z(1-z)\big(6\Delta_-^{[1]\prime\prime} + 3\Delta_-^{[1]\prime} + 8\Delta_-^{[1]}\big), \tag{D.30}$$

$$\hat{d}^{(1)}_{[Q\bar{Q}(a^{[1]})]\to[Q\bar{Q}(^3P_2^{[8]},T2)]} = \frac{1}{48N_c}z(1-z)\Delta_-^{[1]}, \tag{D.31}$$

$$\hat{d}^{(1)}_{[Q\bar{Q}(a^{[8]})]\to[Q\bar{Q}(^3S_1^{[8]},T)]} = \frac{1}{16N_c(N_c^2-1)} z(1-z)\Delta_+^{[8]}, \tag{D.32}$$

$$\hat{d}^{(1)}_{[Q\bar{Q}(a^{[8]})]\to[Q\bar{Q}(^1P_1^{[8]},T)]} = \frac{1}{48N_c(N_c^2-1)} \Big\{ 2(N_c^2-4)\Delta_0\delta(1-z)\Big(- \ln\big[\frac{\mu_\Lambda^2}{m_Q^2}\big] + 2\ln 2 + \frac{1}{2}\Big) + 2\,z\,\Delta_+^{[8]}\Big[\frac{1}{(1-z)_+} - \frac{3}{2}z\Big]\Big\}, \tag{D.33}$$

$$\hat{d}^{(1)}_{[Q\bar{Q}(a^{[8]})]\to[Q\bar{Q}(^3P_1^{[8]},T)]} = \frac{1}{192N_c(N_c^2-1)} z(1-z)\big(6\Delta_-^{[8]\prime\prime} + 9\Delta_-^{[8]\prime} + 16\Delta_-^{[8]}\big), \tag{D.34}$$

$$\hat{d}^{(1)}_{[Q\bar{Q}(a^{[1]})]\to[Q\bar{Q}(^3P_2^{[8]},T1)]} = \frac{1}{192N_c(N_c^2-1)} z(1-z)\big(6\Delta_-^{[8]\prime\prime} + 3\Delta_-^{[8]\prime} + 8\Delta_-^{[8]}\big), \tag{D.35}$$

$$\hat{d}^{(1)}_{[Q\bar{Q}(a^{[1]})]\to[Q\bar{Q}(^3P_2^{[8]},T2)]} = \frac{1}{48N_c(N_c^2-1)} z(1-z)\Delta_-^{[8]}, \tag{D.36}$$

$$\hat{d}^{(1)}_{[Q\bar{Q}(a^{[8]})]\to[Q\bar{Q}(^{2S+1}L_J^{[1]},pol)]} = \hat{d}^{(1)}_{[Q\bar{Q}(a^{[1]})]\to[Q\bar{Q}(^{2S+1}L_J^{[8]},pol)]}, \tag{D.37}$$

where *pol* is the polarization of the outgoing heavy quark pair.

D.4 NLO - Tensor

$$\hat{d}^{(1)}_{[Q\bar{Q}(t^{[1]})]\to[Q\bar{Q}(^3S_1^{[1]},L)]} = 0, \tag{D.38}$$

$$\hat{d}^{(1)}_{[Q\bar{Q}(t^{[1]})]\to[Q\bar{Q}(^1P_1^{[1]},L)]} = 0, \tag{D.39}$$

$$\hat{d}^{(1)}_{[Q\bar{Q}(t^{[1]})]\to[Q\bar{Q}(^3P_1^{[1]},L)]} = 0, \tag{D.40}$$

$$\hat{d}^{(1)}_{[Q\bar{Q}(t^{[1]})]\to[Q\bar{Q}(^3P_2^{[1]},T2)]} = 0, \tag{D.41}$$

$$\hat{d}^{(1)}_{[Q\bar{Q}(t^{[1]})]\to[Q\bar{Q}(^3P_2^{[1]},L)]} = 0, \tag{D.42}$$

$$\hat{d}^{(1)}_{[Q\bar{Q}(t^{[1]})]\to[Q\bar{Q}(^3S_1^{[8]},L)]} = \frac{1}{16N_c} z(1-z)\Delta_-^{[1]}, \tag{D.43}$$

$$\hat{d}^{(1)}_{[Q\bar{Q}(t^{[1]})]\to[Q\bar{Q}(^1P_1^{[8]},L)]} = \frac{1}{48N_c} z(1-z)\Delta_-^{[1]}, \tag{D.44}$$

$$\hat{d}^{(1)}_{[Q\bar{Q}(t^{[1]})]\to[Q\bar{Q}(^3P_1^{[8]},L)]} = \frac{1}{48N_c} \Big\{ 2\Delta_0\delta(1-z)\Big(- \ln\big[\frac{\mu_\Lambda^2}{m_Q^2}\big] + 2\ln 2 + \frac{1}{2}\Big) + z\,\Delta_+^{[1]}\Big[\frac{1}{(1-z)_+} - 4z + 1\Big]\Big\}, \tag{D.45}$$

$$\hat{d}^{(1)}_{[Q\bar{Q}(t^{[1]})]\to[Q\bar{Q}(^3P_2^{[8]},T2)]} = \frac{1}{48N_c}\Big\{2\Delta_0\delta(1-z)\Big(-\ln\big[\frac{\mu_\Lambda^2}{m_Q^2}\big]+2\ln 2+\frac{1}{2}\Big) + z\,\Delta_+^{[1]}\Big[\frac{1}{(1-z)_+}-z+1\Big]\Big\}, \tag{D.46}$$

$$\hat{d}^{(1)}_{[Q\bar{Q}(t^{[1]})]\to[Q\bar{Q}(^3P_2^{[8]},L)]} = \frac{1}{288N_c}\Big\{4\Delta_0\delta(1-z)\Big(-\ln\big[\frac{\mu_\Lambda^2}{m_Q^2}\big]+2\ln 2+\frac{1}{2}\Big) + 12\,z\Delta_+^{[1]\prime\prime}(1-z) - 3\,z\Delta_+^{[1]\prime}(3z-2) + 2\,z\,\Delta_+^{[1]}\Big[\frac{1}{(1-z)_+}-7z+5\Big]\Big\}, \tag{D.47}$$

$$\hat{d}^{(1)}_{[Q\bar{Q}(t^{[8]})]\to[Q\bar{Q}(^3S_1^{[8]},L)]} = \frac{1}{16N_c(N_c^2-1)}z(1-z)\Delta_-^{[8]}, \tag{D.48}$$

$$\hat{d}^{(1)}_{[Q\bar{Q}(t^{[8]})]\to[Q\bar{Q}(^1P_1^{[8]},L)]} = \frac{1}{48N_c(N_c^2-1)}z(1-z)\Delta_-^{[8]}, \tag{D.49}$$

$$\hat{d}^{(1)}_{[Q\bar{Q}(t^{[8]})]\to[Q\bar{Q}(^3P_1^{[8]},L)]} = \frac{1}{48N_c(N_c^2-1)}\Big\{(N_c^2-4)\Delta_0\delta(1-z)\Big(-\ln\big[\frac{\mu_\Lambda^2}{m_Q^2}\big] + 2\ln 2+\frac{1}{2}\Big) + z\,\Delta_+^{[8]}\Big[\frac{1}{(1-z)_+}-4z+1\Big]\Big\}, \tag{D.50}$$

$$\hat{d}^{(1)}_{[Q\bar{Q}(t^{[8]})]\to[Q\bar{Q}(^3P_2^{[8]},T2)]} = \frac{1}{48N_c(N_c^2-1)}\Big\{(N_c^2-4)\Delta_0\delta(1-z)\Big(-\ln\big[\frac{\mu_\Lambda^2}{m_Q^2}\big] + 2\ln 2+\frac{1}{2}\Big) + z\,\Delta_+^{[8]}\Big[\frac{1}{(1-z)_+}-z+1\Big]\Big\}, \tag{D.51}$$

$$\hat{d}^{(1)}_{[Q\bar{Q}(t^{[8]})]\to[Q\bar{Q}(^3P_2^{[8]},L)]} = \frac{1}{288N_c(N_c^2-1)}\Big\{2(N_c^2-4)\Delta_0\delta(1-z)\Big(-\ln\big[\frac{\mu_\Lambda^2}{m_Q^2}\big] + 2\ln 2+\frac{1}{2}\Big) + 12\,z\Delta_+^{[8]\prime\prime}(1-z) - 3\,z\Delta_+^{[8]\prime}(3z-2) + 2\,z\,\Delta_+^{[8]}\Big[\frac{1}{(1-z)_+}-7z+5\Big]\Big\}, \tag{D.52}$$

$$\hat{d}^{(1)}_{[Q\bar{Q}(t^{[8]})]\to[Q\bar{Q}(^{2S+1}L_J^{[1]},pol)]} = \hat{d}^{(1)}_{[Q\bar{Q}(t^{[1]})]\to[Q\bar{Q}(^{2S+1}L_J^{[8]},pol)]}, \tag{D.53}$$

where *pol* is the polarization of the outgoing heavy quark pair.

D.5 ^3P_J operators with orbital angular momentum summed

Notice the T or L for $^3P_J^{[1]}$ and $^3P_J^{[8]}$ are the polarization of final S-wave heavy quarkonium, as explained at the end of Sec. 8.1.

D.5.1 Leading Order

$$\hat{d}^{(0)}_{[Q\bar{Q}(v^{[1]})]\to[Q\bar{Q}(^3P_J^{[1]},T)]} = 0, \tag{D.54}$$

$$\hat{d}^{(0)}_{[Q\bar{Q}(a^{[1]})]\to[Q\bar{Q}(^1P_1^{[1]},L)]} = 0, \tag{D.55}$$

$$\hat{d}^{(0)}_{[Q\bar{Q}(t^{[1]})]\to[Q\bar{Q}(^3P_J^{[1]},L)]} = 0. \tag{D.56}$$

The corresponding color octet channels also vanish.

D.5.2 Next-to-leading order

$$\hat{d}^{(1)}_{[Q\bar{Q}(v^{[1]})]\to[Q\bar{Q}(^3P_J^{[8]},T)]} = \frac{1}{8N_c}z(1-z)\Big\{\Delta_+^{[1]}\ln\big[\frac{\mu_0^2}{m_Q^2}\big] - \Delta_+^{[1]}\Big[2\ln(2(1-z))-1\Big] + \Delta_+^{[1]\prime} + \Delta_+^{[1]\prime\prime}\Big\}, \tag{D.57}$$

$$\hat{d}^{(1)}_{[Q\bar{Q}(v^{[8]})]\to[Q\bar{Q}(^3P_J^{[1]},T)]} = \hat{d}^{(1)}_{[Q\bar{Q}(v^{[1]})]\to[Q\bar{Q}(^3P_J^{[8]},T)]}, \tag{D.58}$$

$$\hat{d}^{(1)}_{[Q\bar{Q}(v^{[8]})]\to[Q\bar{Q}(^3P_J^{[8]},T)]} = \frac{1}{8N_c(N_c^2-1)}z(1-z)\Big\{\Delta_+^{[8]}\ln\big[\frac{\mu_0^2}{m_Q^2}\big] - \Delta_+^{[8]}\Big[2\ln(2(1-z))-1\Big] + \Delta_+^{[8]\prime} + \Delta_+^{[8]\prime\prime}\Big\}, \tag{D.59}$$

$$\hat{d}^{(1)}_{[Q\bar{Q}(a^{[1]})]\to[Q\bar{Q}(^3P_J^{[8]},L)]} = \frac{1}{16N_c}z(1-z)\Big\{(\Delta_-^{[1]} + \Delta_-^{[1]\prime} + \Delta_-^{[1]\prime\prime})\Big[\ln\big[\frac{\mu_0^2}{m_Q^2}\big] - 2\ln(2(1-z))-3\Big] - \Delta_-^{[1]\prime}\Big\}, \tag{D.60}$$

$$\hat{d}^{(1)}_{[Q\bar{Q}(a^{[8]})]\to[Q\bar{Q}(^3P_J^{[1]},L)]} = \hat{d}^{(1)}_{[Q\bar{Q}(a^{[1]})]\to[Q\bar{Q}(^3P_J^{[8]},L)]}, \tag{D.61}$$

$$\hat{d}^{(1)}_{[Q\bar{Q}(a^{[1]})]\to[Q\bar{Q}(^3P_J^{[8]},L)]} = \frac{1}{16N_c(N_c^2-1)}z(1-z)\Big\{(\Delta_-^{[8]} + \Delta_-^{[8]\prime} + \Delta_-^{[8]\prime\prime})\Big[\ln\big[\frac{\mu_0^2}{m_Q^2}\big] - 2\ln(2(1-z))-3\Big] - \Delta_-^{[8]\prime}\Big\}, \tag{D.62}$$

$$\hat{d}^{(1)}_{[Q\bar{Q}(t^{[1]})]\to[Q\bar{Q}(^3P_J^{[8]},L)]} = \frac{1}{16N_c}z(1-z)(2\Delta_+^{[1]} + \Delta_+^{[1]\prime} + \Delta_+^{[1]\prime\prime}), \tag{D.63}$$

$$\hat{d}^{(1)}_{[Q\bar{Q}(t^{[8]})]\to[Q\bar{Q}(^3P_J^{[1]},L)]} = \hat{d}^{(1)}_{[Q\bar{Q}(t^{[1]})]\to[Q\bar{Q}(^3P_J^{[8]},L)]}, \tag{D.64}$$

$$\hat{d}^{(1)}_{[Q\bar{Q}(t^{[8]})]\to[Q\bar{Q}(^3P_J^{[8]},L)]} = \frac{1}{16N_c(N_c^2-1)}z(1-z)(2\Delta_+^{[8]} + \Delta_+^{[8]\prime} + \Delta_+^{[8]\prime\prime}). \tag{D.65}$$

Bibliography

[1] J. Beringer et al. Review of Particle Physics (RPP). *Phys.Rev.*, D86: 010001, 2012. doi: 10.1103/PhysRevD.86.010001.

[2] Eric Braaten and James Russ. J/psi and Upsilon Polarization in Hadronic Production Processes. 2014.

[3] Eric Braaten, Michael A. Doncheski, Sean Fleming, and Michelangelo L. Mangano. Fragmentation production of J/ψ and ψ' at the Tevatron. *Phys.Lett.*, B333:548–554, 1994. doi: 10.1016/0370-2693(94)90182-1.

[4] Michael Kramer. Quarkonium production at high-energy colliders. *Prog.Part.Nucl.Phys.*, 47:141–201, 2001. doi: 10.1016/S0146-6410(01)00154-5.

[5] A. Abulencia et al. Polarization of J/ψ and ψ_{2S} mesons produced in $p\bar{p}$ collisions at $\sqrt{s} = 1.96$-TeV. *Phys.Rev.Lett.*, 99:132001, 2007. doi: 10.1103/PhysRevLett.99.132001.

[6] D. Acosta et al. Υ production and polarization in $p\bar{p}$ collisions at $\sqrt{s} = 1.8$-TeV. *Phys.Rev.Lett.*, 88:161802, 2002. doi: 10.1103/PhysRevLett.88.161802.

[7] Geoffrey T. Bodwin. Theory of Charmonium Production. 2012.

[8] P. Artoisenet, John M. Campbell, J.P. Lansberg, F. Maltoni, and F. Tramontano. Υ Production at Fermilab Tevatron and LHC Energies. *Phys.Rev.Lett.*, 101:152001, 2008. doi: 10.1103/PhysRevLett.101.152001.

[9] Bin Gong and Jian-Xiong Wang. Next-to-leading-order QCD corrections to J/ψ polarization at Tevatron and Large-Hadron-Collider energies. *Phys.Rev.Lett.*, 100:232001, 2008. doi: 10.1103/PhysRevLett.100.232001.

[10] J.F. Amundson, Oscar J.P. Eboli, E.M. Gregores, and F. Halzen. Quantitative tests of color evaporation: Charmonium production. *Phys.Lett.*, B390:323–328, 1997. doi: 10.1016/S0370-2693(96)01417-7.

[11] Yan-Qing Ma, Kai Wang, and Kuang-Ta Chao. $J/\psi(\psi')$ production at the Tevatron and LHC at $\mathcal{O}(\alpha_s^4 v^4)$ in nonrelativistic QCD. *Phys.Rev.Lett.*, 106:042002, 2011. doi: 10.1103/PhysRevLett.106.042002.

[12] Kuang-Ta Chao, Yan-Qing Ma, Hua-Sheng Shao, Kai Wang, and Yu-Jie Zhang. J/ψ Polarization at Hadron Colliders in Nonrelativistic QCD. *Phys.Rev.Lett.*, 108:242004, 2012. doi: 10.1103/PhysRevLett.108.242004.

[13] Mathias Butenschoen and Bernd A. Kniehl. World data of J/psi production consolidate NRQCD factorization at NLO. *Phys.Rev.*, D84:051501, 2011. doi: 10.1103/PhysRevD.84.051501.

[14] Mathias Butenschoen and Bernd A. Kniehl. J/psi polarization at Tevatron and LHC: Nonrelativistic-QCD factorization at the crossroads. *Phys.Rev.Lett.*, 108:172002, 2012. doi: 10.1103/PhysRevLett.108.172002.

[15] Bin Gong, Lu-Ping Wan, Jian-Xiong Wang, and Hong-Fei Zhang. Polarization for Prompt J/psi, psi(2s) production at the Tevatron and LHC. *Phys.Rev.Lett.*, 110:042002, 2013. doi: 10.1103/PhysRevLett.110.042002.

[16] Roel Aaij et al. Measurement of $\psi(2S)$ polarisation in pp collisions at $\sqrt{s} = 7$ TeV. *Eur.Phys.J.*, C74:2872, 2014. doi: 10.1140/epjc/s10052-014-2872-9.

[17] Bin Gong, Lu-Ping Wan, Jian-Xiong Wang, and Hong-Fei Zhang. Complete next-to-leading-order study on the yield and polarization of Upsilon(1S,2S,3S) at the Tevatron and LHC. *Phys.Rev.Lett.*, 112:032001, 2014. doi: 10.1103/PhysRevLett.112.032001.

[18] Geoffrey T. Bodwin, Hee Sok Chung, U-Rae Kim, and Jungil Lee. Fragmentation contributions to J/psi production at the Tevatron and the LHC. *Phys.Rev.Lett.*, 113:022001, 2014. doi: 10.1103/PhysRevLett.113.022001.

[19] Bernard Aubert et al. Observation of the bottomonium ground state in the decay $\upsilon_{3S} \to \gamma\eta_b$. *Phys.Rev.Lett.*, 101:071801, 2008. doi: 10.1103/PhysRevLett.101.071801.

[20] G. Bonvicini et al. Measurement of the eta(b)(1S) mass and the branching fraction for Upsilon(3S) $\to$ gamma eta(b)(1S). *Phys.Rev.*, D81: 031104, 2010. doi: 10.1103/PhysRevD.81.031104.

[21] Bernard Aubert et al. Evidence for the eta(b)(1S) Meson in Radiative Upsilon(2S) Decay. *Phys.Rev.Lett.*, 103:161801, 2009. doi: 10.1103/PhysRevLett.103.161801.

[22] B.G. Fulsom. Recent bottomonium results from BaBar. *PoS*, ICHEP2010:199, 2010.

[23] Zhong-Bo Kang, Jian-Wei Qiu, and George Sterman. Heavy quarkonium production and polarization. *Phys.Rev.Lett.*, 108:102002, 2012. doi: 10.1103/PhysRevLett.108.102002.

[24] Zhong-Bo Kang, Yan-Qing Ma, Jian-Wei Qiu, and George Sterman. Heavy quarkonium production at collider energies: Partonic cross sections and polarization. 2013.

[25] F. Aversa, P. Chiappetta, Mario Greco, and J.P. Guillet. QCD Corrections to Parton-Parton Scattering Processes. *Nucl.Phys.*, B327:105, 1989. doi: 10.1016/0550-3213(89)90288-5.

[26] N. Brambilla, S. Eidelman, B.K. Heltsley, R. Vogt, G.T. Bodwin, et al. Heavy quarkonium: progress, puzzles, and opportunities. *Eur.Phys.J.*, C71:1534, 2011. doi: 10.1140/epjc/s10052-010-1534-9.

[27] John C. Collins, Davison E. Soper, and George F. Sterman. Heavy Particle Production in High-Energy Hadron Collisions. *Nucl.Phys.*, B263: 37, 1986. doi: 10.1016/0550-3213(86)90026-X.

[28] M.B. Einhorn and S.D. Ellis. Hadronic Production of the New Resonances: Probing Gluon Distributions. *Phys.Rev.*, D12:2007, 1975. doi: 10.1103/PhysRevD.12.2007.

[29] S.D. Ellis, Martin B. Einhorn, and C. Quigg. Comment on Hadronic Production of Psions. *Phys.Rev.Lett.*, 36:1263, 1976. doi: 10.1103/PhysRevLett.36.1263.

[30] C.E. Carlson and R. Suaya. Hadronic Production of psi/J Mesons. *Phys.Rev.*, D14:3115, 1976. doi: 10.1103/PhysRevD.14.3115.

[31] Chao-Hsi Chang. Hadronic Production of J/ψ Associated With a Gluon. *Nucl.Phys.*, B172:425–434, 1980. doi: 10.1016/0550-3213(80)90175-3.

[32] Edmond L. Berger and Daniel L. Jones. Inelastic Photoproduction of J/psi and Upsilon by Gluons. *Phys.Rev.*, D23:1521–1530, 1981. doi: 10.1103/PhysRevD.23.1521.

[33] R. Baier and R. Ruckl. Hadronic Production of J/psi and Upsilon: Transverse Momentum Distributions. *Phys.Lett.*, B102:364, 1981. doi: 10.1016/0370-2693(81)90636-5.

[34] R. Baier and R. Ruckl. On Inelastic Leptoproduction of Heavy Quarkonium States. *Nucl.Phys.*, B201:1, 1982. doi: 10.1016/0550-3213(82)90374-1.

[35] R. Baier and R. Ruckl. Hadronic Collisions: A Quarkonium Factory. *Z.Phys.*, C19:251, 1983. doi: 10.1007/BF01572254.

[36] Geoffrey T. Bodwin, Eric Braaten, and G. Peter Lepage. Rigorous qcd analysis of inclusive annihilation and production of heavy quarkonium. *Phys.Rev.*, D51:1125–1171, 1995. doi: 10.1103/PhysRevD.55.5853,10.1103/PhysRevD.51.1125. quarkonium.

[37] Yan-Qing Ma, Kai Wang, and Kuang-Ta Chao. QCD radiative corrections to χ_{cJ} production at hadron colliders. *Phys.Rev.*, D83:111503, 2011. doi: 10.1103/PhysRevD.83.111503.

[38] Mathias Butenschoen and Bernd A. Kniehl. Reconciling J/ψ production at HERA, RHIC, Tevatron, and LHC with NRQCD factorization at next-to-leading order. *Phys.Rev.Lett.*, 106:022003, 2011. doi: 10.1103/PhysRevLett.106.022003.

[39] Kai Wang, Yan-Qing Ma, and Kuang-Ta Chao. $\Upsilon(1S)$ prompt production at the Tevatron and LHC in nonrelativistic QCD. *Phys.Rev.*, D85:114003, 2012. doi: 10.1103/PhysRevD.85.114003.

[40] Zhong-Bo Kang, Yan-Qing Ma, Jian-Wei Qiu, and George Sterman. Heavy Quarkonium Production at Collider Energies: Factorization and Evolution. 2014.

[41] Yu-Jie Zhang, Yan-Qing Ma, Kai Wang, and Kuang-Ta Chao. QCD radiative correction to color-octet J/psi inclusive production at B Factories. *Phys.Rev.*, D81:034015, 2010. doi: 10.1103/PhysRevD.81.034015.

[42] Serguei Chatrchyan et al. Measurement of the Y1S, Y2S and Y3S polarizations in pp collisions at $\sqrt{s} = 7$ TeV. *Phys.Rev.Lett.*, 110:081802, 2013. doi: 10.1103/PhysRevLett.110.081802.

[43] Zhong-Bo Kang, Jian-Wei Qiu, and George Sterman. Factorization and quarkonium production. *Nucl.Phys.Proc.Suppl.*, 214:39–43, 2011. doi: 10.1016/j.nuclphysbps.2011.03.054.

[44] Sean Fleming, Adam K. Leibovich, Thomas Mehen, and Ira Z. Rothstein. The systematics of quarkonium production at the lhc and double parton fragmentation. *Phys.Rev.*, D86:094012, 2012. doi: 10.1103/PhysRevD.86.094012.

[45] Yan-Qing Ma, Jian-Wei Qiu, and Hong Zhang. Heavy quarkonium fragmentation functions from a heavy quark pair. I. S wave. *Phys.Rev.*, D89: 094029, 2014. doi: 10.1103/PhysRevD.89.094029.

[46] Yan-Qing Ma, Jian-Wei Qiu, and Hong Zhang. Heavy quarkonium fragmentation functions from a heavy quark pair. II. P wave. *Phys.Rev.*, D89:094030, 2014. doi: 10.1103/PhysRevD.89.094030.

[47] Yan-Qing Ma, Jian-Wei Qiu, George Sterman, and Hong Zhang. Factorized power expansion for high-p_T heavy quarkonium production. 2014.

[48] Yan-Qing Ma, Kai Wang, and Kuang-Ta Chao. A complete NLO calculation of the J/ψ and ψ' production at hadron colliders. *Phys.Rev.*, D84:114001, 2011. doi: 10.1103/PhysRevD.84.114001.

[49] Murray Gell-Mann. The Eightfold Way: A Theory of strong interaction symmetry. 1961.

[50] Yuval Ne'eman. Derivation of strong interactions from a gauge invariance. *Nucl.Phys.*, 26:222–229, 1961. doi: 10.1016/0029-5582(61)90134-1.

[51] Murray Gell-Mann. A Schematic Model of Baryons and Mesons. *Phys.Lett.*, 8:214–215, 1964. doi: 10.1016/S0031-9163(64)92001-3.

[52] G. Zweig. An SU(3) model for strong interaction symmetry and its breaking. Version 2. pages 22–101, 1964.

[53] S. Okubo. Phi meson and unitary symmetry model. *Phys.Lett.*, 5:165–168, 1963. doi: 10.1016/S0375-9601(63)92548-9.

[54] Jugoro Iizuka. Systematics and phenomenology of meson family. *Prog.Theor.Phys.Suppl.*, 37:21–34, 1966. doi: 10.1143/PTPS.37.21.

[55] M.Y. Han and Yoichiro Nambu. Three Triplet Model with Double SU(3) Symmetry. *Phys.Rev.*, 139:B1006–B1010, 1965. doi: 10.1103/PhysRev.139.B1006.

[56] Jr. Callan, Curtis G. and David J. Gross. High-energy electroproduction and the constitution of the electric current. *Phys.Rev.Lett.*, 22:156–159, 1969. doi: 10.1103/PhysRevLett.22.156.

[57] J.D. Bjorken and Emmanuel A. Paschos. Inelastic Electron Proton and gamma Proton Scattering, and the Structure of the Nucleon. *Phys.Rev.*, 185:1975–1982, 1969. doi: 10.1103/PhysRev.185.1975.

[58] R.P. Feynman. The behavior of hadron collisions at extreme energies. *Conf.Proc.*, C690905:237–258, 1969.

[59] Richard P. Feynman. Very high-energy collisions of hadrons. *Phys.Rev.Lett.*, 23:1415–1417, 1969. doi: 10.1103/PhysRevLett.23.1415.

[60] J.J. Aubert et al. Experimental Observation of a Heavy Particle J. *Phys.Rev.Lett.*, 33:1404–1406, 1974. doi: 10.1103/PhysRevLett.33.1404.

[61] J.E. Augustin et al. Discovery of a Narrow Resonance in e+ e- Annihilation. *Phys.Rev.Lett.*, 33:1406–1408, 1974. doi: 10.1103/PhysRevLett.33.1406.

[62] G.S. Abrams, D. Briggs, William Chinowsky, C.E. Friedberg, G. Goldhaber, et al. The Discovery of a Second Narrow Resonance in e+ e- Annihilation. *Phys.Rev.Lett.*, 33:1453–1455, 1974. doi: 10.1103/PhysRevLett.33.1453.

[63] S.W. Herb, D.C. Hom, L.M. Lederman, J.C. Sens, H.D. Snyder, et al. Observation of a Dimuon Resonance at 9.5-GeV in 400-GeV Proton-Nucleus Collisions. *Phys.Rev.Lett.*, 39:252–255, 1977. doi: 10.1103/PhysRevLett.39.252.

[64] R. Brandelik et al. Evidence for Planar Events in e+ e- Annihilation at High-Energies. *Phys.Lett.*, B86:243, 1979. doi: 10.1016/0370-2693(79)90830-X.

[65] F. Abe et al. Observation of top quark production in $\bar{p}p$ collisions. *Phys.Rev.Lett.*, 74:2626–2631, 1995. doi: 10.1103/PhysRevLett.74.2626.

[66] S. Abachi et al. Search for high mass top quark production in $p\bar{p}$ collisions at $\sqrt{s} = 1.8$ TeV. *Phys.Rev.Lett.*, 74:2422–2426, 1995. doi: 10.1103/PhysRevLett.74.2422.

[67] J. Ashman et al. A Measurement of the Spin Asymmetry and Determination of the Structure Function g(1) in Deep Inelastic Muon-Proton Scattering. *Phys.Lett.*, B206:364, 1988. doi: 10.1016/0370-2693(88)91523-7.

[68] Chen-Ning Yang and Robert L. Mills. Conservation of Isotopic Spin and Isotopic Gauge Invariance. *Phys.Rev.*, 96:191–195, 1954. doi: 10.1103/PhysRev.96.191.

[69] H. Fritzsch, Murray Gell-Mann, and H. Leutwyler. Advantages of the Color Octet Gluon Picture. *Phys.Lett.*, B47:365–368, 1973. doi: 10.1016/0370-2693(73)90625-4.

[70] David J. Gross and Frank Wilczek. Ultraviolet Behavior of Nonabelian Gauge Theories. *Phys.Rev.Lett.*, 30:1343–1346, 1973. doi: 10.1103/PhysRevLett.30.1343.

[71] H. David Politzer. Reliable Perturbative Results for Strong Interactions? *Phys.Rev.Lett.*, 30:1346–1349, 1973. doi: 10.1103/PhysRevLett.30.1346.

[72] L.D. Faddeev and V.N. Popov. Feynman Diagrams for the Yang-Mills Field. *Phys.Lett.*, B25:29–30, 1967. doi: 10.1016/0370-2693(67)90067-6.

[73] John C. Collins, Davison E. Soper, and George F. Sterman. Factorization of Hard Processes in QCD. *Adv.Ser.Direct.High Energy Phys.*, 5:1–91, 1988.

[74] Raymond Brock et al. Handbook of perturbative QCD: Version 1.0. *Rev.Mod.Phys.*, 67:157–248, 1995. doi: 10.1103/RevModPhys.67.157.

[75] G. Curci, W. Furmanski, and R. Petronzio. Evolution of Parton Densities Beyond Leading Order: The Nonsinglet Case. *Nucl.Phys.*, B175:27, 1980. doi: 10.1016/0550-3213(80)90003-6.

[76] Jian-Wei Qiu. Basics of perturbative QCD. *Prog.Theor.Phys.Suppl.*, 187:1–16, 2011. doi: 10.1143/PTPS.187.1.

[77] Jian-wei Qiu and George F. Sterman. Power corrections in hadronic scattering. 1. Leading 1/Q**2 corrections to the Drell-Yan cross-section. *Nucl.Phys.*, B353:105–136, 1991. doi: 10.1016/0550-3213(91)90503-P.

[78] Jian-wei Qiu and George F. Sterman. Power corrections to hadronic scattering. 2. Factorization. *Nucl.Phys.*, B353:137–164, 1991. doi: 10.1016/0550-3213(91)90504-Q.

[79] Eric Braaten and Tzu Chiang Yuan. Gluon fragmentation into heavy quarkonium. *Phys.Rev.Lett.*, 71:1673–1676, 1993. doi: 10.1103/PhysRevLett.71.1673. gluon fragmentation to 1S0[1].

[80] Eric Braaten, King-man Cheung, and Tzu Chiang Yuan. Z0 decay into charmonium via charm quark fragmentation. *Phys.Rev.*, D48:4230–4235, 1993. doi: 10.1103/PhysRevD.48.4230. Heavy Quark Fragmentation to 1S0[1] and 3S1[1].

[81] Eric Braaten and Tzu Chiang Yuan. Gluon fragmentation into P wave heavy quarkonium. *Phys.Rev.*, D50:3176–3180, 1994. doi: 10.1103/PhysRevD.50.3176. Gluon Fragmentation into 3PJ.

[82] F. Abe et al. Production of J/ψ mesons from χ_c meson decays in $p\bar{p}$ collisions at $\sqrt{s} = 1.8$ TeV. *Phys.Rev.Lett.*, 79:578–583, 1997. doi: 10.1103/PhysRevLett.79.578.

[83] J.P. Lansberg. Off-shell and non-static contributions to heavy-quarkonium production. *AIP Conf.Proc.*, 892:324–326, 2007. doi: 10.1063/1.2714407.

[84] J.P. Lansberg. On the mechanisms of heavy-quarkonium hadroproduction. *Eur.Phys.J.*, C61:693–703, 2009. doi: 10.1140/epjc/s10052-008-0826-9.

[85] Harald Fritzsch. Producing Heavy Quark Flavors in Hadronic Collisions: A Test of Quantum Chromodynamics. *Phys.Lett.*, B67:217, 1977. doi: 10.1016/0370-2693(77)90108-3.

[86] F. Halzen. Cvc for Gluons and Hadroproduction of Quark Flavors. *Phys.Lett.*, B69:105, 1977. doi: 10.1016/0370-2693(77)90144-7.

[87] Francis Halzen and Satoshi Matsuda. Hadroproduction of Quark Flavors. *Phys.Rev.*, D17:1344, 1978. doi: 10.1103/PhysRevD.17.1344.

[88] M. Gluck, J.F. Owens, and E. Reya. Gluon Contribution to Hadronic J/psi Production. *Phys.Rev.*, D17:2324, 1978. doi: 10.1103/PhysRevD.17.2324.

[89] W.E. Caswell and G.P. Lepage. Effective Lagrangians for Bound State Problems in QED, QCD, and Other Field Theories. *Phys.Lett.*, B167:437, 1986. doi: 10.1016/0370-2693(86)91297-9.

[90] Kuang-Ta Chao and Yan-Qing Ma. Quarkonium production review. *PoS*, ConfinementX:003, 2012.

[91] P. Artoisenet, J.P. Lansberg, and F. Maltoni. Hadroproduction of J/ψ and υ in association with a heavy-quark pair. *Phys.Lett.*, B653:60–66, 2007. doi: 10.1016/j.physletb.2007.04.031.

[92] CMS Collaboration. J/psi and psi(2S) prompt double-differential cross sections in pp collisions at 7 TeV. 2014.

[93] John Collins. *Foundations of Perturbative QCD*. Cambridge University Press, 2013.

[94] Sean Fleming, Adam K. Leibovich, Thomas Mehen, and Ira Z. Rothstein. Anomalous dimensions of the double parton fragmentation functions. 2013. doi: 10.1103/PhysRevD.87.074022.

[95] G. Peter Lepage and Stanley J. Brodsky. Exclusive Processes in Quantum Chromodynamics: Evolution Equations for Hadronic Wave Functions and the Form-Factors of Mesons. *Phys.Lett.*, B87:359–365, 1979. doi: 10.1016/0370-2693(79)90554-9.

[96] A.V. Efremov and A.V. Radyushkin. Asymptotical Behavior of Pion Electromagnetic Form-Factor in QCD. *Theor.Math.Phys.*, 42:97–110, 1980. doi: 10.1007/BF01032111.

[97] G. Peter Lepage and Stanley J. Brodsky. Exclusive Processes in Perturbative Quantum Chromodynamics. *Phys.Rev.*, D22:2157, 1980. doi: 10.1103/PhysRevD.22.2157.

[98] V.L. Chernyak and A.R. Zhitnitsky. Asymptotic Behavior of Exclusive Processes in QCD. *Phys.Rept.*, 112:173, 1984. doi: 10.1016/0370-1573(84)90126-1.

[99] V.V. Braguta, A.K. Likhoded, and A.V. Luchinsky. The Study of leading twist light cone wave function of eta(c) meson. *Phys.Lett.*, B646:80–90, 2007. doi: 10.1016/j.physletb.2007.01.014.

[100] V.V. Braguta. The study of leading twist light cone wave functions of J/psi meson. *Phys.Rev.*, D75:094016, 2007. doi: 10.1103/PhysRevD.75.094016.

[101] V.V. Braguta, A.K. Likhoded, and A.V. Luchinsky. Leading twist distribution amplitudes of P-wave nonrelativistic mesons. *Phys.Rev.*, D79:074004, 2009. doi: 10.1103/PhysRevD.79.074004.

[102] J.P. Ma and Z.G. Si. NRQCD Factorization for Twist-2 Light-Cone Wave-Functions of Charmonia. *Phys.Lett.*, B647:419–426, 2007. doi: 10.1016/j.physletb.2007.02.040.

[103] Guido Bell and Thorsten Feldmann. Modelling light-cone distribution amplitudes from non-relativistic bound states. *JHEP*, 0804:061, 2008. doi: 10.1088/1126-6708/2008/04/061.

[104] Yu Jia and Deshan Yang. Refactorizing NRQCD short-distance coefficients in exclusive quarkonium production. *Nucl.Phys.*, B814:217–230, 2009. doi: 10.1016/j.nuclphysb.2009.01.025.

[105] Yu Jia, Jian-Xiong Wang, and Deshan Yang. Bridging light-cone and NRQCD approaches: asymptotic behavior of B_c electromagnetic form factor. *JHEP*, 1110:105, 2011. doi: 10.1007/JHEP10(2011)105.

[106] Xiang-Peng Wang and Deshan Yang. The leading twist light-cone distribution amplitudes for the S-wave and P-wave quarkonia and their applications in single quarkonium exclusive productions. *JHEP*, 1406: 121, 2014. doi: 10.1007/JHEP06(2014)121.

[107] Eric Braaten and Jungil Lee. Next-to-leading order calculation of the color octet 3S(1) gluon fragmentation function for heavy quarkonium. *Nucl.Phys.*, B586:427–439, 2000. doi: 10.1016/S0550-3213(00)00396-5. Gluon Fragmentation into 3S1[8].

[108] J.P. Ma. Quark fragmentation into p wave triplet quarkonium. *Phys.Rev.*, D53:1185–1190, 1996. doi: 10.1103/PhysRevD.53.1185.

[109] Eric Braaten and Yu-Qi Chen. Dimensional regularization in quarkonium calculations. *Phys.Rev.*, D55:2693–2707, 1997. doi: 10.1103/PhysRevD.55.2693.

[110] Gang Hao, YaBing Zuo, and Cong-Feng Qiao. The Fragmentation Function of Gluon Splitting into P-wave Spin-singlet Heavy Quarkonium. 2009. Gluon Fragmentation into 1P1[1] and 1S0[8].

[111] Yu Jia, Wen-Long Sang, and Jia Xu. Inclusive h_c Production at B Factories. *Phys.Rev.*, D86:074023, 2012. doi: 10.1103/PhysRevD.86.074023.

[112] Andrea Petrelli, Matteo Cacciari, Mario Greco, Fabio Maltoni, and Michelangelo L. Mangano. NLO production and decay of quarkonium. *Nucl.Phys.*, B514:245–309, 1998. doi: 10.1016/S0550-3213(97)00801-8.

[113] Zhong-Bo Kang, Yan-Qing Ma, and Raju Venugopalan. Quarkonium production in high energy proton-nucleus collisions: CGC meets NRQCD. *JHEP*, 1401:056, 2014. doi: 10.1007/JHEP01(2014)056.

[114] Han-wen Huang and Kuang-ta Chao. QCD radiative correction to the hadronic annihilation rate of 1+- heavy quarkonium. *Phys.Rev.*, D54:3065–3072, 1996. doi: 10.1103/PhysRevD.60.079901,10.1103/PhysRevD.56.7472,10.1103/PhysRevD.54.3065.

[115] Zhi-Guo He, Ying Fan, and Kuang-Ta Chao. QCD prediction for the non-D anti-D annihilation decay of psi(3770). *Phys.Rev.Lett.*, 101: 112001, 2008. doi: 10.1103/PhysRevLett.101.112001.

[116] Zhi-Guo He, Ying Fan, and Kuang-Ta Chao. NRQCD Predictions of D-Wave Quarkonia D-3(J) (J = 1,2,3) Decay into Light Hadrons at Order alpha**3 (S). *Phys.Rev.*, D81:074032, 2010. doi: 10.1103/PhysRevD.81.074032.

[117] Ying Fan, Zhi-Guo He, Yan-Qing Ma, and Kuang-Ta Chao. Predictions of Light Hadronic Decays of Heavy Quarkonium 1D(2) States in NRQCD. *Phys.Rev.*, D80:014001, 2009. doi: 10.1103/PhysRevD.80.014001.

[118] Jian-wei Qiu and George F. Sterman. Single transverse spin asymmetries in hadronic pion production. *Phys.Rev.*, D59:014004, 1999. doi: 10.1103/PhysRevD.59.014004.

[119] Zhong-Bo Kang and Jian-Wei Qiu. Evolution of twist-3 multi-parton correlation functions relevant to single transverse-spin asymmetry. *Phys.Rev.*, D79:016003, 2009. doi: 10.1103/PhysRevD.79.016003.

[120] M. Beneke and Vladimir A. Smirnov. Asymptotic expansion of Feynman integrals near threshold. *Nucl.Phys.*, B522:321–344, 1998. doi: 10.1016/S0550-3213(98)00138-2.

[121] P. Breitenlohner and D. Maison. Dimensional renormalization and the action principle. *Commun.Math.Phys.*, 52:11–38, 1977. doi: 10.1007/BF01609069.

[122] Gerard 't Hooft and M.J.G. Veltman. Regularization and Renormalization of Gauge Fields. *Nucl.Phys.*, B44:189–213, 1972. doi: 10.1016/0550-3213(72)90279-9.

[123] Dirk Kreimer. The γ_5 problem and anomalies: A clifford algebra approach. *Phys.Lett.*, B237:59, 1990. doi: 10.1016/0370-2693(90)90461-E.

[124] J.G. Korner, D. Kreimer, and K. Schilcher. A practicable γ_5 scheme in dimensional regularization. *Z.Phys.*, C54:503–512, 1992. doi: 10.1007/BF01559471.

[125] Dirk Kreimer. The role of γ_5 in dimensional regularization. 1993.

[126] Todd H. West. Feynman parameter and trace - programs for expressing feynman amplitudes as integrals over feynman parameters. *Computer Physics Communications*, 77(2):286 – 298, 1993. ISSN 0010-4655. doi: http://dx.doi.org/10.1016/0010-4655(93)90011-Z. URL http://www.sciencedirect.com/science/article/pii/001046559390011Z. Mathematica, program, gamma5.

[127] Hua-Sheng Shao, Yan-Qing Ma, Kai Wang, and Kuang-Ta Chao. Polarizations of χ_{c1} and χ_{c2} in prompt production at the LHC. *Phys.Rev.Lett.*, 112:182003, 2014. doi: 10.1103/PhysRevLett.112.182003.

[128] Bernd A. Kniehl and Jungil Lee. Polarized J/ψ from chi(cJ) and ψ' decays at the Tevatron. *Phys.Rev.*, D62:114027, 2000. doi: 10.1103/PhysRevD.62.114027.

[129] J. Pumplin, D.R. Stump, J. Huston, H.L. Lai, Pavel M. Nadolsky, et al. New generation of parton distributions with uncertainties from global QCD analysis. *JHEP*, 0207:012, 2002. doi: 10.1088/1126-6708/2002/07/012.

[130] Geoffrey T. Bodwin, U-Rae Kim, and Jungil Lee. Higher-order relativistic corrections to gluon fragmentation into spin-triplet S-wave quarkonium. *JHEP*, 1211:020, 2012. doi: 10.1007/JHEP11(2012)020.

[131] Pietro Faccioli, Valentin Knuenz, Carlos Lourenco, Joao Seixas, and Hermine K. Woehri. Quarkonium production in the LHC era: a polarized perspective. *Phys.Lett.B*, 2014.

[132] Geoffrey T. Bodwin, Eric Braaten, Estia Eichten, Stephen Lars Olsen, Todd K. Pedlar, et al. Quarkonium at the Frontiers of High Energy Physics: A Snowmass White Paper. 2013.

[133] Tzu Chiang Yuan. Perturbative QCD fragmentation functions for production of P wave mesons with charm and beauty. *Phys.Rev.*, D50:5664–5675, 1994. doi: 10.1103/PhysRevD.50.5664. Heavy Quark Fragmentation to 1P1[1], 3PJ[1], 1S0[8], 3S1[8].